

Late Cenozoic (13-0 Myr) glacimarine sedimentology, facies analysis, and sequence
stratigraphy from the Western Ross Embayment, Antarctica:
Implications for the variability of the Antarctic Ice Sheets.

by

Robert Murray McKay

A thesis
submitted to Victoria University of Wellington
in fulfilment of the requirements for the degree of
Doctor of Philosophy
in Geology

Victoria University of Wellington

2008



ABSTRACT

Sedimentary processes related to oscillations of the marine-based sector of Antarctic Ice Sheet (AIS) in the Ross Embayment over the past 13 Myr are examined at various timescales from stratigraphic records of glacial advance and retreat obtained from the McMurdo Sound region. An initial sedimentary model was developed from short (<2 m) sediment cores collected from beneath the present-day McMurdo Ice Shelf and seasonally open water in the Ross Island region. These cores document sedimentary processes associated with subglacial, ice shelf and open marine environments since the Last Glacial Maximum (LGM) in the Ross Sea Embayment. A radiocarbon chronology from these short cores implies that lift-off of grounded ice in the 900 m-deep marine basins surrounding Ross Island occurred by ~10,100 ^{14}C yr BP. Following lift-off, the ice shelf calving line retreated toward its present position. By ~8,900 ^{14}C yr BP, seasonally open marine conditions extended as far south as Ross Island. Glacial retreat was rapid and preceded the timing of Meltwater Pulse 1B. Since 8,900 ^{14}C yr BP, the calving line of the Ross Ice Shelf has remained pinned to Ross Island despite warmer-than-present temperatures during the mid-Holocene.

Depositional models developed for the LGM to recent sediments were then applied to the interpretation of the 1284-m-long ANDRILL McMurdo Ice Shelf core (AND-1B) to documenting oscillations of the AIS in the Ross Embayment over the past 13 Myr. A sequence stratigraphic framework for grounding-line fluctuations of under a variety of glacial regimes, with three distinct types of glacimarine cycle (sequence motif) identified. Motif 1 (Pleistocene and Mid to early Late Miocene) is dominated by thick sub-glacial diamictite, deposited during glacial advance, with occasional thin interbeds of sparsely- to non-fossiliferous mudstone that marks an ice shelf setting during interglacial maxima. Motif 2 (Pliocene) comprises subglacial to glacimarine diamictite overlain by thin, proglacial deposits and capped with substantial beds of diatom-bearing mudstone or diatomite formed under open-marine conditions. Motif 3 (Late Miocene) extends from subglacial diamictite into a thick proglacial succession that includes a combination of stratified diamictite, graded sandstone, conglomerate, and rhythmically-stratified mudstone. The differences in these facies successions (motifs) are associated with the long-term evolution of the AIS in the Ross Embayment from a cold glacial regime with limited volumes of subglacial meltwater (Motif 1) to warmer styles (Motifs 2 and 3) of glaciation with increased subglacial meltwater discharge, before passing back to the cold style of glaciation that characterises the present-day AIS (i.e., limited subglacial meltwater). Each motif was interpreted on the basis of modern analogues of glacimarine sedimentation from a range of climatic/glacial settings, recording a fundamental change in the mass balance for the AIS in

the Ross Embayment. For cold glacial regimes similar to the present day Antarctic Ice Sheets, ablation was largely controlled by calving at the marine margin and the melting of the underside of ice shelves by oceanic processes. For warmer regimes, in particular for Motif 3, ablation by melting was a significant influence on mass balance.

This sedimentary model was then applied in detail to interpret the Pleistocene section of AND-1B (upper 150 m) with a chronostratigraphic interpretation constrained by sequence stratigraphy, $^{40}\text{Ar}/^{39}\text{Ar}$ dating of volcanic ashes, and magneto-stratigraphy. The glacial-marine sequences in AND-1B drill core correlate one-to-one with cycles in the benthic $\delta^{18}\text{O}$ record for the past ~ 0.8 Myr (Marine Isotope Stages 20-2), and are interpreted as recording fluctuations of the AIS in the Ross Embayment with a 100-kyr cyclicity. In this “100-kyr world”, the AIS is relatively stable, with subglacial to grounding-zone sedimentation dominating at the AND-1B drill site, with only thin intervals of ice-shelf sedimentation during interglacials and little evidence for open-marine conditions during the Late Pleistocene “super-interglacials”. An unconformity spans (~ 200 kyr) most of the Mid-Pleistocene Transition and is inferred to represent large scale expansion of AIS at ~ 0.8 Myr. Prior to this, Early Pleistocene glacial/interglacial cycles had a 40-kyr frequency, with interglacial periods characterised by open water deposits that contain volcanoclastic debris and diatomaceous sediments. This upper 150 m of AND-1B provides clear evidence for both a change in the frequency (40- to 100-kyr cycles), and a reduction in the sensitivity of a cooler marine-based AIS in the Ross Embayment.

ACKNOWLEDGEMENTS

This thesis has benefited from the support and guidance by numerous people over the past three years.

Peter Barrett and Tim Naish supervised the project. Both have provided me with incredible opportunities, support and experiences that are too numerous to list. Above all, they have made this undertaking a thoroughly enjoyable experience. Thanks guys.

Lionel Carter and Gavin Dunbar have essentially acted as additional supervisors throughout this project, and their input to this work was invaluable.

All the staff and students at the Antarctic Research Centre - Tamsin Falconer, Alex Pyne and Michelle Dow, in particular have ensured that the logistical, technical, scientific and administrative aspects of this project have run smoothly. Nancy Bertler provided ice core material (and advice) and the use of lab facilities. Valerie Claymore, at GNS, also provided assistance with ice core processing.

Matthew Wood helped with the processing of difficult samples for grain size analysis. His care and dedication to this task was exceptional. Margaret Harper is thanked for her discussions and help regarding diatoms and their identification. Stewart Bush is thanked for thin section processing, and John Carter is thanked for assistance with the Sedigraph.

I am also thankful to many scientists who I have interacted with during various aspects of this work, in particular; Ross Powell, Greg Browne, Ellen Cowan, Mike Hannah, Huw Horgan, Larry Krissek, Phil Kyle, Richard Levy, Christian Ohneiser, Jake Ross, Reed Scherer, Franco Talarico, Thomas Wilch, Gary Wilson, Dene Carroll, Cliff Atkins, and the entire ANDRILL McMurdo Ice Shelf on-ice team. Eugene Domack, Phil Bart, Chris Fielding, Mike Hambrey are thanked for reviews of papers that make up chapters in this thesis. The staff at the Antarctic Research Facility at Florida State University are thanked for assistance with analysing the Deep Freeze and AND-1B cores.

I am especially grateful to Doug MacAyeal and his research group for their hospitality during my visit to University of Chicago. Although aspects of that work did not eventuate for this project, it was an invaluable learning experience.

This work was financially supported by the New Zealand Foundation for Research Science and Technology (FRST) contract COX0410 and the Marsden Fund (Grant 04-GNS—010).

Antarctica New Zealand is thanked for logistical support. The Royal Society of New Zealand, Geological Society of New Zealand, INQUA, SCAR, and the Transantarctic Association are thanked for financial assistance to attend conferences and present aspects of this work.

Thanks also to all my friends and family. Most of all, thank you to Jo.

TABLE OF CONTENTS

ABSTRACT	i
ACKNOWLEDGEMENTS	iii
TABLE OF CONTENTS	iv
LIST OF FIGURES.....	xi
LIST OF TABLES.....	xiv
INTRODUCTION	1
CHAPTER 1: CONTROLS ON LATE CENOZOIC SEDIMENTATION IN THE MCMURDO ICE SHELF REGION, ANTARCTICA	9
1.1 Geological history of the McMurdo Sound region.....	11
1.1.1 Pre-Gondwana break-up	11
1.1.2 Mid-Jurassic: Initiation of West Antarctic Rift and Gondwana break-up....	12
1.1.3 Paleocene to Eocene: Transantarctic Mountain uplift and depression of the Ross Embayment	14
1.1.4 Latest Eocene to Oligocene: Development of the Victoria Land Basin and the main rifting phase	14
1.1.5 Early Miocene: Initiation of the Terror Rift	15
1.1.6 Pliocene to Pleistocene: Continued rifting and the formation of Ross Island	15
1.2 Ice Sheet history: Paleogene to Neogene	17
1.2.1 Geological evidence for major Antarctic climatic events	17
1.2.2 Oligocene onset of widespread Antarctic glaciation	17
1.2.3 Late Oligocene to Early Miocene boundary: Continued cooling or widespread deglaciation?.....	18
1.2.4 Drivers for initial ice sheet development.....	19
1.2.5 Early Miocene development of large ephemeral ice sheets	20
1.2.6 Mid-Miocene cooling	20
1.2.7 Pliocene warming	21
1.2.8 Late Pliocene/Early Pleistocene cooling	22

1.2.9 Drivers for Late Pliocene/Early Pleistocene glacial/interglacial cycles	23
1.2.10 The Mid-Pleistocene Transition and the onset of 100-kyr Late Pleistocene glacial/interglacial cycles	24
1.2.11 Drivers for the Mid-Pleistocene Transition and the 100-kyr cycles.....	25
1.3 The configuration of past ice sheet advance and retreat in the Western Ross Embayment.....	27
1.4 Retreat of the Antarctic Ice Sheet in the Ross Embayment since the Last Glacial Maximum.....	29
1.4.1 Geological evidence	29
1.4.2 Geophysical evidence of glacial advance in the western Ross Sea.....	30
1.5 Regional setting at the present-day AND-1B site	32
1.5.1 The McMurdo Ice Shelf	32
1.6 Bathymetry and oceanography in the Ross Sea and McMurdo Sound	33
1.6.1 Biogenic production	34
1.7 Summary.....	35
1.8 References	35
 CHAPTER 2: THE RETREAT OF THE ANTARCTIC ICE SHEET (ROSS ICE SHELF) IN THE ROSS EMBAYMENT SINCE THE LAST GLACIAL MAXIMUM	45
2.1 Introduction	47
2.2 Regional setting	50
2.3 Methods	52
2.3.1 Core collection and description.....	52
2.3.2 Grain size analysis.....	53
2.3.3 Sand fraction petrology	53
2.3.4 X-ray diffraction.....	55
2.3.5 Diatom analysis	55
2.3.6 Windless Bight ice core analysis.....	56
2.3.7 Radiocarbon chronology.....	56
2.4 Stratigraphy	58
2.4.1 Clast-rich sandy diamict unit.....	58

2.4.2	Clast-rich muddy diamict unit	59
2.4.3	Silty-clay unit	60
2.4.4	Diatom mud and ooze with dispersed clasts.....	61
2.5	Chronology	65
2.6	Discussion.....	68
2.6.1	Sub-ice shelf diamict facies.....	68
2.6.2	Sub-ice shelf sand and mud facies.....	69
2.6.3	Open water diatom mud and ooze facies.....	71
2.7	Sediment provenance and ice shelf dynamics	72
2.8	Timing and magnitude of grounding and calving retreat: Relationships to Meltwater Pulses 1A and 1B.	73
2.9	Conclusions	78
2.10	References	79
2.11	Supplementary data: Core logs.....	84
2.12	Supplementary data: X radiographs	93
2.13	Supplementary data: Grain size results	96
2.14	Supplementary data: Grain size statistics	98
2.15	Supplementary data: Sand grain petrology.....	100
2.16	Supplementary data: XRD results	101
2.17	Supplementary data: Diatom counts.....	102
2.18	Supplementary data: Ice core analysis.....	103
2.18.1	Methods	103
2.18.2	Control samples	104
2.18.3	Determining the rate of sedimentation	104
2.18.4	Results	105

CHAPTER 3: THE STRATIGRAPHIC SIGNATURE OF LATE CENOZOIC OSCILLATIONS OF THE ANTARCTIC ICE SHEETS IN THE ROSS EMBAYMENT, ANTARCTICA	107
3.1 Introduction	110
3.1 Previous high-latitude glacimarine depositional models.....	113
3.2 Geological setting.....	117
3.3 Glacial setting.....	117
3.4 AND-1B lithofacies scheme.....	119
3.4.1 Facies 1: Diatomite.....	119
3.4.2 Facies 2: Mudstone.....	122
3.4.3 Facies 3: Interstratified mudstone and sandstone.....	123
3.4.4 Facies 4: Mudstone with dispersed/common clasts.....	124
3.4.5 Facies 5: Rhythmically interlaminated mudstone with siltstone or sandstone	124
3.4.6 Facies 6: Sandstone	125
3.4.7 Facies 7: Conglomerate	126
3.4.8 Facies 8: Breccia.....	126
3.4.9 Facies 9: Stratified diamictite.....	126
3.4.10 Facies 10: Massive diamictite.....	127
3.4.11 Facies 11: Volcanic rocks and sediments.....	128
3.5 Sequence stratigraphic framework	128
3.5.1 Motif 1: Diamictite dominant.....	129
3.5.2 Motif 2: Interstratified diamictite and diatomite	131
3.5.3 Motif 3: Interstratified diamictite and mudstone.....	134
3.6 Discussion: Sedimentation models of glacimarine deposition at AND-1B ..	136
3.6.1 Sedimentation during a cold, polar glacial regime	136
3.6.2 Sedimentation during a dynamic polar/sub-polar glacial regime.....	139
3.6.3 Sedimentation during a dynamic sub-polar glacial regime	143
3.7 Conclusions	146
3.8 References	147
3.9 Supplementary report: Grain size analysis	154
3.9.1 Grain size method.....	154

3.9.2	Facies 1: Diatomite	155
3.9.3	Facies 2: Mudstone	155
3.9.4	Facies 3: Interstratified mudstone and sandstone	156
3.9.5	Facies 4: Mudstone with dispersed/common clasts.....	157
3.9.6	Facies 5: Rhythmically interlaminated mudstone with siltstone or sandstone	158
3.9.7	Facies 6: Sandstone	158
3.9.8	Facies 7: Conglomerate	159
3.9.9	Facies 8: Breccia.....	160
3.9.10	Facies 9: Stratified diamictite	160
3.9.11	Facies 10 – Massive diamictite.....	161
3.10	References	163
3.10.1.1	Supplementary data: Grain-size frequency from AND-1B	164
3.10.1.2	Supplementary data: Grain-size statistical data from AND-1B	169

CHAPTER 4: THE PLEISTOCENE GLACIAL HISTORY OF THE ANTARCTIC ICE SHEET IN THE ROSS EMBAYMENT, BASED ON SEDIMENT DRILL CORE FROM BENEATH THE MCMURDO ICE SHELF.175

4.1	Introduction	177
4.2	Proxy records of Pleistocene ice volume and sea level fluctuations	178
4.3	Evidence for WAIS “collapse” during the Pleistocene?	180
4.4	Methods	183
4.5	Pleistocene glacial/interglacial sequence stratigraphy of the AND-1B drill core	184
4.5.1	Sequence 1: Diamictite with interbedded sands and muds (10.08 to 0 mbsf).....	184
4.5.2	Sequence 2: Interbedded sandstone and mudstone overlying interbedded stratified and massive diamictite (41.1 to 26.68 mbsf)	187
4.5.3	Sequence 3: Diamictite overlain by conglomerate, mud with dispersed clasts and silty claystone (47.70 to 41.90 mbsf).....	189
4.5.4	Sequence 4: Diamictite overlain by conglomerate and mudstone with dispersed clasts (51.10 to 47.86 mbsf)	190

4.5.5	Sequence 5: Diamictite overlain by thin interbedded sandstone and mudstone (56.49 to 51.10 mbsf).....	191
4.5.6	Sequence 6: Diamictite overlain by thin interbedded sandstone and mudstone (67.10 to 56.49 mbsf).....	192
4.5.7	Sequences 7-9: Interbedded diamictites (82.60 to 67.10 mbsf)	195
4.5.8	Sequence 10: Interbedded diamictites overlain by mudstone (interbedded with volcanogenic facies), diatomite, and mudstones with lapilli tuff and volcanic ash beds. (99.25 to 82.60 mbsf)	196
4.5.9	Sequence 11: Diamictite, volcanic sandstone and silty claystone (103.72 to 99.58 mbsf).....	198
4.5.10	Sequence 12: Diamictite overlain by mudstone with dispersed clasts (109.42 to 103.72 mbsf)	200
4.5.11	Sequence 13: Volcanic sandstones and mudstones, mudstone with dispersed clasts, diatomite, and diamictite (125.00 to 109.42)	201
4.5.12	Sequence 14: Diamictite, volcanic sandstones, mudstone with dispersed clasts and silty claystones (150.73 to 125 mbsf)	202
4.6	Subglacial, glacimarine and marine processes of the Antarctic Ice Sheet system in the Ross Embayment during the Pleistocene	204
4.7	Sedimentary evidence for erosion and unconformities	208
4.8	Chronostratigraphy and correlation to the marine oxygen isotope timescale	209
4.9	Identifying periods of past retreat and expansion of the Antarctic Ice Sheet in the Ross Embayment during the Pleistocene	213
4.9.1	The Late Pleistocene (0.8 Myr to present)	213
4.9.2	Mid-Pleistocene Transition	215
4.9.3	The Early Pleistocene	216
4.10	Conclusions	217
4.11	References	218
CHAPTER 5: SAND PROVENANCE OF THE AND-1B DRILL CORE		223
5.1	Introduction	225
5.2	Methods	228
5.3	Results	229

5.4	Discussion.....	230
5.4.1	Long-term provenance signal shifts in diamictite facies	230
5.4.2	Glacial to interglacial variability	234
5.5	Conclusions	237
5.6	References	240
CHAPTER 6: SYNTHESIS.....		243
6.1	Development of a sedimentary model for the seafloor beneath the McMurdo Ice Shelf since the Last Glacial Maximum	246
6.2	Sedimentary model associated with a cold-polar marine-based ice sheet in the Ross Embayment: Motif 1	246
6.3	Sedimentary model associated with a dynamic sub-polar marine-based ice sheet in the Ross Embayment: Motif 2.....	247
6.4	Sedimentary model associated with a dynamic sub-polar WAIS: Motif 3 ...	248
6.5	Response of WAIS to Late Cenozoic climate cycles	248
6.6	Timing of the retreat of AIS in the Ross Embayment since the Last Glacial Maximum and the sub-orbital Holocene record	249
6.7	Determining the response of WAIS to orbitally influenced climate cycles during the Pleistocene.....	251
6.8	Comparison with Neogene geologic records from East Antarctica	251
6.8.1	Prydz Bay region	251
6.8.2	Transantarctic Mountains	253
6.9	Correlation to global proxies and implication for orbital control of the Late Cenozoic Antarctic Ice Sheets.....	254
6.10	References	258

LIST OF FIGURES

Figure 1: Map of Antarctica and McMurdo Sound region.....	12
Figure 2: Geological map (after Craddock <i>et al.</i> , 1970) of the Ross embayment sector	13
Figure 3: Geological cross-section of McMurdo Sound	15
Figure 4: Proxy for temperature and ice volume.....	19
Figure 5: Ice core and deep sea proxies for determining past temperatures and ice volume (from Jouzel <i>et al.</i> , 2007 and Lisiecki and Raymo, 2005) matched against orbital forcing parameters.....	26
Figure 6: Ice Sheet growth in the Ross Embayment	28
Figure 7: Retreat of LGM grounding line	31
Figure 8: Radarsat mosaic showing the drainage into the Ross Ice Shelf.....	32
Figure 9: Simplification of interactions of oceanic water masses occurring on the present-day Ross Sea continental shelf.	33
Figure 10: Map of Ross Island region showing the core sites in this study	51
Figure 11: Photos of various sand grains in HWD03 cores	59
Figure 12: Diatom abundances in cores DF80-189 (top) and DF80-133 (bottom).....	62
Figure 13: Examples of diatom taxa observed in DF80 cores. Scale Bar = 10µm.....	63
Figure 14: Examples of diatom taxa observed in DF80 cores. Scale Bar = 10µm.....	64
Figure 15: Composite logs of DF80-189 and HWD03-1	66
Figure 16: Composite logs of DF80-133 and HWD03-2.....	67
Figure 17: Core logs, lithological characteristics, and selected x-rays of representative facies from HWD03-1 and DF80-189..	71
Figure 18: Sediment transport paths during three stages of glacial retreat.	72
Figure 19: A chronology for the retreat of the Antarctic Ice Sheet from this study.....	75
Figure 20: The retreat history of the ice sheet/shelf grounding and calving line.....	76
Figure 21: Core log for HWD03-1 (from Barrett <i>et al.</i> , 2005).	84
Figure 22: Core log for HWD03-2 (from Barrett <i>et al.</i> , 2005).	85
Figure 23: Core log for HWD06.	86
Figure 24: Core log for DF80-70	87
Figure 25: Core log for DF80-78.	88
Figure 26: Core log for DF80-79.	89
Figure 27: Core log for DF80-133.	90
Figure 28: Core log for DF80-138	91
Figure 29: Core log for DF80-189.	92
Figure 30: X-radiograph for DF80-70.....	93

Figure 31: X-radiograph for DF80-78.....	93
Figure 32: X-radiograph for DF80-79.....	94
Figure 33: X-radiograph for DF80-133.....	94
Figure 34: X-radiograph for DF80-138.....	95
Figure 35: X-radiograph for DF80-189.....	95
Figure 36: Map of Antarctic continent and McMurdo Sound.....	112
Figure 37: Stratigraphic log, Lithostratigraphic Units (LSU), and interpretation of AND-1B core.	120
Figure 38: Example stratigraphic log of a Motif 1 sequence from AND-1B.....	130
Figure 39: Example stratigraphic log of a Motif 2a sequence from AND-1B.	132
Figure 40: Example stratigraphic log of a Motif 2b sequence from AND-1B.....	133
Figure 41: Example stratigraphic log of a Motif 3 sequence from AND-1B.....	135
Figure 42: Sedimentary model for Motif 1.	138
Figure 43: Sedimentary model for Motif 2	140
Figure 44: Sedimentary model for Motif 3	145
Figure 45: Grain-size results for Facies 1	155
Figure 46: Grain-size results for Facies 2.	156
Figure 47: Grain-size results for Facies 3.	157
Figure 48: Grain size results for Facies 4.....	157
Figure 49: Grain-size results for Facies 5.	158
Figure 50: Grain-size results for Facies 6.	159
Figure 51: Grain-size results for Facies 7.	160
Figure 52: Grain-size results for Facies 9.	160
Figure 53: Top: Grain-size results for Facies 10.....	162
Figure 54: Map of Antarctica and Ross Island (RI) region.....	180
Figure 55: Stratigraphic log (0-52 mbsf).....	186
Figure 56: Representative photos of facies and GSEs from Sequences 2 to 3 AND-1B.	188
Figure 57: Representative photos of facies and GSEs from Sequences 3 to 5 AND-1B.	191
Figure 58: Stratigraphic log (48-100 mbsf).....	194
Figure 59: Representative photos of facies and GSEs from Sequences 5 to 10 in AND-1B. ...	196
Figure 60: Stratigraphic log (98-154 mbsf).....	199
Figure 61: Representative photos of facies and GSEs from Sequences 10 to 11 in AND-1B..	200
Figure 62: Representative photos of facies and GSEs from Sequences 11 to 13 in AND-1B..	202
Figure 63: Representative photos of facies and GSEs from Sequences 13 to 15 in AND-1B..	204
Figure 64: Cartoon to illustrate simply the tidal pumping process.	207

List of figures

Figure 65: Age model based on integration of magnetostratigraphy, tephrochronology and the sequence stratigraphic model.....	212
Figure 66: Geological map (after Craddock 1970 and Borg <i>et al.</i> , 1989).....	226
Figure 67: Paleogeography reconstructions based on the known chronology of volcanism in the McMurdo region.....	227
Figure 68: Hypothesised effect on glacial flowlines for two different glacial maxima.	228
Figure 69: Sequence motifs, Lithostratigraphic Units (LSU) and of AND-1B.....	231
Figure 70: Petrographic results for the upper 150 m of the AND-1B drill core.	235
Figure 71: Correlation of AND-1B to $\delta^{18}\text{O}$ marine records.....	256

LIST OF TABLES

Table 1: Lithologies and minerals categories for modal analysis of sand fraction.	54
Table 2: Reported and corrected radiocarbon (AIO) dates used in this study.....	57
Table 3: Grain size results for HWD06 and DF80 cores.	97
Table 4: Grain size statistics for HWD06 and DF80 cores.	99
Table 5: Modal analysis results for sand grain fraction	100
Table 6: XRD results for DF80 and HWD cores	101
Table 7: Diatom results from DF80 cores.	102
Table 8: Ice core control sample results.....	104
Table 9: Ice core sediment results	105
Table 10: Modern (post-LGM) analogues from various glacial thermal regimes.....	115
Table 11: Summary of lithofacies documented in the core.	120
Table 12: Grain-size frequency data for AND-1B..	168
Table 13: Grain-size statistics for AND-1B samples.	173
Table 14: Percentage data from modal analysis of sand fraction from AND-1B.....	239

Introduction

During the austral summer of 2006-2007, the ANtarctic geological DRILLing (ANDRILL) Programme collected its first geological drill core from a platform on the McMurdo Ice Shelf, at the northwest corner of the Ross Ice Shelf. Termed the “McMurdo Ice Shelf Project”, the key aim was to recover a succession of Miocene, Pliocene and Pleistocene sediments that documented past ice shelf/sheet response to climatic forcings.

The aim of this thesis is two-fold:

- To provide an initial model of sedimentation for beneath the McMurdo Ice Shelf; and develop a retreat history of the Antarctic Ice Sheet in the Ross Embayment since the Last Glacial Maximum (LGM; ~20 kyr). This model was developed from short sediment cores collected during ANDRILL site survey seasons (2003 and 2006), as well as archived cores from the McMurdo region.
- To develop and apply this sedimentation model to the ANDRILL McMurdo Ice Shelf drill core (AND-1B) at a variety of time scales; and using this model to interpret to climatic implications. AND-1B recovered 1284.87 m of drill core at 98% recovery.

This thesis comprises six chapters, most of which are modified from papers that have resulted, or will result from this thesis. Each chapter is intended to be a distinct piece of research that relates to one of the two aims stated above. The very nature of the ANDRILL project is collaborative, and all of the papers derived from this thesis are multi-authored. The paragraphs below detail the aims of each chapter, and the extent of my contribution to each. Where other authors have provided data, I have referenced this in the text of each chapter.

Chapter 1 is an overview of the geologic and tectonic setting of Antarctica, with a focus on the Ross Sea sector. It then outlines the major developments in Antarctic climatic evolution with a focus on the development of its ice sheets, before discussing the retreat of grounded ice sheet in the Ross Sea embayment since the LGM. It finishes by

Introduction

providing background information on the present-day oceanographic and ecological setting. This chapter is intended to provide a context for the following chapters, and to present the state of knowledge prior to undertaking of this thesis. More detailed and critical analysis of the published literature is provided and cited within each of the following chapters.

Chapter 2 develops a sedimentary lithofacies model and glacial retreat history for the Ross Ice Shelf and the Antarctic Ice Sheet (AIS) system in the McMurdo region from the LGM to present. This chapter was based on a series of gravity cores collected from beneath the McMurdo Ice Shelf during 2003 (HWD03) and 2006 (HWD06), as well as archived marine cores (DF80) collected in McMurdo region. Sediments in the HWD03 cores were described by Peter Barrett and Gavin Dunbar prior to my involvement in this project. Diatom analysis from HWD03 cores in this paper was done by Margaret Harper, and this is referenced when used. Tim Naish, Gavin Dunbar, and I described the sediments in the HWD06 and DF80 cores. I conducted the diatom and grain size analysis for the DF80 and HWD06 cores, as well as the petrology and IRD analysis from HWD03, HWD06, and DF80 cores. I also undertook dust content analysis on an ice core from Windless Bight. The synthesis of the sediment model and the chronology for the retreat of the Antarctic Ice Sheet/Ice Shelf system in the Ross Embayment since the LGM was presented in McKay *et al.* (2008), with input from all co-authors.

Chapter 3 extends the sedimentary model developed in the previous chapter to the entire AND-1B drill core. It outlines the sedimentary facies successions associated with advance and retreat of the Antarctic Ice Sheet across the drillsite for the past 13 Myr. It also documents large-scale changes in the behaviour of the Antarctic Ice Sheet in the Ross Embayment, and provides sedimentary models for deposition under three different thermal ice sheet regimes. The interpretation of past glacial regimes made in this chapter are based on modern analogues of sedimentation in sub-polar (e.g., Greenland/Spitsbergen) and polar (e.g. Antarctica) glacial environments. For this thesis, a “sub-polar glacial regime” is defined as a glacier/ice sheet that has a vertical temperature profile that has a significant zone that is below pressure melting point, but also has significant zones that are at pressure melting point, especially at the ice sheet

Introduction

bed. Polar glaciers are below pressure melting throughout the vertical temperature profile, with the possible exception of a thin zone of water/unfrozen sediments at the bed. The use of “wet(warm)-based”, “polythermal” or “dry(cold)-based” was considered ambiguous in the context of interpreting past glacial marine sedimentation, as the present-day Antarctic Ice Sheet is now known to contain a significant subglacial drainage network, and therefore there is potential for some “wet-based” glacial deposition in the modern Antarctic environment. I developed the facies descriptions and analysis, and interpretations of glacial proximity/environments, with input from Greg Browne, Lionel Carter, Tim Naish and Ross Powell. Facies analysis was based on the core logging of ANDRILL sedimentology/stratigraphy team during the on-ice core characterisation phase of the ANDRILL project. Greg Browne and I identified the three sedimentary motifs. I developed the sedimentary model presented in this chapter, and in McKay *et al.* (in review), with input from the ANDRILL sedimentology/stratigraphy team. At the end of this chapter a supplementary report documents the textural characteristics of each facies type by presenting the grain-size frequency distributions of 162 samples. Interpretations made in this report are intended to supplement the facies descriptions and process interpretations made earlier in the chapter.

Chapter 4 provides a history for the Antarctic Ice Sheet in the Ross Embayment throughout the Pleistocene. This is based on core descriptions of the upper 150 m of AND-1B. It uses the detailed core descriptions provided by ANDRILL Sedimentology/Stratigraphy team (Greg Browne, Lionel Carter, Ellen Cowan, Gavin Dunbar, Larry Krissek, Rob McKay, Thomas Wilch), as well as a re-description of the upper 150 m conducted by Tim Naish, Ross Powell and me at Florida State University in 2007. From these descriptions, concepts for a high-resolution sequence stratigraphic model for the Pleistocene section of the AND-1B drill core were developed. This interpretation incorporates elements of the sedimentary models developed in Chapters 2 and 3, and applies a new chronostratigraphic framework for this thesis. This framework is constrained by $^{40}\text{Ar}/^{39}\text{Ar}$ dating of volcanic ashes and magnetostratigraphy of AND-1B (Wilson *et al.*, 2007) and the $\delta^{18}\text{O}$ benthic marine record of Lisiecki and Raymo (2005). This chapter will constitute the basis of a paper that is in the final stages of preparation. The exact scope and conclusions in this paper will be determined once the

Introduction

age model is finalised by additional $^{40}\text{Ar}/^{39}\text{Ar}$ dating of volcanic ashes, which are due in mid-2008. However, despite the absence of these data Chapter 6 provides clear sedimentary evidence for a fundamental change in the response of AIS to orbital forcing parameters at 0.8 Myr. Prior to 0.8 Myr, the AIS in the Ross Embayment fluctuated between a subglacial and open marine state at the AND-1B drillsite, and responded at a ~ 40 kyr frequency. After 0.8 Myr, the AIS was more stable, and fluctuated at a 100-kyr frequency between a subglacial and ice shelf state.

Chapter 5 provides an overview of the provenance signal of grounded ice passing over the AND-1B drill site as determined from the sand grain petrographic results. Provenance shifts are noted at interglacial/glacial frequencies. A long-term shift in glacially transported detritus from EAIS outlet glacier to the south of the drill site is also noted at 0.8 Myr, from basement- into Beacon Supergroup-derived quartz. However, whether this is a result of changes in paleogeography due to Plio-Pleistocene volcanic cone building, or the progressive down-cutting of outlet glaciers flowing through the Transantarctic Mountains is difficult to determine. The conclusions in this chapter are necessarily subjective, reflecting the uncertainties associated with interpreting the provenance signal. The data and results presented here will be integrated into a publication lead by Franco Talarico and Sandra Sandroni (Università di Sienna), who have documented the clast content at 10 cm intervals for the entire AND-1B drill core.

Chapter 6 summarises the main results of this thesis, in particular the changes in the stratigraphic signature of the AIS in the Ross Embayment during the Late Cenozoic, and the inferences that can be drawn on the variability in the extent and thermal regime of the AIS in the Ross Embayment over this time. The relevance of the AND-1B is then discussed in the context of the on-land Neogene geological record from Antarctica, as well as our understanding of global proxy records.

Peer-reviewed publications resulting from this thesis

- McKay, R.M., Dunbar, G.B., Naish, T., Barrett, P.J., Carter, L., and Harper, M., 2008. Retreat history of the Ross Ice Sheet (Shelf) since the Last Glacial Maximum from deep-basin sediment cores around Ross Island. *Palaeogeography, Palaeoclimatology, Palaeoecology* v.260, p 168-183.
- McKay, R.M., Browne, G.H., Carter, L., Cowan, E.A., Dunbar, G.B., Krissek, L.A., Naish, T.R., Powell, R.D., Reed, J.A., Wilch, T.I., and the ANDRILL MIS Science Team, in review. The stratigraphic signature of Late Cenozoic oscillations of the Antarctic Ice Sheet in Ross Embayment. *In review with Geological Society of America Bulletin*.
- Naish, T., Powell, R., Levy, R., Krissek, L., Niessen, F., Pompilio, M., Scherer, R., Talarico, F., Wilson, G., Wilson, T., McKay, R., Ross, J., Winter, D., Barrett, P., Browne, G., Carter, L., Cody, R., Cowan, E., Crampton, J., DeConto, R., Dunbar, G., Dunbar, N., Florindo, F., Gebhardt, C., Graham, I., Hannah, M., Harwood, D., Hansaraj, D., Henrys, S., Helling, D., Kuhn, G., Kyle, P., Läufer, A., Maffioli, P., Mogens, D., Mandernack, K., McIntosh, W., Millan, C., Morin, R., Ohneiser, C., Paulsen, T., Persico, D., Pollard, D., Reed, J., Raine, I., Schmitt, D., Sagnotti, L., Sjunneskog, C., Strong, P., Taviani, M., Vogel, S., Wilch, T., Williams, T., (in review). Late Cenozoic Antarctic ice sheet oscillations. *In review with Nature*.

Publications, in prep (for peer-reviewed journals) likely to result from this thesis

- McKay, R., Naish, T., Powell, R., Ross, J. *et al.*, in prep. Pleistocene stability of the Antarctic Ice Sheet. *Short format paper to submit to Nature, Science or Geology (based on Chapter 4)*.
- Carter, L., McKay, R., Dunbar, G., Naish, T., *et al.*, in prep. Late Cenozoic variability of the Antarctic Ice Sheet and its influence on SW Pacific ocean-climate. *To be submitted Global and Planetary Change (includes work from Chapter 4)*. 31p.
- Franco Talarico, Sonia Sandroni, McKay, R., *et al.*, Provenance and ice flow history from the AND-1B drill core. *To be submitted Global and Planetary Change (includes work from Chapter 5)*.

Non-peer reviewed publications resulting from this thesis

- Krissek, L.A., Browne, G.H., Carter, L., Cowan, E.A., Dunbar, G.B., McKay, R.M., Naish, T., Powell, R., Reed, J., Wilch, T.I and the ANDRILL MIS Science Team 2007. Sedimentology and Stratigraphy of the AND-1B Core, ANDRILL McMurdo Ice Shelf Project, Antarctica. *Terra Antartica* v.14, p.185-222.
- G. Dunbar, G., Niessen, F., Vogel, S., Tulaczyk, S., Mandernack, K., Krissek, L., Carter, L., Cowan, E., Wilch, T., Peng, C., Strong, C.P., Scherer, R., Sjunneskog, C., Winter, D., McKay, R., Talarico, F., Pompilio, M., and the ANDRILL-MIS Science Team. Late Pleistocene to Holocene Strata from Soft-Sediment Coring at the AND-1B site, ANDRILL McMurdo Ice Shelf Project, Antarctica. *Terra Antartica* v.14, p141-154.
- Pompilio, M., Dunbar, N., Gebhardt, A., Helling, D., Kuhn, G., Kyle, P., McKay, R., Talarico, F., Tulaczyk, S., Vogel, S., Wilch, T., and the ANDRILL MIS Science Team. 2007. Petrology and Geochemistry of the AND-1B Core, ANDRILL McMurdo Ice Shelf Project, Antarctica. *Terra Antartica* v.14, p.255-288.

- Wilson, G., Levy, R., Browne, G., Dunbar, N., Florindo, F., Henry, S., Graham, I., McIntosh, W., McKay, R., Naish, T., Ohneiser, C., Powell, R., Ross, J., Sagnotti, L., Scherer, R., Sjunneskog, C., Strong, C.P., Taviani, M., Winter, D., and the ANDRILL MIS Science Team. 2007. Preliminary Integrated Chronostratigraphy of the AND-1B Core, ANDRILL McMurdo Ice Shelf Project, Antarctica. *Terra Antarctica* v.14, p.297-316.
- Carter, L., Dunbar, G., McKay, R. and Naish, T., 2007. Sedimentation and oceanography beneath the McMurdo Ice Shelf at Windless Bight, 2006. *Antarctic Data Series* v.32, Antarctic Research Centre, Victoria University of Wellington.
- Barrett, P.J., Carter, L., Dunbar, G.B., Dunker, E., Giorgetti, G., Harper, M.A., McKay, R.M., Niessen, F., Nixdorf, U., Pyne, A.R., Riesselmann, C., Robinson, N., Hollis, C., and Strong, P., 2005. Oceanography and sedimentation beneath the McMurdo Ice Shelf in Windless Bight, Antarctica. *Antarctic Data Series* v.25, Antarctic Research Centre, Victoria University of Wellington. 100p.

Conference publications resulting from this thesis

- McKay, R.M., Browne, G.H., Carter, L., Cowan, E.A., Dunbar, G.B., Krissek, L.A., Naish, T.R., Powell, R.D., Reed, J.A., Wilch, T.I., and the ANDRILL MIS Science Team. 2008. The stratigraphic signature of Late Cenozoic oscillations of the West Antarctic Ice Sheet in Ross Embayment. *Joint SCAR-IASC Open Science Conference 2008*.
- Talarico, F., McKay, R., and Sandroni, S., 2008. Clast provenance and sand petrology in ANDRILL (AND-1B) cores: Implications For the Late Cenozoic Paleoclimatic evolution in the Ross Embayment. *Joint SCAR-IASC Open Science Conference 2008*.
- McKay, R.M., Carter, L., Browne, G.H., Cowan, E.A., Dunbar, G.B., Krissek, L.A., Naish, T.R., Powell, R.D., Reed, J.A., Wilch, T.I., and the ANDRILL MIS Science Team. 2008. A 13 million year history of ice advance and retreat in the Western Ross Embayment – stratigraphic evidence from ANDRILL Site 1B. EGU General Assembly *Geophysical Research Abstracts* v.10, EGU2008-A-00000.
- McKay, R.M., Dunbar, G.B., Naish, T., Barrett, P.J., Carter, L., and Harper, M. (2007) A sediment model and retreat history for the Ross Ice (Sheet) Shelf since the Last Glacial Maximum. *14th Annual WAIS 2007 workshop*.
- Powell, R.D., Naish, T.R., Krissek, L.A., Browne, G.H., Carter, L., Cowan, E.A., Dunbar, G.B., McKay, R.M., Wilch, T.I. and the ANDRILL MIS Science Team. (2007) Antarctic Ice Sheet dynamics through the Neogene from evidence in the ANDRILL–McMurdo Ice Shelf Project drill core (AND-1B) *International Symposium on Antarctic Earth Sciences X*.
- Krissek, L.A., Browne, G.H., Carter, L., Cowan, E.A., Dunbar, G.B., McKay, R.M., Naish, T.R., Powell, R.D., Reed, J.A., Wilch, T.I., and the ANDRILL MIS Science Team (2007) Sedimentology and stratigraphy of the ANDRILL McMurdo Ice Shelf (AND-001B) core. *International Symposium on Antarctic Earth Sciences X*.
- McKay, R.M., Dunbar, G.B., Naish, T., Barrett, P.J., Carter, L., and Harper, M. (2007) A glacial to interglacial sediment model and retreat history for the Ross Ice (Sheet) Shelf in Western Ross Sea since the Last Glacial Maximum. *International Symposium on Antarctic Earth Sciences X*.

Introduction

- Wilson, G.S., Levy, R.H., Browne, G.H., Florindo, F., Henrys, S.A., Graham, I., McIntosh, W.C., McKay, R.M., Naish, T.R., Ohneiser, C., Powell, R.D., Ross, J.I., Sagnotti, L., Scherer, R., Sjunneskog, C., Strong, P., Taviani, M., Winter, D. (2007) Preliminary chronostratigraphy for the upper 700 m (upper Miocene – Pleistocene) of the AND-1B drill core recovered from beneath the McMurdo Ice Shelf, Antarctica. *International Symposium on Antarctic Earth Sciences X*.
- McKay, R.M., Dunbar, G.B., Naish, T., Barrett, P.J., Carter, L., and Harper, M. (2007) Retreat history of the West Antarctic Ice Sheet since the Last Glacial Maximum from deep basin and sub-ice shelf sediment cores in the South Western Ross Sea. *Quaternary International* v.167-168, p278.
- McKay, R., Barrett, P.J. and Dunbar G., 2006. Provenance and Depositional History beneath the McMurdo Ice Shelf in Windless Bight, Ross Sea. *Poster presented at SCAR XXIX Open Science Conference, Hobart, Australia*.
- McKay, R., Barrett, P., Dunbar, G., Naish, T., Harper, M and Carter, L., 2005. A preliminary sedimentation model for beneath the McMurdo Ice Shelf. *Geological Society of New Zealand Miscellaneous Publication* v.119A. p.55.

The work described in this thesis was carried out while I was a full-time student at the Antarctic Research Centre, Victoria University of Wellington between 1 June 2005 and 30 May 2008. Except where mentioned in the text, the research described here is my own. No part of this thesis has been submitted to any other university or similar institution.

Robert McKay

May 2008

CHAPTER 1

Controls on Late Cenozoic sedimentation in the McMurdo Ice Shelf region, Antarctica

Introduction

Sedimentation at the ANDRILL (ANtarctic DRILLing) McMurdo Ice Shelf (MIS) site is influenced by interactions between the physiography of the region with glaciological, and to a lesser extent, oceanographic and biological processes. This chapter first discusses the bedrock geology and tectonic history of the Transantarctic Mountains and the West Antarctic Rift System, providing background on provenance, paleogeography, and volcanism relevant to documenting past configurations of Antarctic Ice Sheets. This is followed by an overview of the glacial and paleoclimatic history for the Antarctic continent (with a focus on the Ross Embayment) throughout the Cenozoic, examining history and mechanisms for ice sheet initiation, variations in the past ice extent and glacial terminations. The third section focuses on local controls in the McMurdo Sound region and provides a summary of both the on-land and marine geological record documenting the retreat of the Antarctic Ice Sheet in the Ross Embayment since the Last Glacial Maximum. A better chronology will be needed to understand adequately the forcings that drove this retreat. The last section outlines the present-day oceanographic and biogenic controls at the ANDRILL McMurdo Ice Shelf project site, and the influences these may have had on past sedimentation.

1.1 Geological history of the McMurdo Sound region

Understanding of the bedrock geology within the Ross Sea Embayment is based largely on outcrops in the uplifted Transantarctic Mountains (TAM; Figure 1). The geology exposed within the TAM is representative of the western margin of the East Antarctic craton, with Mesozoic to Cenozoic uplift and igneous activity associated with the break-up of Gondwana and the development of the West Antarctic Rift system (Figure 2).

1.1.1 Pre-Gondwana break-up

The oldest rocks in the region are metasedimentary clastics and carbonates deposited in a broad shallow marine basin along the present site of the TAM in late Precambrian and Cambrian times when Antarctica was part of the Gondwana supercontinent (Tingey,

1991; Goodge, 2002). These were folded and intruded by granitic magmas during the Ross Orogeny, 500-450 Myr (Granite Harbour Intrusive Complex; Laird, 1991). The mid-continental mountains of the Ross Orogeny were eroded down in Silurian times to a peneplain that reached across Antarctica to the other Gondwana continents. This surface is overlain by subhorizontal strata that are largely terrestrial in origin and reach a thickness of ~2 km (Beacon Supergroup, 390-180 Myr, Barrett, 1991).

1.1.2 Mid-Jurassic: Initiation of West Antarctic Rift and Gondwana break-up

A reorganisation of the global plate system led to the break-up of the Gondwana supercontinent during the Middle Jurassic, and the initiation of the West Antarctic Rift System with associated volcanism that formed the deposits of the Ferrar Large Igneous Group – which includes the Kirkpatrick Basalt, Ferrar Dolerite, and volcanoclastic deposits that intrude the sediments of the Beacon Supergroup (Dalziel, 1992; Dalziel and Elliot, 1982; Elliot, 1975). Further rifting and crustal stretching during the Early Cretaceous resulted in rotated crustal blocks separated by thinned crust that form the archipelago that now lies beneath the ice of West Antarctica (Fitzgerald, 2002).

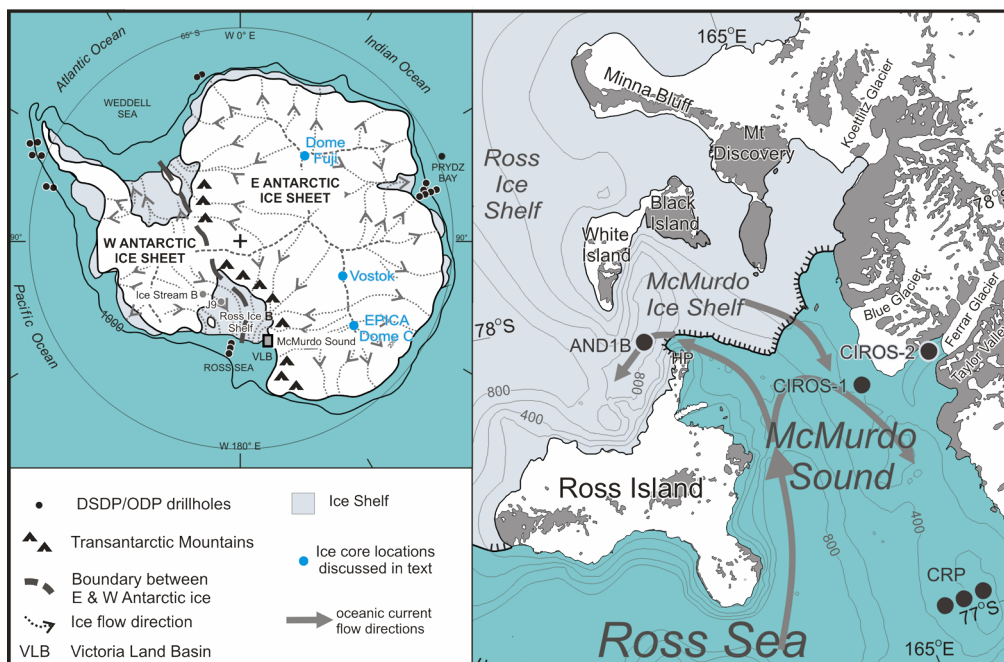


Figure 1: Map of Antarctica (modified from Barrett, 1996) and McMurdo Sound region, showing locations discussed in text. Topographic data is from the Antarctic Digital Database. Bathymetry (200 m contours) is based on data from GNS Sciences archives. Oceanic currents are from Robinson (2004).

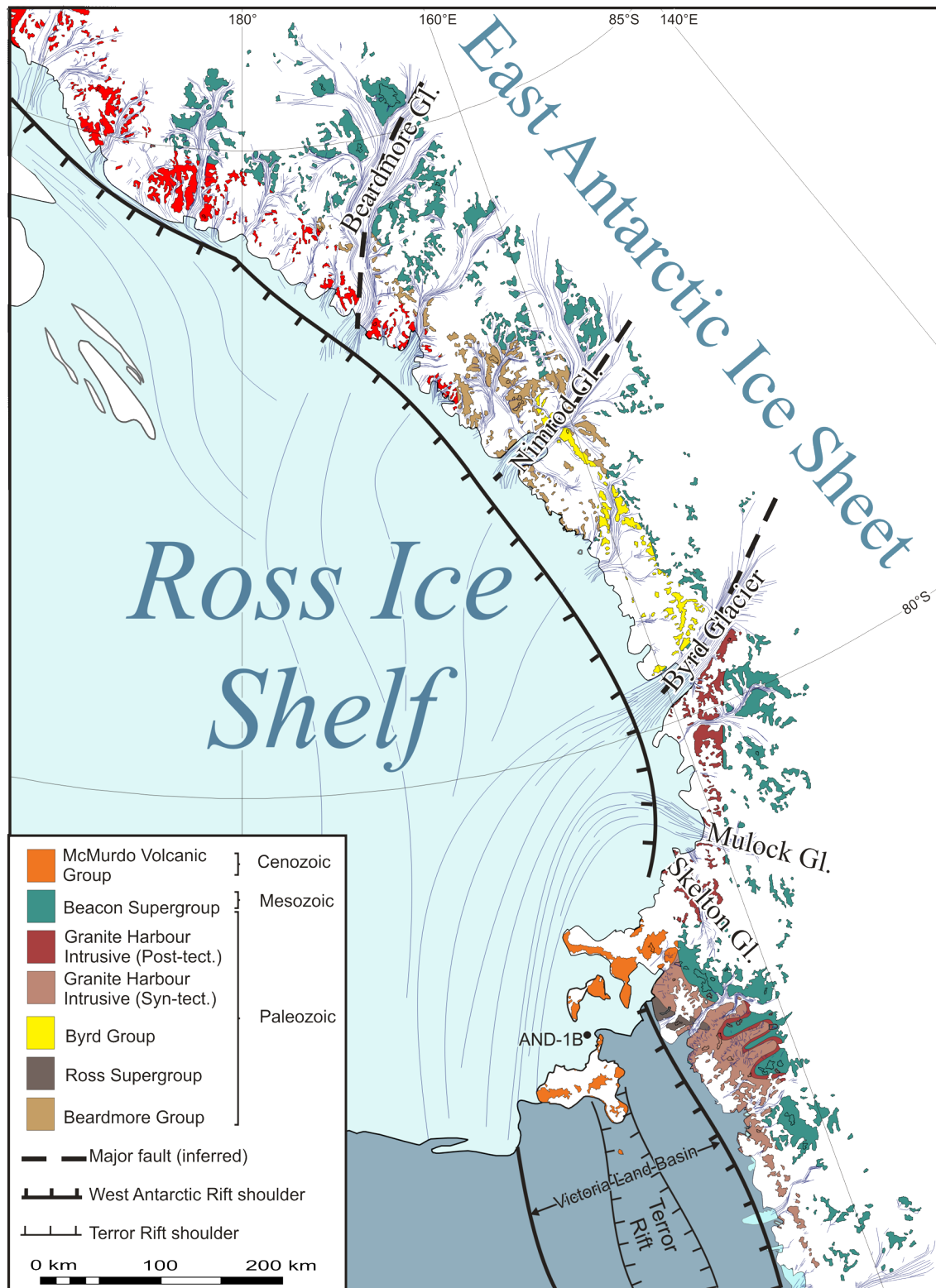


Figure 2: Geological map (after Craddock *et al.*, 1970) of the Ross embayment sector of the Transantarctic Mountains with major features of the West Antarctic Rift system (after Cooper and Davey, 1987). Ice flow directions are from Fahnestock *et al.* (2000). The AND-1B drill site is also shown. Topographic data is from the Antarctic Digital Database.

1.1.3 Paleocene to Eocene: Transantarctic Mountain uplift and depression of the Ross Embayment

The TAM are over 3000 km long, have elevations reaching up to 4500 m, and form one shoulder of the West Antarctic Rift (Figure 2). They have formed along a divergent margin, which is unusual for mountains of this height (Fitzgerald, 2002). Stern *et al.* (2005) attribute up to 2000 m (50%) of uplift to isostatic response following glacial incision. The age of the TAM uplift episodes are difficult to obtain due to gaps in the geological record. Using fission track data, initial uplift of the TAM appears to have occurred in several phases from ~115 Myr (Fitzgerald, 1994). Most exhumation began around 50-55 Myr (Fitzgerald, 1994) with provenance studies from offshore drilling indicating that the Transantarctic Mountains had achieved most of their present height by 34 Myr (Smellie, 2001).

1.1.4 Latest Eocene to Oligocene: Development of the Victoria Land Basin and the main rifting phase

Crustal extension and thinning during the Mesozoic rift period led to the development of sedimentary basins within the Ross Sea. The Victoria Land Basin, an east tilting half-graben approximately 350 km long is hinged at the TAM front in the west, and its eastern margin is bounded by a major fault extending from Ross Island to Terra Nova Bay (Figure 2). Seismic records indicate it contains sediments up to 12 km in thickness (Cooper and Davey, 1987). Drill core chronology indicates that the basin begun subsiding rapidly between 34 Myr and 31 Myr, and then gradually slowed (e.g., Figure 3; Fielding *et al.*, 2008). In the past ~20 Myr, sedimentation in the Victoria Land Basin has kept pace with subsidence.

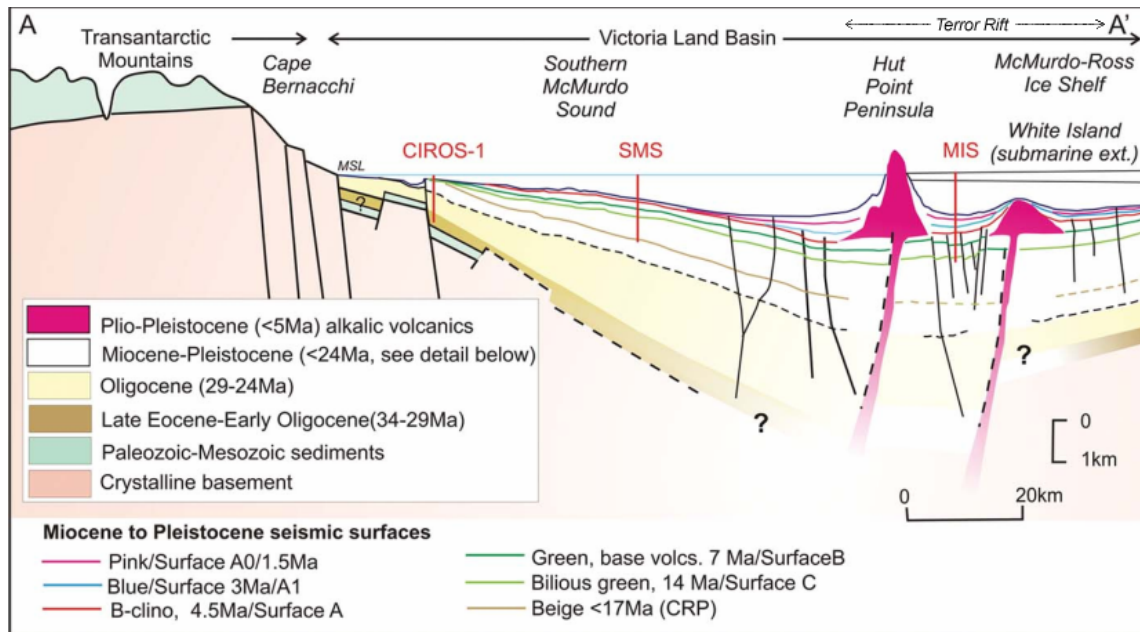


Figure 3: Geological cross-section of McMurdo Sound derived from seismic stratigraphy and drill core data, including CIROS-1, the McMurdo Ice Shelf project (MIS), the Southern McMurdo Sound project, and the Cape Robert Project (from Naish *et al.*, 2006).

1.1.5 Early Miocene: Initiation of the Terror Rift

The MSSTS and CRP drill cores (Figure 1) indicate that volcanism associated with extension of the Terror Rift (Figure 2 and Figure 3) has been occurring in the region since ~25 Ma (Barrett *et al.*, 1986; McIntosh, 2000). The Terror Rift is a 40 km-wide graben currently bound by Mt Erebus and Mt Melbourne, 350 km to the north. It is the most recent phase of extension within the Victoria Land Basin (Esser *et al.*, 2004), and is represented by the stratigraphic section overlying the beige (Rf) seismic reflector in Figure 3.

1.1.6 Pliocene to Pleistocene: Continued rifting and the formation of Ross Island

The McMurdo Volcanic Province is currently dominated in the McMurdo region by Ross Island and centred on Mt Erebus (3,794 m). Older volcanoes lie to the south of Ross Island, notably Black Island, White Island, Mt Discovery and Mt Morning. Ross Island consists of four major volcanic centres - Mt Bird, Mt Terror and Hut Point Peninsula, which surround the active Mt Erebus in radially symmetrical pattern, suggesting that hot spot/plume activity is responsible for the volcanism (Kyle and Cole, 1974). Continued extension associated with the Terror Rift has occurred throughout the late Neogene (Fielding *et al.*, 2008).

Basaltic shield volcanism on Ross Island began between 4.6 and 1.3 Myr, first centred around Mt Bird between 4.6-3.8 Myr (Wright and Kyle, 1990a), followed by Mt Terror from approximately 1.7-1.3 Myr (Wright and Kyle, 1990b). $^{40}\text{Ar}/^{39}\text{Ar}$ dating indicates that the oldest sub-aerial eruption of Mt Erebus is 1.3 Myr (Esser *et al.*, 2004). Three phases in the evolution of Mt. Erebus are documented, beginning with a shield-building phase of low-viscosity mafic volcanism between 1.3 and 1.0 Myr (Esser *et al.*, 2004). This was followed by a cone building phase, with more differentiated, higher-viscosity eruptions of tephrites, basanites and phonotephrites (moderately higher alkali and silica content). Since 250 ka, Mt Erebus has been characterised by anorthoclase-phyric tephriphonolite and phonolite eruptions (i.e., much higher silica and alkali content).

The loading of the lithosphere by Ross Island has resulted in up to 1.8 km of net subsidence beneath Ross Island. A subcircular offshore flexural moat has formed around the island, providing accommodation space for significant volumes of Plio-Pleistocene sediment (Stern *et al.*, 1991; ten Brink *et al.*, 1997; Horgan *et al.*, 2005). The blue seismic (Rj) reflector in Figure 3 represents the oldest stratigraphic horizon associated with this flexural loading and is dated at <3 Myr (Fielding *et al.*, 2008; Henrys *et al.*, in prep.)

The stratigraphic interval above the blue reflector (<3 Myr) may also be associated with extensive erosion of the western margin of the Victoria Land Basin, probably by grounded ice, and a change to a dominant sediment supply from the south (Fielding *et al.*, 2008). The presence of large clinoform sets evident in seismic cross sections suggests that prior to this, sediment was largely sourced from the western margin of the basin (Fielding *et al.*, 2008).

1.2 Ice Sheet history: Paleogene to Neogene

1.2.1 Geological evidence for major Antarctic climatic events

The $\delta^{18}\text{O}$ isotopic ratio from deep-sea benthic foraminifera is influenced by both sea water temperature and ice volume. Compilations for the Cenozoic Era (e.g., Zachos *et al.*, 2001) give relatively low values ($<1.8\text{‰}$) that suggest an ice sheet-free world in Cretaceous and Paleocene times with a gradual cooling through the Eocene. Two significant events mark this record (Figure 4), and were recognised in the earliest measurements (Shackleton and Kennett, 1975) - a rapid $\sim 1\text{‰}$ increase at approximately 34 Myr, interpreted to signify the development of extensive Antarctic sea-ice formation, with the initiation of Antarctic bottom water production, and another rapid $\sim 1\text{‰}$ increase at 14 Myr, signifying the development of the EAIS as a permanent feature (Shackleton and Kennett, 1975; Kennett and Shackleton, 1976).

1.2.2 Oligocene onset of widespread Antarctic glaciation

The CIROS-1 drill hole provided the first direct record of Antarctic ice advance from the late Eocene to early Miocene period (Barrett, 1989; Hannah *et al.*, 1997; Wilson *et al.*, 1998). Late Eocene to early Oligocene strata consisted of deep-water turbidite facies with lone-stones, indicating some glacial influence, whereas the late Oligocene-early Miocene section contained diamictite, sandstone and mudstone (Hambrey *et al.*, 1989) typical of near-shore glacial marine sedimentation from fluctuating ice sheets. This provided the first evidence that dynamic Antarctic ice sheets reached the Victoria Land coast as early late Oligocene times. Drilling in Prydz Bay on the other side of the continent reached back to latest Eocene-early Oligocene diamictites (Hambrey *et al.*, 1991), indicating the TAM was a barrier to the earliest Antarctic ice sheets reaching the Ross Sea. Zachos *et al.* (1992) confirmed an earliest Oligocene age for the first ice sheets from an ice-rafting event in cores off the Kerguelen Plateau, and inferred earliest Oligocene ice volumes similar to the present day ice sheet. Individual Oligocene glaciation events inferred on the basis of discrete positive excursions in the benthic $\delta^{18}\text{O}$ record (Figure 4), are believed to represent glaciation over the entire Antarctic continent at volumes of 125% relative to the present day Antarctic Ice Sheet, while ice volumes

during glacial minima were ~50% of the present day ice sheet (Miller *et al.*, 1991; Miller *et al.*, 2005; Pekar *et al.*, 2006).

1.2.3 Late Oligocene to Early Miocene boundary: Continued cooling or widespread deglaciation?

Zachos *et al.* (2001) infer a significant warming during the late Oligocene (Figure 4) with widespread deglaciation of the Antarctic continent and warmer bottom water temperatures at this time. However, this contrasts with the pollen record from the Cape Roberts Project that shows several species of *Nothofagus* (southern beech) indicating a cool temperate climate persisted throughout the Oligocene, with perhaps a slight cooling indicated (Prebble *et al.*, 2006; Barrett, 2007). Between 24 and 17 Myr, the pollen record shows just one species of *Nothofagus* along with taxa reflecting a herb-moss tundra (Askin and Raine, 2000) and periods of extensive grounded ice (Barrett, 2007). Naish *et al.* (2001) used well-dated volcanic ashes to show that the sedimentary cyclicity in the CRP record is orbitally forced, and also linked a large erosional hiatus at 23.7 Myr with large-scale ice sheet expansion coinciding the Mi-1 isotope event (Figure 4; Naish *et al.*, 2001). Pekar *et al.* (2006) explain the abrupt decrease in the benthic $\delta^{18}\text{O}$ record at 25 Myr (Figure 4) as an artefact of the Zachos *et al.* (2001) curve being spliced together at this interval, with more southerly drilling sites sampled below 25 Myr, while equatorial Atlantic sites were sampled above. Pekar and Christie-Blick's (2008) calibration of the $\delta^{18}\text{O}$ curve against back-stripped continental margin records suggests limited deglaciation, which is more in-line with Cape Roberts Project results and does not require climatic decoupling from the atmospheric CO_2 record, which shows declining levels throughout the Oligocene through to the early Miocene (Pagani *et al.*, 2005).

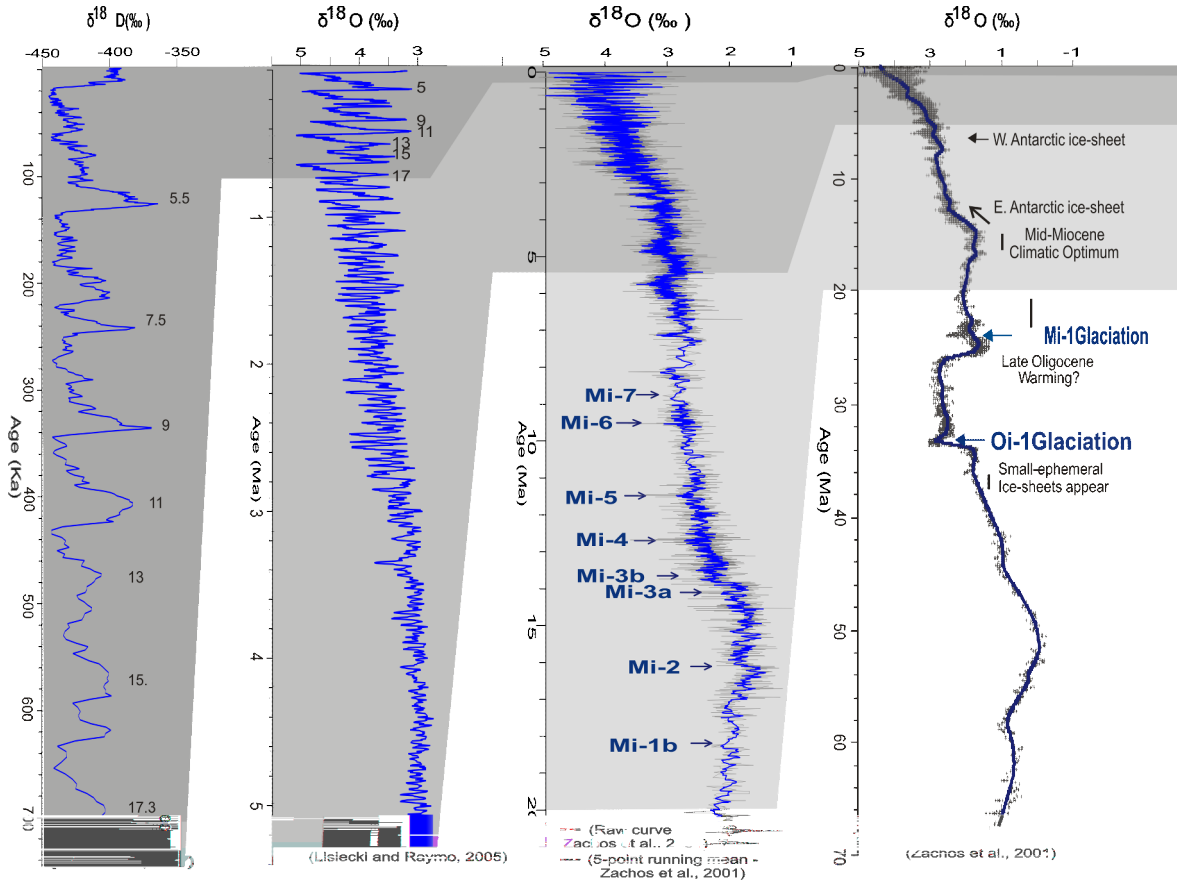


Figure 4: From left to right: Deuterium record from EPICA Dome C ice core (Jouzel *et al.*, 2007) provides a proxy for temperature over the past 740 kyr; $\delta^{18}\text{O}$ benthic stack (Lisiecki and Raymo, 2005) shows change from low-amplitude to high-amplitude 40-kyr cycles at 3 to 2.5 Myr associated with onset of Northern Hemisphere glaciation, and the onset of 100-kyr cycles at ~900-700 kyr; $\delta^{18}\text{O}$ benthic composite record showing large Mi-glacial events followed by a gradual cooling (Zachos *et al.*, 2001; Miller *et al.*, 1991); $\delta^{18}\text{O}$ benthic stack of Zachos *et al.* (2001) showing the major climatic events in the Cenozoic.

1.2.4 Drivers for initial ice sheet development

Antarctica has been in a polar position since Early Cretaceous, yet it appears to have remained highly vegetated and relatively ice-free until the Eocene/Oligocene boundary (approximately 34 Myr; Barrett, 1996). It had long been thought that the thermal isolation after continental break-up, and the development of the Antarctic Circumpolar Current during the Eocene and Oligocene, directly led to the development of the first Antarctic ice sheets (Kennett, 1977). However, a recent coupled GCM (climate)-ice sheet model suggests that thermal isolation may play a secondary role, with the major influence in the development of the first ice sheets being the decline in atmospheric CO_2 (DeConto and Pollard, 2003). This model predicts a three-phase development of the ice

sheets. Declining CO₂ initially leads to small scale, temperate/dynamic glaciations at high elevations. Continuing decline through a CO₂ threshold (between 2-3x present day CO₂) results in rapid glacial expansion, with dynamic, ephemeral ice sheets controlled by orbital variations eventually coalescing into a single, continental-scale East Antarctic Ice Sheet.

1.2.5 Early Miocene development of large ephemeral ice sheets

Although the Early Miocene is generally seen as a period relative warmth, marine sediment cores from DSDP site 270 indicate periods of extensive grounded ice (West Antarctic Ice Sheet) within the Ross Sea embayment since at least the Early Miocene (Barrett, 1975; Leckie and Webb, 1983; Bart *et al.*, 2000). Prior to this, glaciarmarine processes within the Ross Sea appear to be restricted to iceberg-related processes (Leckie and Webb, 1983). The $\delta^{18}\text{O}$ and $\delta^{13}\text{C}$ isotope records also provide evidence for major transient glacial advances in Antarctica as early as the Late Oligocene to Early Miocene (Zachos *et al.*, 2001). The Mi-1 event at ~23 Myr is characterised by a 200 kyr-long positive $\delta^{18}\text{O}$ excursion and may represent an expansion of the EAIS close to, or exceeding, its present day volume (Miller *et al.*, 1991; Zachos *et al.*, 2001; Pekar and DeConto, 2006). Subsequent glaciations (Mi events) are also noted in the oxygen isotope record throughout the Miocene (Figure 4), with large ephermal glaciations corresponding to 100 kyr orbital cycles (Miller *et al.*, 1991; Naish *et al.*, 2001; Pekar and DeConto, 2006).

1.2.6 Mid-Miocene cooling

The 1‰ increase in the $\delta^{18}\text{O}$ at 13.9 Myr (Figure 4; Shackleton and Kennett, 1975; Zachos *et al.*, 2001) is widely attributed to the development of a more stable East Antarctic Ice Sheet, similar to that of today. Recent $^{40}\text{Ar}/^{39}\text{Ar}$ dating of volcanic ashes incorporated into glaciogenic deposits in the Dry Valleys sector of the TAM indicate that the transition from wet-based to cold based polar glaciation occurred between 13.94 and 13.62 Myr (Lewis *et al.*, 2007).

1.2.7 Pliocene warming

The Early to mid-Pliocene (5.3-3 Myr) is characterised by a relatively stable interval with low amplitude cycles in the $\delta^{18}\text{O}$ record (Figure 4). However, the behaviour of the Antarctic Ice Sheet during this time has been hotly debated for over two decades since Webb *et al.* (1984) reported marine diatoms, some as young as Pliocene, in “wet-based” glacial deposits, named the Sirius Formation (later Group) at high elevations in the TAM. Webb *et al.* (1984) argued that diatomaceous sediments must have been deposited in seas in the East Antarctic interior, subsequently to be glacially eroded and transported over the TAM, and deposited within Sirius Group sediments. This required the loss of at least 2/3 of East Antarctic ice and a final phase of wet-based ice overriding the TAM during the mid-Pliocene (~3 Myr). The Sirius Group is also notable for the presence of *Nothofagus* fossils, indicating that coeval vegetation existed at the time of its deposition (Francis and Hill, 1996).

A dynamic Pliocene East Antarctic Ice Sheet was seen by many as inconsistent with more recent geomorphic evidence of extremely slow landscape evolution in the Dry Valleys (e.g., Denton *et al.*, 1993; Summerfield *et al.*, 1999), and prolonged cold conditions in the Transantarctic Mountains of southern Victoria Land for the past 14 Myr (Marchant *et al.*, 1996). The hypothesised Pliocene collapse was also inconsistent with the deep-sea oxygen isotope record, which did not show a large enough $\delta^{18}\text{O}$ increase to reflect such a widespread loss of Antarctic ice (Kennett and Hodell, 1993).

Studies have since shown the diatoms to be extremely rare in Sirius deposits (~1 specimen/gram) and to occur also in moraines and local snow (Stroeve *et al.*, 1996; Kellogg and Kellogg, 1996; Barrett *et al.*, 1997; McKay *et al.*, 2008). Data in these papers also suggests that the diatoms are less abundant at depth and more abundant in Sirius diamictites with higher porosity. As a consequence, the marine Pliocene diatoms are interpreted as contaminants, and not age-diagnostic for the deposits in which they are found.

Other notable Pliocene strata outcrop in the mountains of the Prydz Bay/Amery Ice Shelf region of East Antarctica (Figure 1). The Sørsdal Formation in the Vestfold Hills

currently lies 25 m.a.s.l (metres above sea level) and consists of Early Pliocene (4.5 to 4.1 Myr) diatomaceous siltstone and sandstones, as well as sandy diamictites. It does not contain evidence of coeval terrestrial vegetation during its deposition, but indicates marine conditions (Quilty *et al.*, 2000), and that the margin of EAIS was reduced in Pliocene times. The Pagodroma Group outcrops in the Prince Charles Mountains that flank the present-day Amery Ice Shelf, and consist of early Miocene to Pliocene/Early Pliocene glacimarine strata. The Late Pliocene (early Pleistocene?) strata in the Pagodroma Group (Bardin Bluffs Formation) are dominated by diamictites, but contain occasional laminated (sandstone/mudstone) facies, and silty sandstone facies with rare-IRD. These deposits provide evidence of “wet-based” fjordal glaciers, interpreted as a similar regime to present-day tidewater glaciers of East Greenland, and are associated with advance of the East Antarctic Ice Sheet (Hambrey and McKelvey, 2000). Combined, these deposits indicate an oscillating margin of the East Antarctic Ice Sheet (in the Prydz Bay region) between the middle Miocene and Late Pliocene, with periodical marine incursions occurring at least 450 km in land from the present-day ice Amery Ice Shelf calving line (Whitehead *et al.*, 2006).

1.2.8 Late Pliocene/Early Pleistocene cooling

The Late Pliocene $\delta^{18}\text{O}$ record (Figure 4) is characterised by a significant step between 3 and 2.5 Myr, with the record displaying higher amplitudes and gradually increasing $\delta^{18}\text{O}$ values, interpreted as representing the onset of widespread Northern Hemisphere glaciation (Shackleton and Opdyke, 1997; Ravelo *et al.*, 2004). Kennett and Barker (1990) attributed decreased sedimentation rates in the Weddell Sea Abyssal Plain to the expansion of the West Antarctic Ice Sheet to the continental shelf margin between 3 and 2.4 Myr. They also noted an increase in sea ice extent at this time. Seismic reflection data from the Ross Sea indicate a major glacial unconformity, believed to be Late Pliocene in age, and inferred to be the result of expansion of the grounded WAIS onto the Ross Sea continental shelf (Bart, 2000).

1.2.9 Drivers for Late Pliocene/Early Pleistocene glacial/interglacial cycles

Milankovitch (1941) hypothesised that periods of weaker intensity of insolation during summer promoted glacial growth in the Northern Hemisphere. Periods of weak summer insolation occur during periods of low obliquity (axial tilt; cycles of ~41 kyr) and when aphelion occurs during Northern Hemisphere summer. During the 1970's, the development of deep-sea $\delta^{18}\text{O}$ records showed that over the past 450,000 years, the dominant frequency of glacial/interglacial cycles averaged ~100 kyr, and was largely in phase with orbital eccentricity (Hays *et al.*, 1976). Although eccentricity has little direct influence on insolation compared to precession and obliquity, it does modulate the amplitude of the insolation forced by precession. For example, during periods of low eccentricity (i.e., more circular orbit) the effect of precession is more subdued.

The benthic $\delta^{18}\text{O}$ stack of Lisiecki and Raymo (2005) shows a strong 41 kyr co-variance during the Late Pliocene to early Pleistocene (Figure 4). The forcing for these 41-kyr cycles is debated, as precession (23 kyr cycles) has a more profound influence on insolation intensity, yet the precession signal is not as strong as would be expected in $\delta^{18}\text{O}$ records (Figure 5). Huybers and Denton (in press) suggests that total integrated summer insolation controlled by the duration of summer, rather than peak intensity insolation, was the critical factor in determining the extent of ice sheet melting in the Southern Hemisphere. Due to Kepler's second law of planetary motion (the Earth travels fastest at perihelion) precession is largely cancelled out by the fact that more intense summers are of shorter duration, leaving changes in obliquity to exert a greater influence on the total integrated summer insolation. Huybers and Tzipermann (2008) present an ice sheet/energy balance model that generates 40-kyr glacial cycles for an ice sheet subjected to a warmer climate and a thinner profile resulting from increased subglacial deformation (i.e., sliding at the base). They favour this obliquity-based forcing, as it is in phase between hemispheres.

Raymo *et al.* (2006) postulate that precession is the dominant driver for ice growth and decay. Using a non-dimensional northern versus Southern Hemisphere ice volume model, they demonstrated that because precession-based insolation forcing is out of phase between hemispheres, the precession signal will be cancelled out in global

proxies such as the $\delta^{18}\text{O}$ isotope record. Due to differences in isotope ratios between northern versus Southern Hemisphere ice sheets, relatively small changes in Antarctic ice volume will cancel out larger changes in the Northern Hemisphere. Therefore, this should result in obliquity periodicity dominating global proxies for ice volume and sea level records, as it is in phase between hemispheres. This is largely what is observed in the deep-sea isotope record prior to the Mid-Pleistocene Transition.

1.2.10 The Mid-Pleistocene Transition and the onset of 100-kyr Late Pleistocene glacial/interglacial cycles

Between 900 and 700 kyr, the $\delta^{18}\text{O}$ benthic marine record indicates that glacial/interglacial cycles switched from a ~41 kyr to ~100 kyr period. Ice core records display a strong correlation to $\delta^{18}\text{O}$ benthic marine record (Figure 4), and provide the highest resolution record of atmospheric conditions over time. Unlike marine records, ice cores also record atmospheric gas composition and deuterium proxies for temperature.

The Vostok ice core shows that the past four glacial terminations all display similar trends – an increase in temperature initially accompanied by steady increases in CH_4 and CO_2 . This is then followed by a rapid increase in CH_4 and a reduction in $\delta^{18}\text{O}_{\text{atm}}$, inferred to coincide with collapse of the Northern Hemisphere ice sheets. These patterns suggest that orbital forcing is amplified initially by greenhouse gases, then by deglaciation and ice albedo feedback mechanisms (Petit *et al.*, 1999).

The pattern of interglacial periods is not uniform, with the length of the current stable warm conditions of the Holocene (~11 kyr) far exceeding the length of the previous four interglacial maxima. These display shorter warm periods followed by rapid cooling and then slower temperature decreases (Petit *et al.*, 1999). The longest continuous ice core to date, EPICA Dome C, provides a climate record for the past 800,000 yrs (Jouzel *et al.*, 2007). A total of 10 glacial cycles are recorded in the core, including a complete record of Marine Isotope Stage 11 (~410 ka). Marine Isotope Stage 11 is an interglacial period considered to be an analogue to the Holocene period, as it had prolonged warm conditions at the interglacial peak, and corresponds to prolonged period of low-

amplitude eccentricity (Figure 5). The period prior to Marine Isotope Stage 11 is characterised by less warm, but longer glacial maxima (EPICA Community Members, 2004).

1.2.11 Drivers for the Mid-Pleistocene Transition and the 100-kyr cycles

The cause(s) for the transition to 100 kyr glacial/interglacial cycles has yet to be determined. Understanding why northern and Southern Hemisphere climate records are in phase may be the key to answering this question. The effect of precession on insolation is out of phase between hemispheres, and therefore if it is the main control (i.e., modulated by eccentricity cycles at 100ka periodicity), then these records should be out of phase. Huybers and Wunsch (2005) suggest that obliquity is still the primary control. They note that glacial terminations actually occur at ~80 and 120 kyr periods, and point to “beat-skipping” of the obliquity cycle. They speculate that beat skipping may occur because obliquity has a greater effect on insolation at high latitudes. The effect of obliquity on insolation is more sustained than precession, and is therefore more likely to influence basal melting, as it takes ~10 kyr for surface temperature to penetrate to the base of a thick ice sheet (precession makes little impact at this timescale). When ice sheets are thinner, basal ice sheet temperatures and pressure are lower, and are therefore less susceptible to increased insolation – and when the ice sheets are thicker, more basal melt and sliding results. This may promote glacial terminations, as increased sliding thins the ice sheet, moving more ice into the lower-latitude ablation zone, or the ocean. Under this model, the warmer climate of the Late Pliocene and early Pleistocene is more likely to result in terminations every obliquity cycle.

Using a single column atmospheric model, Huybers and Denton (in press) show that using the duration of summer in the Southern Hemisphere (Figure 5) to drive the model temperatures that correlate strongly to the ice core record at Dome Fuji can be reconstructed. They conclude that glacial terminations may be driven by long summers in the south (e.g., less sea ice, increased outgassing of CO₂ from Southern Ocean, etc) and more intense summers (e.g., positive degree day ablation of ice sheets) in the Northern Hemisphere. Due to Kepler’s second law resulting in longer summers having lower peak insolation (and vice versa), both signals are almost identical and are in phase at both the precession and obliquity timescales.

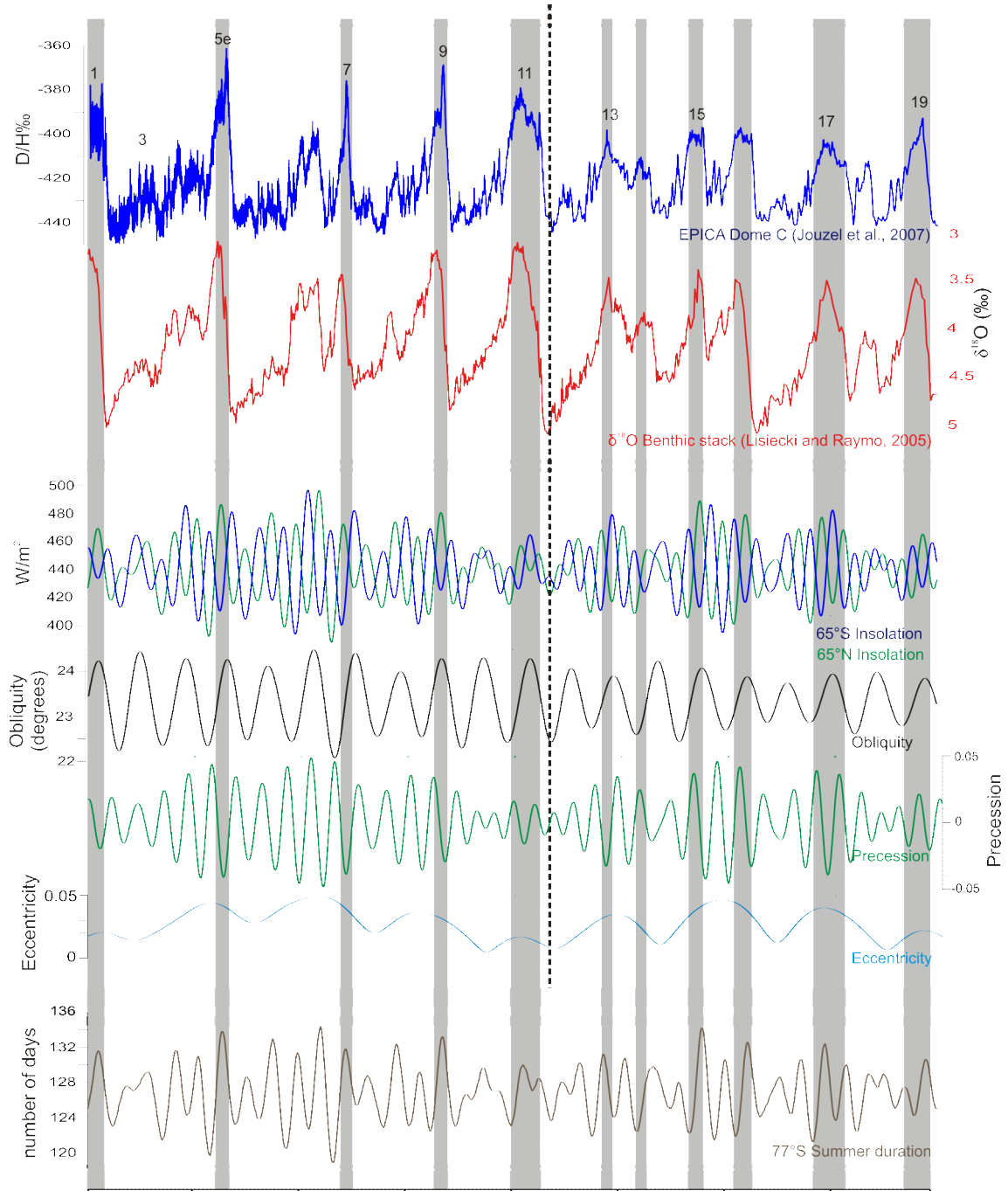


Figure 5: Ice core and deep sea proxies for determining past temperatures and ice volume (from Jouzel *et al.*, 2007 and Lisiecki and Raymo, 2005) matched against orbital forcing parameters (Berger and Loutre, 1991). Summer duration at 77°S was determined using a Matlab script for daily insolation provided by Huybers (2006), and summing the number of day where insolation exceeds 250 W/m^2 .

Raymo *et al.* (2006) point to precession, modulated by eccentricity as the prime control. They postulate that the Antarctic Ice Sheet cooled to a degree that the margin became marine-based around ~1 Myr. Therefore, changes in Antarctic Ice Sheet were driven largely by eustatic sea level fluctuations associated with Northern Hemisphere glacial/interglacial cycles, i.e., north drives south, resulting in an in-phase signal.

1.3 The configuration of past ice sheet advance and retreat in the Western Ross Embayment

Approximately two-thirds of the present-day Ross Ice Shelf is nourished by ice streams that drain the WAIS, yet its western margin is fed by EAIS outlet glaciers (Fahnestock *et al.*, 2000; Figure 6A). Glaciological reconstructions at the LGM, indicates grounded ice expansion within the Ross Embayment to near the edge of the Ross Sea continental shelf (Denton and Hughes, 2002) with an almost even contribution from East and West Antarctic sourced ice (e.g. Figure 6B). Previous studies of till provenance in the Ross Island region indicate that glacial transport by ice sourced from EAIS outlet glaciers to the south of the drill site occurred during the last period of grounded ice deposition at the LGM (Licht *et al.*, 2005). This distal provenance source indicates that grounded ice event at the LGM in the Windless Bight region was the result of large-scale ice sheet advance in the Ross Embayment, rather than localised glacial advance from Ross Island or outlet glaciers in the McMurdo Sound region.

In the Windless Bight region, past ice sheets were grounded well below sea level and were therefore likely to be highly responsive to oceanographic-related mass balance controls, such as eustasy, iceberg calving and ice front/sub-ice shelf melting. Of critical importance with regard to ice sheet retreat within the greater Ross Embayment (including sections of the presently-grounded WAIS) is that marine ice-sheet grounding lines are inherently unstable on reverse bedslopes (Schoof, 2007). When this reverse bedslope is combined with an overdeepened bed, forcings such as rising sea levels, decreased accumulation rates, increased ice sheet temperature profile and/or basal slipperiness may result in the ice sheet being forced into irreversible retreat. This implies that once retreat was initiated for past configurations of the ice sheet, it was likely to occur across the entire Ross Embayment,

similar to the pattern of retreat documented for the last glacial interglacial cycle (e.g. Conway et al., 1999, Denton and Hughes, 2002; see following section for details).

Taking into account LGM reconstructions, mass balance considerations, and the overdeepened/reverse slope nature of the Ross Sea continental shelf since the Late Neogene (De Santis et al., 1995), the record of grounded ice sheet deposition at Windless Bight is expected to be intimately tied to the overall state of the AIS in the Ross Embayment as a whole. Provided the provenance signal of subglacial deposits indicates at distal EAIS outlet glacier source, the sedimentary record of glacial advance and retreat at Windless Bight is interpreted in this thesis as documenting widespread changes in the volume of marine-based sector of the Antarctic Ice Sheet (fed by both the EAIS and WAIS) in the Ross Embayment (e.g. Figure 7E).

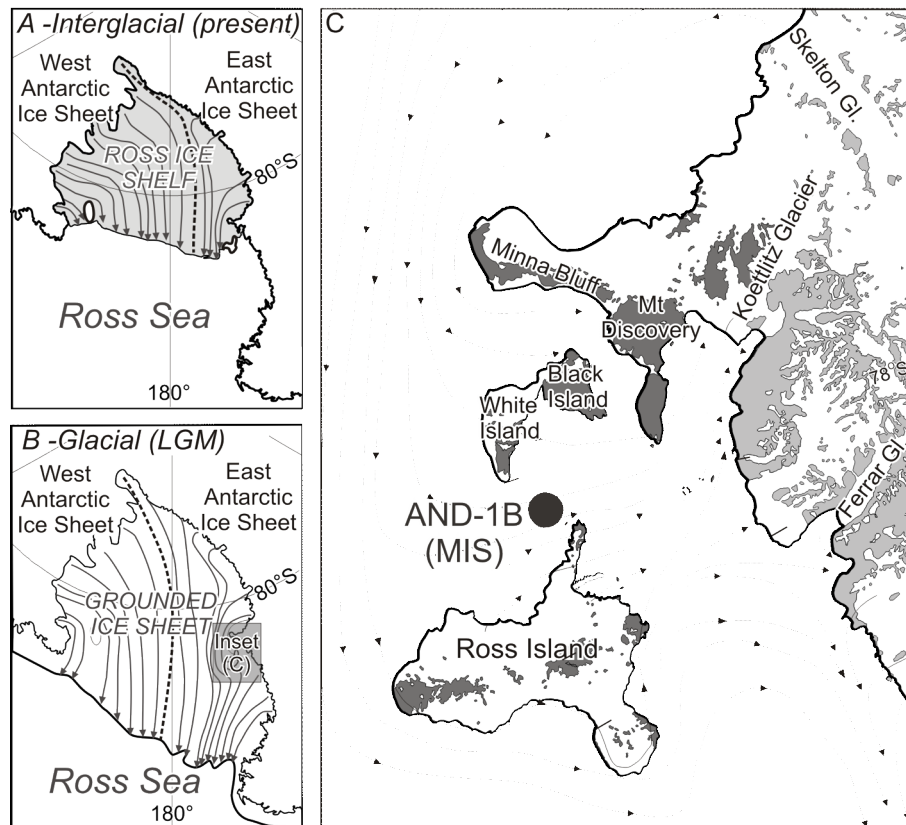


Figure 6: Ice flow-line pathways for (A) the present day Ross Ice Shelf showing WAIS vs. EAIS contributions (after Fahnestock et al. 2000) and (B) a reconstruction of the grounded ice sheet in the Ross Embayment at Last Glacial Maximum, showing the WAIS vs. EAIS contribution (after Denton and Hughes, 2002); (C) A high-resolution inset of LGM flow-line reconstruction for the McMurdo Sound Region based on geological and geomorphic evidence (Denton and Hughes, 2002). This shows the pathway for ice sourced from the southern TAM outlet glaciers into Windless Bight during periods of glacial expansion and grounded ice.

1.4 Retreat of the Antarctic Ice Sheet in the Ross Embayment since the Last Glacial Maximum

1.4.1 Geological evidence

The Ross Sea Drift covers an extensive portion of the McMurdo Sound region and consists of drift sheets that are relatively unweathered and are commonly ice-cored in coastal McMurdo Sound. ^{14}C dates of shell material incorporated in the Ross Sea Drift indicates that it is Last Glacial Maximum (LGM) age, and it is interpreted as representing an advance of a grounded ice sheet during Marine Isotope Stage 2 (Stuiver *et al.*, 1981; Denton and Marchant, 2000). The drift reaches a maximum elevation of 710 m at the eastern side of Ross Island (Cape Crozier), while along the Scott Coast it reaches elevations of 250 m, suggesting that ice was grounded across McMurdo Sound and the profile of the LGM ice sheet sloped landward across McMurdo Sound. The grounded ice advanced westward from McMurdo Sound, and acted to dam the mouths of the Dry Valleys, resulting in large proglacial lakes within the Dry Valleys (Denton *et al.*, 1991). ^{14}C dates indicate that Taylor Valley was still blocked by grounded ice in McMurdo Sound between 8900 and 8340 ^{14}C yr BP (Denton *et al.*, 1991). Emerged marine deposits near Marble Point indicate that grounded ice had receded by 6430 ± 70 ^{14}C yr BP (~ 7500 cal yr BP) (Stuiver *et al.*, 1981). ^{14}C dates imply that the Taylor Glacier (draining from the EAIS) actually receded during LGM, suggesting little change in EAIS surface height in this region since the LGM (Denton *et al.*, 1991).

Since the LGM, the Antarctic Ice Sheet (including the Ross Ice Shelf) is inferred to have retreated over 1300 km along the western margin of the Ross Embayment (Conway *et al.*, 1999), while remaining relatively stable in the east. Drewry (1979) suggested that although the grounding advanced northward during the last glacial, floating ice shelves dominated the Ross Sea embayment and grounding occurred mostly on local topographical highs (i.e., Crary, Mawson, Pennell and Ross Banks), but agreed with Denton *et al.* (1971) that the entire of McMurdo Sound was grounded with ice 1-1.3km in thickness at the LGM, based on evidence of glacial advance from the Ross Sea region into the Dry Valleys. Using geological data to extend existing ice sheet flowlines and surface contours, Stuiver *et al.* (1981) placed the maximum extent of LGM grounding line at the continental shelf edge. Denton *et al.* (1991) also placed the LGM grounding line at the continental shelf margin,

based on foredeepening features in the Northern Basin, interpreted as being formed by grounded ice - although Kellogg *et al.* (1996) noted that these features may represent an earlier phase of ice advance.

Sediment cores and geophysical studies place the grounding line of the western sector of the Ross Ice Shelf just north of Coulman Island, ~200 km to the south of the continental shelf at a latitude of 73°28 S (Figure 7). This is based on the locations of sediment wedges interpreted from seismic profiles, and an absence on diamictites north of this point, (e.g., Figure 7; Anderson *et al.*, 2002; Shipp *et al.*, 1999; Domack *et al.*, 1999; Conway *et al.*, 1999). Licht *et al.* (1996) studying sediment cores, placed it 100 km to the south of Coulman Island.

1.4.2 Geophysical evidence of glacial advance in the western Ross Sea

Multibeam swath bathymetry in the Ross Sea reveal geomorphic features associated with grounded ice. These include drumlins, grooves, flutes, megascale lineations that extend right across the continental shelf (Figure 7; Anderson *et al.*, 2002; Shipp *et al.*, 1999). Iceberg furrows and meltwater channels are also evident. Shipp *et al.* (1999) identified five seismic facies associated with sedimentation of the last glacial cycle in the Ross Sea. Each facies is distinguished by external geometry, bounding surface features, acoustic signatures and internal reflectors. Deposits are thicker in troughs than on the banks. The results were correlated with the lithofacies identified by Domack *et al.* (1999) and the bathymetry to determine the extent of the last glacial advance and retreat in the Ross Sea (Figure 7).

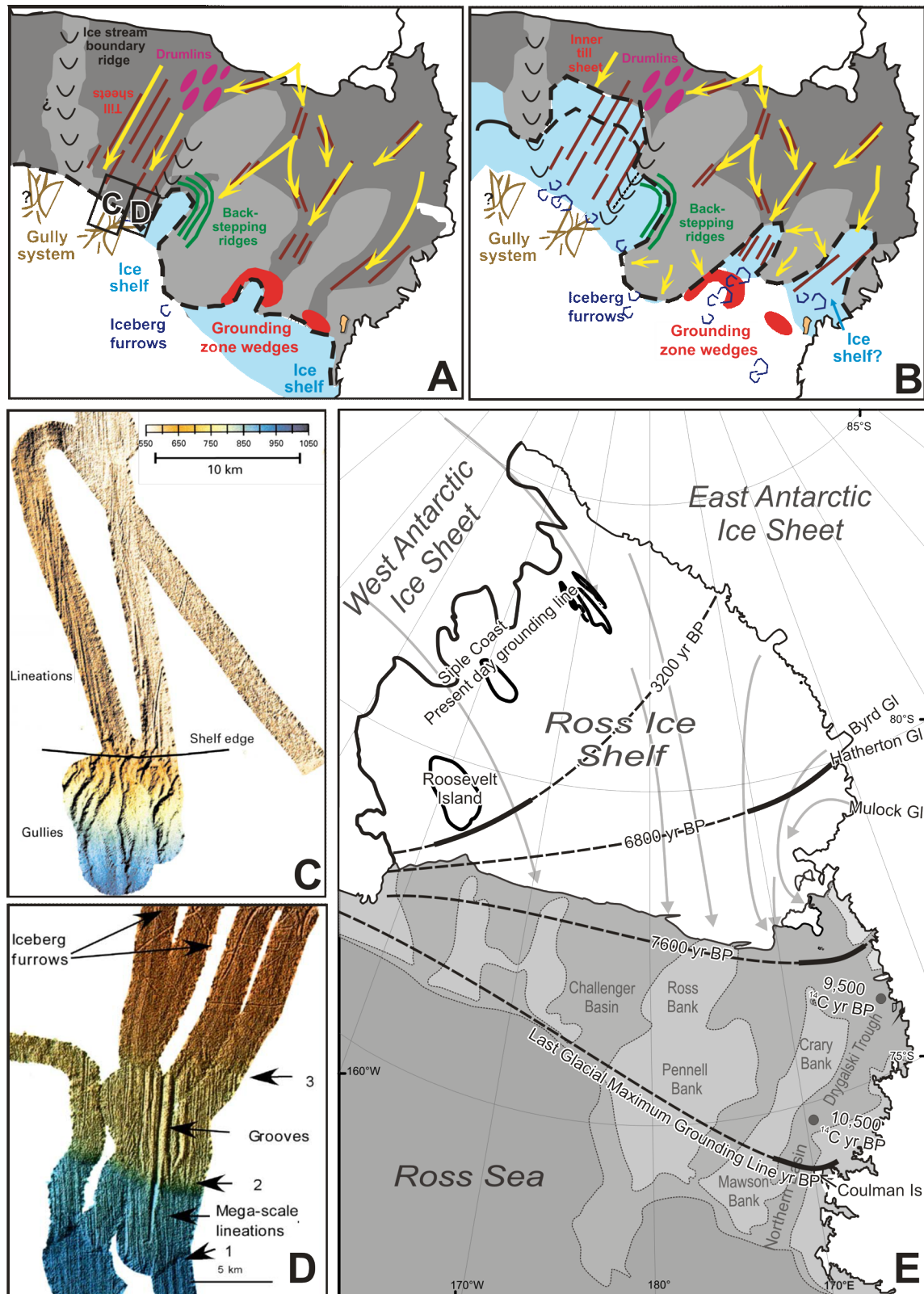


Figure 7: A) Reconstruction of LGM glacial configuration based on seafloor geomorphology and seismic profiling (from Shipp *et al.*, 1999); B) Reconstruction of post-LGM glacial retreat, showing accelerated glacial retreat along the marine troughs, in particular the Northern Basin and Drygalski Troughs (from Shipp *et al.*, 1999); C/D) Examples of swath bathymetry, similar to those used to develop reconstructions in A and B (from Mosola and Anderson, 2006); E) Chronology for retreat of LGM grounding line (cal. years) after Conway *et al.* (1999), including two ^{14}C age (grey circles) from marine cores in Domack *et al.*, 1999).

1.5 Regional setting at the present-day AND-1B site

1.5.1 The McMurdo Ice Shelf

The McMurdo Ice Shelf is bound by Ross Island to the northeast, Victoria Land to the west, McMurdo Sound to the north (Figure 8). Its flow near the AND-1B site is $\sim 150 \text{ m yr}^{-1}$, compared to ($>700 \text{ m yr}^{-1}$) for the Ross Ice Shelf, from which it is separated by a shear zone that extends from the Cape Crozier on the eastern edge of Ross Island to Mina Bluff (McCrae, 1984; Whillans and Merry, 1996). The eastern section is characterised by surface accumulation and the western section by net ablation (McCrae, 1984). Oxygen Isotope compositions indicate that the source of glacial ice is variable across the McMurdo Ice Shelf (Kellogg *et al.*, 1996). The western sector contains large volumes of ice derived from much higher elevations (i.e., EAIS), probably via the Mulock Glacier to the south. Oxygen isotope analysis indicates that most of the surface ice in the western ablation zone is derived from seawater, suggesting that bottom freezing processes are the dominant contributor to the mass balance to the western sector of the McMurdo Ice Shelf (Kellogg *et al.*, 1990). Melting near the grounding line (and surface ablation) minimise the contribution of ice from the Koettlitz Glacier (Gow and Epstein, 1972).

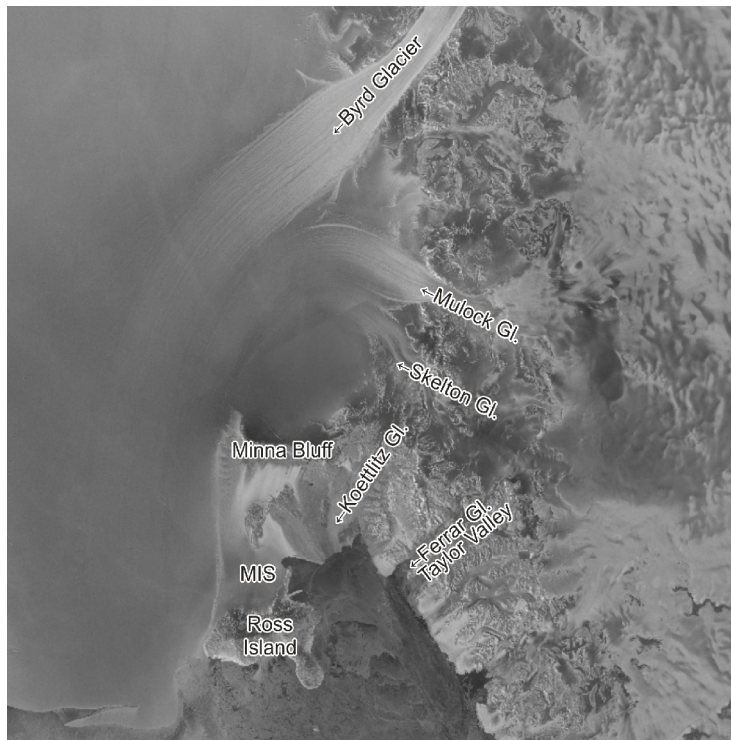


Figure 8: Radarsat mosaic showing the drainage of the Byrd, Mulock and Skelton glaciers into the Ross Ice Shelf. The zone of shearing between Minna Bluff and to the right of Ross Island separates the McMurdo Ice Shelf (MIS) from the Ross Ice Shelf (Source: Atlas of Antarctic Research -www.usgs.gov).

1.6 Bathymetry and oceanography in the Ross Sea and McMurdo Sound

Bathymetry plays an important role in oceanic water mass transfer, and therefore biogenic production and sedimentation. It is also an important factor in reconstructing past ice grounding events. The western Ross Sea consists of a series of banks and troughs (see Figure 7), that trend in a north-south direction and extend beneath the Ross Ice Shelf. The volcanic centres and flexural moats around McMurdo Sound interrupt this pattern, and at Windless Bight, the bathymetry consists of a NE-SW trending trough that extends to a maximum depth of 950 m and gradually shallows eastwards to 810 m (Figure 1; Horgan *et al.*, 2005).

The upwelling of warm, nutrient-rich Circumpolar Deep Water onto the continental shelf region of the Ross Sea is important, as it moderates ice cover, provides a warm environment for animals, and supplies nutrients for primary production. Once Circumpolar Deep Water has been transported onto the Ross Sea continental shelf, it is modified into several types of water masses by such factors as sea ice production, glacial meltwater and precipitation. Processes in the Ross Sea region are dominated by large polynyas in the southwest Ross Sea. These polynyas provide large areas of open water (formed by wind and upwelling of warmer water) that allow for high volumes of new sea ice production. Brine rejection during this sea ice formation in the Ross Sea modifies Circumpolar Deep Water into High-Salinity Shelf Water (Assmann, 2003),

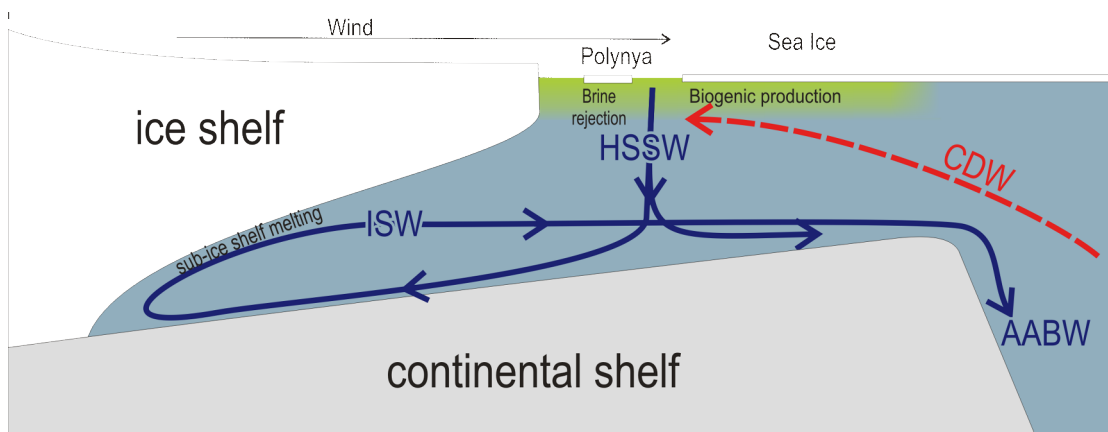


Figure 9: Simplification of interactions of oceanic water masses occurring on the present-day Ross Sea continental shelf, as discussed in the text (modified from Jacobs *et al.*, 1992). Acronyms: Circumpolar Deep Water (CDW); Antarctic Bottom Water (AABW); High Salinity Shelf Water (HSSW), Ice Shelf Water (ISW).

and its interaction with other water masses (Figure 9) is an important driver of Antarctic Bottom Water – and ultimately, global thermohaline circulation. High-Salinity Shelf Water that enters the sub-ice shelf cavity is super cooled into Ice Shelf Water, and is responsible for significant volumes of sub-ice shelf melting, as well as basal freezing process (Jacobs *et al.*, 1992)

The main inflows of these shelf waters to the Ross Ice Shelf cavity are located in eastern McMurdo Sound and to the east of Ross Island (Assmann *et al.*, 2003; Figure 1). The western part of the Sound is dominated by northward flow from beneath the Ross Ice Shelf, with ^{14}C and tritium measurements suggesting a six-year residence time for the water under ice shelf (Michel *et al.*, 1979). The flow under the McMurdo Ice Shelf passes Hut Point Peninsula in an easterly to northeasterly direction (depending on bathymetry) at mean speeds of $\sim 6.5 \text{ cm s}^{-1}$. The maximum sub-ice shelf current speed recorded at Windless Bight was 22 cm s^{-1} , but there was a noticeable tidal effect on current speed and direction, and possible disruption of currents during the period of measurements by a large iceberg (B-15) immediately to the north of Ross Island (Barrett *et al.*, 2005).

Due to re-suspension processes, sediments from depths shallower than 400 m tend to be richer in sand, gravel and coarse sponge spicules, while being depleted in organic carbon and opal. Also of note is a layer of suspended sediment at the ocean floor in McMurdo Sound, which ranges between 25-250 m in thickness (Dunbar *et al.*, 1989).

1.6.1 Biogenic production

During the summer, as the Ross Sea polynyas enlarge and daylight hours increase, primary productivity rapidly increases. One of the largest phytoplankton blooms in the Southern Ocean forms in the southern Ross Sea during the early spring (Comiso *et al.*, 1993). In the deep water regions of McMurdo Sound, the organic carbon accumulation rates average $45 \text{ mg C m}^{-2} \text{ day}^{-1}$, which is an order of magnitude higher than the world average for continental margins (Dunbar *et al.*, 1989).

Leventer and Dunbar (1988) noted that the surface sediments in the sound are dominated by *Fragilariopsis curta*, a common member of sea ice and open water communities, and *Thalassiosira* spp., which is rarely found in sea ice samples and is representative of open water primary production. *Fragilariopsis curta* is most abundant in the southwest of the sound, where sea ice is more prevalent, while *Thalassiosira* is most abundant in the east and northwest Sound.

1.7 Summary

Changes in past glacial extent are likely to be the primary control on sedimentation at the AND-1B drill site beneath the present day McMurdo Ice Shelf (Figure 1), with glacial maxima dominated by subglacial deposits of sediments sourced from Transantarctic Mountain outlet glaciers feeding into the marine-based AIS in the Ross Embayment. Glacial minima are influenced by a combination of biogenic, oceanographic and glacimarine processes. This thesis attempts to identify sedimentary processes associated with advance and retreat of the marine-based AIS grounding line in the Ross Embayment for the past ~13 Ma. Attempts are also made to identify changes in glacial thermal regime and extent over time, from non-climatic forcings. One example of a non-climatic forcing is volcanic cone building, which may alter glacial flowlines or ice shelf pinning points. Tectonics are also important, but large-scale changes in bathymetry are not predicted in the context of AND-1B (past ~13 Myr) due to the tectonic overprint of the Terror Rift, which has been active since 25 Ma.

1.8 References

- Anderson, J. B., Shipp, S. S., Lowe, A. L., Wellner, J. S., and Mosola, A. B., 2002. The Antarctic ice sheet during the Last Glacial Maximum and its subsequent retreat history; a review. *Quaternary Science Reviews* v.21, p.49-70.
- Askin, R. A., and Raine, J. I., 2000. Oligocene and early Miocene terrestrial palynology of CRP-2/2A, Victoria Land Basin, Antarctica. *Terra Antartica* v. 7, p.493-501.
- Assmann K.M., 2003. The effect of McMurdo Sound topography on water mass exchange across the Ross Ice Shelf front. *Annual report of the Filchner-Ronne Ice Shelf Program (FRISP)* v.15.
- Assmann, H., Hellmer, H.H., and Beckmann, A., 2003. Seasonal Variation in Circulation and Water Mass Distribution on the Ross Sea Continental Shelf. *Antarctic Science* v.15, p.3–11.

- Barrett, P.J., 1975. Textural characteristics of Cenozoic preglacial and glacial sediments at site 270, Ross Sea, Antarctica. In: Hayes, D.E., and Frakes, L.A., (eds.), *Initial Reports of the Deep Sea Drilling Project* v. 28, p.757–767.
- Barrett, P.J. (ed.), 1986. Antarctic Cenozoic history from the MSSTS-1 drillhole, McMurdo Sound, Antarctica. *NZ DSIR Bulletin* v.237, 174 p.
- Barrett, P.J. (ed.), 1989. Antarctic Cenozoic history from the CIROS-1 drillhole, McMurdo Sound, Antarctica. *NZ DSIR Bulletin* v.245, 254p.
- Barrett, P. J., 1991. The Devonian to Triassic Beacon Supergroup of the Transantarctic Mountains and correlatives in other parts of Antarctica. In: Tingey, R. J. (ed.) *The geology of Antarctica: Oxford Monographs on Geology and Geophysics* v. 17, p.120-152.
- Barrett, P.J. 1996. Antarctic Paleoenvironment through Cenozoic times – a review. *Terra Antarctica* v.3, p.103-119.
- Barrett, P.J., 2007. Cenozoic climate and sea level history from glaci-marine strata off the Victoria Land coast, Cape Roberts Project, Antarctica. In: Hambrey, M.J., Christoffersen, P., Glasser, N.F. and Hubbard, B. (eds.) *Glacial Processes and Products*. International Association of Sedimentologists Special Publication.
- Barrett, P.J., Bleakley, N.L., Dickinson, W.W., Hannah, M.H. and Harper, M.A., 1997. Distribution of siliceous microfossils on Mount Feather, Antarctica, and the age of the Sirius Group. In: Ricci, C.A. (Ed.), *The Antarctic Region: geological evolution and processes*. Siena, Museo Nazionale dell' Antartide, p.763-770.
- Barrett, P.J., Carter, L., Dunbar, G.B., Dunker, E., Giorgetti, G., Harper, M.A., McKay, R.M., Niessen, F., Nixdorf, U., Pyne, A.R., Riesselmann, C., Robinson, N., Hollis, C., and Strong, P., 2005. Oceanography and sedimentation beneath the McMurdo Ice Shelf in Windless Bight, Antarctica. *Antarctic Data Series* v. 25, Victoria University of Wellington, 100p.
- Bart, P.J., Anderson, J.B., Trincardi, F., Shipp, S.S., 2000. Seismic data from the Northern basin, Ross Sea, record extreme expansions of the East Antarctic Ice Sheet during the late Neogene. *Marine Geology* v.166, p.31-50.
- Berger, A. and Loutre, M. F. 1991. Insolation Values for the Climate of the Last 10 Million Years. *Quaternary Science Reviews* v.10, p.297–317.
- Conway, H., Hall, B. L., Denton, G. H., Gades, A. M., and Waddington, E. D., 1999. Past and future grounding-line retreat of the West Antarctic Ice Sheet. *Science* v.286, p.280-283.
- Cooper, A. K., and Davey, F. J., 1987. *The Antarctic Continental Margin: Geology and Geophysics of the Western Ross Sea*. Houston, Texas, Circum-Pacific Council for Energy and Mineral Resources, Earth Science Series, 253 p.
- Comiso, J.C., McClain, C.R., Sullivan, C.W., Ryan, J.P. and Leonard, C.L., 1993. Coastal zone color scanner pigment concentration in the Southern Ocean and relationships to geophysical surface features. *Journal of Geophysical Research* v.98(C), p.2419–2451.
- Craddock, C, 1970. Geological map of Antarctica. In: Craddock, C. (ed.), *Antarctic Geoscience: Madison* (University of Wisconsin Press).
- Dalziel, I. W. D. 1992. Antarctica; A Tale of Two Supercontinents? *Annual Review of Earth and Planetary Sciences* v.20, p.501-526.

- Dalziel, I. W. D., and Elliot, D. H. 1982. West Antarctica; problem child of Gondwanaland. *Tectonics* v.1, p.3-19,
- DeConto, R. M., and Pollard, D. 2003. Rapid Cenozoic glaciation of Antarctica induced by declining atmospheric CO₂. *Nature* v.421, p.245-249.
- Denton and Marchant, D.R., 2000. The Geological Basis for a Reconstruction of a Grounded Ice Sheet in McMurdo Sound, Antarctica, at the Last Glacial Maximum *Geografiska Annaler* v.82A, p.167-211.
- Denton, G. H., and Hughes, T. J., 2002. Reconstructing the Antarctic ice sheet at the last glacial maximum: *Quaternary Science Reviews* v.21, p.193-202.
- Denton, G. H., Armstrong, R. L., and Stuiver, M., 1971. The Late Cenozoic glacial history of Antarctica. In: Turekian, K. K. (ed.) *The Late Cenozoic glacial ages*. Yale University Press. p.267-306.
- Denton, G. H., Prentice, M. L., and Burckle, L. H., 1991. Cainozoic history of the Antarctic ice sheet. In: Tingey, R. J. (ed.) *The geology of Antarctica: Oxford Monographs on Geology and Geophysics* v.17, p.365-433.
- Denton, G.H., Sugden, D.E., Marchant, D.R., Hall, B.L. and Wilch, T.I., 1993. East Antarctic Ice Sheet sensitivity to Pliocene climatic change from a Dry Valley perspective. *Geografiska Annaler* v.75A, p.155-204.
- De Santis, L., Anderson, J.B., Brancolini, G., and Zayatz, I., 1995. Seismic record of late Oligocene through Miocene glaciation on the central and eastern continental shelf of the Ross Sea, in Cooper, A.K., et al., eds., *Geology and seismic stratigraphy of the Antarctic Margin: American Geophysical Union Antarctic Research Series*, v. 68, p. 235–260.
- Domack, E.W., Jacobson, E.A., Shipp, S., and Anderson, J. B., 1999. Late Pleistocene-Holocene retreat of the West Antarctic ice-sheet system in the Ross Sea; Part 2, Sedimentologic and stratigraphic signature. *Geological Society of America Bulletin* v.111, p.1517-1536.
- Drewry, D.J. 1979. Late Wisconsin reconstruction for the Ross Sea region, Antarctica. *Journal of Glaciology* v.24, p.231-244.
- Dunbar, R. B., Leventer, A. R., Stockton, W. L., 1989. Biogenic sedimentation in McMurdo Sound, Antarctica. *Marine Geology* v.85, 155-179.
- Elliot, D. H. 1975. Tectonics of Antarctica; a review. *American Journal of Science* v.275(A), p.45-106,
- EPICA Community Members, 2004. Eight glacial cycles from an Antarctic ice core. *Nature* v.429, p.623-628.
- Esser, R.P., Kyle P.R., McIntosh W.C., 2004. ⁴⁰Ar/³⁹Ar dating of the eruptive history of Mount Erebus, Antarctica: Volcano evolution. *Bulletin of Volcanology*. v.66, p.671–686.
- Fahnestock, M.A., Scambos, T.A., Bindshadler, R.A., Kvaran, G., 2000. A millennium of variable ice flow recorded by the Ross Ice Shelf, Antarctica. *Journal of Glaciology* v.46, p.652-664.
- Fielding, C.R., Whittaker, J., Henrys, S.A., Wilson, T.J., and Naish, T.R., 2008. Seismic facies and stratigraphy of the Cenozoic succession in McMurdo Sound, Antarctica: implications for tectonic, climatic and glacial history. *Palaeogeography, Palaeoclimatology, Palaeoecology* v.260, p.8–29.

- Fitzgerald, P. G., 1994. Thermochronologic constraints on post-Paleozoic tectonic evolution of the central Transantarctic Mountains, Antarctica. *Tectonics* v. 13, p.818-836.
- Fitzgerald, P.G., 2002. Tectonics and landscape evolution of the Antarctic plate since the breakup of Gondwana, with an emphasis on the West Antarctic rift system and the Transantarctic Mountains, In: Gamble, J., and Skinner, D. A., eds., *Antarctica at the Close of a Millennium*, Royal Society of New Zealand Bulletin v.35, p.453–469.
- Francis, J.E. and Hill, R.S., 1996. Fossil plants from the Pliocene Sirius Group, Transantarctic Mountains: Evidence for climate from growth rings and fossil leaves. *Palaaios* v.11, p.389-396.
- Goodge, J.W., 2002. From Rodinia to Gondwana: Supercontinent evolution in the Transantarctic Mountains: In: Gamble, J., and Skinner, D. A., eds., *Antarctica at the Close of a Millennium*, Royal Society of New Zealand Bulletin 35, Proceedings of the 8th International Symposium on Antarctic Earth Science. p.61-74.
- Gow, A. J. and Epstein, S., 1972. On the use of stable isotopes to trace the origins of ice in a floating ice tongue. *Journal of Geophysical. Research* v.77, p.6552-6557.
- Hannah, M.J., Cita, M.B., Coccioni, R., and Monechi, S., 1997. The Eocene/Oligocene boundary at 70°South, McMurdo Sound, Antarctica. *Terra Antartica*, v.4, p.79-87.
- Hambrey, M. J., Barrett, P. J., and Robinson, P. H., 1989. Stratigraphy Antarctic Cenozoic history from the CIROS-1 drillhole, McMurdo Sound. *DSIR Bulletin* v.245, p.23-48.
- Hambrey, M.J., Ehrmann, W.U., and Larsen, B., 1991. The Cenozoic glacial record from the Prydz Bay continental shelf, East Antarctica. In: J. Barron and B. Larsen (eds.), *Leg 119, Ocean Drilling Program, Scientific Results* p.77–132.
- Hambrey, M. J., and McKelvey, B., 2000. Neogene fjordal sedimentation on the western margin of the Lambert Graben, East Antarctica. *Sedimentology* v. 47, p.577-607.
- Hays, J.D., Imbrie, J., and Shackleton, N.J., 1976. Variations in the Earth's orbit; pacemaker of the ice ages. *Science* v.194, p.1121-1132.
- Henrys, S., Hansaraj, D., Wilson, T., Fielding, C., Paulsen, T., Ross, J., McIntosh, W., Dunbar, N., Naish, T.R., Powell, R. and the ANDRILL MIS Science Team, in prep. Neogene rifting in the Victoria Land Basin: Implications for East-West Antarctica Plate Motion. To be submitted to *Geology*.
- Horgan, H., Naish, T., Bannister, S., Balfour, N., and Wilson, G., 2005. Seismic stratigraphy of the Plio-Pleistocene Ross Island flexural moat-fill: a prognosis for ANDRILL Program drilling beneath McMurdo-Ross Ice Shelf. *Global and Planetary Change* v.45, p.83-97.
- Huybers, P.W., 2006. Early Pleistocene glacial cycles and the integrated summer insolation forcing. *Science* v.313, p.508-511.
- Huybers, P.W., Wunsch, C., 2005. Obliquity pacing of the Late Pleistocene glacial terminations. *Nature* v.434, p.491-494.
- Huybers, P.W. and Denton, G.H., in press. Interpolar climate symmetry at orbital time scales and the duration of Southern Hemisphere summer. *In press with Nature*.
- Huybers, P., and E. Tziperman 2008. Integrated summer insolation forcing and 40,000-year glacial cycles: The perspective from an ice-sheet/energy-balance model, *Paleoceanography*, v.23, PA1208, doi:10.1029/2007PA001463.

- Jacobs, S.J., Hellmer, H.H., Doake, C.S.M., Jenkins, A. and Frolich, R.M., 1992. Melting of ice shelves and the mass balance of Antarctica. *Journal of Glaciology* v.38, p.375–387.
- Jouzel, J., Masson-Delmotte, V., Cattani, O., Dreyfus, G., Falourd, S., Hoffmann, G., Minster, B., Nouet, J., Barnola, J. M., Chappel-laz, J., Fischer, H., Gallet, J. C., Johnsen, S., Leuenberger, M., Lulergue, L., Luethi, D., Oerter, H., Parrenin, F., Raisbeck, G., Raynaud, D., Schilt, A., Schwander, J., Selmo, E., Souchez, R., Spahni, R., Stauffer, B., Steffensen, J. P., Stenni, B., Stocker, T.F., Tison, J. L., Werner, M., and Wolff, E. W., 2007. Orbital and millennial Antarctic climate variability over the last 800 000 years. *Science*, v.317, p.793–796.
- Kellogg, D. E., and Kellogg, T. B., 1996. Diatoms in South Pole ice; implications for eolian contamination of Sirius Group deposits. *Geology*, v.24, p.115-118.
- Kellogg, T. B., Kellogg, D. E. and Stuiver, M., 1990. Late Quaternary history of the southwestern Ross Sea: evidence from debris bands on the McMurdo Ice Shelf, Antarctica. *Antarctic Research Series* v.50, p.25-56.
- Kellogg, T. B., Hughes, T., and Kellogg, D. E., 1996. Late Pleistocene interactions of East and West Antarctic ice-flow regimes; evidence from the McMurdo Ice Shelf. *Journal of Glaciology* v.42, p.486-500.
- Kennett, J. P., 1977. Cenozoic evolution of Antarctic glaciation, the Circum-Antarctic Ocean, and their impact on global paleoceanography. *Journal of Geophysical Research* v.82, p.3843-3860.
- Kennett, J. P., and Shackleton, N. J., 1976. Oxygen isotopic evidence for the development of the psychrosphere 38 Myr ago. *Nature* v. 260, p.513-515.
- Kennett, J.P., Barker, P.F., 1990. Latest Cretaceous to Cenozoic climate and oceanographic developments in the Weddell Sea, Antarctica: An ocean drilling perspective. In Barker, P.F., Kennett, J.P., (eds.) *Proceedings of the Ocean Drilling Program, Scientific Results* v.113, p.93-960.
- Kennett, J.P. and Hodell, D.A., 1993. Evidence for the relative climatic stability of Antarctica during the early Pliocene: A marine perspective. *Geografiska Annaler* v.75A, p.205-220.
- Kyle P.R., and Cole, J.W., 1974. Structural control of volcanism in the McMurdo Volcanic Group, Antarctica. *Bulletin of Volcanology* v.38. p.16–25
- Laird, M.G., 1991. The Late Proterozoic–Middle Palaeozoic rocks of Antarctica. In: Tingey, R.J. (ed.) *The Geology of Antarctica*. Oxford University Press. p.74–119.
- Leckie, R.M., and Webb, P.-N., 1983. Late Oligocene-early Miocene glacial record of the Ross Sea, Antarctica; evidence from DSDP Site 270. *Geology* v.11, p.578-582.
- Leventer, A. R. and Dunbar, R. B., 1988. Recent diatom record of McMurdo Sound, Antarctica: Implications for history of sea ice extent. *Paleoceanography* v.3, p.259 – 274.
- Lewis, A.R., Marchant, D.R., Ashworth, A.C., Hemming, S.R., and Machlus, M.L., 2007. Major middle Miocene global climate change: Evidence from East Antarctica and the Transantarctic Mountains: *Geological Society of America Bulletin* v.119, p.1449-1461.
- Licht, K. J., Jennings, A. E., Andrews, J. T., and Williams, K. M., 1996. Chronology of late Wisconsin ice retreat from the western Ross Sea, Antarctica. *Geology* v.24, p.223-226.

- Licht, K.J., Lederer, J.R., Swope, J., 2005. Provenance of LGM glacial till (sand fraction) across the Ross embayment, Antarctica: *Quaternary Science Reviews* v.24, p.1499-1520.
- Lisiecki, L.E., Raymo, M.E., 2005. A Pliocene-Pleistocene stack of 57 globally distributed benthic $\delta^{18}\text{O}$ records. *Paleoceanography* v.20. PA1003, doi:10.1029/2004PA001071.
- Marchant, D.R., Denton, G.H., Swisher III, C.C., Potter Jr., N., 1996. Late Cenozoic Antarctic paleoclimate reconstructed from volcanic ashes in the Dry Valleys region of southern Victoria Land. *Geological Society of America Bulletin* v.108, p.181-194.
- McCrae, I.R., 1984. A summary of glaciological measurements made between 1960 and 1984 on the McMurdo Ice Shelf, Antarctica. *Auckland: School of Engineering Report* v.360, Department of Theoretical and Applied Mechanics, University of Auckland.
- McIntosh, W.C. 2000. $^{40}\text{Ar}/^{39}\text{Ar}$ Geochronology of tephra and volcanic clasts in CRP-2A, Victoria Land Basin, Antarctica. *Terra Antarctica* v.7, p.621-630.
- McKay, R., Barrett, P., Harper, M., and Hannah, M., 2008. Atmospheric transport and concentration of diatoms in the Allan Hills, Transantarctic Mountains. *Palaeogeography, Palaeoclimatology, Palaeoecology* v.260, p.245-261.
- Michel, R.L., Linick, T.W. and Williams, P.M. 1979. Tritium and carbon-14 Distributions in Seawater from under the Ross Ice Shelf Project Ice Hole. *Science* v.203, p.445-446.
- Milankovitch, M.M., 1941. Canon of Insolation and the Ice-Age Problem, Beograd: Koniglich Serbische Akademie.
- Miller, K.G., Wright, J.D., Fairbanks, R.G., 1991. Unlocking the icehouse: Oligocene-Miocene oxygen isotopes, eustasy, and margin erosion. *Journal of Geophysical Research* v.96, p.6829-6848.
- Miller, K.G., Kominz, M.A., Browning, J.V., Wright, J.D., Mountain, G.S., Katz, M.E., Sugarman, P.J., Cramer, B.S., Christie-Blick, N., Pekar, S.F., 2005. The Phanerozoic record of global sea-level change. *Science* v.312, p.1293-1297.
- Mosola, A.B., and Anderson, J.B., 2006. Expansion and rapid retreat of the West Antarctic Ice Sheet in eastern Ross Sea: possible consequence of over-extended ice streams? *Quaternary Science Reviews* v.25, p.2177-2196.
- Naish, T.R., Woolfe, K.J., Barrett, P.J., Wilson, G.S., Cliff, A., Bohaty, S.M., Buckner, C.J., Claps, M., Davey, F.J., Dunbar, G.B., Dunn, A.G., Fielding, C.R., Florindo, F., Hannah, M.J., Harwood, D.M., Henrys, S.A., Krissek, L.A., Lavelle, M., van der Meer, J.J.M., McIntosh, W.C., Niessen, F., Passchier, S., Powell, R.D., Roberts, A.P., Sagnotti, L., Scherer, R.P., Strong, P.C., Talarico, F., Verosub, K.L., Villa, G., Watkins, D.K., Webb, P.-N., Wonik, T., 2001. Orbitally induced oscillations in the East Antarctic ice sheet at the Oligocene/Miocene boundary. *Nature* v.413, p.719-723.
- Naish, T.R., Levy, R.H., Powell, R.D., ANDRILL MIS Science and Operations Teams, 2006. ANDRILL McMurdo Ice Shelf Scientific Logistical Implementation Plan, *ANDRILL Contribution* v. 7, University of Nebraska, Lincoln, 117p.
- Pagani, M., Zachos, J.C., Freeman, K.H., Tipple, B., Bohaty, S., 2005. Marked decline in atmospheric carbon dioxide concentrations during the Paleogene. *Science* v.309, p.600-603.

- Pekar, S.F., and Christie-Blick, N., 2008. Resolving apparent conflicts between oceanographic and Antarctic climate records and evidence for a decrease in pCO₂ during the Oligocene through early Miocene (34–16 Ma). *Palaeogeography, Palaeoclimatology, Palaeoecology* v.260, p.41–49.
- Pekar, S.F., and DeConto, R.M., 2006. High-resolution ice-volume estimates for the early Miocene: evidence for a dynamic ice sheet in Antarctica. *Palaeogeography, Palaeoclimatology, Palaeoecology* v.231, p.101–109.
- Pekar, S.F., DeConto, R.M., Harwood, D.M., 2006. Resolving a late Oligocene conundrum: deep-sea warming versus Antarctic glaciation. *Palaeogeography, Palaeoclimatology, Palaeoecology* v.231, p.29–40.
- Petit, J. R., Jouzel, J., Raynaud, D., Barkov, N. I., Barnola, J. M., Basile, I., Bender, M., Chappellaz, J., Davis, M., Delaygue, G., Delmotte, M., Kotlyakov, V. M., Legrand, M., Lipenkov, V. Y., Lorius, C., Pepin, L., Ritz, C., Saltzmann, E., and Stievenard, M., 1999. Climate and atmospheric history of the past 420,000 years from the Vostok ice core, Antarctica. *Nature* v.399, p.429–436.
- Prebble, J.G., Raine, J.I., Barrett, P.J., Hannah, M.J., 2006. Vegetation and climate from two Oligocene glacioeustatic sedimentary cycles (31 and 24 Ma) cored by the Cape Roberts project, Victoria Land Basin, Antarctica. *Palaeogeography, Palaeoclimatology, Palaeoecology* v.231, p.41–57.
- Quilty, P.G., Lirio, J.M., and Jillett, D., 2000. Stratigraphy of the Pliocene Sørsdal Formation, Marine Plain, Vestfold Hills, East Antarctica. *Antarctic Science* v.12, p.205–216.
- Ravelo, A.C., Andreasen D.H., Lyle, M., Lyle A.O., and Wara M.W., 2004. Regional climate shifts caused by gradual global cooling in the Pliocene epoch. *Science* v.429, p.263–267.
- Raymo, M. E., Lisiecki, L. E., and Nisancioglu, K. H., 2006. Plio-pleistocene ice volume, Antarctic climate, and the global delta O-18 record. *Science* v.313, p.492–495.
- Rebesco, M., Camerlenghi, A., Geletti, R., Canals, M., 2006. Margin architecture reveals the transition to the modern Antarctic ice sheet ca. 3 Myr. *Geology* v.34, p.301–304.
- Robinson, N.J. 2004. An oceanographic study of the cavity beneath the McMurdo Ice Shelf, Antarctica. *Unpublished MSc Thesis*. Victoria University of Wellington.
- Schoof, C. 2007, Ice sheet grounding line dynamics: steady states, stability and hysteresis: *Journal of Geophysical Research*, v.112, F03S28, doi:10.1029/2006JF000664.
- Shackleton, N. J., 2000. The 100,000-year ice-age cycle identified and found to lag temperature, carbon dioxide, and orbital eccentricity: *Science* v.289, p.1897–1902.
- Shackleton, N. J., and Kennett, J. P., 1975. Paleotemperature history of the Cenozoic and the initiation of Antarctic glaciation; oxygen and carbon isotope analyses in DSDP sites 277, 279, and 281: *Initial Reports of the Deep Sea Drilling Project* v.29, p.743–755.
- Shackleton, N. J., and Opdyke, N. D., 1977. Oxygen isotope and paleomagnetic evidence for early Northern Hemisphere glaciation. *Nature* v.270, p.216–219.

- Shipp, S., Anderson, J. B., and Domack, E. W., 1999. Late Pleistocene-Holocene retreat of the West Antarctic ice-sheet system in the Ross Sea; Part 1, Geophysical results. *Geological Society of America Bulletin* v.111, p.1486-1516.
- Smellie, J. L., 2001. History of Oligocene erosion, uplift and unroofing of the Transantarctic Mountains deduced from sandstone detrital modes in CRP-3 drill core, Victoria Land Basin, Antarctica. *Terra Antarctica* v.8, p.481-489.
- Stern, T. A., Davey, F. J., and Delisle, G., 1991. Lithospheric flexure induced by the load of Ross Archipelago, southern Victoria Land, Antarctica. In: Thomson, M. R. A., Crame, J. A. and Thomson, J. W., (eds.) *Geological Evolution of Antarctica*. Cambridge University Press. p.323-328.
- Stern, T.A., Baxter, A.K. and Barrett, P., 2005. Isostatic rebound due to glacial erosion within the Transantarctic Mountains. *Geology* v.33, p.221-224.
- Stroeven, A.P., and Prentice, M., 1997. A case for Sirius Group alpine glaciation at Mount Flemming, South Victoria Land, Antarctica: A case against Pliocene East Antarctic Ice Sheet reduction. *Geological Society of America Bulletin* v.109, p.825-840.
- Stuiver, M., Denton, G. H., Hughes, T. J., Fastook, J. L., 1981. History of the marine ice sheet in West Antarctica during the last glaciation; a working hypothesis: In: Denton, G. H., and Hughes, T. J. (eds.) *The last great ice sheets*, p.319-436.
- Summerfield, M.E., Sugden, D.E., Denton, G.H., Marchant, D.R., Cockburn, H.A.P. and Stuart, M.F., 1999. Cosmogenic isotope data support previous evidence of extremely low rates of denudation in the Dry Valleys region, southern Victoria Land, Antarctica. *Geological Society Special Publications* v.16, p.255-267.
- ten Brink, U. S., Hackney, R. I., Bannister, S. C., Stern, T. A., and Makovsky, Y., 1997. Uplift of the Transantarctic Mountains and the bedrock beneath the East Antarctic ice sheet. *Journal of Geophysical Research* v.102(B), p.27,603-27,621.
- Tingey, R.J., 1991. The regional geology of Archaean and Proterozoic rocks in Antarctica: in Tingey, R.J., (ed.), *The geology of Antarctica*. Oxford University Press, p.1-73.
- Webb, P.N., Harwood, D.M., McKelvey, B.C., Mercer, J.H. and Stott, L.D., 1984. Cenozoic marine sedimentation and ice-volume variation on the East Antarctic craton. *Geology* v.12, p.287-291.
- Whillans, I.M. and Merry, C.J., 1996. Kinematics of the shear zone between Ross Ice Shelf and McMurdo Ice Shelf, March 1996. *Internal Report to Antarctic Support Associates*, 18p.
- Whitehead, J.M., Quilty, P.G., McKelvey, O'Brien, P.E., 2006. A review of the Cenozoic Stratigraphy and Glacial History of the Lambert Graben-Prydz Bay region, East Antarctica. *Antarctic Science* v.18, p.83-99.
- Wilson, G. S., Roberts, A. P., Verosub, K. L., Florindo, F., and Sagnotti, L., 1998. Magnetobiostratigraphic chronology of the Eocene-Oligocene transition in the CIROS-1 core, Victoria Land margin, Antarctica: implications for Antarctic glacial history. *Geological Society of America Bulletin* v.110, p.35-47.
- Wright, A. C., and Kyle, P. R., 1990a. Mount Bird. In: LeMasurier, W. E., and Thomson, J. W., (eds.), *Volcanoes of the Antarctic plate and Southern Ocean*, *Antarctic Research Series* v.48. Washington D.C., American Geophysical Union, p.97-98.
- Wright, A. C., and Kyle, P. R. 1990b. Mount Terror. In: LeMasurier, W. E., and Thomson, J. W., (eds.), *Volcanoes of the Antarctic plate and Southern Ocean*, *Antarctic Research Series* v.48. Washington D.C., American Geophysical Union, p.99-102.

- Zachos, J. C., Berggren, W. A., Aubry, M.-P., Mackensen, A., Wise, S. W., Jr., Schlich, R., Palmer Julson, A. A., Bitschene, P. R., Blackburn, N. A., Breza, J. R., Coffin, M. F., Harwood, D. M., Heider, F., Holmes, M. A., Howard, W. R., Inokuchi, H., Kelts, K., Lazarus, D. B., Maruyama, T., Munschy, M., Pratson, E. L., Quilty, P. G., Rack, F. R., Salters, V. J. M., Sevigny, J. H., Storey, M., Takemura, A., Watkins, D. K., Whitechurch, H., and Zachos, J., 1992. Isotope and trace element geochemistry of Eocene and Oligocene foraminifers from Site 748, Kerguelen Plateau. *Proceedings of the Ocean Drilling Program sites* v.120, p.839-854.
- Zachos, J.C., Pagni, M., Sloan, L., Thomas, E., and Billups, K., 2001. Trends, rhythms, and aberrations in global climate 65 Myr to present. *Science* v.292, p.686-693.

CHAPTER 2

The retreat of the Antarctic Ice Sheet (Ross Ice Shelf) in the Ross Embayment since the Last Glacial Maximum

Abstract

Radiocarbon-dated sediment cores from deep basins beneath the McMurdo Ice Shelf, and seasonally-open water north of Ross Island, McMurdo Sound, display a characteristic succession of sedimentary facies that document the retreat of the Antarctic Ice Sheet in the Ross Embayment at the Last Glacial Maximum to its present ice shelf configuration. The facies succession records a transition from a nearly-grounded ice sheet to open-marine environments (north of Ross Island) that comprises in ascending stratigraphic order: (1) slightly-consolidated, clast-rich muddy diamict dominated by basement clasts from the Transantarctic Mountains, and interpreted as melt-out from the basal layer debris proximal to a retreating grounding zone; (2) sparsely-fossiliferous (reworked diatom frustules) and non-bioturbated mud lacking limestones, interpreted as a sub-ice shelf facies; and (3) diatom mud and diatom ooze indicative of open marine conditions with evidence of iceberg rafting. The succession in the open-marine Lewis Basin north of Ross Island is similar, though the diamict is much sandier and sedimentation rates 1-2 orders of magnitude higher. A radiocarbon chronology from total organic carbon is presented that implies that lift-off of grounded ice in the 900 m-deep marine basins surrounding Ross Island occurred by $\sim 10,100$ ^{14}C yr BP. Following lift-off, an ice shelf was maintained to the north of Ross Island until $\sim 8,900$ ^{14}C yr BP. A phase of accelerated retreat at that time between the Drygalski Trough and Ross Island is identified, and immediately precedes the timing of Meltwater Pulse 1b. At $\sim 8,900$ ^{14}C yr BP, the calving line became pinned to Ross Island, significantly decoupling from the grounding line, and marking the transition from a retreating ice sheet to the development of the present ice shelf.

2.1 Introduction

The Ross Ice Shelf, Antarctica, is the largest ice shelf in the world ($560,000 \text{ km}^2$) and is fed by outlet glaciers that drain the East Antarctic Ice Sheet (EAIS) along its western margin (e.g., Denton and Hughes, 2002), although most of the ice shelf is nourished directly by fast-flowing ice streams that drain the West Antarctic Ice Sheet (WAIS; Bindshadler, 1998). Future stability of the Ross Ice Shelf, which is coupled to the

behaviour of the WAIS, has been of wide interest (Mercer, 1978) in the context of current global warming projections (IPCC, 2007). Despite calving of a 30 km-wide strip of ice from its northern margin in 2000, the Ross Ice Shelf is currently considered to be stable, as the mean summer temperature is around -8°C (Oppenheimer, 1998). Recent glaciological evidence indicates that the Ross Ice Shelf is becoming increasingly undernourished with one of its ice stream feeders from West Antarctica stagnating and at least one other slowing down (Joughin and Tulaczyk, 2002; Joughin *et al.*, 2005).

Fluctuations in flow velocity of the ice streams near the WAIS grounding line have been observed (Joughin *et al.*, 2002; Bindshadler *et al.*, 2003; Bougamont *et al.*, 2003), and suggest that over timescales of decades to centuries ice shelves represent the most vulnerable element of the WAIS-Ross Ice Shelf system, and that their collapse could come rapidly (MacAyeal, 1992). Their demise may be the precursor to eventual collapse of the WAIS (Mercer, 1978).

Collapse of the Ross Ice Shelf could affect climate, WAIS extent, and sea level in several ways: Firstly, production of dense bottom water could be disrupted by an initial large-scale discharge of low density meltwater, reducing the production of bottom water around Antarctica. Such an effect could alter the global thermohaline ocean circulation system (Clark *et al.*, 2002; Weaver *et al.*, 2003; Stocker, 2003). Secondly, Earth's albedo will decrease as 560,000 km² of permanent ice cover is replaced with dark ocean, albeit with seasonal sea ice cover, consequently amplifying regional warming. Lastly, the exchange of heat and water vapour between the ocean and the atmosphere could lead to accelerated loss and eventual collapse of the marine-based WAIS in as little time as a few centuries, raising sea level by 5 to 6 m (e.g., Alley and Bindshadler, 2001). Of particular concern is that the fundamental behaviour of the Ross Ice Shelf is poorly understood and models on which predictions are based need to be constrained by new data (Bentley, 2004; Huybrechts, 2004), including those gathered from records of the ancient Ross Ice Shelf during the last major global warming event from the Last Glacial Maximum (LGM) ~ 22 kyr to present.

Between 26.5 and 19.5 kyr (LGM), a grounded ice sheet expanded to near the edge of the continental shelf (~Coulman Island) at approximately 700 m below present day sea level (Anderson *et al.*, 1992; Domack *et al.*, 1999; Bart *et al.*, 2000), and the retreat of both grounding and calving lines since then have been reconstructed using cores collected from the open Ross Sea and ice seismic reflection profiles (e.g., Licht *et al.*, 1996; Conway *et al.*, 1999; Domack and Harris, 1998; Domack *et al.*, 1999; Shipp *et al.*, 1999). Based on a series of piston cores, Domack *et al.* (1999) proposed a sedimentary model describing the LGM-Holocene retreat of the Antarctic Ice Sheet (AIS) in the western Ross Sea. Their lithologic succession in ascending stratigraphic order comprises: (1) Massive mud-rich, over-consolidated diamicton reflecting a sub-glacial setting; (2) a thin, stratified and loosely compacted granulated facies indicative of the glacier “sole” lift-off zone; (3) a terrigenous mud sub-ice shelf facies; (4) a siliceous mud and ooze characteristic of seasonally-open marine conditions.

Radiocarbon dating of organic matter in the cores provided a chronology for post-LGM retreat of the AIS in the Ross Embayment that showed the grounding line withdrew from the outer Drygalski Trough to the vicinity of Ross Island between ~11 and 7 kyr ¹⁴C BP (Domack *et al.*, 1999; Conway *et al.*, 1999). While the grounding line has continued to retreat during the Holocene, the calving line has remained pinned at Ross Island (Figure 10).

This chapter examines the sedimentary evidence for Holocene stability of the McMurdo Ice Shelf, a small body of permanent floating ice at the northwest corner of the Ross Ice Shelf (Figure 10), based on new sediment cores and oceanographic data from beneath the McMurdo Ice Shelf, and from seasonally open water immediately to the north of Ross Island. It documents a Holocene retreat history of the AIS in the Ross Embayment, and provides a revised chronology for the timing of grounding and calving-line retreat in southern McMurdo Sound. These observations are then related to the retreat history of the AIS in the Ross Embayment since the LGM.

2.2 Regional setting

The McMurdo Ice Shelf (area of 2500 km²) is at the northwest corner of the much larger Ross Ice Shelf (560,000 km²) and is fed by mainly by glaciers flowing from the Transantarctic Mountains and Ross Island and surface accumulation of ~0.3 m/year. It is buttressed against the much larger Ross Ice Shelf along a shear zone extending from Minna Bluff to Cape Crozier (McCrae, 1984; Whillans and Merry, 1996; Kellogg *et al.*, 1996; Figure 10), and the presence of the Ross Ice Shelf in this region allows for the survival of the McMurdo Ice Shelf. The area over Windless Bight where the cores for this study were taken is melting at the base but is free of sediment. A simple calculation based on ice flow velocity (100 m yr⁻¹), ice shelf thickness (70 to 150 m) and ice shelf accumulation balanced by basal melting shows that basal glacial debris sourced even as close as Ross Island would have melted out a few km beyond the grounding line, and long before the shelf ice reached the Windless Bight core sites.

Sediment in the western Ross Sea today is accumulating primarily in north-south-trending troughs between 600 and 1200 m deep, once sites of former ice streams draining the WAIS and EAIS-sourced outlet glaciers during the Last Glacial Maximum (Hughes, 1977; Mosola and Anderson, 2006). However, 500 km south of the continental shelf edge, and 300 km south of the LGM grounding line, volcanic Ross Island is surrounded by a basin over 900 m deep, termed a “flexural moat”, formed by lithospheric loading (Stern *et al.*, 1991; ten Brink *et al.*, 1997; Horgan *et al.*, 2005). The moat is interrupted only for a few kilometres southwest of Hut Point Peninsula (Figure 10), where the sea floor rises to 600 m, accelerating the ocean current flow between McMurdo Sound and Windless Bight.

Sea floor sediment in the Ross Sea is a mix of biogenic silica (largely diatom remains from algal growth in the open ocean or sea ice), terrigenous mud carried in suspension from the adjacent continent, and sand and gravel carried by floating ice. Sediment-bearing ice can be sea-ice with sand windblown from land, McMurdo Ice Shelf fragments from the western ablation zone with volcanic surface debris or basal debris from TAM outlet glaciers (Barrett *et al.*, 1983). Terrigenous mud dominates the sea floor sediment throughout the Ross Sea, even though locally biogenic silica can exceed 40% in the deeper open water basins (Dunbar *et al.*, 1985). Ice-rafted sand and gravel is widespread but forms only a few percent of sea floor sediment (Barrett *et al.*, 1983). Sediment origin can be readily determined from mineralogy and clast composition – quartz-free dark basic to intermediate volcanic rocks come from Ross Island and the

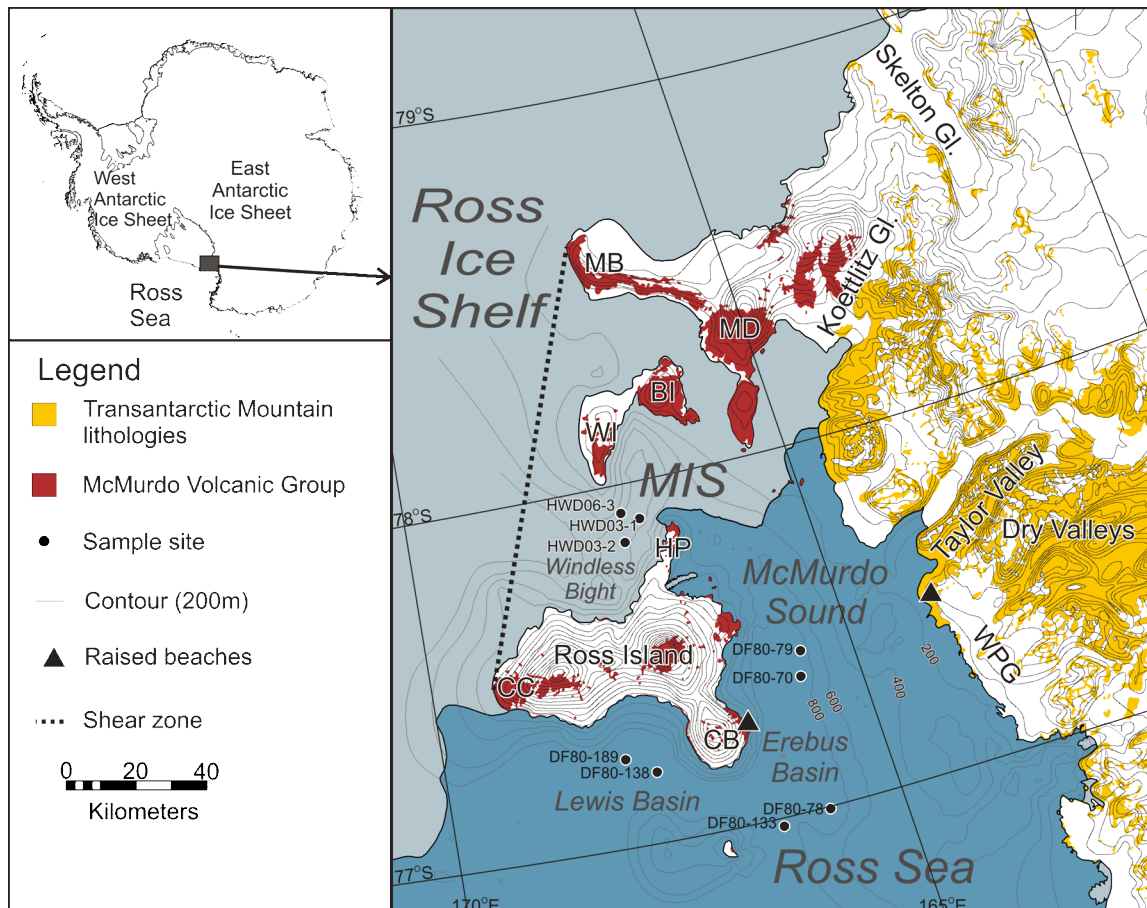


Figure 10: Map of Ross Island region showing the core sites in this study, and localities mentioned in text. The two main provenance areas and raised beaches locations (Dochat *et al.*, 2000; Hall and Denton, 1999) discussed in text are also shown. BI = Black Island, CB = Cape Bird, CC = Cape Crozier, HP = Hut Point Peninsula, MB = Minna Bluff, MD = Mount Discovery, WI = White Island, WPG = Wilson Piedmont Glacier.

volcanoes of southern McMurdo Sound (Kyle, 1990), whereas quartz grains and granitoid or metasedimentary rocks come from the quartz-rich Cambro-Ordovician basement and overlying Beacon Supergroup strata of the Transantarctic Mountains (Craddock, 1970, Plate 13).

Diatom blooms generate frustules that settle to the sea floor largely as medium sand-sized pellets from browsing zooplankton in the open waters of the Ross Sea and McMurdo Sound (Dunbar *et al.*, 1985). However, some of the frustules remain singular and in suspension long enough to be carried by currents beneath the McMurdo Ice Shelf. The net current flow is from McMurdo Sound into Windless Bight with a mean speed of approximately 7 cm s^{-1} , though there is a strong tidal influence with direction reversing and speeds reaching 22 cm s^{-1} (Robinson and Pyne, 2004). The net flow is sufficient to carry frustules and terrigenous mud, but not pellets or sand for tens to hundreds of kilometres beneath the ice (Barrett *et al.*, 2005).

2.3 Methods

2.3.1 Core collection and description

Three sediment gravity cores from beneath the McMurdo Ice Shelf, collected during 2003 (HWD03) and 2006 (HWD06), and six piston cores from the Erebus Basin (in McMurdo Sound) and the Lewis Basin (north of Ross Island), collected by the *USCGC Glacier* as part of Operation Deep Freeze (DF) in 1979-80 (Figure 10), were analysed. To sample beneath the McMurdo Ice Shelf, three Hot Water Drill (HWD) access holes were made, through which a gravity corer was deployed (details in Barrett *et al.*, 2005). Detailed logging, sampling, and x-ray imaging of the Deep Freeze 80 cores were conducted at the Antarctic Marine Geology Research Facility at Florida State University. Core descriptions follow the terminology of Hambrey *et al.* (1997), and are based on visual observations, smear slide analysis, and x-radiography. Undrained shear strength was measured using a shear vane. Ice-rafted debris (IRD) was quantified by summing the number of grains visible on x-radiographs and exceeding 2 mm in size, in 1-cm-thick horizontal bands following the method of Grobe (1987). Grains were counted to a maximum of 10 grains in each cm-band because quantities higher than this

were difficult to determine accurately as individual grains began to overlap in the x-ray image. Therefore, a maximum value of 10 grains >2 mm to these intervals was arbitrarily assigned. This readily allows for diamicton to be distinguished from fine-grained sediment with ice-rafted debris. Descriptions and logs for the cores analysed in this study are provided in the supplementary material at the end of this chapter (Figure 21 to Figure 35).

2.3.2 Grain size analysis

Dry sieving and Sedigraph analysis determined grain-size frequency distribution at 0.5 phi intervals for the sand and mud fractions (Dunbar and Barrett, 2005). All sediment was unconsolidated and lacking any significant carbonate. Therefore, disaggregation was minimal and consisted of Hydrogen Peroxide treatment to remove the organic fraction, and stirring in sodium hexametaphosphate (1g/L) in an ultrasonic tank prior to wet sieving and Sedigraph analysis. Grain size data is provided as supplementary material at the end of this chapter and is presented in Figure 15 and Figure 16.

2.3.3 Sand fraction petrology

The 63-500 µm fraction of each sample was saturated in epoxy to produce pellets for sectioning. The pellets were cut into thin sections to give a maximum quartz birefringence colour of white. The textural and compositional characteristics of each slide were described and point counts of between 300 and 400 grains were undertaken. Sand grains were grouped into one of the categories detailed in Table 1. Modal petrographic analysis (300+ grain point count) for the 63-500 µm fraction was undertaken on grain mount thin sections. The rock fragments and minerals characterised in these counts are summarised in Table 1. To determine the provenance of the sand grains, individual minerals and rock fragments were grouped into those of lithologies found solely or largely in the Transantarctic Mountains and those of more local McMurdo Volcanic Group origin (Figure 2).

<i>Mineral/Lithics</i>	<i>Description</i>	<i>Provenance</i>
Calcite:	Mostly organic in origin, although rare grains of metamorphic calcite with twinning and zoning were noted in the basal unit of HWD03-1.	Byrd Group Ross Supergroup
Volcanic lithics:	Vary from unweathered, angular basaltic groundmass with K-feldspar, plagioclase, olivine or pyroxene phenocrysts to reworked volcanic grains (epiclasts). The epiclasts are usually well rounded and display significant quantities of clay minerals enclosing feldspars, olivine and pyroxenes and are inferred to be the result of significant weathering and transport of volcanic source rocks. In HWD03-1 (24-31 cm), these weathered epiclast may be calcite-cemented diamictite intraclasts and they are grouped together (as they are difficult to distinguish, and like MVG grains are interpreted to be locally sourced). The volcanic lithics are all inferred to be sourced from the MVG, although no distinction of individual volcanic centres (i.e., Ross Island, Black Island) is made.	McMurdo Volcanic Group
Volcanic glass	Vary from colourless/light brown to red brown. Angular to subrounded and often highly vesicular. Rare olivine/plagioclase phenocrysts.	McMurdo Volcanic Group
Plagioclase	Angular to rounded grains, with a tabular form and cleavage at $\sim 90^\circ$, multiple twinning or local alteration to sericite.	Granite Harbour Intrusive Complex
Feldspar	Angular to rounded grains, displaying significant alteration (visible in plain polarised light) to sericite or albite.	Granite Harbour Intrusive Complex Beacon Supergroup Ferrar Dolerite Byrd Group McMurdo Volcanic Group
K-Feldspar	Tabular grains with simple twinning.	McMurdo Volcanic Group Ferrar Dolerite
Microcline	Feldspar with cross-hatched twinning, indicative of a granitic source	Granite Harbour Intrusive Complex
Quartz	Varies from angular to well-rounded. Most grains are monocrystalline with straight to strong undulose extinction. Some grains have fluid inclusions. Smaller grains of quartz lacking distinguishing features may have been identified as feldspar. Polycrystalline quartz grains were also included in this group. Likely sources of this quartz are from Beacon Supergroup sediments, basement granitoids, and basement metasediments (esp. polycrystalline quartz)	Granite Harbour Intrusive Complex Beacon Supergroup
Rounded quartz (\pm overgrowths)	Rounded to well-rounded quartz (\pm overgrowths) likely derived from Taylor group (Beacon Supergroup; Korsch 1974).	Beacon Supergroup
Sedimentary lithics	Range from quartz arenite to arkose lithics.	Beacon Supergroup Ross Supergroup
Pyroxene with exsolution laminae	Includes pigeonite displaying distinctive chevron style twinning and exsolution laminae, likely derived from Ferrar Dolerite (Smellie, 1998).	Ferrar Dolerite
Heavy minerals	Generally lacking distinguishable features. Pyroxenes, amphiboles and biotite are noted.	McMurdo Volcanic Group Ferrar Dolerite Granite Harbour Intrusive Complex

Table 1: Lithologies and minerals categories for modal analysis of sand fraction.

The most distinctive indicator of the Transantarctic Mountains provenance is quartz, which is absent in the McMurdo Volcanic Group (Kyle, 1990), but can be attributed to granites and metasediments, and quartz arenite and arkosic sandstone of the Beacon Supergroup that crops out throughout the Transantarctic Mountains. Notably, rounded quartz with overgrowths can be directly attributed to Devonian Taylor Group (Beacon Supergroup) sandstones (Korsch, 1974). Pyroxene is another important provenance marker, with pigeonite being of Ferrar Dolerite origin, and augite of McMurdo Volcanic Group origin (Smellie, 1998). In the absence of cleavage, alteration or twinning, feldspars could be difficult to distinguish from quartz, except where conchoidal fractures, undulose extinction or overgrowths could be seen. Distinguishing feldspar from quartz could be normally done with confidence for larger grains ($>200\text{ }\mu\text{m}$).

2.3.4 X-ray diffraction

Bulk mineralogy was quantified by XRD. These measurements were undertaken by R. Soong at GNS Science, New Zealand using a Philips *X'Pert Pro X-ray* diffractometer, and quantified using *Siroquant*, a Rietveld synthesis algorithm (e.g., Taylor, 1991). X-ray diffraction results are provided in Table 6.

2.3.5 Diatom analysis

Diatom abundances and concentrations for the DF80 cores were determined by settling known amounts of suspended sediment using the method of Scherer, (1994). Diatom assemblages for the HWD cores are detailed in Barrett *et al.* (2005), where analysis was conducted by Margaret Harper (Victoria University of Wellington). Diatom results are shown in detail in Figure 12, while Figure 13 and Figure 14 show photographs of representative examples of the various taxa documented from the DF80 cores. Particular importance is assigned to the relative abundance of *F. curta*, as it is an indicator of proximal sea-ice formation (e.g., Cunningham *et al.*, 1999; Leventer, 1998). Diatom concentration was used as a proxy for biogenic productivity/reworking. Changes in the relative abundance of fossil diatom species was used as proxy measure of reworking following Sjunneskog and Scherer (2005), who interpreted an increase in fossil diatom taxa in glacial diamicts relative to overlying muds in short sediment cores from the Ross

Sea to be the result of reworking from a variety of older source beds. Diatom results are provided in Table 7.

2.3.6 Windless Bight ice core analysis

To test for the presence of supraglacial debris that might have passed through the McMurdo Shelf at Windless Bight site, a 20-m-long ice core from near HWD03-01 was melted and filtered at 1-m intervals. The cellulose filters (2.5µm) were dissolved by acetoysis mixture (9 parts acetic anhydride, 1 part concentrated sulphuric acid). The precipitate was washed in distilled water and weighed. This weight was then combined with the ice accumulation estimates of McCrae (1984) to determine the sediment flux of supraglacial material that is passing through the ice shelf. The data and methodology for determining the sediment flux rate is provided on page 103.

2.3.7 Radiocarbon chronology

Twenty three ^{14}C ages were obtained from bulk organic carbon in acid insoluble organic (AIO) residues at the Rafter Radiocarbon Laboratory, Lower Hutt. Establishing radiocarbon chronologies for Pleistocene to recent sediments on the Antarctic margin is difficult (e.g., Licht and Andrews, 2002; Mosola and Anderson, 2006; Domack *et al.*, 1999; Conway *et al.*, 1999). Firstly, the marine reservoir correction (1200-1300 years) is substantially greater than for most of the world's oceans as a consequence of enhanced upwelling of "old" deep waters in the region (Gordon and Harkness, 1992; Andrews *et al.*, 1999). Secondly, reworking of sediment containing ^{14}C from organic matter that is "dead" (i.e., beyond the usable limit of radiocarbon $\sim >50$ kyr in age) appears to be significant in the Ross Sea (e.g., Licht *et al.*, 1999). This process increases the measured ^{14}C age in proportion to the ratio of "dead" to contemporaneous AIO material.

To place the chronology into context with previous studies, the technique of Andrews *et al.* (1999) is adopted, correcting the AIO dates by subtracting the surface ^{14}C date from stratigraphically-lower ^{14}C dates. This technique appears to give consistent results with a precision of around ± 500 yrs (Andrews *et al.*, 1999) for diatomaceous-rich sediments,

which are abundant in the Ross Sea. However, it is less reliable for the transitional ice shelf/grounded glacial sediments, where the reworking of old carbon and a lack of primary production leads to errors that are likely to be several thousand years too old (e.g., Domack *et al.*, 1999; Licht *et al.*, 1998). For the glacially reworked diamicts, this error may exceed 10,000 years. Following the techniques reported in these earlier studies, ages are given as both reported and corrected (Table 2). However, they are not calibrated or adjusted to calendar years.

<i>Lab Code</i>	<i>CORE/ DEPTH</i>	<i>Depth (cm)</i>	<i>Reported (14C yrs)</i>	<i>Age Percent Modern</i>	$\delta^{13}C$	$\delta^{14}C$	<i>Corrected age (14C yrs BP)</i>
NZA26112	DF80-78	224-226	22510±120	6.03	-23.3	-939.5	NA
NZA25999	DF80-79	24-26	18613±85	9.79	-25.2	-902.1	NA
NZA26000	DF80-79	108.5-111	17667±75	11.01	-24.3	-889.7	NA
NZA25912	DF80-133	136-138	8024±35	36.58	-26	-635	NA
NZA26113	DF80-138	6-8	26310±180	3.76	-24.2	-962.4	NA
NZA26114	DF80-138	143-145	30930±320	2.11	-23.9	-978.8	NA
NZA26111	DF80-138	244-246	20780±100	7.47	-25.9	-925.4	NA
NZA25941	DF80-189	7-9	2470±35	73.03	-27.7	-273.7	0
NZA25939	DF80-189	96-98	7168±35	40.69	-26.7	-594.5	4698
NZA25913	DF80-189	127-129	11331±45	24.24	-25.2	-757.7	8861
NZA25940	DF80-189	176-178	21830±120	6.56	-16.5	-933.3	NA
NZA18135	HWD03-1	0-1	4343±55	58	-27.2	-423.9	0*
NZA18846	HWD03-1	4-5	5845±35	48	-25.2	-520.3	1380
NZA18136	HWD03-1	20-21	18080±100	10	-24.9	-895.3	16480
NZA18137	HWD03-1	33-34	24550±190	5	-23.1	-953.1	NA
NZA18856	HWD03-1	45-46	25750±190	4	-22.6	-959.5	NA
NZA18857	HWD03-1	58-59	22550±170	6	-25	-939.6	NA
NZA18138	HWD03-2	1-2.5	2701±50	71	-26.9	-292.9	0*
NZA18847	HWD03-2	9-10	4743±40	55	-25.3	-449.8	2042
NZA18139	HWD03-2	28-29	6562±45	44	-25.7	-561.6	3861
NZA18140	HWD03-2	58-59	12797±85	20	-25	-798	10096
NZA25403	HWD06-3	0.5-2.5	4675±40	55.5	-28	-448.4	NA
NZA25420	HWD06-3	31-32.5	10982±60	25.31	-24.3	-746.5	NA

Table 2: Reported and corrected radiocarbon (AIO) dates used in this study. Dates were corrected by subtracting the reported surface age for each core. Corrections are only made on muds and diatom oozes with a reported age of <20ka.

2.4 Stratigraphy

The core stratigraphy is summarised in Figure 15 and Figure 16. The descriptions are focused on the cores from beneath the McMurdo Ice Shelf (HWD03-1, HWD03-2 and HWD06-1) and from the Lewis Basin (DF80-189), where ^{14}C ages in the postglacial sediments are in stratigraphic order and sedimentation rates are relatively constant. DF80-133 is included because it contains similar lithologies to the other cores. However, DF80-133 contains some core disturbance and therefore only one radiocarbon date was obtained. Lithologies encountered in these cores include diamicts, muds, diatom-bearing muds and diatomaceous ooze.

2.4.1 *Clast-rich sandy diamict unit*

A moderately-compacted diamict is present at the base of DF80-189 (1.46-1.96 m) and DF80-133 (1.47-2.47 m). It consists of poorly-sorted gravel clasts in a muddy, coarse sand matrix. The gravel clasts are generally <50 mm in length, (although core diameter would not allow larger clasts to be recovered) and are a wide range of lithologies, including granite, quartz, meta-sedimentary, and basalt. Faceted and striated clasts are common. Undrained shear strength was not measured on the DF cores, as they have dried out during storage. However, qualitatively no sediments appeared overconsolidated. A thickness for the diamict was unable to be determined, as the cores could not penetrate this unit any further than 1 m.

Grain size (Figure 15 and Figure 16) is characterised by a distinct medium sand mode. Mud content is between 10-15%, which is low compared to the other diamicts. This relative lack of mud may have resulted from winnowing during or soon after deposition or from washing in the core tube, as there is evidence of some core disturbance.

Sand grain provenance (Table 5) shows a clear Transantarctic Mountain signal (up to 50%), with common grains of rounded quartz and sandstone lithics (from the Beacon Supergroup), as well as varying proportions of microcline (from Granite Harbour Intrusives) and pigeonite (from Ferrar Dolerite). The maximum size of Transantarctic Mountain grains in this unit was 500 μm (i.e., the upper limit of the size fraction

studied). XRD analysis also confirms a generally higher abundance (~25-30%) of quartz relative to the overlying units.

The diatom concentration is very low in this unit ($<8 \times 10^6$ v/g), both in DF-133 and DF80-189. The unit in DF80-133 is highly disturbed, and although this should not affect petrographic results for the 63-500 μm fraction, it may have had some influence on the diatom and grain size results. On this account, only the top and bottom of the unit in this core was sampled. However, the results support this correlation with DF80-189. The increase in Transantarctic Mountain lithologies, higher quartz values as determined by XRD, and a general decrease in the proportion of *F. curta* also support the correlation (Figure 15 and Figure 16). This, combined with an age of 8,020 (uncorrected) ^{14}C yr BP in the overlying undisturbed mud at 1.36-1.38 m, suggests that the diamict in DF80-133 has a similar origin to that of DF80-189.

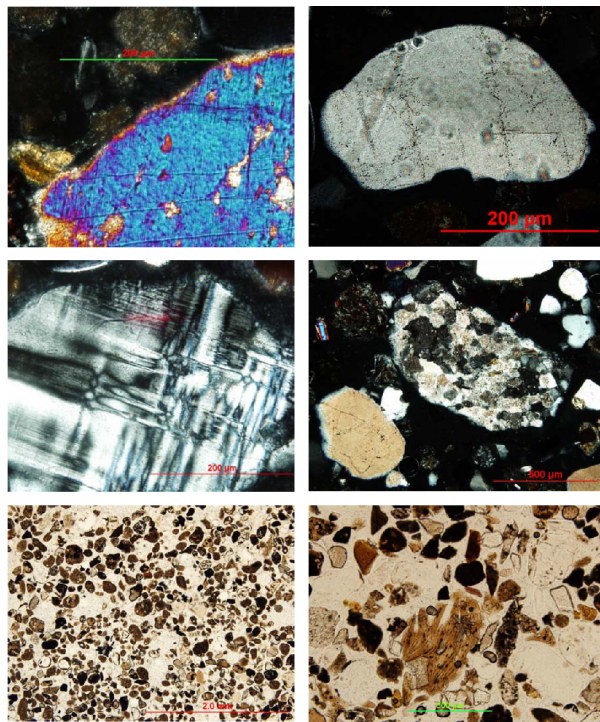


Figure 11: Photos of various sand grains in HWD03 cores. Top left: Pigeonite from Ferrar Dolerite (HWD03-1, 3 cm). Top right: Rounded Quartz with overgrowth from Devonian Beacon Supergroup (HWD03-1, 0 cm). Centre left: Microcline from granitoid (HWD03-1, 0 cm). Centre right: Sedimentary lithic from Transantarctic Mountains. Bottom left: Well-sorted grains from black sand (HWD03-1, 29 cm). Bottom right: Sandy mud from upper 10 mm of HWD03-1 containing vesicular volcanic glass, volcanic lithics quartz, and feldspar (HWD03-1, 0 cm).

2.4.2 Clast-rich muddy diamict unit

This unit is present in sub-ice shelf cores HWD03-1 (0.31-0.62 m), and HWD06-3 (0-0.34 m). It is characterised by poorly sorted, angular to subrounded pebbles (generally <25 mm) in a sandy mud matrix. The clasts are of mixed lithologies, and display facets and striated faces. Like the sandy diamict, the sand grain petrology and XRD analysis

show a distinct Transantarctic Mountain provenance. Grain-size distribution indicates broad frequency distribution with no distinct mode and a mud content of approximately 80%. Diatom concentration is $<10 \times 10^6$ valves per gram of dry sediment (v/g), and TOC values are consistently low at c.0.25% (Barrett *et al.*, 2005).

Undrained shear strength was measured at 8 to 22 kPa (Barrett *et al.*, 2005). The base of this unit in HWD06-3 (0.32-0.34 m) is notably stiffer than overlying sediment, which suggests compaction beneath grounded ice. The shear vane could not be used in this section of the core due to the abundance of gravel clasts. In HWD03-1, Total Organic Carbon (TOC) in this unit varies between 0.10 and 0.18% (Barrett *et al.*, 2005).

2.4.3 Silty-clay unit

Directly overlying the diamicts are silty clays, although HWD03-1 includes intervals 0.05 to 0.08 m thick of fine sandy mud, and both HWD03-1 and -2 have such an interval for the upper few cm. No grains exceed 2 mm, and almost none exceed 0.5 mm (Figure 15). Sand provenance is largely from the McMurdo Volcanic Group. Petrographic analysis indicates that the sand is composed of rounded, weathered lithics that are heavily calcite cemented, and containing volcanic lithics, feldspar and glass. This interval likely represents sediment gravity flows, and indicates that this site experienced some sediment redeposition immediately following grounding line retreat, perhaps as a result of a tidal pumping mechanism (Domack and Williams, 1990).

Diatom concentrations are low (Figure 12), between 1×10^7 (HWD03-2) and 5.5×10^7 v/g (DF80-189). The assemblages observed are highly fragmented with a mixture of reworked oceanic and fossil forms (e.g., *Actinocyclus* spp., *Paralia sulcata*, *Coscinodiscus* spp., *Thalassiosira* spp., *Rouxia* spp., *Denticulopsis* spp; Figure 13 and Figure 14). The modern sea ice diatom *F.curta* constitutes <20% of the assemblage (see Harper in Barrett *et al.*, 2005).

The lack of IRD or basally transported Transantarctic Mountain grains (Figure 15 and Figure 16) suggests deposition beneath an ice shelf that lacks subglacial debris. Sediment recovered from the surficial ice core at the Windless Bight site indicates that

the present day flux of supraglacial material passing through the ice shelf at the Windless Bight site and being deposited on the seafloor is $0.05\text{--}0.55\ \mu\text{m yr}^{-1}$ (see ice core analysis on page 103), accounting for between 0.1 and 1% of the total sediment accumulating on the seafloor.

The maximum unit thickness is 0.60 m (HWD03-2). Radiocarbon ages (Table 2) from the HWD sites imply accumulation rates of between 0.01 and $0.05\ \text{mm yr}^{-1}$, and TOC values for this unit throughout the cores vary between 0.1 and 0.7% (Barrett *et al.*, 2005; Licht *et al.*, 1999).

2.4.4 Diatom mud and ooze with dispersed clasts

Diatom mud and ooze dominate the upper 1.20–1.40 m in both DF80-133 and DF80-189, taken from the seasonally open water sites of McMurdo Sound and Lewis Basin. They consist of a poorly sorted mud that is distinguished from the underlying Silty-clay unit by its higher concentrations of diatoms (between 2×10^8 and 1.2×10^9 v/g) which constitute >50% of the sediment. This unit is further distinguished by the presence of dispersed oversized grains >2 mm. The diatom assemblage is dominated by *F.curta*, and fossil diatom taxa are statistically insignificant. The Transantarctic Mountain signal in the sand grain petrology fluctuates between 0 and 20%. The sedimentation rate of $0.19\ \text{mm yr}^{-1}$ is significantly higher than underlying deposits. For DF80-189, TOC values vary between 1 and 2% (Licht *et al.*, 1999).

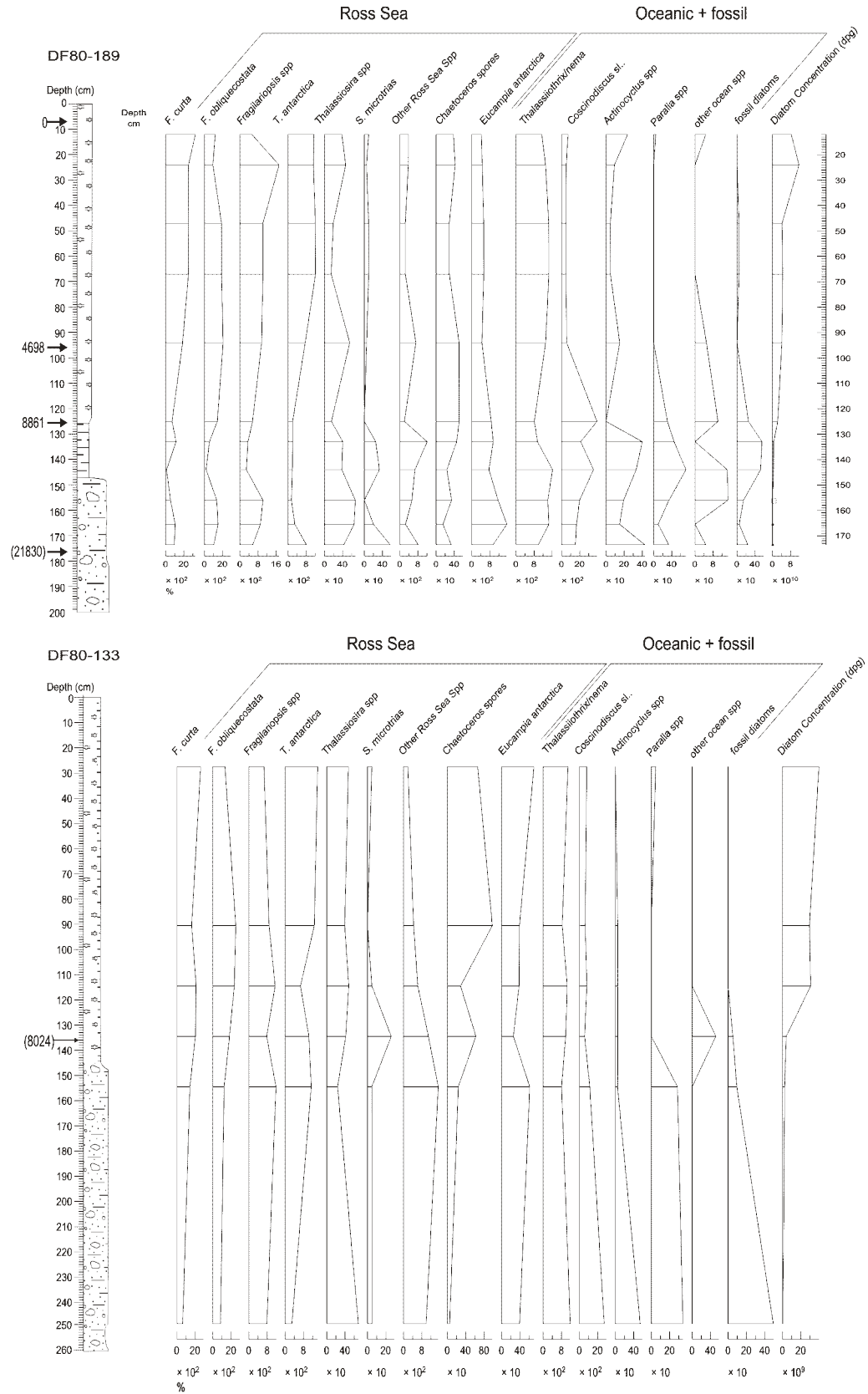


Figure 12: Diatom abundances in cores DF80-189 (top) and DF80-133 (bottom). (note: diatom analysis for HWDO3 cores was conducted by M.Harper and are presented in Barrett *et al.*, 2005).

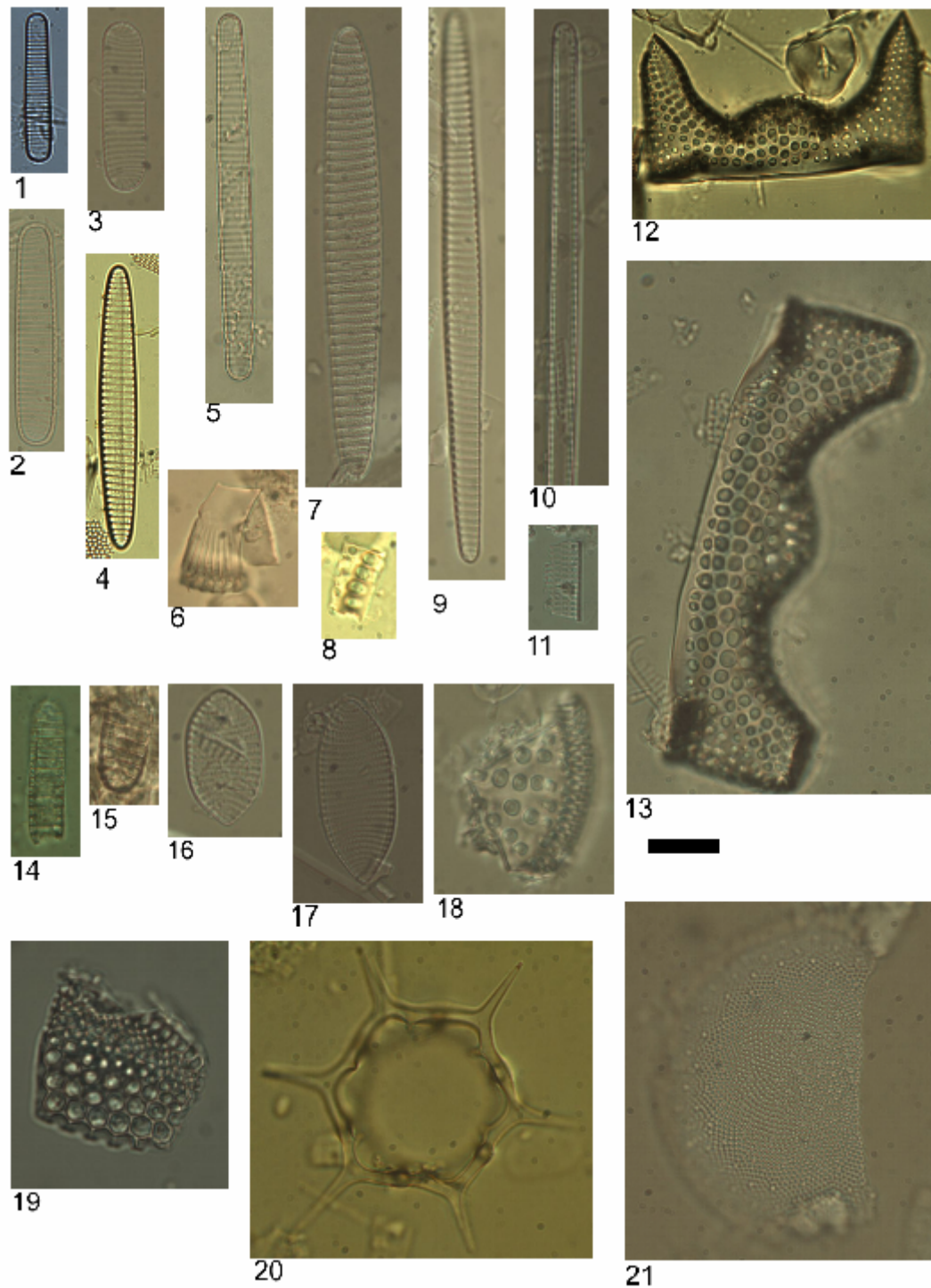


Figure 13: Examples of diatom taxa observed in DF80 cores. Scale Bar = 10µm.

1-3) *Fragilariopsis curta*; 4) *F. obliquecostata*; 5) *F. curta*; 6) *Paralia sulcata*; 7) *F. obliquecostata*; 8) unidentified pennate fragment; 9) *F. sublineata*; 10) *Thalassiothrix antarctica*; 11) *Rouxia* sp?; 12) *Eucampia antarctica*; 13) *E. antarctica*; 14, 15) *Denticulopsis* sp?; 16) *F. separanda*; 17) *F. angulata*; 18) unidentified?; 19) *Thalassiosira torokina*; 20) Silicoflagellate, genus *Distephanus*; 21) *Porosira glacialis*.

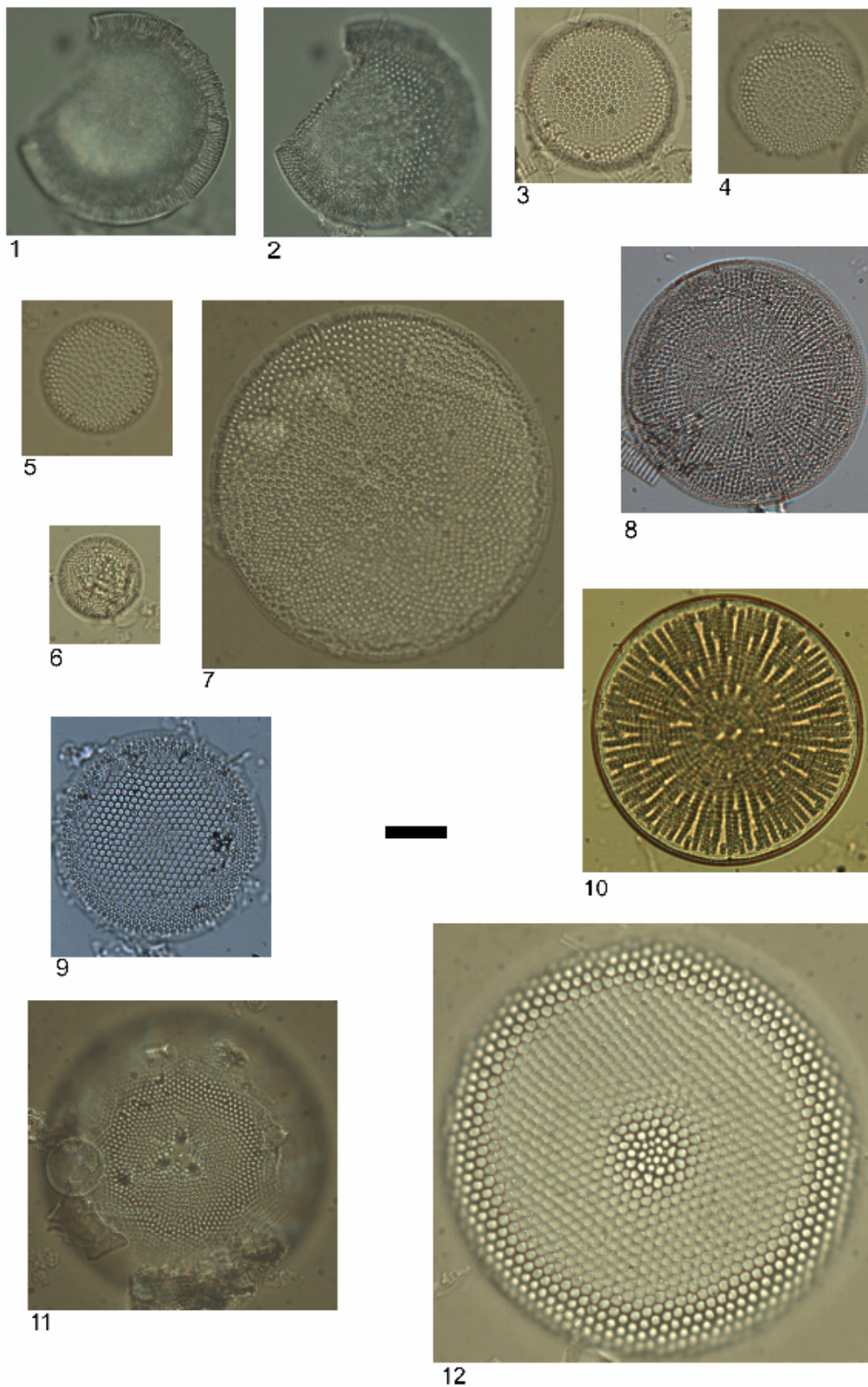


Figure 14: Examples of diatom taxa observed in DF80 cores. Scale Bar = 10µm.

1,2) *Thalassiosira oliverana*; 3-5) *Thalassiosira antarctica*; 6) *Thalassiosira* sp?; 7,8) *Thalassiosira lentiginosa*; 9) *Thalassiosira tumida*; 10) *Actinocyclus actinochilus*; 11) *Stellirima microtaia*; 12) *T. tumida*.

2.5 Chronology

Radiocarbon ages from cores DF80-78 and DF80-79 in the Erebus Basin, and DF80-138 from the Lewis Basin are not in stratigraphic order, and surface values range from 18.6 kyr to 26.3 kyr ^{14}C BP (Table 1), indicating that any sedimentation throughout the Holocene has been dominated by reworking in these cores. Ages taken from the diamict at the base of most cores varied between 20.8 and 25.8 kyr ^{14}C BP, and are not in stratigraphic order. This is to be expected, given the reworked nature of glacially deposited sediments. The fact that the ^{14}C ages are finite indicates incorporation of post-LGM carbon, and that the diamicts are glacimarine, rather than deposited by grounded ice during the LGM. In all cores, smear slide analysis indicates that organic matter is almost entirely restricted to biogenic silica, mostly diatoms, with some sponge spicules.

Four cores provide a stratigraphically ordered chronology of the transition from regionally grounded ice to sub-ice shelf and open ocean conditions. These cores are the main focus of this study, as they show the least reworking and the most complete facies sequence. Two are from Windless Bight (HWD03-1 and HWD03-2), one is from northern McMurdo Sound (DF80-133), and another is from the Lewis Basin (DF80-189). On account of reworking in the cores in central McMurdo Sound (DF80-70 and DF80-79), it is difficult to reconstruct the timing of ice shelf retreat through McMurdo Sound itself, but a retreat history to the immediate north and south can be constrained.

The near-surface ages of these four cores lie between 2.57 and 4.68 kyr ^{14}C BP. This range is similar to those reported in previous studies from the Ross Sea (e.g., Mosola and Anderson, 2006; Licht *et al.*, 1996; Domack *et al.*, 1999; and Andrews *et al.*, 1999).

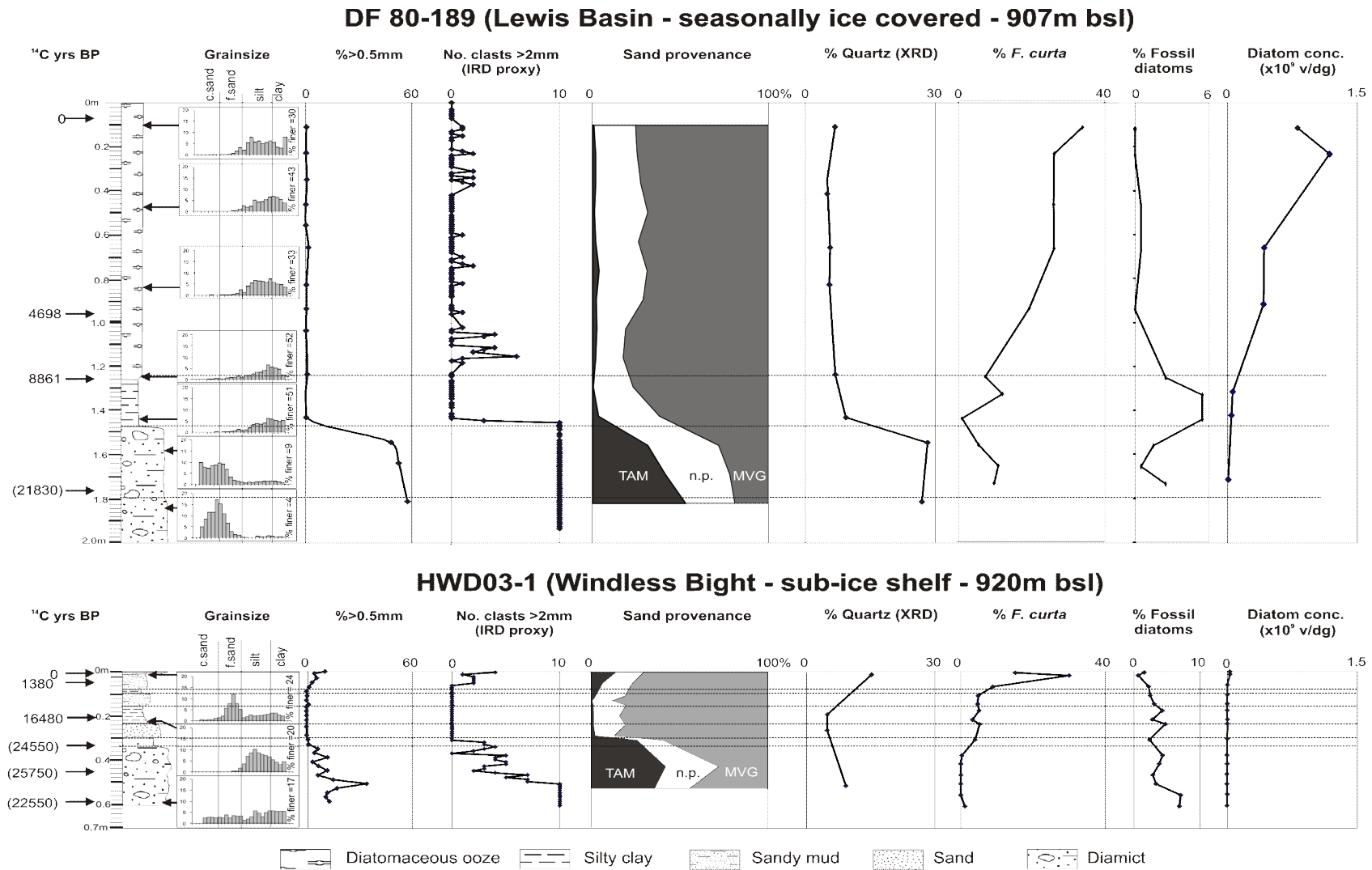


Figure 15: Composite logs of DF80-189 and HWD03-1, with corrected radiocarbon ages, grain-size histograms, % grains >0.5 mm and >2.0 mm, 63-500 μ m (sand) provenance, % quartz measured by XRD, and diatom abundances. Bracketed ^{14}C dates are reported (uncorrected) ages.

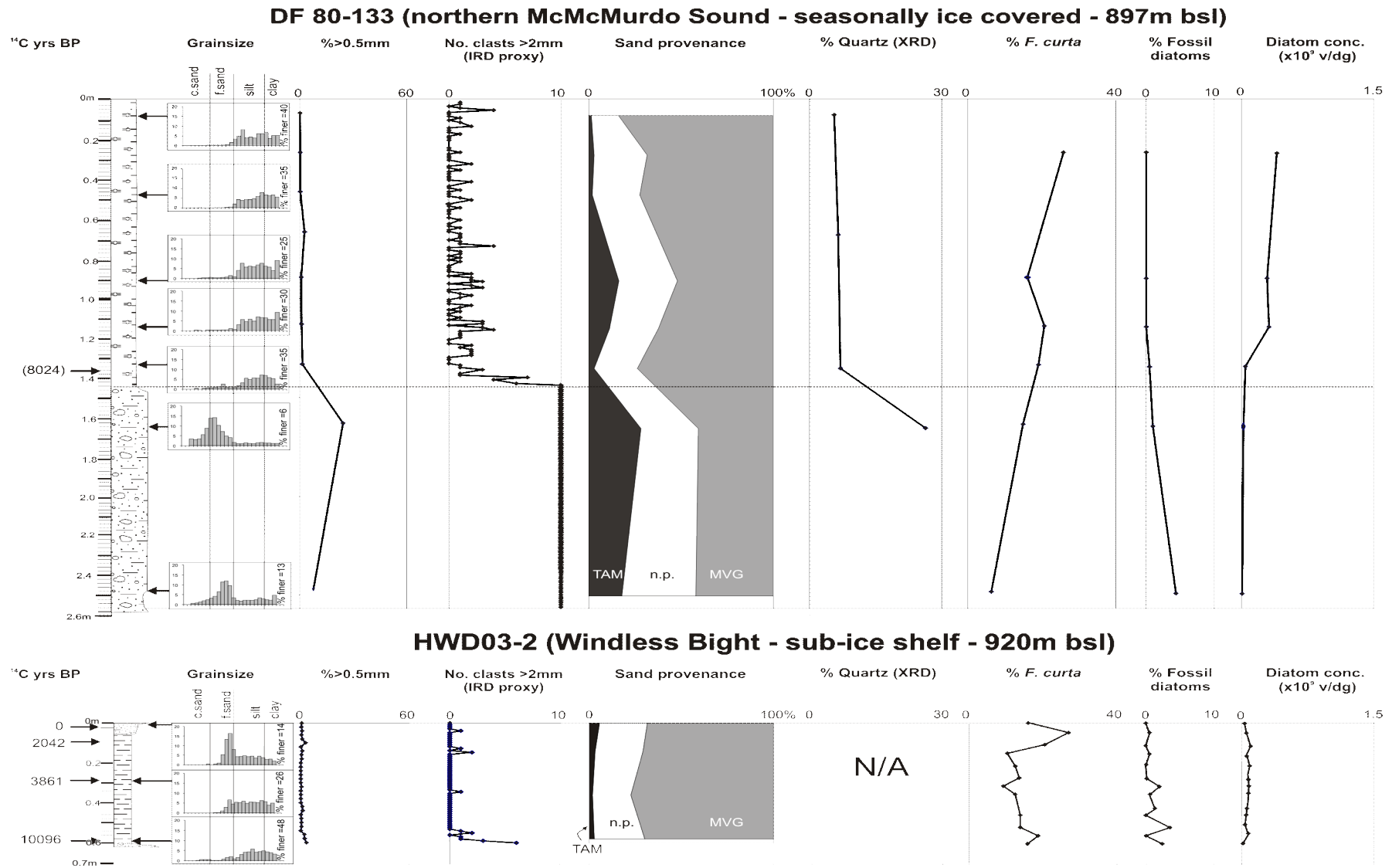


Figure 16: Composite logs of DF80-133 and HWD03-2, with corrected radiocarbon ages, grain-size histograms, % grains >0.5 mm and >2.0 mm, 63-500 μ m (sand) provenance, % quartz measured by XRD, and diatom abundances. Bracketed ¹⁴C dates are reported (uncorrected) ages.

2.6 Discussion

The lithological units can be interpreted as facies with distinct biogenic and sedimentary markers for constraining the position of the grounding and calving lines of the McMurdo/Ross Ice Shelves around Ross Island. The facies model presented here is developed from that of Domack *et al.* (1999) for the Central and Western Ross Sea, with some differences.

Developing an accurate chronology of events is complicated by difficulties in ^{14}C dating Ross Sea sediments (see Methods section). In particular, the “dead” carbon in many samples through reworking of older sediment has resulted in ages representing a maximum value, rather than the depositional age of the sample. This is especially evident in McMurdo Sound. However, this effect is minimised in sediments with relatively high accumulation rates of contemporaneous carbon (e.g., Licht *et al.*, 1999), allowing us to provide a chronology for the retreat history of the ice sheet/shelf system in the Ross Sea that is comparable with previous studies from the marine record (e.g., Licht *et al.*, 1996; Licht and Andrews, 2002; Andrews *et al.*, 1999; Domack *et al.*, 1999).

Three distinct facies are identified here, from which the retreat of both the grounding line and calving line of the Ross Ice Shelf is inferred: 1) sub-ice shelf diamict; 2) sub-ice shelf sand and mud; and 3) open-water diatom mud and ooze with IRD.

2.6.1 *Sub-ice shelf diamict facies*

The sub-ice shelf diamict facies is distinguished by its lithology and Transantarctic Mountain provenance. Diatom concentrations are low, and valves are usually broken. The assemblages also have relatively higher abundances of fossil and oceanic forms. There was no evidence within any of the diamict units that is indicative of deposition beneath grounded ice. Given its unconsolidated nature, the diamict is likely to have resulted from meltout from the basal debris zone shortly after the retreat of regionally grounded ice. However, over-consolidation is not a prerequisite for indicating grounded

ice, as sediment cores that have penetrated megascale lineations on the seafloor have recovered diamictos with low shear strengths and high water contents (Anderson, 1999). The ages measured from this unit in the HWD and DF80 cores range between 20.78 kyr and 25.75 kyr ^{14}C BP, which significantly postdate the 26.86 kyr ^{14}C BP age for grounded ice in McMurdo Sound (Dochat *et al.*, 2000), and suggest some input of post-LGM carbon, which could not have occurred if the sediment were deposited beneath grounded ice. The fact that this unit could not be penetrated by the gravity corer may be due to either the presence of an underlying compacted till or the presence of large clasts. Coring under the McMurdo Ice Shelf, by the ANDRILL Project, near the vicinity of HWD03-1, has revealed an over-consolidated till at 1.94 m below the seafloor underlying the less consolidated diamict that constitutes this facies in the short cores presented here (Naish *et al.*, 2007).

Domack *et al.*'s (1999) muddy pelletised gravel and sand (granulated) facies is not included in the model presented here. Domack *et al.* (1999) noted that this facies is stratified, coarsens upwards, has dropstones, and is mineralogically identical to the underlying diamict. It is inferred to be derived from the basal glacial debris zone, and represents the lift-off of the grounded ice sheet from the sea floor, with a gradual increase in sub-ice shelf reworking as the thickness of ice shelf cavity increases. None of the diamicts in the HWD or DF80 cores are stratified, suggesting that marine deposition or reworking of sediments by sub-ice shelf currents was minimal. However, the diamict from Lewis Basin and northern McMurdo Sound (DF80-133 and DF80-189) has lower mud content than the diamict at the Windless Bight site (HWD cores), and could relate to the granulated facies of Domack *et al.* (1999).

2.6.2 Sub-ice shelf sand and mud facies

Sub-ice shelf sand and mud (HWD03 sites; DF80-189, 1.22-1.45 m) are distinguished by low diatom concentrations (with a low percentage of sea-ice forms), a lack of grains >2 mm in diameter (Figure 15 and Figure 17), a lack of sand grains derived from the Transantarctic Mountains, and a slow sedimentation rate (0.01-0.05 mm yr⁻¹). However, the upper 0.05 m of HWD03-1 shows an increase in coarse sand (up to 500 μm) with a Transantarctic Mountain provenance and includes fine gravel with a mixed provenance.

The presence of these grains would normally be associated with the calving line of the ice shelf. This site is currently beneath the McMurdo Ice Shelf, 5 km from the calving line and these grains are too coarse to be transported via sub-ice shelf currents in a settling water column. Modern sub-ice shelf currents ($<22 \text{ cm s}^{-1}$) are only capable of laterally transporting settling fine sand grains (at most) 1 km beneath the ice shelf (Barrett *et al.*, 2005).

Therefore, the presence of these sand grains indicates that either the ice shelf front has retreated and then re-advanced over this site, or that reworking of the older diamicts is currently taking place beneath the ice shelf. If the ice shelf had retreated past this site during the Holocene, a significant increase in diatom deposition and a rapid increase in the sedimentation rate would be expected (e.g., DF80-189 and DF80-133). This is not the case at either HWD03-1 or HWD03-2 (Figure 15 and Figure 16), indicating that there has been no period of seasonally open water above or near the site during the Holocene, despite the temperature reconstructions based on deuterium isotopes from a number of Antarctic ice cores suggesting an early Holocene optimum up to 2.5°C warmer than present in this region (Steig *et al.*, 2000; Masson *et al.*, 2000). If there has been a period of calving-line retreat over the site, it was almost certainly very short lived.

An alternative explanation is the reworking of exposed diamict on the seafloor from local bathymetric highs, in particular, the hummocks, drumlins, and lineations that are commonly associated with glacial-marine deposition elsewhere in the Ross Sea (e.g., Shipp *et al.*, 1999). Perhaps sub-ice shelf bottom currents increased in strength as the ice shelf front approached the site in the late Holocene. This increased flow could have winnowed fine grained material from exposed seafloor diamicts, resulting in localised slope instability. This facies is absent in DF80-133, as grains $>2 \text{ mm}$ are persistent throughout the core. This suggests that either the ice shelf did not persist at this site for a significant length of time, or this unit has been reworked and eroded.

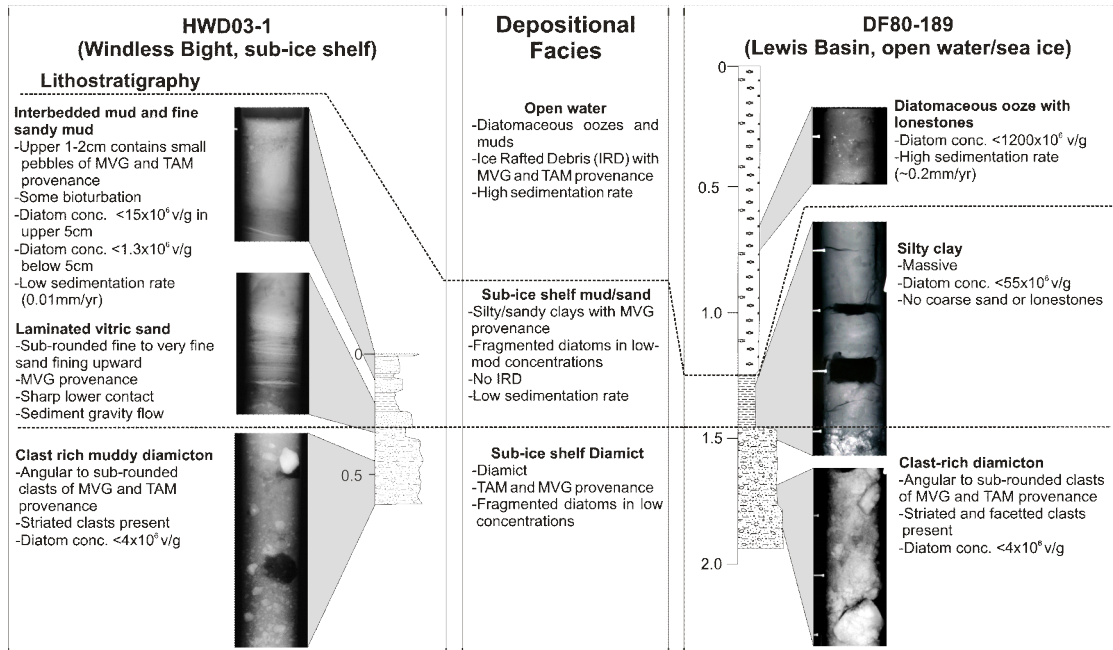


Figure 17: Core logs, lithological characteristics, and selected x-rays of representative facies from HWD03-1 and DF80-189. Note lack of outsized sand grains in sub-ice shelf mud/sands in both cores relative to the open water diatomaceous ooze/mud in DF80-189. The laminated vitric sand in HWD03-1 is interpreted as a sediment gravity flow.

In HWD03-1, a distinctive dark interval (0.24-0.31 m) of well-sorted, soft, muddy fine to very fine sand (63-97% sand) with mm-scale mud laminations occurs directly above the underlying diamict facies. The sand has a sharp lower contact with load features. Petrographic analysis indicates that the sand is composed of rounded, weathered volcanic glass and lithics. This interval likely represents a series of small sediment gravity flows following grounding line retreat.

2.6.3 Open water diatom mud and ooze facies

This facies is distinguished by its higher accumulation rate (0.2 mm yr^{-1}) associated with primary biogenic production. Diatom concentrations are one to two orders of magnitude higher (between 5×10^8 and 12×10^9 v/g; Figure 12) than for the underlying sub-ice shelf facies ($4\text{--}5 \times 10^7$ v/g) and marked by the high abundance of *F. curta*, a diatom that dominates seasonal sea ice and the adjacent water column in the Ross Sea (Leventer, 1998). Associated with this biogenic deposition is the presence of ice-rafted coarse sand and pebbles most likely derived from icebergs calving from glaciers along the Victoria Land coast and Ross Island (Figure 17).

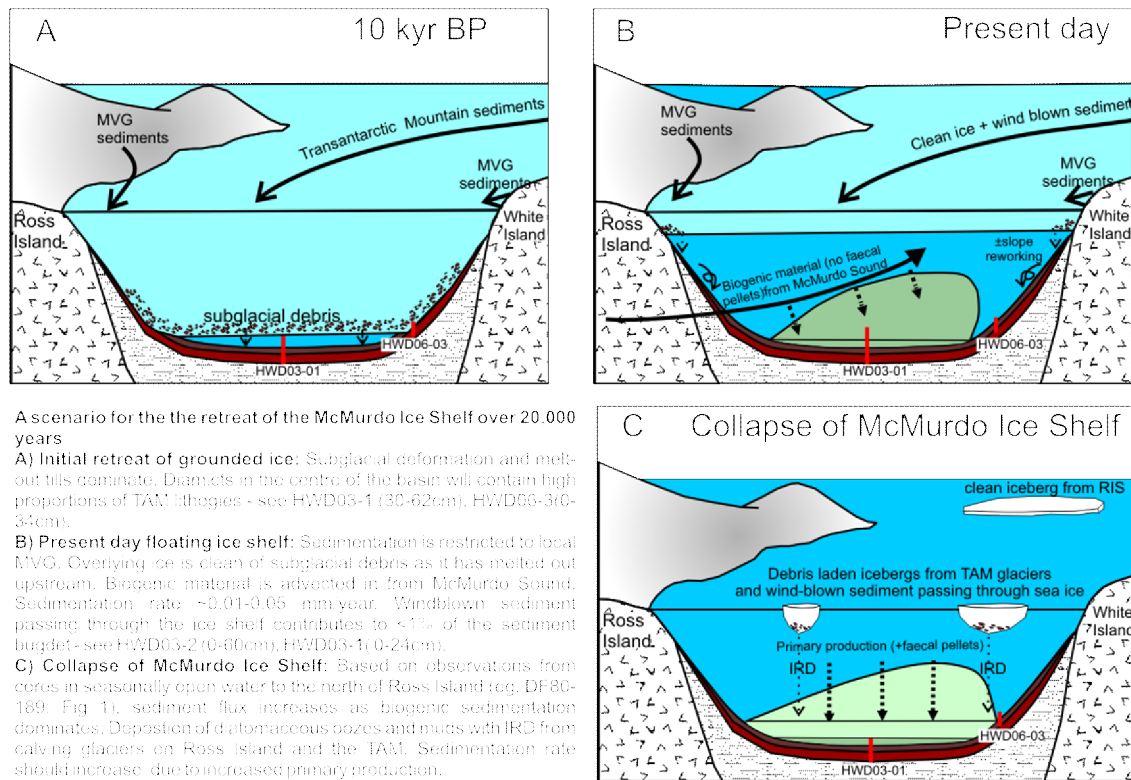


Figure 18: Sediment transport paths during three stages of glacial retreat in McMurdo Sound.

2.7 Sediment provenance and ice shelf dynamics

A strong relationship between sand provenance and the position of the Ross/McMurdo Ice Shelf calving lines is identified. During periods of glacial advance, regionally grounded ice transports large volumes of sediment derived from the Transantarctic Mountains into Windless Bight, and Erebus and Lewis basins (Figure 18). Transantarctic Mountain lithologies contribute up to 50% of the 63-500 μm fraction. This signal is also evident in the XRD results, with quartz generally exceeding 30% of the mineral assemblage. These results are consistent with reconstructions (e.g., Stuiver *et al.*, 1981; Denton and Marchant, 2000) of the grounded Ross Ice Shelf transporting sediment from the Transantarctic Mountains to the south of Minna Bluff into Windless Bight, and around Cape Bird into McMurdo Sound.

The retreat of the grounding line and the development of ice shelf conditions are represented by a dramatic increase in the proportion of locally derived McMurdo Volcanic Group grains. XRD analysis suggests quartz constitutes <10% of the mineral

assemblage, while Transantarctic Mountain-derived sand in the 63-500 μm fraction generally contributes <4%. However, there is potential for localised slope instability that may distort this signal (Figure 18). Instability may result from ice withdrawal or from the winnowing of fine material higher up the slope due to increasing oceanic current influence. As the calving line retreated over the site, sediment provenance was still dominated by material derived from the McMurdo Volcanic Group, although there is a noticeable increase in Transantarctic Mountain lithologies (~10-15%) in the 63-500 μm fraction. These may result from poorly-sorted ice-rafted debris, well-sorted wind-blown sand passing through sea ice, or reworking of older seafloor diamicts (Figure 18).

2.8 Timing and magnitude of grounding and calving retreat: Relationships to Meltwater Pulses 1A and 1B.

Within the uncertainties associated with Antarctic radiocarbon ages, the corrected AIO ages are consistent with those of previous studies. However, contamination of some samples with “dead” carbon is clearly evident in intervals where ages are not in chronological order. Nonetheless, two cores are identified where the chronology is likely to be reliable. The corrected age of 8.9 kyr ^{14}C BP for DF80-189 (1.27-1.29 m), a mud with high diatom concentrations ($\sim 5.5 \times 10^7$ v/g; Figure 12) is likely to be robust for two reasons: (1) the age was corrected by the AIO age at 0.07 m depth (2.47 kyr ^{14}C BP), not the surface and therefore calculating the age from the surface age would result in an age >8.86 kyr ^{14}C BP. For example, using the sedimentation rates determined between 0.07 and 0.96 m depth (0.19 mm yr^{-1}) to extrapolate the expected age at 0 m depth (2.05 kyr ^{14}C yr), would have given a corrected age at 1.27-1.29 m of 9.28 kyr ^{14}C BP. However, the simple correction to 0.07 m is used, and rounded up to 8.90 kyr ^{14}C BP for the chronology. (2) It coincides with the first signal in the diatom record of primary production, which would have provided the first significant influx of non-reworked carbon and the first signal of IRD (Figure 15). (3) Overlying ages are in chronological order and there is no major lithological change. This date indicates that open marine conditions were developing above this site at ~ 8.9 kyr ^{14}C BP.

The underlying glacial sediments are usually low in diatomaceous material, and hence contemporaneous carbon, making ages less reliable for dating the retreat of the grounding line. However at HWD03-2, the base of 0.60 m-thick mud (which overlies a pebbly sandy mud) gives a corrected age of 10.1 kyr ^{14}C BP (Figure 15). This age is likely to be reliable given that: (1) It has a moderate diatom concentration ($>10 \times 10^6$ v/g) dominated by modern Ross Sea taxa (e.g., *F. curta*, *F. obliquecostata*), (2) there is a lack of fossil diatoms which is an indicator of reworking from older sediment (Sjunneskog and Scherer, 2005); and (3) overlying sediments are of a uniform lithology and the ages are in chronological order, defining a linear age-depth relationship (Figure 15).

Thus HWD03-2 constrains the age for lift-off of grounded ice 920 m below sea level immediately to the south of Ross Island to earlier than 10.1 kyr ^{14}C BP. This is further constrained by the ~ 8.9 kyr ^{14}C BP age obtained for open marine conditions immediately to the north of Ross Island from DF80-189. These are included in Figure 19, which shows the revised chronology for the retreat of the LGM ice sheet in the Ross Embayment.

On the basis of these ages and the lithostratigraphy recorded in the HWD and DF80 cores, the grounding and calving lines of the ice sheet are postulated to have retreated at similar rates until between 8.0 and 9.0 kyr ^{14}C BP, when the calving line became pinned to Ross Island. Since then it has remained there, while the grounding line continued to retreat to its present day position.

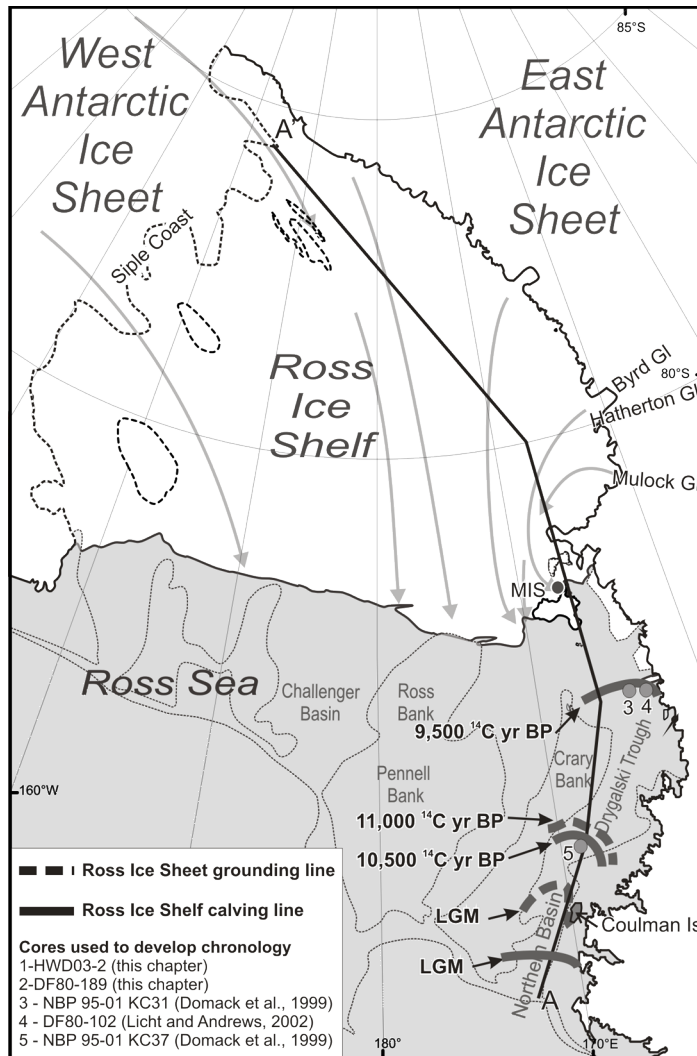


Figure 19: A chronology for the retreat of the ice sheet in the Ross Embayment from this study (black lines and circles) and previous workers (dark grey). Solid lines indicate the maximum position of the calving line for the Ross Ice Shelf, while dashed lines indicate the maximum position of the grounding line, including its present day position along the Siple Coast. Ice shelf extent at the LGM is poorly constrained and is based on a sedimentary hiatus observed in sediment cores (Licht *et al.*, 1996). Transect line A-A' for Figure 20 is also shown. Regional bathymetry (500 m contours) and modern ice flow for the Ross Ice Shelf (after Fahnestock *et al.*, 2000) is also shown. Localities mentioned in the text are also labelled.

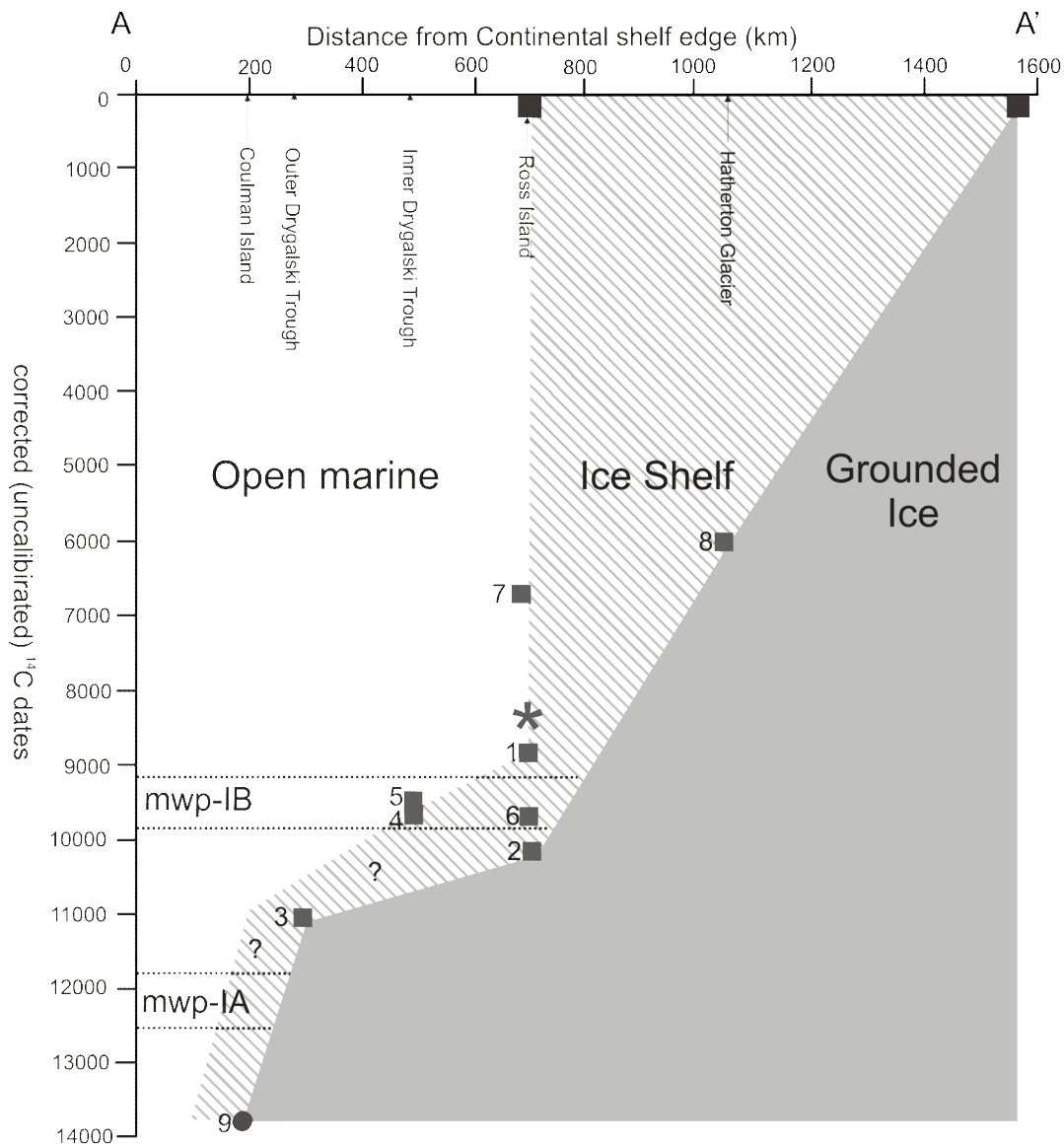


Figure 20: The retreat history of the ice sheet/shelf grounding and calving line in the Ross Embayment, using corrected ^{14}C dates from this study, and those of previous workers. Corrected (but uncalibrated) age ranges for Meltwater Pulse (mwp) events 1A and 1B (after Fairbanks, 1989) are also plotted. Sources for this chronology are: (1) DF80-189, AIO ^{14}C date from diatomaceous ooze with IRD, (this chapter); (2) HWD03-2, AIO ^{14}C date from sub-ice shelf diatom-bearing mud, (this chapter); (3) KC37, AIO ^{14}C date from sediment core (Domack *et al.*, 1999); (4) DF80-102, AIO ^{14}C date from muddy diatom ooze, Licht and Andrews, 2002); (5) KC31 (AIO ^{14}C date from sediment core, Domack *et al.*, 1999); (6) Oldest penguin bone at Cape Bird (Dochat *et al.*, 2000); (7) DF80-57, Oldest marine shell in McMurdo Sound (Licht *et al.*, 1999); (8) algal date adjacent to Hatherton Glacier (Bockheim *et al.*, 1989); (9) Inferred extent of grounded ice at the Last Glacial Maximum from seismic profiling in the Western Ross Sea (after Shipp *et al.*, 1999), while timing of grounding line extent at 13.8 kyr ^{14}C BP (ref 9) is based on a reworked foram in diamict from a sediment core (NBP9501-7) in the central Ross Sea (Licht and Andrews, 2002); * Terrestrial evidence for grounded ice in McMurdo Sound (Hall *et al.*, 2000).

The timing of lift-off of grounded ice at Windless Bight just after 10.1 kyr ^{14}C BP is slightly earlier than previous estimates from marine sediment cores further north in the Ross Sea (e.g., Domack *et al.*, 1999; Conway *et al.*, 1999; Licht and Andrews, 2002), and earlier than the timing of ice retreat based on ages from proglacial lakes in the Taylor Valley at 8.34 kyr ^{14}C BP (Hall *et al.*, 2000). These proglacial lakes are inferred to have been formed as the result of the grounded ice sheet in McMurdo Sound. If correct, this revised chronology indicates that the retreat of the ice sheet in the Ross Embayment was more rapid and earlier than previously believed, and raises questions over its relationship to Meltwater Pulses 1A and 1B (mwp-1A and mwp-1B). Domack *et al.* (1999) implied that the initial post-LGM retreat of the Ross Ice Shelf grounding line from near Coulman Island at ~ 11 kyr ^{14}C BP postdated, and was thus not the cause of, a 20 m rise in sea level between ~ 12.5 and 11.8 kyr ^{14}C BP (mwp-1A; Fairbanks, 1989; Bard *et al.*, 1996). The chronology presented in this chapter agrees with this, but also indicates that the retreat of the grounding line from the outer Drygalski Trough to Ross Island occurred rapidly (within 1,000 years), and appears to immediately precede mwp-1B, a ~ 10 m sea level rise that occurred between ~ 9.2 and 9.8 kyr ^{14}C BP (Fairbanks, 1989; Bard *et al.*, 1996).

Considering the uncertainties associated with ^{14}C ages in the Ross Sea, and the uncertainties that surround mwp-1B, the chronology is cautiously interpreted in the context of global eustatic sea level changes. Taken at face value, the chronology suggests that initial lift-off of grounded ice at Windless Bight preceded mwp-1B (Figure 20), implying that the AIS could have been a significant contributor to eustatic rise. Nevertheless, a Northern Hemisphere origin for mwp-1B, which may have destabilised the marine-based Ross Embayment sector of the ice sheet and triggered the transition from an ice sheet to the present ice shelf, cannot be ruled out.

The chronology from this study also places the retreat of grounded and shelf ice from the marine basins north of Ross Island much earlier than the chronology derived from raised beaches at Cape Bird, where *in situ* penguin remains date the oldest raised beach ridge at 3.59 kyr ^{14}C BP (Dochat *et al.*, 2000) and provide a minimum age for ice shelf retreat. However, reworked penguin bones within beach deposits at Cape Bird have

been dated at 9.74 kyr ^{14}C BP (Dochat *et al.*, 2000), implying earlier open water conditions at this location. Raised beaches along the Scott Coast in McMurdo Sound suggest deglaciation shortly before 6.5 kyr ^{14}C yr BP (Hall and Denton, 1999). The raised beaches at Cape Bird and the Scott Coast can form only in the absence of an ice shelf, and therefore provide a minimum age for grounded ice retreat. The extensive reworking in DF80-78 and DF80-79 (supported by the non-stratigraphic order of the radiocarbon ages; Table 2) prevents us from determining the timing of ice shelf retreat within McMurdo Sound itself where the raised beaches are located (Figure 10). Therefore, it is possible that an ice shelf remained in McMurdo Sound until 6.5 kyr ^{14}C BP, while open ocean conditions prevailed to the north and east of Ross Island.

The persistence of proglacial lakes in the Dry Valleys until 8.34 kyr ^{14}C BP (Hall *et al.*, 2000) provides a maximum age for the retreat of grounded ice in McMurdo Sound, if it is assumed they were dammed by grounded ice. However, the presence of these lakes does not indicate the extent of grounding within McMurdo Sound itself, and it is possible that localised grounding occurred along the western shoreline of McMurdo Sound until 8.34 kyr ^{14}C BP, perhaps as a seaward and southward extension of the modern Wilson Piedmont Glacier, ~1.5 kyr after the ice lifted off the floors of the deeper basins.

2.9 Conclusions

- The ice sheet grounding line retreated rapidly across the Ross Sea continental shelf from the outer Dryglaski Trough to south of Ross Island between 11 and 10 kyr ^{14}C BP.
- By ~8.9 kyr ^{14}C BP, there were open marine conditions immediately to the north of Ross Island.
- The Ross Ice Shelf has been pinned to Ross Island since ~8.9 kyr ^{14}C BP while the grounding line has continued to retreat towards the Siple Coast. Its calving line has not retreated past its present position during this time, despite ice core evidence for a mid-Holocene climatic optima 1-2°C warmer than present (Steig *et al.*, 1998).

- It is suggested that the post-LGM retreat of the ice sheet in the Ross Embayment shifted to its contemporary ice shelf mode when the calving line became pinned by Ross Island.
- This revised chronology implies an earlier and more rapid retreat history than previously reported, and allows for the possibility that the retreat of the marine based sectors of the Antarctic Ice Sheet was associated with global eustatic sea-level pulses.

2.10 References

- Alley, R. B., and Bindshadler, R. A., 2001. The West Antarctic ice sheet and sea-level change. *Antarctic Research Series* v.77, p.1-11.
- Anderson, John B. 1999. *Antarctic Marine Geology*. Cambridge University Press, UK, 289p.
- Anderson, J. B., Shipp, S. S., Bartek, L. R., and Reid, D. E., 1992. Evidence for a grounded ice sheet on the Ross Sea continental shelf during the late Pleistocene and preliminary paleodrainage reconstruction. *Antarctic Research Series* v.57, p.39-62.
- Andrews, J. T., Domack, E. W., Cunningham, W. L., Leventer, A., Licht, K. J., Jull, A. J. T., DeMaster, D. J., and Jennings, A. E., 1999. Problems and possible solutions concerning radiocarbon dating of surface marine sediments, Ross Sea, Antarctica: *Quaternary Research* v.52, p.206-216.
- Bard, E., Hamelin, B., Arnold, M., Montaggioni, L., Cabioch, G., Faure, G., Rougerie, F., 1996. Deglacial sea-level record from Tahiti corals and the timing of global meltwater discharge. *Nature* v.382, p.241-244.
- Barrett, P. J., Pyne, A. R., and Macpherson, A. J., 1983. Observations on the sea floor of McMurdo Sound and Granite Harbour. *New Zealand Antarctic Record* v.5, p.16-22.
- Barrett, P.J., Carter, L., Dunbar, G.B., Dunker, E., Giorgetti, G., Harper, M.A., McKay, R.M., Niessen, F., Nixdorf, U., Pyne, A.R., Riesselmann, C., Robinson, N., Hollis, C., and Strong, P., 2005. Oceanography and sedimentation beneath the McMurdo Ice Shelf in Windless Bight, Antarctica. *Antarctic Data Series* v.25, Victoria University of Wellington, 100p.
- Bart, P.J., Anderson, J.B., Trincardi, F. and Shipp, S.S. 2000. Seismic data from the Northern basin, Ross Sea, record extreme expansions of the East Antarctic Ice Sheet during the late Neogene. *Marine Geology* v.166, p.31-50.
- Bentley C.R., 2004. Mass balance of the Antarctic Ice Sheet: observational aspects. In: Bamber, J.L. and Payne, A.J. (eds.), *Mass Balance of the Cryosphere*. Cambridge University Press, UK, p.459-489.
- Bindshadler, R., 1998. Monitoring ice sheet behavior from space. *Reviews of Geophysics* v.36, 79-104.

- Bindschadler, R. A., King, M. A., Alley, R. B., Anandakrishnan, S., and Padman, L., 2003. Tidally controlled stick-slip discharge of a West Antarctic ice stream. *Science* v.301, p.1087-1089.
- Bockheim, J. G., Wilson, S. C., Denton, G. H., Andersen, B. G., and Stuiver, M., 1989. Late Quaternary ice-surface fluctuations of Hatherton Glacier, Transantarctic Mountains. *Quaternary Research* v.31, p.229-254.
- Bougamont, M., Tulaczyk, S., and Joughin, I., 2003. Numerical investigations of the slow-down of Whillans ice stream, West Antarctica; is it shutting down like Ice Stream C? *Annals of Glaciology* v.37, p.239-246.
- Carter, L., Dunbar, G., McKay, R. and Naish, T., 2007. Sedimentation and oceanography beneath the McMurdo Ice Shelf at Windless Bight, 2006. *Antarctic Data Series* v.32, Victoria University of Wellington, 31p.
- Clark, P. U., Mitrovica, J. X., Milne, G. A., and Tamisiea, M. E., 2002. Sea-level fingerprinting as a direct test for the source of global meltwater pulse IA. *Science* v.295, p.2438-2441.
- Conway, H., Hall, B. L., Denton, G. H., Gades, A. M., and Waddington, E. D., 1999. Past and future grounding-line retreat of the West Antarctic ice sheet: *Science* v.86, p.280-283.
- Craddock, C., 1970. *Antarctic Map Folio Series* v.12, 6p.
- Cunningham, W. L., Andrews, J. T., Jennings, A. E., Licht, K. J., and Leventer, A., 1999. Late Pleistocene-Holocene marine conditions in the Ross Sea, Antarctica; evidence from the diatom record. *The Holocene* v.9, p.129-139.
- Denton, G. H., and Hughes, T. J., 2002. Reconstructing the Antarctic ice sheet at the last glacial maximum: *Quaternary Science Reviews* v.21, p.193-202.
- Denton, G. H., and Marchant, D. R., 2000. The geologic basis for a reconstruction of a grounded ice sheet in McMurdo Sound, Antarctica, at the last glacial maximum: *Geografiska Annaler*. v.82(A), p.167-211.
- Dochat, T. M., Marchant, D. R., and Denton, G. H., 2000. Glacial geology of Cape Bird, Ross Island, Antarctica. *Geografiska Annaler*. v.82(A), p.237-247.
- Domack, E. W., and Harris, P. T., 1998. A new depositional model for ice shelves, based upon sediment cores from the Ross Sea and MacRobertson Shelf, Antarctica: *Annals of Glaciology* v.27, p.281-284.
- Domack, E. W., and Williams, C. R., 1990. Fine structure and suspended sediment transport in three Antarctic fjords. *Antarctic Research Series* v.50, p.71-89.
- Domack, E. W., Jacobson, E. A., Shipp, S., and Anderson, J. B., 1999. Late Pleistocene-Holocene retreat of the West Antarctic ice-sheet system in the Ross Sea; Part 2, Sedimentologic and stratigraphic signature. *Geological Society of America Bulletin* v.111, p.1517-1536.
- Dunbar, G. B., and Barrett, P. J., 2005. *Antarctic Data Series* v.24, Victoria University of Wellington, 55p.
- Dunbar, R. B., Anderson, J. B., Domack, E. W., and Jacobs, S. S., 1985. Oceanographic influences on sedimentation along the Antarctic continental shelf. *Antarctic Research Series* v.43, p.291-312.
- Fairbanks, R. G., 1989. A 17,000-year glacio-eustatic sea level record; influence of glacial melting rates on the Younger Dryas event and deep-ocean circulation: *Nature* v.342, 637-642.

- Fahnestock, M.A., Scambos, T.A., Bindshadler, R.A., Kvaran, G., 2000. A millennium of variable ice flow recorded by the Ross Ice Shelf, Antarctica. *Journal of Glaciology* v.46, p.652-664.
- Gordon, J. E., and Harkness, D.D., 1992. Magnitude and geographic variation of the radiocarbon content in Antarctic marine life; implications for reservoir corrections in radiocarbon dating. *Quaternary Science Reviews* v.11, p.697-708.
- Grobe, H., 1987. A simple method for the determination of ice-rafted debris in sediment cores. *Polarforschung* v.57, p.123-126.
- Hall, B.L., and Denton, G.H., 1999. New relative sea-level curves for the southern Scott Coast, Antarctica; evidence for Holocene deglaciation of the western Ross Sea. *Journal of Quaternary Science* v.14, p.641-650.
- Hall, B.L., Denton, G.H., Hendy, C.H., Denton, G.H., and Hall, B.L., 2000. Evidence from Taylor Valley for a grounded ice sheet in the Ross Sea, Antarctica: *Geografiska Annaler* v.82(A), p.275-303.
- Hambrey, M., Krissek, L., Powell, R., Barrett, P., Camerlenghi, A., Claps, M., Ehrmann, W., Fielding, C. R., Howe, J., and Woolfe, K., 1997. Cape Roberts Project Core Logging Manual. *Antarctic Data Series* v.21, Victoria University of Wellington, 89p.
- Horgan, H., Naish, T., Bannister, S., Balfour, N., and Wilson, G. S., 2005. Seismic stratigraphy of the Plio-Pleistocene Ross Island flexural moat-fill; a prognosis for ANDRILL Program drilling beneath McMurdo-Ross Ice Shelf. *Global and Planetary Change* v.45, p.83-97.
- Hughes, T., 1977. West Antarctic ice streams. *Reviews of Geophysics and Space Physics* v.15, p.1-46.
- Huybrechts, P., 2004. Antarctica: modelling. In Bamber, J.L. and Payne, A.J. (Eds), 2004. *Mass Balance of the Cryosphere*. Cambridge University Press, Cambridge, UK, p.491-523.
- IPCC, 2007. Working group I contribution to the IPCC fourth assessment report climate change 2007. The physical science basis. Cambridge University Press, UK. 365p.
- Joughin, I., Bindshadler, R. A., King, M. A., Voigt, D., Alley, R. B., Anandakrishnan, S., Horgan, H., Peters, L., Winberry, P., Das, S. B., and Catania, G., 2005. Continued deceleration of Whillans ice stream, West Antarctica. *Geophysical Research Letters* v.32, p.4.
- Joughin, I., and Tulaczyk, S., 2002. Positive mass balance of the Ross ice streams, West Antarctica. *Science* v.295, p.476-480.
- Joughin, I., Tulaczyk, S., Bindshadler, R., and Price, S. F., 2002. Changes in west Antarctic ice stream velocities; observation and analysis. *Journal of Geophysical Research* v.107, p.32.
- Kellogg, T.B., Hughes, T., and Kellogg, D.E., 1996. Late Pleistocene interactions of East and West Antarctic ice-flow regimes; evidence from the McMurdo Ice Shelf. *Journal of Glaciology* v.42, p.486-500.
- Korsch, R.J., 1974. Petrographic comparison of the Taylor and Victoria groups (Devonian to Triassic) in South Victoria Land, Antarctica. *New Zealand Journal of Geology and Geophysics* v.17, p.523-541.
- Kyle, P. R., 1990. McMurdo Volcanic Group, western Ross Embayment; introduction: *Antarctic Research Series* v.48, p.19-25.

- Leventer, A., 1998. The fate of Antarctic "sea ice diatoms" and their use as paleoenvironmental indicators. *Antarctic Research Series* v.73, p.121-137.
- Licht, K. J., and Andrews, J. T., 2002. The ^{14}C record of late Pleistocene ice advance and retreat in the central Ross Sea, Antarctica. *Arctic, Antarctic, and Alpine Research* v.34, p.324-333.
- Licht, K. J., Jennings, A. E., Andrews, J. T., and Williams, K. M., 1996. Chronology of late Wisconsin ice retreat from the western Ross Sea, Antarctica. *Geology* v.24, p.223-226.
- Licht, K. J., Cunningham, W. L., Andrews, J. T., Domack, E. W., and Jennings, A. E., 1998. Establishing chronologies from acid-insoluble organic ^{14}C dates on Antarctic (Ross Sea) and Arctic (North Atlantic) marine sediments. *Polar Research* v.17, p.203-216.
- Licht, K. J., Dunbar, N. W., Andrews, J. T., and Jennings, A. E., 1999. Distinguishing subglacial till and glacial marine diamictos in the western Ross Sea, Antarctica; implications for a last glacial maximum grounding line. *Geological Society of America Bulletin* v.111, p.91-103.
- MacAyeal, D. R., 1992. Irregular oscillations of the West Antarctic ice sheet. *Nature* v.359, p.29-32.
- Masson, V., Vimeux, F., Jouzel, J., Morgan, V., Delmotte, M., Ciais, P., Hammer, C., Johnsen, S., Lipenkov, V. Y., Mosley-Thompson, E., Petit, J.-R., Steig, E. J., Stievenard, M., and Vaikmae, R., 2000. Holocene climate variability in Antarctic based on 11 ice-core isotopic records. *Quaternary Research* v.54, p.348-358.
- McCrae, I.R., 1984. A summary of glaciological measurements made between 1960 and 1984 on the McMurdo Ice Shelf, Antarctica. Auckland. *School of Engineering Report* v.360, University of Auckland.
- Mercer, J. H., 1978. West Antarctic ice sheet and CO_2 greenhouse effect; a threat of disaster. *Nature* v.271, p.321-325.
- Mosola, A.B., and Anderson, J.B., 2006. Expansion and rapid retreat of the West Antarctic Ice Sheet in eastern Ross Sea: possible consequence of over-extended ice streams? *Quaternary Science Reviews* v.25, p.2177-2196.
- Naish, T.R., Powell, R.D., Levy, R.L., and the ANDRILL science team., 2007. AND-1B Initial Science Results, ANDRILL McMurdo Ice Shelf Project. *Terra Antarctica* v.14, p.121-328.
- Oppenheimer, M., 1998. Global warming and the stability of the West Antarctic Ice Sheet. *Nature* v.393, p.325-332.
- Robinson, N. and Pyne, A., 2004. Water Column Current Profile Analysis from beneath the McMurdo Ice Shelf at Windless Bight and under the sea ice in Granite Harbour, Antarctica. *Antarctic Data Series* v.26, Victoria University of Wellington. 30p.
- Scherer, R.P., 1994. A new method for the determination of absolute abundance of diatoms and other silt-sized sedimentary particles. *Journal of Paleolimnology* v.12, p.171-179.
- Shipp, S., Anderson, J. B., and Domack, E. W., 1999. Late Pleistocene-Holocene retreat of the West Antarctic ice-sheet system in the Ross Sea; Part 1, Geophysical results: *Geological Society of America Bulletin* v.111, p.1486-1516.
- Sjunneskog, C., and Scherer, R. P., 2005. Mixed diatom assemblages in glacial sediment from the central Ross Sea, Antarctica. *Palaeogeography, Palaeoclimatology, Palaeoecology* v.218, p.287-300.

- Smellie, J. L., 1998. Sand grain detrital modes in CRP-1; provenance variations and influence of Miocene eruptions on the marine record in the McMurdo Sound region: *Terra Antarctica* v.5, p.579-587.
- Steig, E. J., Hart, C. P., White, J. W. C., Cunningham, W. L., Davis, M. D., and Saltzman, E. S., 1998. Changes in climate, ocean and ice-sheet conditions in the Ross Embayment, Antarctica, at 6 ka. *Annals of Glaciology* v.27, p.305-310.
- Steig, E. J., Morse, D. L., Waddington, E. D., Stuiver, M., Grootes, P. M., Mayewski, P. A., Twickler, M. S., Whitlow, S. I., Denton, G. H., and Hall, B. L., 2000. Wisconsinan and Holocene climate history from an ice core at Taylor Dome, western Ross Embayment, Antarctica. *Geografiska Annaler* v.82(A), p.213-235.
- Stern, T. A., Davey, F. J., and Delisle, G., 1991. Lithospheric flexure induced by the load of Ross Archipelago, southern Victoria Land, Antarctica. In: Thomson, M. R. A., Crame, J. A., and Thomson, J. W., (eds.) *Geological Evolution of Antarctica*. Cambridge University Press, p.323-328.
- Stocker, T. F., 2003. South dials north: *Nature* v.424, p.496-497.
- Stuiver, M., Denton, G. H., Hughes, T. J., and Fastook, J. L., 1981. History of the marine ice sheet in West Antarctica during the last glaciation; a working hypothesis. In: Denton, G. H., and Hughes, T. J. (eds.), *The Last Great Ice Sheets*. John Wiley and Sons, New York.
- Taylor, J.C., 1991. Computer Programs for Standardless Quantitative Analysis of Minerals Using the Full Powder Diffraction Profile. *Powder Diffraction* v.6, p.2-9.
- ten Brink, U. S., Hackney, R. I., Bannister, S. C., Stern, T. A., and Makovsky, Y., 1997. Uplift of the Transantarctic Mountains and the bedrock beneath the East Antarctic ice sheet: *Journal of Geophysical Research* v.102, p.27,603-27,621.
- Weaver, A. J., Saenko, O. A., Clark, P. U., and Mitrovica, J. X., 2003. Meltwater pulse 1A from Antarctica as a trigger of the Bolling-Allerod warm interval. *Science* v.299, p.1709-1713.
- Whillans, I.M. and Merry, C.J., 1996. Kinematics of the shear zone between Ross Ice Shelf and McMurdo Ice Shelf, March 1996. *Internal Report to Antarctic Support Associates*, p.18.

2.11 Supplementary data: Core logs

SITE HWD03-1

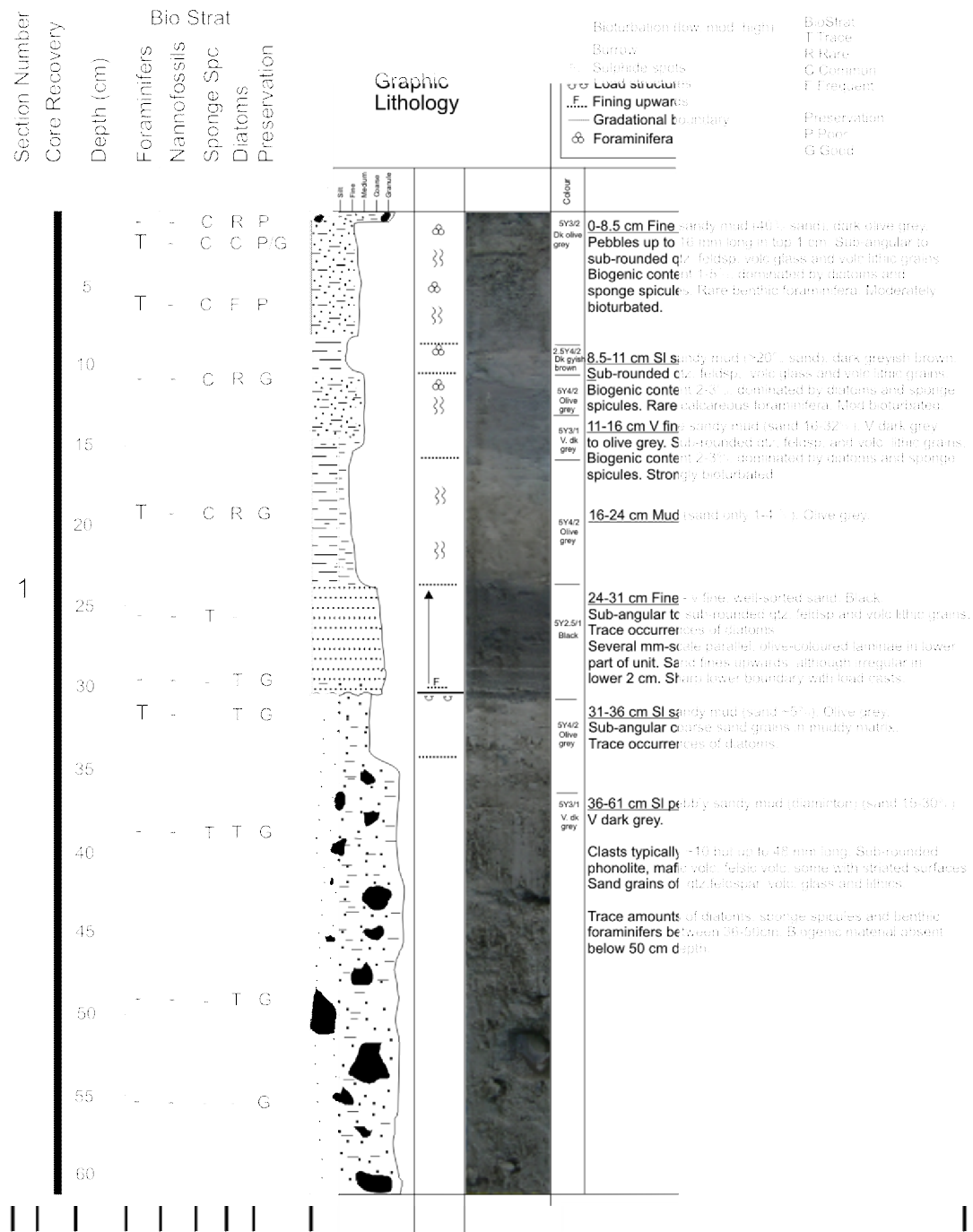
CORE #: 4
Total length (m) 0.61
Lat 77 53.308 S
Long 167 17.753 E
Water depth (m) 921

DATE: CORING/LOGGING

LOGGED BY: GG/GD
SCALE:

SHEET #: 1 of 1

REMARKS: grease used on
the inside of the liner to aid core recovery.
Core froze in storage.

Figure 21: Core log for HWD03-1 (from Barrett *et al.*, 2005).

SITE HWD03-2

CORE #: 4

Total length (m) 0.62

Lat 77°50.111 S

Long 167°20.209 E

Water depth (m) 923

DATE: CORING/LOGGING 29-1-03

LOGGED BY: GG/GD

SCALE:

SHEET #: 1 of 1

REMARKS: Grease used on the inside of the liner to aid core recovery. Core froze in storage.

Section Number	Core Recovery	Depth (cm)	Bio Strat					Graphic Lithology	Colour	Description
			Foraminifers	Nannofossils	Sponge Spc	Diatoms	Preservation			
1		5	-	-	C	C	G	Py	5Y4/2 Olive grey	0-3 cm V fine sandy mud (sand ~40%). Olive grey. Subangular pebbles to 16 mm long in top 1 cm. Sand and silt fraction is subangular to subrounded qtz, feldsp with volc lithic fragments and rare volc glass. Visible biogenic silica 2-5%, mostly round and elongate diatoms and sponge spicules. Moderately bioturbated. Occasional 1-2 mm black sulphide? "blebs"
		10	-	-	C	C	G	Py	5Y5/1 grey	3-5 cm Irregular, bioturbated contact 7 cm sponge spicule-filled lens up to 20 mm in length
		15	-	-	C	C	G	Py	10Y5/1 Greenish grey	slightly stiffer layer
		20	-	-	C	C	G	Py	10Y4/1 Dk greenish grey	5-58 cm SI v fine sandy mud (sand 3-12%). Grey to dark greenish grey.
		25	-	-	C	C	G	Py	10Y4/1 Dk greenish grey	Subangular to subrounded qtz, feldsp, heavy minerals. Variable biogenic silica in the mud fraction, predominantly diatoms and sponge spicules with some silicoflagellates (est 10% at 7 cm, 3% at 13 cm, 6% at 30 cm and 1% at 61cm). Highly bioturbated with burrows, spicule-filled lenses up to 10 mm in diameter and 50 mm in length.
		30	-	-	C	C	G	Py	10Y4/1 Dk greenish grey	
		35	-	-	C	C	G	Py	10Y4/1 Dk greenish grey	
		40	-	-	C	C	G	Py	10Y4/1 Dk greenish grey	
		45	-	-	C	C	G	Py	10Y4/1 Dk greenish grey	
		50	-	-	C	C	G	Py	10Y4/1 Dk greenish grey	
		55	-	-	C	C	G	Py	10Y4/1 Dk greenish grey	
		60	-	-	R	R	G	Py	10Y4/1 Dk greenish grey	58-59 cm gradational contact 59-62 cm SI pebbly sl sandy mud. Dark greenish grey. Common sub-angular granules and rare clasts up to 16 mm long in a muddy matrix.

Figure 22: Core log for HWD03-2 (from Barrett *et al.*, 2005).




SITE Windless Bight							DATE: CORING/LOGGING 15-02-06/04-04-06			
CORE #8							LOGGED BY: RM/GD			
Total length (m) 0.34							REMARKS:			
Lat 77.9168°S							Samples taken for C14 dating at 0.5-2.5cm and 31-32.5cm. Grain size and petrology samples taken every 2cm (eg, 0-2cm, 2-4cm, etc). Core froze in storage.			
Long 167.309°E										
Water depth (m) 841							SHEET #: 1 of 1			
Section Number	Core Recovery	Depth (cm)	Bio Strat				Firmness	Graphic Lithology	Colour	
			Foraminifers	Nannofossils	Sponge spc	Diatoms	Preservation			Biostrat T Trace R Rare C Common F Frequent Preservation P Poor G Good
										Description
1		0	R	-	F	T	P/G			0-2.5 cm Medium sand (sand ~60%) moderately sorted silty med sand with abundant sponge spicules (~10mm in length, fibrous). Sand fraction includes subangular to well-rounded quartz. Approximately 50% quartz and feldspar, 50% volcanic lithics. No bedding evident.
			R	-	C	R	P/G			2.5-3.5cm gradational, undulating contact.
			T	-	-	T	P/G			3.5-27cm Sandy mud (sand ~20-40%) Sandy mud with grains up to 1mm common. Occasional pebbles up to 10 mm in length. No bedding evident. Includes well-rounded quartz. No fossil/spicules.
		10	T	-	-	-	-			6-8cm - volcanic pebble, 25mm length. 21-22cm - volcanic pebble, 10mm length.
			-	-	-	-	-			
		20	-	-	-	-	-			
			-	-	-	-	-			
			-	-	-	-	-			
		30	-	-	-	-	-			
			-	-	-	-	-			
									27cm gradational contact 27-32cm Pebbly sandy mud (sand ~40%) V.poorly sorted with pebbles up to 10mm in length.	
									32-34cm Pebbly sandy mud (sand ~40%)V.poorly sorted, noticeably stiffer than above layers. Sand fraction includes subangular to well-rounded quartz and feldspar (~50%). Subrounded basalt pebbles (up to 35mm in length) with striated surfaces, keels and horizontally aligned facets (facing upwards).	
		40						Firm		

Figure 23: Core log for HWD06.

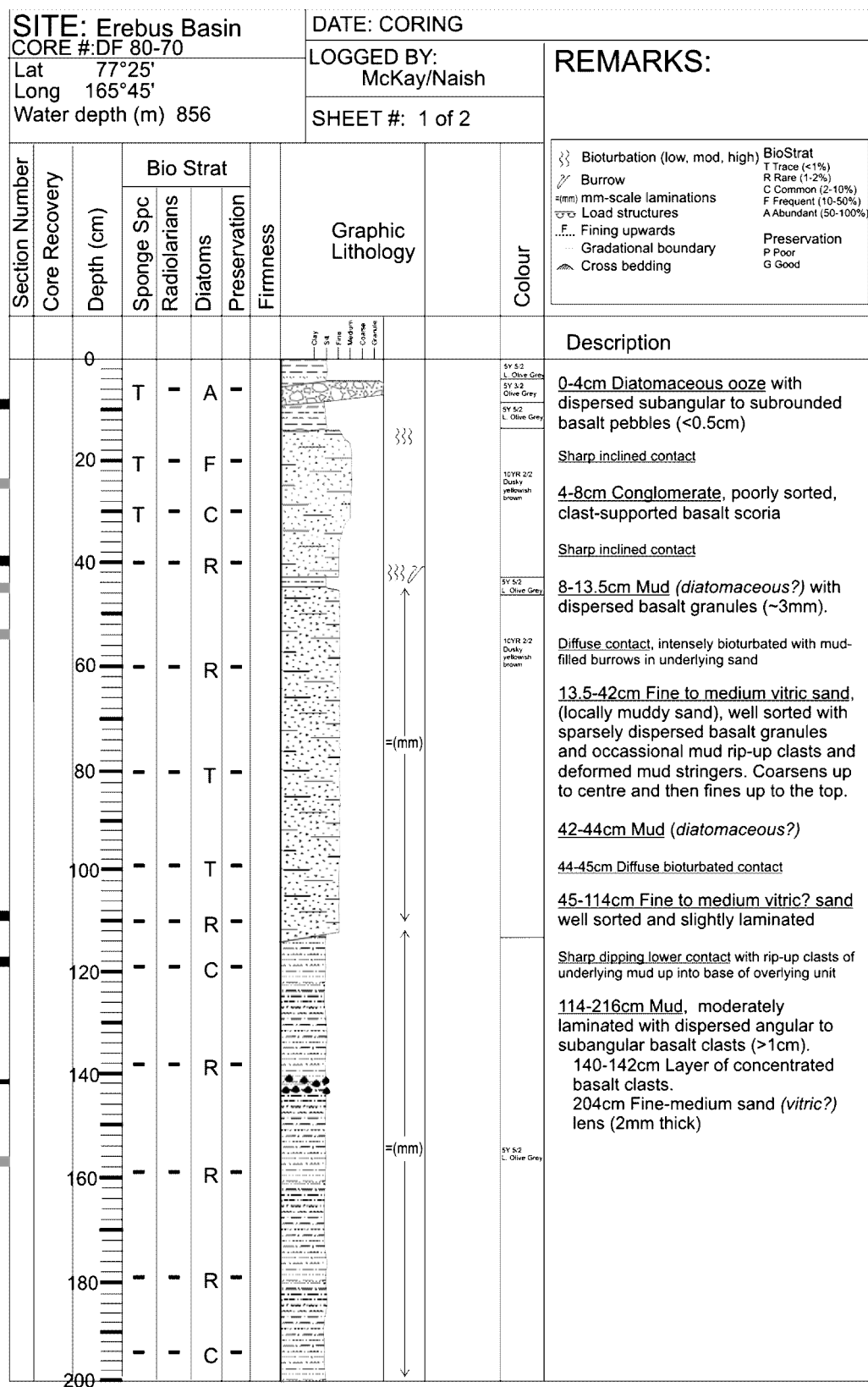


Figure 24: Core log for DF80-70

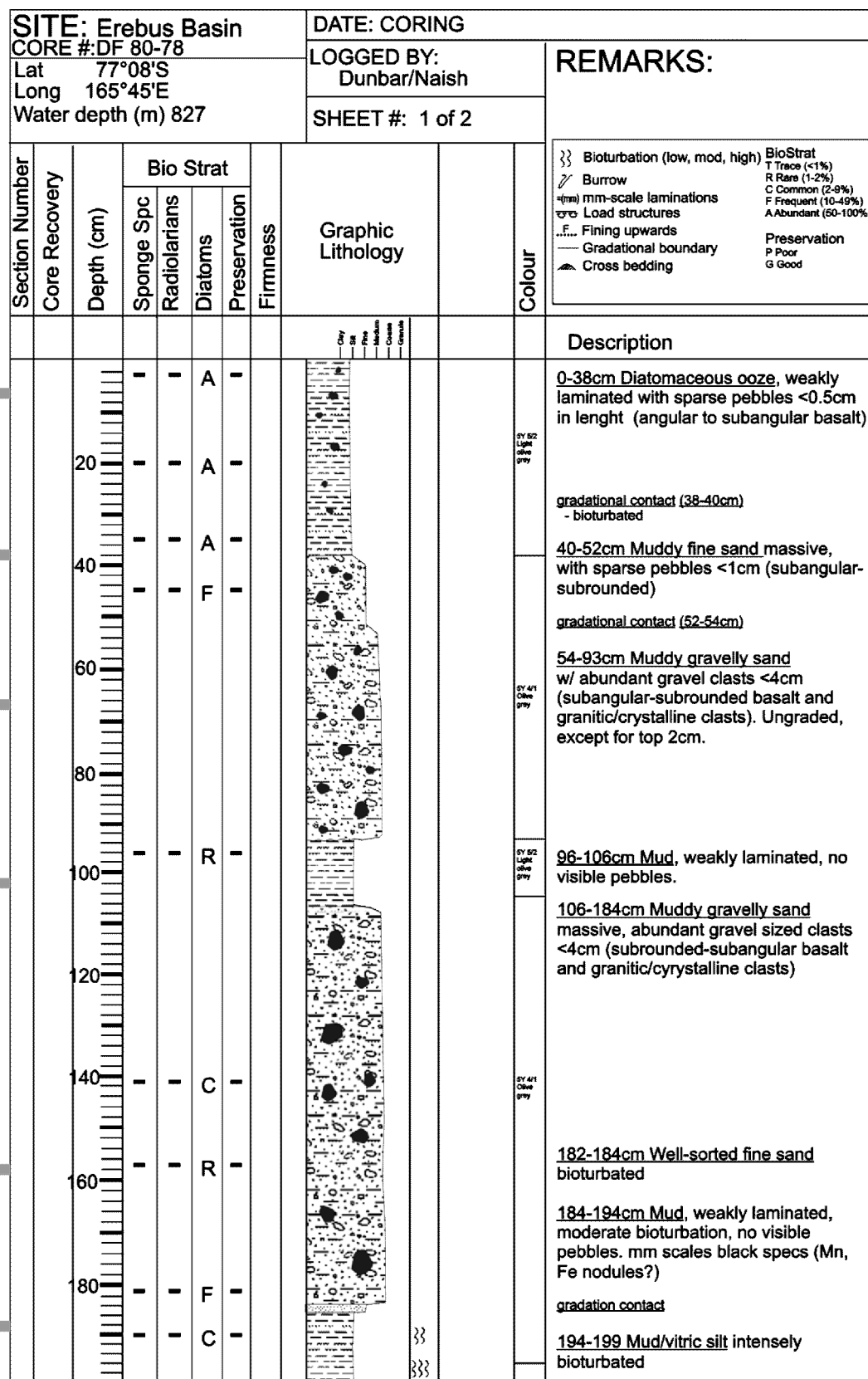


Figure 25: Core log for DF80-78.

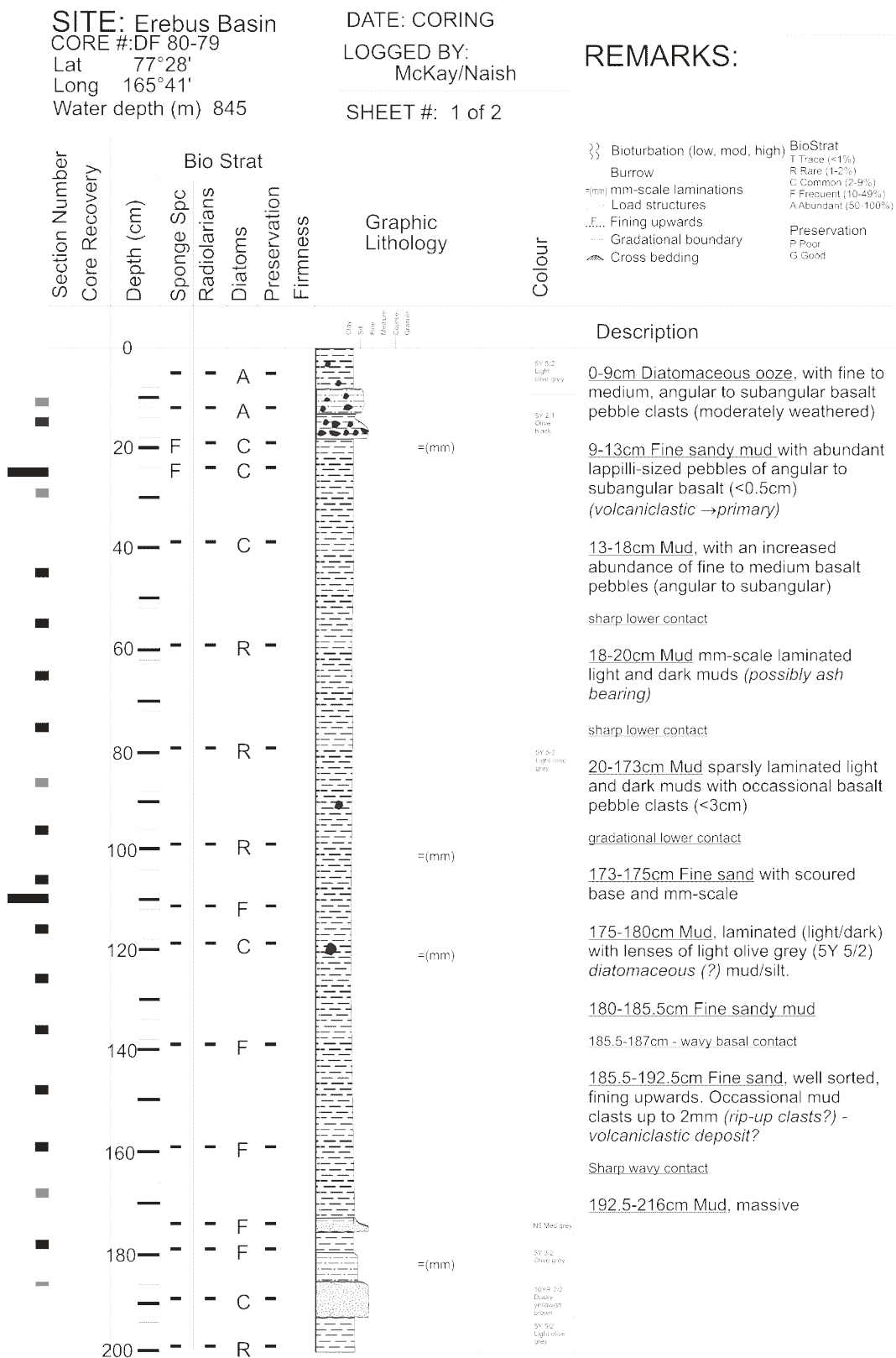


Figure 26: Core log for DF80-79.

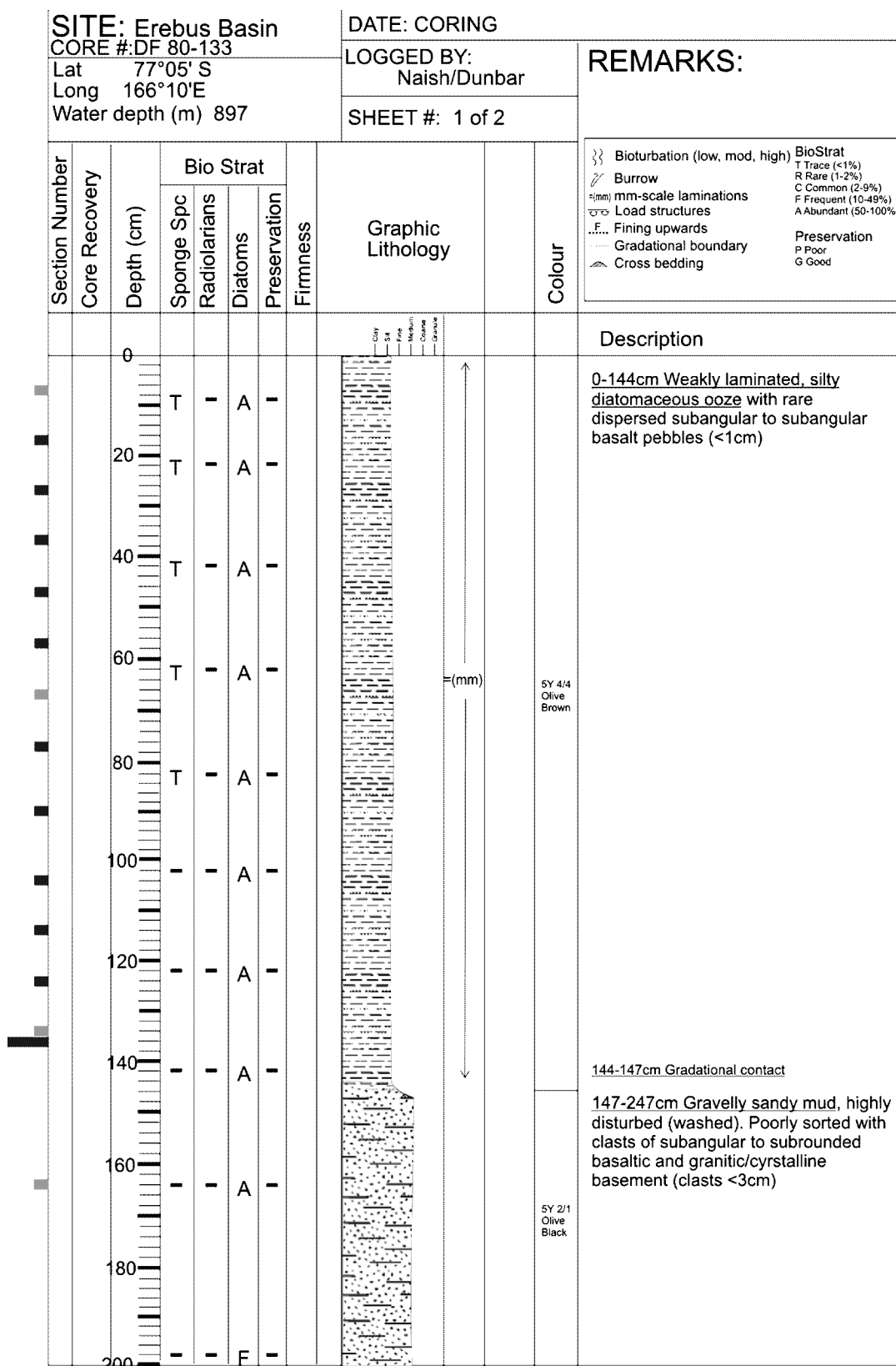


Figure 27: Core log for DF80-133.

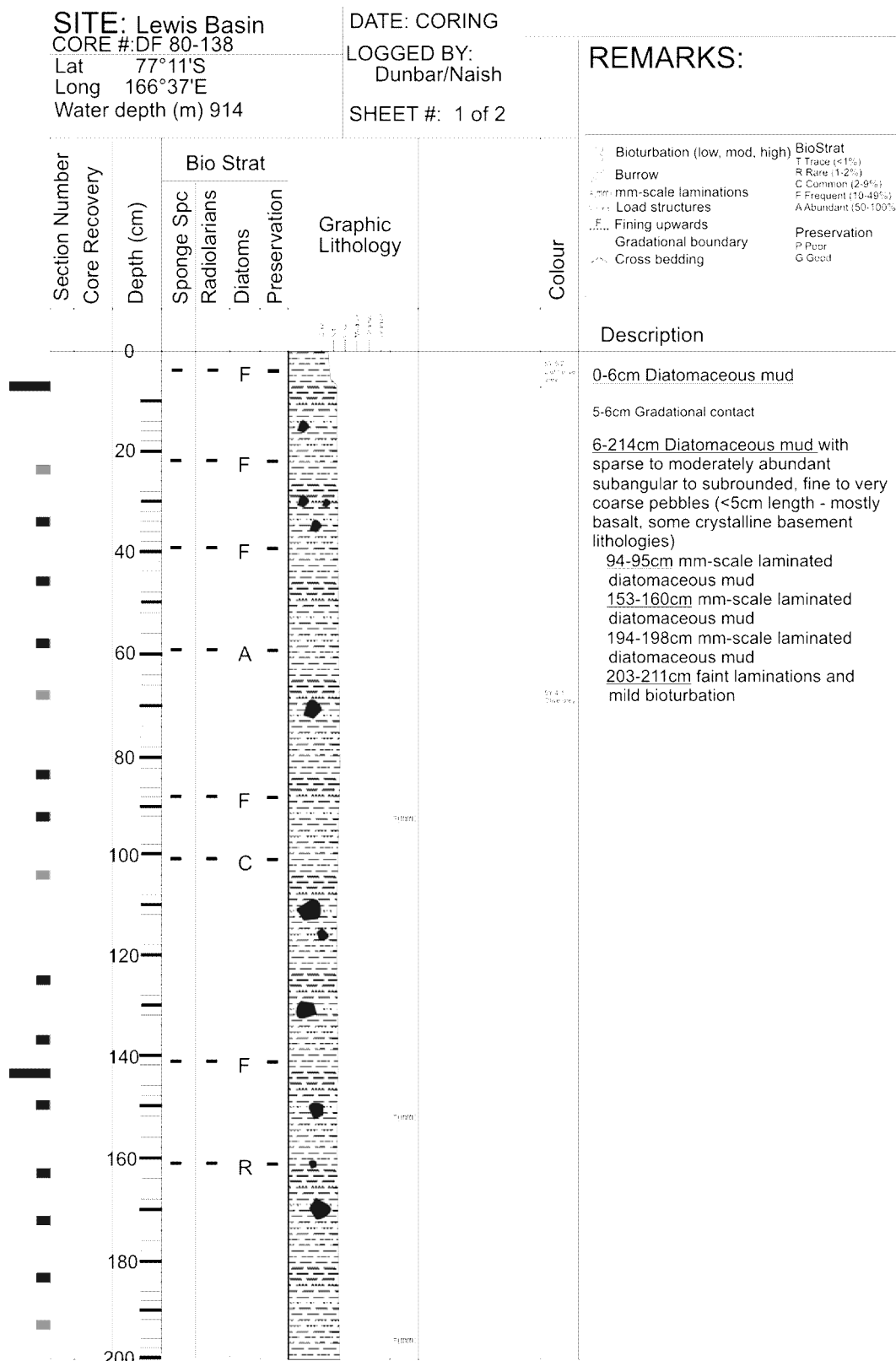


Figure 28: Core log for DF80-138

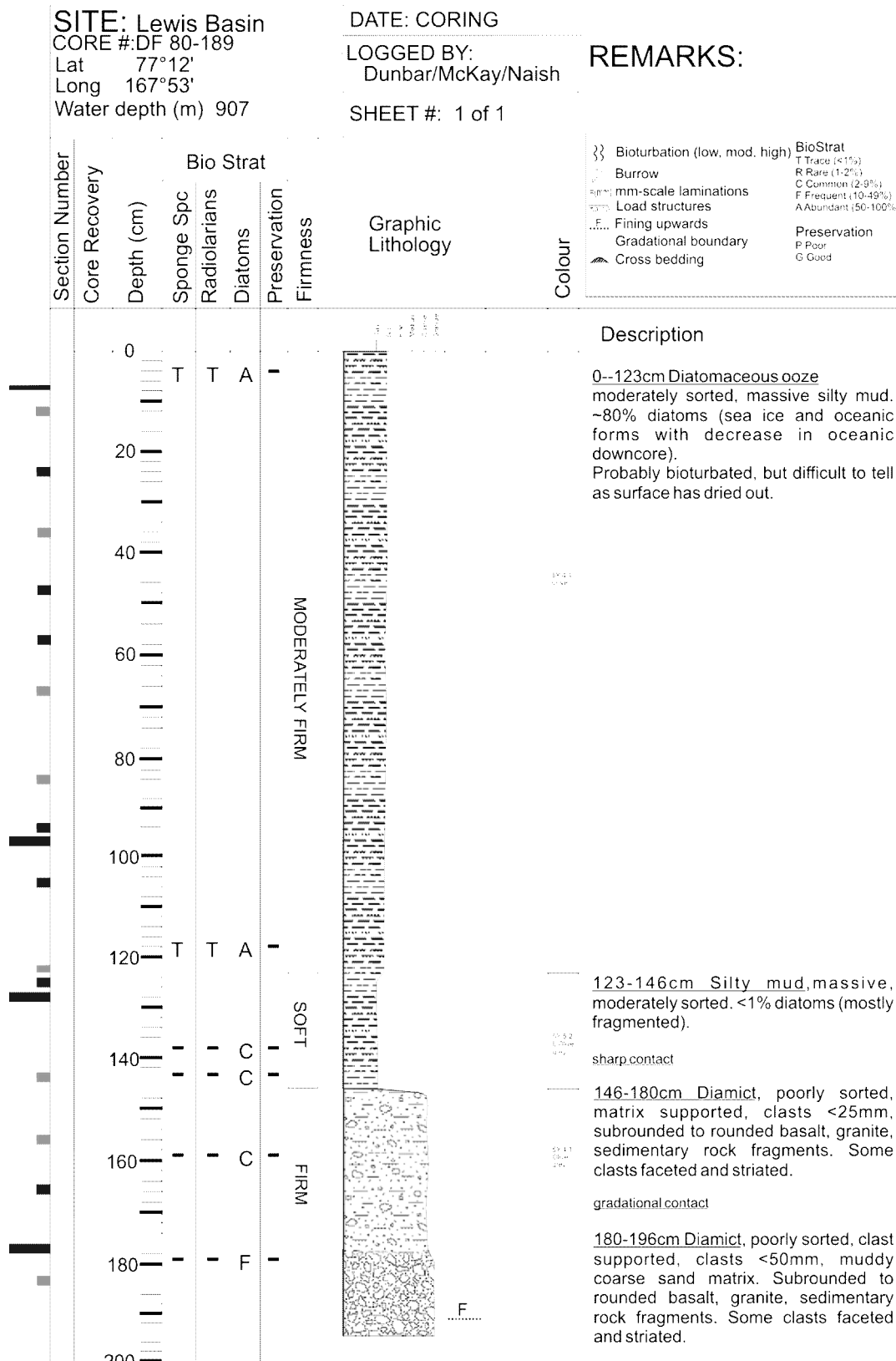


Figure 29: Core log for DF80-189.

2.12 Supplementary data: X radiographs

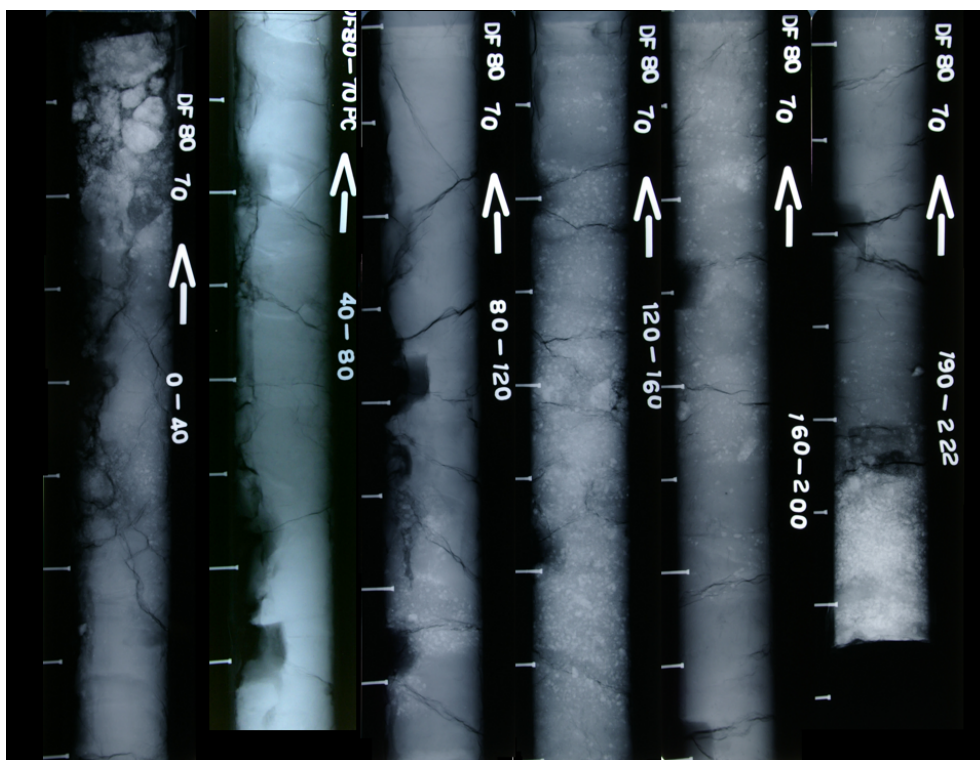


Figure 30: X-radiograph for DF80-70.

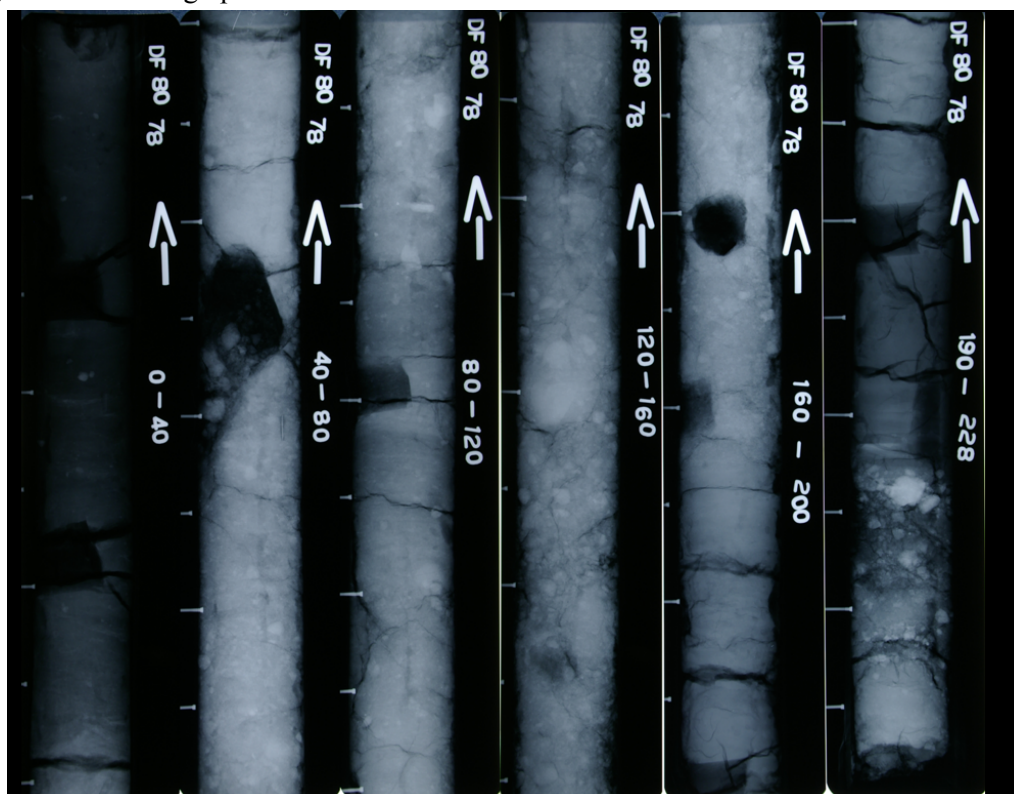


Figure 31: X-radiograph for DF80-78.

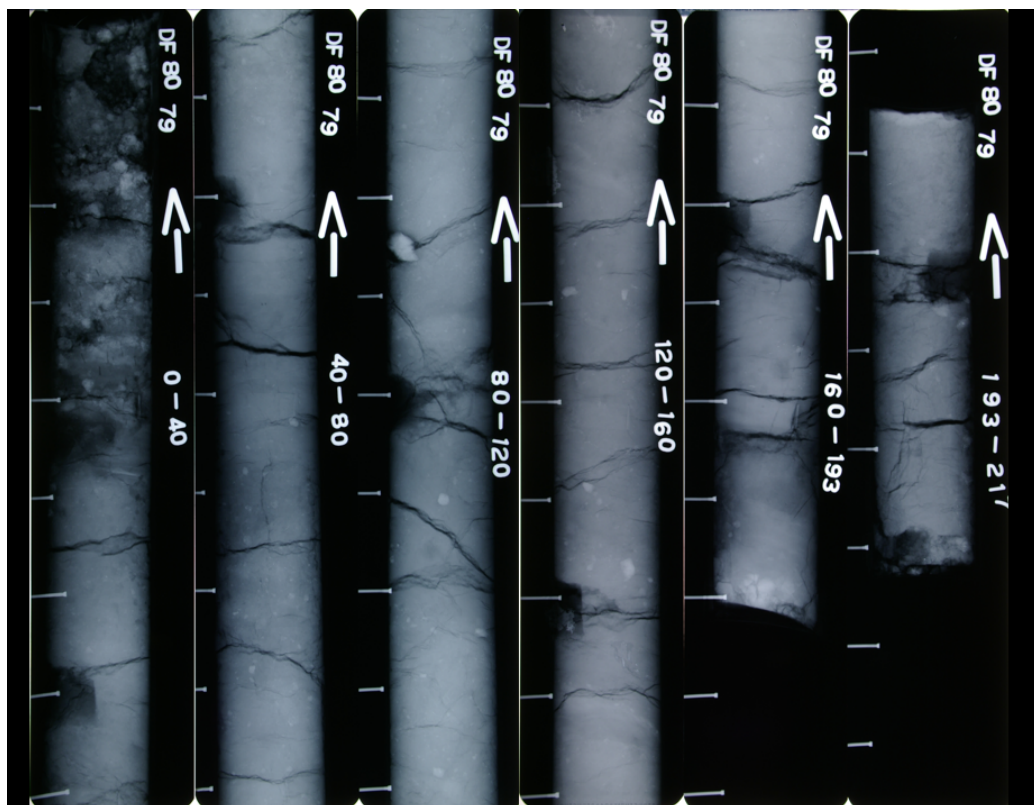


Figure 32: X-radiograph for DF80-79.

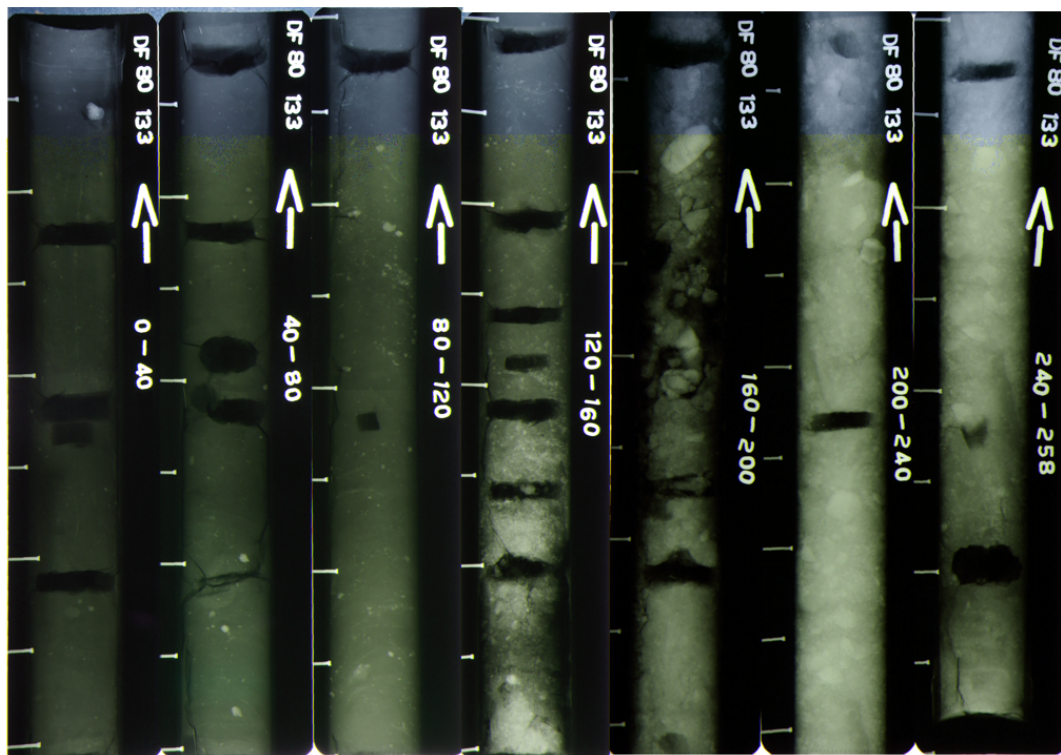


Figure 33: X-radiograph for DF80-133.

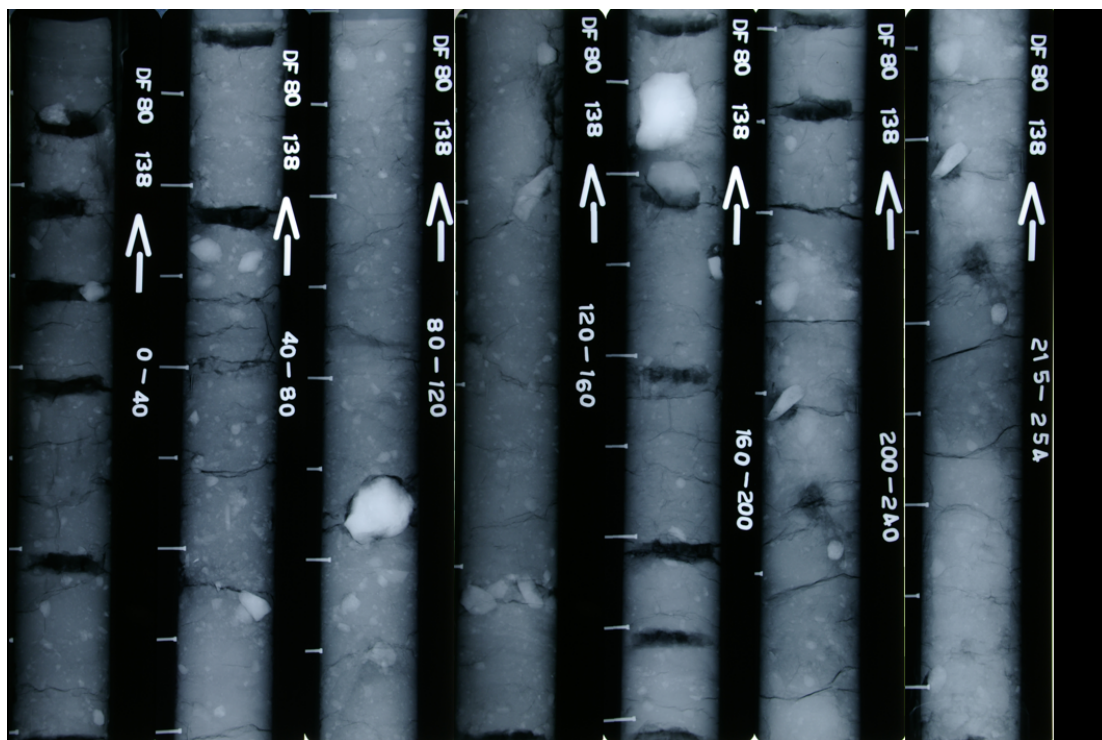


Figure 34: X-radiograph for DF80-138.

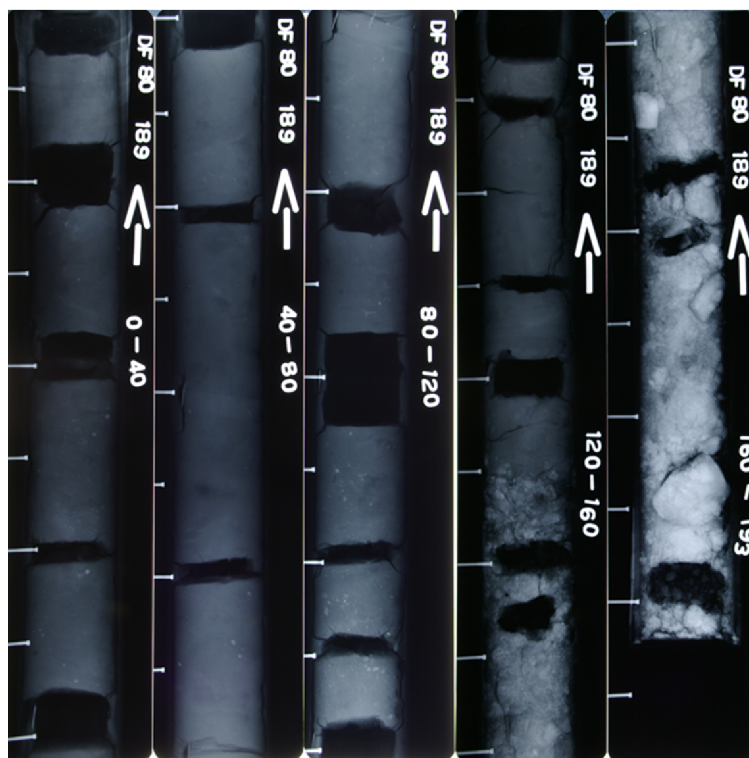


Figure 35: X-radiograph for DF80-189.

2.13 Supplementary data: Grain size results

SUMMARY DATA

Frequency

Class midpts	-2.00	-1.25	-0.75	-0.25	0.25	0.75	1.25	1.75	2.25	2.75	3.25	3.75	4.25	4.75	5.25	5.75	6.25	6.75	7.25	7.75	8.25	8.75	9.25	9.75	12.50
Class limits	-1.50	-1.00	-0.50	0.00	0.50	1.00	1.50	2.00	2.50	3.00	3.50	4.00	4.50	5.00	5.50	6.00	6.50	7.00	7.50	8.00	8.50	9.00	9.50	10.0	Rest
HWD06 (0-2cm)	4.81	4.17	5.73	4.15	4.83	7.36	8.06	8.97	9.20	8.66	7.13	5.80	2.48	1.65	1.76	1.46	1.34	1.04	0.94	0.98	0.80	0.64	0.68	0.54	6.84
HWD06 (2-4cm)	2.56	3.18	3.52	4.20	4.39	5.87	7.27	8.46	8.64	7.98	6.27	6.16	2.14	1.56	2.02	1.81	1.78	1.50	1.62	1.75	1.41	1.38	1.35	0.98	12.20
HWD06 (4-6cm)	1.57	1.73	1.24	1.70	2.40	3.41	3.84	4.43	4.76	5.99	5.90	5.46	2.01	2.09	2.91	2.56	3.08	2.91	2.79	4.25	3.14	2.91	2.68	3.14	23.10
HWD06 (6-8cm)	1.23	0.60	1.12	0.86	1.52	1.99	2.70	3.10	3.44	4.33	4.59	5.23	1.94	1.87	3.87	2.77	4.01	3.11	3.04	3.74	3.53	3.11	2.70	2.42	33.20
HWD06 (8-10cm)	1.96	2.33	2.18	2.63	2.56	2.19	2.63	2.81	3.03	3.88	4.03	4.38	2.63	1.77	2.47	3.52	2.73	3.65	2.99	3.91	2.80	2.93	2.73	1.89	31.38
HWD06 (10-12cm)	1.70	1.47	1.09	1.32	1.79	2.10	2.75	3.18	3.42	4.05	4.15	4.38	2.46	2.18	3.06	3.40	3.94	3.53	3.94	4.35	4.42	4.01	3.74	3.87	25.69
HWD06 (12-14cm)	0.98	0.00	0.88	0.80	0.95	1.24	1.49	1.94	2.28	2.99	3.37	4.06	1.77	2.47	4.17	4.01	4.72	3.77	5.03	4.56	4.40	3.38	2.91	0.94	36.88
HWD06 (14-16cm)	0.43	0.36	1.44	1.12	1.28	1.71	2.31	2.67	3.02	3.80	4.10	4.68	2.95	1.89	3.25	3.32	4.04	3.32	3.97	4.55	4.69	4.11	4.19	3.97	28.80
HWD06 (16-18cm)	0.43	0.25	0.94	0.98	1.59	1.94	2.10	2.52	2.86	3.75	4.13	4.84	2.77	3.05	2.96	3.18	3.83	3.54	3.90	4.62	4.48	4.26	3.90	2.82	30.39
HWD06 (18-20cm)	1.70	1.06	0.99	0.87	0.91	1.40	1.69	2.06	2.26	2.90	3.25	3.89	2.48	2.23	2.12	3.34	3.19	3.49	3.34	4.48	3.79	3.72	3.26	2.96	38.62
HWD06 (20-22cm)	0.00	1.74	1.68	1.46	1.41	1.70	2.08	2.31	2.68	3.47	4.16	5.11	2.33	2.38	2.98	3.05	2.70	3.62	3.41	3.83	3.26	2.91	2.55	3.41	35.76
HWD06 (22-24cm)	0.00	0.47	1.42	1.56	1.95	2.36	3.02	3.52	4.03	4.93	5.30	6.25	2.68	2.76	2.81	3.07	3.00	3.13	3.39	3.83	4.09	3.71	3.64	4.15	24.93
HWD06 (24-26cm)	0.00	4.96	0.47	0.60	0.57	0.71	0.93	1.26	1.62	2.29	2.78	4.01	2.82	2.80	3.95	4.42	5.21	4.34	3.95	4.26	3.95	2.60	2.53	4.42	34.57
HWD06 (26-28cm)	2.14	0.72	0.96	1.11	1.31	1.59	1.90	2.28	2.64	3.70	4.76	5.86	3.12	2.85	3.33	4.37	4.99	3.81	4.23	3.60	3.33	2.56	2.29	2.63	29.93
HWD06 (28-30cm)	0.62	1.39	1.21	2.27	2.30	2.52	2.91	3.44	3.80	4.73	5.01	5.93	3.16	3.63	4.27	4.78	4.34	2.95	3.21	3.14	2.26	2.14	1.89	0.82	27.28
HWD06 (30-32cm)	2.21	0.60	1.58	1.63	1.51	2.26	2.98	3.90	4.55	5.68	6.57	7.23	3.39	2.48	3.18	3.64	3.59	2.72	2.95	3.18	2.60	2.08	1.91	1.00	26.58
HWD06 (32-34cm)	1.85	3.34	2.82	2.17	2.81	2.88	3.34	3.64	3.80	4.35	5.12	6.89	3.25	2.10	2.59	2.48	2.86	2.64	2.59	2.70	2.37	2.20	2.04	1.49	27.70
DF80-189 (11-13cm)	0.00	0.00	0.00	0.17	0.14	0.05	0.09	0.20	0.25	0.66	1.55	3.29	2.09	5.31	7.81	5.67	6.23	5.02	5.58	6.42	5.49	3.35	3.07	8.00	29.57
DF80-189 (23-25cm)	0.00	0.00	0.00	0.19	0.08	0.06	0.08	0.09	0.14	0.36	1.13	2.54	3.32	3.34	4.93	3.88	4.26	5.87	5.02	6.63	6.06	5.31	5.31	6.54	34.87
DF80-189 (35-37cm)	0.00	0.00	0.00	0.00	0.33	0.22	0.59	0.39	0.31	0.53	1.00	2.40	3.50	3.35	5.86	5.29	7.27	6.71	5.48	6.33	5.57	5.95	5.29	0.66	32.96
DF80-189 (46.5-48.5cm)	0.00	0.00	0.00	0.00	0.00	0.00	0.04	0.04	0.00	0.13	0.32	1.15	2.72	1.90	2.24	5.07	4.20	4.49	5.27	6.64	6.83	6.44	5.47	3.90	43.14
DF80-189 (56-58cm)	0.00	0.00	0.00	0.00	0.03	0.00	0.00	0.06	0.02	0.10	0.18	1.00	1.36	3.12	4.65	3.88	4.85	5.14	5.33	6.79	6.69	6.01	6.11	6.11	38.58
DF80-189 (66-68cm)	0.00	0.70	0.66	0.00	0.06	0.04	0.10	0.09	0.26	0.59	1.36	3.51	3.46	2.71	2.71	5.88	6.60	6.87	6.33	8.05	5.97	4.79	4.97	5.06	29.21
DF80-189 (83-85cm)	0.00	0.00	0.00	0.23	0.05	0.06	0.12	0.12	0.12	0.36	0.86	2.40	1.33	4.15	5.55	6.79	6.31	6.22	5.84	7.17	5.84	5.17	4.78	3.64	32.91
DF80-189 (93-95cm)	0.00	0.00	0.00	0.15	0.11	0.24	0.20	0.13	0.14	0.33	0.67	1.41	1.59	2.06	4.92	5.90	4.72	5.90	5.41	6.20	5.41	5.21	4.82	3.74	40.73
DF80-189 (104-106cm)	0.00	0.00	0.00	0.05	0.04	0.03	0.10	0.18	0.40	0.44	0.82	1.48	0.36	3.33	5.39	5.39	5.49	6.47	5.88	7.45	5.69	6.08	5.59	5.39	33.93
DF80-189 (124-126cm)	0.00	0.00	0.00	0.14	0.23	0.55	0.38	0.40	0.69	0.88	1.10	1.68	1.07	1.93	1.68	2.43	3.36	3.27	4.02	6.54	5.61	5.14	4.58	2.15	52.15
DF80-189 (143.5-145.5cm)	0.00	0.00	0.00	0.00	0.02	0.17	0.08	0.13	0.18	0.28	0.65	1.17	0.65	1.12	1.93	3.28	3.86	3.57	4.15	6.27	5.79	5.30	4.73	5.30	51.40
DF80-189 (155-157cm)	9.63	8.90	7.21	6.70	7.88	7.91	8.79	8.26	6.13	3.14	1.72	1.48	0.99	0.68	0.90	0.75	1.17	1.13	1.25	1.46	1.40	1.31	1.19	0.79	9.23
DF80-189 (164.5-166.5cm)	6.59	6.73	7.19	7.46	10.3	14.1	12.0	9.23	6.09	2.79	1.44	1.17	0.71	0.32	0.68	0.50	0.49	0.77	0.89	1.08	0.80	0.77	0.82	0.10	6.84

SUMMARY DATA

Frequency

Class midpts	-2.00	-1.25	-0.75	-0.25	0.25	0.75	1.25	1.75	2.25	2.75	3.25	3.75	4.25	4.75	5.25	5.75	6.25	6.75	7.25	7.75	8.25	8.75	9.25	9.75	12.50
Class limits	-1.50	-1.00	-0.50	0.00	0.50	1.00	1.50	2.00	2.50	3.00	3.50	4.00	4.50	5.00	5.50	6.00	6.50	7.00	7.50	8.00	8.50	9.00	9.50	10.0	Rest
DF80-189 (182-184cm)	10.9	4.34	7.37	9.98	10.0	14.8	13.3	9.50	5.78	2.61	1.28	1.07	0.32	0.13	0.07	0.02	0.68	0.54	0.37	0.77	0.66	0.40	0.47	0.27	4.17
DF80-133 (6-8cm)	0.00	0.00	0.00	0.00	0.00	0.16	0.10	0.12	0.17	0.35	0.49	1.44	3.54	4.85	8.26	4.04	4.28	3.79	6.10	6.11	6.84	3.60	5.17	5.10	35.48
DF80-133 (26-28cm)	0.00	0.00	0.00	0.00	0.05	0.14	0.19	0.23	0.16	0.20	0.49	0.65	0.49	3.42	4.68	5.07	4.09	4.48	6.82	7.60	6.82	6.24	5.17	5.95	37.04
DF80-133 (46-48cm)	0.00	0.00	0.00	0.11	0.03	0.07	0.08	0.13	0.09	0.13	0.29	0.61	1.95	4.32	3.87	4.45	4.35	4.83	5.99	7.93	6.67	6.38	6.67	5.61	35.47
DF80-133 (66-68cm)	0.00	1.28	1.21	0.00	0.11	0.07	0.18	0.17	0.47	1.07	2.48	6.40	8.57	8.60	9.54	6.74	4.88	3.50	5.47	4.25	5.69	4.01	3.04	4.41	17.86
DF80-133 (89-91cm)	0.00	0.00	0.00	0.09	0.32	0.40	0.42	0.36	0.30	0.54	0.62	1.54	0.82	4.11	7.57	5.73	6.21	5.92	6.89	7.67	6.21	5.63	3.88	9.03	25.72
DF80-133 (113-115cm)	0.00	0.00	0.39	0.22	0.05	0.28	0.39	0.35	0.35	0.49	0.54	1.10	0.69	3.01	5.71	4.57	5.81	4.85	7.04	6.66	6.47	5.71	5.62	9.33	30.36
DF80-133 (133-135cm)	0.00	0.00	0.48	0.00	0.41	0.59	0.65	0.96	1.33	2.64	0.97	1.27	0.76	1.78	3.19	5.48	4.93	5.75	5.57	7.21	7.03	5.93	5.38	2.65	35.04
DF80-133 (163-165cm)	0.34	3.34	3.14	3.41	5.49	8.83	13.9	14.1	10.2	7.21	4.80	4.08	1.55	0.96	1.05	1.39	1.13	0.99	1.39	1.61	1.31	1.27	1.11	1.07	6.42
DF80-133 (247-249cm)	0.37	0.70	0.86	1.33	1.98	2.49	3.25	4.18	6.50	11.4	12.1	9.58	3.43	2.09	1.73	2.25	2.29	2.16	2.42	3.35	2.89	2.38	2.29	4.71	13.24
DF80-79 (10-12cm)	2.29	0.72	2.68	3.55	3.98	6.60	8.36	8.30	7.29	6.33	5.00	5.53	2.71	2.34	2.59	2.88	2.62	3.48	2.17	2.77	2.32	2.39	1.61	2.39	9.12
DF80-79 (18-19cm)	0.00	0.66	0.22	0.55	0.73	0.52	0.76	0.78	0.89	0.87	0.58	1.75	1.06	2.60	2.56	2.47	2.56	2.28	2.28	2.92	3.38	3.01	3.29	1.92	61.36
DF80-79 (28-30cm)	0.00	0.00	0.00	0.27	0.34	0.32	0.34	0.33	0.42	1.11	2.15	6.19	5.70	5.32	4.89	4.52	5.34	3.94	4.19	4.52	4.60	4.68	4.27	2.71	33.84
DF80-79 (54-56cm)	0.00	0.00	0.00	0.00	0.00	0.00	0.05	0.08	0.09	0.20	0.81	3.40	2.63	3.82	4.58	4.48	5.92	5.92	6.49	8.20	7.82	7.16	6.01	7.63	24.71
DF80-79 (74-76cm)	0.00	0.00	0.22	0.15	0.14	0.14	0.25	0.23	0.28	0.44	0.82	1.89	0.71	2.63	5.06	5.15	5.63	4.96	6.01	6.20	6.87	5.54	5.44	6.11	35.12
DF80-79 (85-87cm)	0.00	0.00	0.53	0.36	0.25	0.18	0.26	0.30	0.39	0.58	1.01	3.26	3.54	2.71	4.65	7.20	5.47	5.93	6.56	6.29	6.29	5.84	5.11	8.21	25.07
DF80-79 (105-107cm)	0.00	0.25	0.00	0.06	0.04	0.10	0.09	0.11	0.13	0.23	0.33	1.36	1.27	0.07	0.78	5.47	4.78	4.98	6.35	8.10	8.88	7.71	7.52	7.71	33.68
DF80-79 (125-127cm)	0.00	0.00	0.00	0.19	0.15	0.25	0.35	0.43	0.46	0.65	1.09	1.92	2.36	3.51	4.77	4.68	5.33	4.21	5.70	7.39	5.89	5.99	5.14	4.77	34.79
DF80-79 (147-149cm)	0.00	0.00	0.27	0.24	0.17	0.15	0.20	0.21	0.24	0.35	0.59	1.44	0.82	1.98	4.50	4.60	4.50	6.04	5.17	6.42	5.17	5.65	4.22	2.01	45.03
DF80-79 (158-160cm)	0.00	0.00	0.00	0.35	0.04	0.10	0.19	0.22	0.28	0.30	0.44	0.55	1.43	3.46	6.44	8.79	8.30	6.25	6.64	6.83	5.76	5.08	4.69	2.34	31.53
DF80-79 (167-169cm)	0.00	0.00	0.00	0.15	0.20	0.28	0.49	0.56	0.63	0.87	1.02	1.73	1.74	4.65	7.14	6.58	6.86	5.38	5.56	6.03	5.28	4.36	4.82	3.52	32.17
DF80-79 (177-179cm)	0.00	0.36	0.00	0.00	0.03	0.01	0.02	0.01	0.02	0.06	0.26	1.04	0.39	0.98	2.15	2.34	3.71	4.10	6.25	5.76	6.44	6.15	6.05	2.54	51.35
DF80-79 (185-186cm)	0.00	0.00	0.00	0.00	0.04	0.07	0.04	0.05	0.32	3.47	8.75	9.00	4.63	2.81	4.78	3.43	3.66	3.73	4.78	5.30	4.93	4.78	4.10	1.57	29.77
DF80-79 (194-196cm)	0.00	0.00	0.00	0.00	0.00	0.01	0.02	0.01	0.02	0.09	0.43	0.54	0.66	0.20	0.79	1.19	1.98	3.17	4.55	6.03	7.52	8.01	7.62	6.53	50.64
DF80-79 (209-211cm)	0.00	0.00	0.00	0.04	0.01	0.00	0.01	0.00	0.01	0.05	0.15	0.20	0.69	1.26	1.26	3.89	5.88	6.72	9.45	10.4	11.1	9.35	7.98	8.93	22.58

Table 3: Grain size results for HWD06 and DF80 cores. Note: results for HWD03-1 and HWD03-2 are available in Barrett *et al.*, 2005.

2.14 Supplementary data: Grain size statistics

	Percentiles								Moment measures				Graphic (Folk)				Inman		Proportions			
	1%	5%	16%	25%	50%	75%	84%	95%	Mean	StDev	Skew	Kurt	Mean	StDev	Skew	Kurt	StDev	Skew	Gravel	Sand	Silt	Clay
HWD06 (0-2cm)	-2.53	-1.47	-0.34	0.60	2.10	3.66	5.28	11.97	7	3.53	1.37	4.66	2.35	3.44	0.30	1.80	2.81	0.13	8.98	69.87	11.65	9.50
HWD06 (2-4cm)	-2.01	-1.09	0.30	1.09	2.62	5.71	8.47	15.09	3.84	4.09	0.98	2.95	3.80	4.49	0.49	1.43	4.08	0.43	5.74	62.75	14.19	17.32
HWD06 (4-6cm)	-1.78	-0.35	1.51	2.49	5.61	9.69	11.30	14.56	6.12	4.44	0.16	1.77	6.14	4.71	0.18	0.85	4.89	0.16	3.30	39.14	22.60	34.96
HWD06 (6-8cm)	-1.75	0.40	2.42	3.45	7.29	11.82	14.26	19.20	7.31	4.40	-0.16	1.73	7.99	5.81	0.22	0.92	5.92	0.18	1.83	28.87	24.35	44.96
HWD06 (8-10cm)	-1.89	-0.82	1.41	2.85	6.81	11.80	14.84	21.03	6.79	4.72	-0.13	1.69	7.69	6.67	0.25	1.00	6.71	0.20	4.29	30.31	23.67	41.73
HWD06 (10-12cm)	-1.89	-0.21	2.09	3.26	7.00	10.09	11.47	14.28	6.86	4.32	-0.13	1.89	6.86	4.54	-0.02	0.87	4.69	-0.05	3.18	28.23	26.86	41.73
HWD06 (12-14cm)	-0.99	1.06	3.37	4.96	7.84	16.81	23.23	36.28	7.97	4.09	-0.33	1.97	11.48	10.30	0.58	1.22	9.93	0.55	0.98	20.00	30.50	48.51
HWD06 (14-16cm)	-0.89	0.62	2.73	3.80	7.53	10.51	11.93	14.81	7.36	4.13	-0.18	1.86	7.40	4.45	-0.01	0.87	4.60	-0.05	0.79	26.15	27.29	45.77
HWD06 (16-18cm)	-0.78	0.73	2.83	3.87	7.55	11.02	13.05	17.17	7.45	4.13	-0.17	1.83	7.81	5.05	0.12	0.94	5.11	0.08	0.68	25.65	27.84	45.83
HWD06 (18-20cm)	-2.01	0.22	3.03	4.41	8.31	12.52	14.61	18.85	7.99	4.34	-0.47	2.04	8.65	5.72	0.11	0.94	5.79	0.09	2.76	20.21	24.67	52.36
HWD06 (20-22cm)	-1.07	0.05	2.64	3.73	7.73	11.72	13.50	17.12	7.59	4.41	-0.27	1.76	7.96	5.30	0.08	0.88	5.43	0.06	1.74	26.07	24.30	47.90
HWD06 (22-24cm)	-0.74	0.41	2.22	3.17	6.64	9.99	11.26	13.85	6.76	4.20	0.05	1.73	6.71	4.30	0.05	0.81	4.52	0.02	0.47	34.34	24.67	40.52
HWD06 (24-26cm)	-1.16	-0.95	3.47	4.86	7.77	11.18	12.55	15.32	7.80	4.22	-0.42	2.17	7.93	4.73	-0.01	1.05	4.54	0.05	4.96	15.24	31.74	48.07
HWD06 (26-28cm)	-2.72	0.03	2.69	3.67	6.81	11.00	13.15	17.52	7.11	4.30	-0.12	1.91	7.55	5.26	0.22	0.98	5.23	0.21	2.85	26.11	30.29	40.74
HWD06 (28-30cm)	-1.31	-0.09	1.91	2.98	5.79	11.44	17.99	31.31	6.47	4.39	0.15	1.77	8.56	8.78	0.57	1.52	8.04	0.52	2.01	34.12	29.48	34.38
HWD06 (30-32cm)	-3.04	-0.30	1.92	2.84	5.53	10.81	16.11	26.88	6.30	4.45	0.18	1.79	7.86	7.66	0.53	1.40	7.09	0.49	2.81	37.89	25.12	34.18
HWD06 (32-34cm)	-1.76	-1.02	1.02	2.29	5.32	10.94	14.59	22.01	6.11	4.76	0.12	1.67	6.98	6.88	0.41	1.09	6.79	0.37	5.19	37.81	21.21	35.79
DF80-189 (11-13cm)	2.60	3.82	5.16	5.81	7.96	10.31	11.04	12.52	8.42	3.12	0.05	1.82	8.05	2.79	0.05	0.79	2.94	0.05		6.39	44.14	49.47
DF80-189 (23-25cm)	3.01	4.06	5.48	6.55	8.69	10.83	11.76	13.66	8.92	3.05	-0.18	1.88	8.64	3.02	0.01	0.92	3.14	-0.02		4.66	37.26	58.08
DF80-189 (35-37cm)	1.41	3.86	5.30	6.09	8.04	16.42	25.21	43.09	8.53	3.18	-0.02	1.89	12.85	10.92	0.76	1.56	9.96	0.73		5.78	43.78	50.44
DF80-189 (46.5-48.5cm)	3.76	4.67	6.29	7.26	9.23	12.54	14.16	17.46	9.54	2.86	-0.30	1.74	9.90	3.91	0.27	0.99	3.94	0.25		1.69	32.53	65.78
DF80-189 (56-58cm)	3.86	4.89	6.18	7.06	9.06	11.23	12.25	14.32	9.34	2.82	-0.17	1.71	9.16	2.95	0.08	0.93	3.04	0.05		1.39	35.12	63.49
DF80-189 (66-68cm)	-0.74	3.69	5.46	6.23	8.00	10.45	11.57	13.86	8.42	3.17	-0.21	2.54	8.34	3.07	0.16	0.99	3.06	0.17	0.70	6.66	42.62	50.02
DF80-189 (83-85cm)	2.94	4.27	5.55	6.24	8.20	11.18	12.80	16.10	8.71	3.03	0.00	1.84	8.85	3.60	0.30	0.98	3.62	0.27		4.31	43.37	52.33
DF80-189 (93-95cm)	2.54	4.51	5.86	6.71	8.93	12.31	13.98	17.39	9.23	3.05	-0.29	1.92	9.59	3.98	0.28	0.94	4.06	0.24		3.39	36.70	59.91
DF80-189 (104-106cm)	2.76	4.69	5.83	6.62	8.58	10.91	12.02	14.29	8.94	2.92	-0.08	1.86	8.81	3.00	0.15	0.92	3.10	0.11		3.54	39.78	56.68
DF80-189 (124-126cm)	1.11	3.70	6.43	7.59	10.50	16.74	19.70	25.71	9.81	3.18	-0.83	2.66	12.21	6.65	0.38	0.99	6.64	0.39		6.05	24.32	69.63
DF80-189 (143.5-145.5cm)	3.15	5.16	6.86	7.81	10.13	12.65	13.85	16.28	10.04	2.81	-0.68	2.31	10.28	3.43	0.08	0.94	3.50	0.06		2.66	24.82	72.51
DF80-189 (155-157cm)	-2.76	-1.92	-1.12	-0.55	1.10	3.13	7.25	13.43	2.38	4.21	1.31	3.64	2.41	4.42	0.54	1.71	4.19	0.47	18.53	59.23	8.32	13.92
DF80-189 (164.5-166.5cm)	-2.54	-1.67	-0.80	-0.19	0.91	2.10	3.48	20.37	1.87	3.62	1.84	5.73	1.20	4.41	0.48	3.95	2.14	0.20	13.32	71.90	5.44	9.33
DF80-189 (182-184cm)	-4.16	-2.50	-0.94	-0.37	0.75	1.70	2.30	8.88	1.27	3.08	2.27	8.50	0.70	2.54	0.19	2.25	1.62	-0.04	15.25	75.88	2.91	5.97

	Percentiles								Moment measures				Graphic (Folk)				Inman		Proportions			
	1%	5%	16%	25%	50%	75%	84%	95%	Mean	StDev	Skew	Kurt	Mean	StDev	Skew	Kurt	StDev	Skew	Gravel	Sand	Silt	Clay
DF80-133 (6-8cm)	3.13	4.34	5.31	6.18	8.45	11.13	12.32	14.75	8.86	3.08	-0.07	1.67	8.69	3.33	0.16	0.86	3.50	0.10		2.82	40.98	56.20
DF80-133 (26-28cm)	3.03	4.88	6.03	7.05	8.85	11.12	12.15	14.26	9.22	2.87	-0.19	1.92	9.01	2.95	0.12	0.95	3.06	0.08		2.11	36.67	61.22
DF80-133 (46-48cm)	3.57	4.71	5.99	6.97	8.82	11.03	12.11	14.33	9.14	2.85	-0.15	1.90	8.98	2.99	0.11	0.97	3.06	0.07		1.53	37.68	60.79
DF80-133 (66-68cm)	-1.03	3.10	4.17	4.68	6.32	9.05	10.23	12.30	7.03	3.28	0.23	2.61	6.91	2.91	0.30	0.86	3.03	0.29	1.28	12.15	51.56	35.02
DF80-133 (89-91cm)	1.25	4.26	5.44	6.18	8.04	10.04	10.66	11.91	8.41	2.93	-0.01	2.25	8.05	2.47	0.01	0.81	2.61	0.00		4.60	44.92	50.48
DF80-133 (113-115cm)	1.09	4.53	5.78	6.61	8.59	10.32	10.95	12.24	8.80	2.97	-0.26	2.49	8.44	2.46	-0.07	0.85	2.59	-0.09		4.15	38.36	57.49
DF80-133 (133-135cm)	0.61	2.62	5.59	6.46	8.43	12.06	14.33	18.94	8.70	3.33	-0.39	2.35	9.45	4.66	0.32	1.19	4.37	0.35		9.31	34.66	56.03
DF80-133 (163-165cm)	-1.29	-0.76	0.52	1.02	1.91	3.54	6.12	10.78	2.99	3.41	1.53	4.67	2.85	3.15	0.52	1.88	2.80	0.50	3.68	75.11	10.05	11.17
DF80-133 (247-249cm)	-1.04	0.45	2.07	2.66	3.75	8.08	9.69	11.34	5.29	3.81	0.66	2.33	5.17	3.56	0.48	0.82	3.81	0.56	1.07	53.71	19.72	25.50
DF80-79 (10-12cm)	-2.90	-0.61	0.73	1.32	2.99	6.67	8.39	11.17	4.15	3.85	0.78	2.72	4.04	3.70	0.40	0.90	3.83	0.41	3.01	57.62	21.54	17.83
DF80-79 (18-19cm)	-0.37	2.44	5.80	7.65	12.86	19.54	22.71	29.15	10.00	3.59	-1.21	3.39	13.79	8.27	0.19	0.92	8.45	0.17	0.66	7.65	18.73	72.96
DF80-79 (28-30cm)	1.12	3.45	4.41	5.26	8.01	11.76	13.95	18.41	8.30	3.47	-0.05	1.70	8.79	4.65	0.32	0.94	4.77	0.24		11.47	38.42	50.11
DF80-79 (54-56cm)	3.40	4.08	5.54	6.42	8.21	9.98	10.69	12.13	8.49	2.78	0.12	2.00	8.15	2.51	-0.03	0.93	2.57	-0.04		4.63	42.04	53.33
DF80-79 (74-76cm)	1.73	4.31	5.81	6.63	8.70	10.91	11.91	13.94	8.98	3.02	-0.26	2.18	8.81	2.98	0.07	0.92	3.05	0.05		4.56	36.36	59.08
DF80-79 (85-87cm)	0.24	3.70	5.29	5.99	8.04	10.00	10.67	12.03	8.27	3.07	-0.11	2.42	8.00	2.61	-0.03	0.85	2.69	-0.02		7.12	42.36	50.51
DF80-79 (105-107cm)	3.00	5.52	6.60	7.40	8.93	10.62	11.41	13.00	9.27	2.69	-0.29	2.63	8.98	2.33	0.06	0.95	2.40	0.03	0.25	2.44	31.80	65.51
DF80-79 (125-127cm)	1.60	3.89	5.49	6.40	8.56	11.12	12.39	14.97	8.84	3.12	-0.22	2.03	8.81	3.40	0.13	0.96	3.45	0.11		5.47	37.95	56.58
DF80-79 (147-149cm)	1.40	4.59	6.03	6.90	9.15	15.42	18.58	24.99	9.42	3.12	-0.48	2.23	11.25	6.23	0.53	0.98	6.28	0.50		3.88	34.04	62.08
DF80-79 (158-160cm)	2.21	4.69	5.64	6.15	7.96	11.49	13.95	18.96	8.60	2.99	0.09	1.93	9.18	4.24	0.49	1.10	4.16	0.44		2.46	48.14	49.40
DF80-79 (167-169cm)	1.40	3.75	5.28	5.93	8.01	11.10	12.76	16.14	8.49	3.20	-0.04	1.92	8.68	3.75	0.29	0.98	3.74	0.27		5.92	43.93	50.15
DF80-79 (177-179cm)	3.65	5.44	7.05	7.79	10.26	15.55	18.06	23.16	10.06	2.76	-0.70	2.70	11.79	5.44	0.44	0.94	5.51	0.42	0.36	1.44	25.67	72.53
DF80-79 (185-186cm)	2.65	3.09	3.70	4.36	7.54	11.61	15.18	22.46	7.82	3.55	0.14	1.58	8.81	5.81	0.44	1.10	5.74	0.33		21.75	33.11	45.15
DF80-79 (194-196cm)	3.91	6.28	7.71	8.36	10.05	12.10	13.07	15.04	10.31	2.43	-0.60	2.27	10.28	2.67	0.13	0.96	2.68	0.13		1.12	18.56	80.32
DF80-79 (209-211cm)	4.41	5.70	6.71	7.27	8.45	9.86	10.45	11.64	8.87	2.29	0.34	2.32	8.53	1.84	0.07	0.94	1.87	0.07		0.47	39.56	59.98

Table 4: Grain size statistics for HWD06 and DF80 cores. Note: results for HWD03-1 and HWD03-2 are available in Barrett *et al.*, 2005.

2.15 Supplementary data: Sand grain petrology

		TAM						Uncertain			MVG	
Core	Depth (m)	Dolerite/Pigeonite	Sedimentary lithic	Carbonates	Beacon Quartz	Quartz	Microcline	Plagioclase	Plain feldspar	Heavy Minerals	Volc glass/lithics	Total
DF80-189	0.12	0	0	0	0	1	0	6	46	19	227	300
	0.24	0	0	0	0	5	0	7	53	11	224	300
	0.36	0	0	0	1	4	0	12	43	22	218	300
	0.48	0	1	0	0	2	0	4	59	28	206	300
	0.57	0	0	0	0	5	0	9	45	19	222	300
	0.67	0	3	4	0	4	0	12	55	15	207	300
	0.84	0	2	0	0	4	0	9	48	23	214	300
	0.94	1	1	0	0	5	0	5	33	11	244	300
	1.05	0	2	0	0	3	0	4	34	9	248	300
	1.25	0	0	0	0	1	0	7	48	13	231	300
	1.45	2	2	0	2	3	1	9	80	15	186	300
	1.56	6	23	3	18	41	3	18	89	14	85	300
	1.66	9	39	7	28	39	2	10	75	25	66	300
	1.83	11	53	5	33	55	2	13	46	25	57	300
DF80-133	0.07	0	0	1	0	3	0	1	18	21	230	274
	0.27	0	1	0	0	8	0	10	58	18	205	300
	0.47	0	0	2	0	4	0	3	48	26	217	300
	0.90	0	5	3	8	31	2	16	63	16	156	300
	1.14	0	4	2	7	21	0	13	53	13	187	300
	1.34	0	1	0	1	7	0	7	47	16	221	300
	1.64	7	18	1	28	30	1	14	66	13	122	300
	2.48	2	7	0	16	29	0	15	93	12	126	300
HWD03-1	0.00	2	1	1	11	42	0	7	33	23	280	400
	0.05	1	2	4	6	17	0	29	26	14	301	400
	0.11	1	0	4	0	6	2	18	34	15	320	400
	0.13	0	0	6	0	2	0	22	13	10	347	400
	0.15	0	0	4	0	4	0	38	28	9	317	400
	0.20	0	0	10	0	5	0	33	12	14	326	400
	0.24	0	0	4	0	4	1	14	24	34	319	400
	0.29	0	0	6	0	7	1	2	26	16	342	400
	0.31	2	7	2	23	72	0	34	20	4	237	401
	0.43	0	21	13	34	107	6	63	40	17	99	400
	0.53	4	3	12	30	102	4	13	57	9	166	400
HWD03-2	0.00	1	0	4	0	18	0	48	39	17	273	400
	0.14	0	0	2	0	11	0	41	59	4	283	400
	0.36	0	0	3	0	4	0	47	29	7	310	400
	0.58	0	0	1	0	9	1	57	33	19	280	400
DF80-79	0.11	0	1	0	1	0	0	29	20	14	235	300
	0.19	0	1	1	1	8	0	17	37	22	213	300
	0.29	0	2	0	0	4	0	6	43	11	234	300
	0.55	0	0	0	0	3	0	9	44	7	225	288
	0.75	1	1	1	1	6	1	9	38	20	208	286
	0.86	0	2	1	0	3	0	0	29	7	258	300
	1.06	1	5	0	14	13	0	8	52	16	192	301
	1.18	0	1	0	4	4	1	9	10	22	249	300
	1.26	0	1	1	3	9	1	6	43	12	224	300
	1.48	0	2	2	4	9	0	7	39	8	229	300
	1.59	1	3	0	8	18	2	13	48	26	182	301
	1.68	1	7	0	7	21	1	10	36	13	204	300
	1.86	0	0	0	0	0	0	5	21	6	268	300

Table 5: Modal analysis results for sand grain fraction.

2.16 Supplementary data: XRD results

X-ray Diffraction Quantitative Analysis of Antarctica Samples													
Sample ID	Quartz	Plagioclase	K-feldspar	Amphibole	Pyroxene	Halite	Zeolite	Gypsum	Goethite	Illite	Random mixed-layer illite/Smectite	Chlorite	X-ray amorphous content
DF80/70, 23.5-25.5 cm	22.7	23	5.9	3.2	5.6	1.2	-	-	-	3.7	11	3.1	20.6
DF80/70, 44-46 cm	6.1	20.5	4.2	1.8	5.5	1	-	-	-	2.1	13.5	2	43.3
DF80/70, 53-55 cm	6.6	22.2	4.7	3	6.2	0.9	-	-	-	2.6	9.5	1.8	42.5
DF80/70, 141-142 cm	2.6	20.7	3.8	2.3	9.3	0.3	-	-	-	2	11.1	1.1	46.8
DF80/70, 156-158 cm	4.2	17.6	3	1.6	5.3	0.7	-	-	-	4.2	14	2.5	46.9
DF80/70, 220-221 cm	4.1	22.8	4.1	1.7	18.6	0.3	0.7	-	-	6	3.9	1	36.8
DF80/78, 5-7 cm	4.8	11	1.6	-	3	3.7	-	-	0.1	2.9	9.7	1.7	61.5
DF80/78, 66-68 cm	23	25	5.1	1.6	4.7	0.3	-	-	-	2.9	12.8	1	23.6
DF80/78, 101-103 cm	15.8	21.3	5	1.8	3.3	0.7	-	-	-	4	12.9	3	32.2
DF80/78, 157-159 cm	23.5	24.8	6.1	2.1	5.7	0.1	-	-	-	3.3	8.5	1.4	24.5
DF80/78, 187-189 cm	9.3	18.8	4	1.5	3.5	0.8	-	-	-	3.6	15.9	3.1	39.5
DF80/78, 227-228 cm	10.1	15.3	5	-	4.3	3.6	-	-	-	6.6	21.7	5.4	28
DF80/79, 10-12 cm	1.2	31.8	7.8	-	5.4	0.6	-	-	0.4	0.6	8.2	0.1	43.9
DF80/79, 28-30 cm	4.7	17.4	2.1	-	3.7	0.4	-	-	-	2.5	21.2	2.9	45.1
DF80/79, 85-87 cm	5.4	14.9	3.1	-	4.2	1.5	-	-	-	3.7	19.2	3.8	44.2
DF80/79, 167-169 cm	6.5	16	4.8	-	5.8	2.8	-	-	-	4.9	17.8	5	36.4
DF80/19, 185-186 cm	4.8	15.8	3.5	-	4.2	1.3	-	-	-	4.3	15.7	4.1	46.3
DF80/133, 6-8 cm	5.6	10.9	3	1.3	3.2	5.6	-	-	-	3.4	8.7	2.5	55.8
DF80/133, 66-68 cm	6.5	12.6	3.3	-	3.2	5.4	-	-	-	3.1	12	3.2	50.7
DF80/133, 133-135 cm	7	13.6	3.7	-	3.5	4	-	-	-	3.7	10.7	3	50.8
DF80/133, 163-165 cm	26.3	26.3	8.7	1.1	4.3	0.1	-	-	-	2.4	6.4	2.4	22
DF80/138, 23-25 cm	14.8	16.4	4.1	1	3.1	2	-	-	-	7.4	18.8	4.7	27.7
DF80/138, 91-93 cm	15.3	18	4.4	0.9	2.4	0.8	-	-	-	5.5	17.8	3	31.9
DF80/138, 192-194 cm	10.1	14.3	3.5	-	3.1	1.5	-	-	-	7.9	17.8	5.4	36.4
DF80/138, 214-216 cm	26.7	30.1	10.5	0.3	2.8	1	-	-	-	3.9	11.9	1.7	11.1
DF80/189, 11-13 cm	6.8	11.3	2.9	1.4	3.1	5.5	-	-	-	4.1	10.6	3.1	51.2
DF80/189, 35-37 cm	5	7.4	1.5	-	1.5	5.8	-	-	-	2.6	12.2	2.4	61.6
DF80/189, 66-68 cm	5.7	10.3	1.7	-	2.8	4.8	-	0.8	-	3.1	11.1	2.3	57.4
DF80/189, 83-85 cm	5.5	10.6	2	-	2.2	4.2	-	-	-	3	10	1.9	60.6
DF80/189, 124-126 cm	6.9	12.9	2.6	0.8	2.2	2.9	-	-	-	5.5	14.2	3.5	48.5
DF80/189, 143.5-145.5 cm	9.3	14.2	2.8	-	2	2.9	-	-	-	8.2	13.6	5.2	41.8
DF80/189, 155-157 cm	28.2	28.4	5.5	0.3	2.9	1.3	-	-	-	6.5	10.9	6.3	9.7
DF80/189, 182-184 cm	26.9	21.7	7	1.1	4.5	0.3	-	-	-	3.9	13.6	4.9	16.1
HWD03/1, 1-2 cm	15.2	19	4	1.2	3.7	0.2	-	-	-	4.5	14.5	3	34.7
HWD03/1, 19-20 cm	4.8	14.8	2.6	-	4.6	0.6	-	-	-	4	12.9	3	52.7
HWD03/1, 26-27.5 cm	4.8	16.5	2.2	-	6.9	-	-	-	-	2.8	12	1.5	53.3
HWD03/1, 51-52 cm	9.2	23.7	4.6	-	3.3	0.2	-	-	-	4	14.8	3.2	37
HWD06/3, 0-2 cm	18.9	23.3	5.2	1	6	0.7	-	-	-	7.9	8.6	2.4	26
HWD06/3, 16-18 cm	14.5	20.2	3.9	-	4.6	0.6	-	-	-	4.3	16.3	4	31.6
HWD06/3, 32-34 cm	15	22.4	5.2	-	6.1	0.1	-	-	-	3.6	14.2	3.4	30

Table 6: XRD results for DF80 and HWD cores.

2.17 Supplementary data: Diatom counts

	DF80-189 (11-13cm)	DF80-189 (23-25cm)	DF80-189 (46-48cm)	DF80-189 (66-68cm)	DF80-189 (93-95cm)	DF80-189 (124-126cm)	DF80-189 (132-134cm)	DF80-189 (143-145cm)	DF80-189 (155-157cm)	DF80-189 (164.5-166.5cm)	DF80-189 (173-174cm)	DF80-133(26-28cm)	DF80-133(89-91cm)	DF80-133(113-115cm)	DF80-133(133-135cm)	DF80-133(163-165cm)	DF80-133(247-249cm)
<i>Actinocyclus actinochilus</i> and <i>A.ingens</i>	5	2	1	1	3	0	8	7	3	2	9	0	1	1	1	1	11
<i>Actinocyclus</i> spp	0	0	0		0	0	0	0	1	1	0	0	0	0	0	0	0
<i>Asteromphalus</i> spp	0	0	0		1	0	0	0	3	0	0	0	0	0	1	0	0
<i>Chaet. setae</i> (bulb,llel,spiny, punct)	0	1	0		3	0	0	0	0	0	0	1	7	0	0	2	0
<i>Chaetoceros</i> spores (flange, globe)	0	8	6	6	7	0	0	5	7	3	7	13	13	6	1	0	0
<i>Chaetoceros dictyota</i> spores PLAIN	8	0	0		0	10	9	0	0	0	0	0	0	0	11	3	1
<i>Coscinodiscus</i> spp <i>C. marginatus</i>	1	0	0		0	2	0	3	0	0	1	0	0	0	0	0	0
<i>Eucampia antarctica</i>	9	10	11	11	9	17	19	16	24	31	20	15	8	8	5	13	8
<i>Nitzschia angulata</i>	1	0	2	2	3	0	0	0	0	0	2	4	2	3	1	2	1
<i>Nitzschia curta</i>	69	54	52	52	37	14	23	2	11	21	20	55	33	44	39	30	13
<i>Nitzschia cylindrus</i>	3	4	0		0	0	1	1	1	1	0	0	0	3	2	4	3
<i>Nitzschia kerguelensis</i>	0	1	0		1	0	2	2	0	1	0	0	0	1	2	0	1
<i>Nitzschia obliquecostata</i>	25	20	39	39	41	28	11	4	28	30	22	28	51	49	35	26	17
<i>Nitzschia separanda</i>	2	4	1	1	1	3	0	0	1	0	0	0	1	2	2	0	0
<i>Nitzschia sublineata</i>	5	28	18	18	14	8	4	3	19	16	10	9	15	15	8	19	8
<i>Nitzschia</i> sp.	0	0	0		0	0	0	0	0	0	0	1	0	0	0	0	3
<i>Paralia sulcata</i>	1	0	0		0	6	9	15	7	2	7	1	0	0	0	6	7
<i>Porosira</i> spp. (<i>glacialis pseudodentic.</i>)	7	7	4	4	13	3	24	14	11	5	17	4	9	13	21	31	20
<i>Proboscia seta</i>	0	2	0		0	0	2	0	0	0	0	1	1	1	2	0	0
<i>Rhizosolenia</i> tips	1	0	0		1	0	1	0	2	1	1	0	1	2	0	0	1
<i>Stellarima microtrias</i>	2	1	2	2	1	0	5	7	0	4	12	1	0	1	5	1	1
<i>Thalassiosira antarctica</i>	24	24	25	25	15	4	4	4	3	6	17	30	26	14	20	24	6
<i>Thalassiosira gracilis</i>	3	0	0		0	1	0	0	1	0	1	0	0	3	3	0	1
<i>Thalassiosira lentiginosa</i>	3	3	0		1	0	6	8	3	0	3	1	4	3	2	1	9
<i>Thalassiosira oliverana</i>	0	0	0		0	0	0	0	3	2	0	0	0	0	0	0	0
<i>Thalassiosira tumida</i>	2	7	2	1	9	2	1	0	2	1	4	6	4	4	1	2	3
<i>Thalassiosira</i> spp.	0	0	2	2	1	0	1	0	5	10	1	3	0	0	2	2	1
<i>Thalassiothrix/nema</i> frags	24	28	30	30	26	16	19	34	29	29	21	23	17	22	19	17	24
Centric Hex	15	11	10	10	11	77	42	74	41	33	32	17	13	17	11	24	55
Other pennates (including unknown)	0	0	0		0	0	0	1	0	0	1	0	2	0	3	1	0
Fossil (eg. <i>Denticulopsis</i>)	0	0	0		0	1	4	2	1	0	1	0	0	0	0	0	2
<i>Rouxia</i> spp	0	0	0		0	4	6	7	0	0	4	0	0	0	1	2	8
<i>Stephanopyxis</i> (turrell, other)	0	0	1	1	0	0	1	0	0	0	0	0	0	0	0	0	0
<i>Thalassiosira torokina</i>	0	0	0		0	0	0	2	2	1	0	0	0	0	0	0	0
Corethrona	0	0	0		0	3	0	0	2	0	0	0	0	1	0	0	0
<i>Dactyliosolen antarctica</i>	0	0	1	1	2	0	0	0	0	1	1	0	0	0	0	0	0
<i>Synedra</i> spp.	1	1	1	1	1	1	0	0	0	0	0	0	0	0	0	1	0
<i>Odontella weissfloggi</i>	0	0	0		1	0	0	0	0	0	0	0	0	0	0	0	0
<i>Navicula gibbula</i>	0	0	0	0	0	0	0	0	0	0	0	0	0	0	0	0	5
<i>Melosira</i> sp.	0	0	0	0	0	0	0	0	0	0	0	1	0	0	0	0	0
<i>Amphora</i> sp.	0	0	0	0	0	0	0	0	0	0	0	0	1	0	0	0	0
<i>Nitzschia stellata</i>	0	0	0	0	0	0	0	0	0	0	0	0	0	0	0	0	2
Total	211	216	208	207	202	200	202	211	210	201	214	214	209	213	198	213	211
Fields of View	33	18	25	25	30	12	107	58	483	495	95	10	18	36	17	78	393
Sample Weight (g)	.003	.004	.008	.007	.006	.028	.013	.03	.04	.016	.109	.021	.015	.008	.111	.044	.047

Table 7: Diatom results from DF80 cores. Note: results for HWD03-1 and HWD03-2 are available in Barrett *et al.*, 2005.

2.18 Supplementary data: Ice core analysis

Accumulation of eolian detritus passing through the ice shelf is a potential source of introducing sediments to the seafloor beneath the McMurdo Ice Shelf. To test the hypothesis that windblown TAM and MVG-derived sand grains may pass through the ice shelf and be deposited on the seafloor, a 21-m long ice core from Windless Bight was analysed for dust content. This allowed the rate of seafloor sedimentation of eolian-derived detritus that has passed through the McMurdo Ice Shelf to be determined.

2.18.1 Methods

The ice core was collected on 23 October 2004 by Nancy Bertler (Victoria University of Wellington) at latitude 77°53.3 S, longitude 167°17.8 E, near the HWD03-1 site. One metre lengths of the core were sealed in polyurethane sleeves and melted. This was then filtered at 2.5µm, using Grade 5 Whatman cellulose filter papers. To recover the filtrate, acetolysis treatment was used to dissolve the cellulose filter paper. Acetolysis is commonly used in pollen processing techniques to make cellulose content soluble (Erdtman, 1960).

The filters were placed into 50 ml centrifuge tubes and dehydrated by washing twice in glacial acetic acid. Nine parts acetic anhydride was slowly added to one part sulphuric acid. 20 ml of this mixture was then added to each sample. The sample was then placed in a gently boiling water bath for 30 minutes, or until filter paper was completely dissolved. The sample was washed in glacial acetic acid and centrifuged at 3000rpm for five minutes (repeated once). The sample was then washed in distilled water and centrifuged at 3000rpm for five minutes (repeated six times). The remaining precipitate was then dried onto pre-weighed cover slips. The difference in weight of the cover slips determined the weight of sediment per metre length of ice core. The cover slips were then mounted onto slides using Canada Balsam. Several sample bags leaked during the melting phase, which explains the gaps in the sampling intervals of 1 m (Table 9).

2.18.2 Control samples

Dissolving the filter paper was preferred to incineration as it should not destroy the clay fraction, although this was an untested technique. To test the integrity of the sampling and processing technique, several control samples were run using the above technique:

- An unused filter paper to test solubility by acetolysis mixture (10 ml). A faint precipitate was recovered with a 0.003 g error (Table 8). Addition of an additional 10 ml of acetolysis mixture was added to all other samples and this appears to reduce this error (e.g., controls 2 and 3)
- Four filter papers: Up to four filter papers were used for some samples. For these, it was observed that some filters did not dissolve properly on the first acetolysis treatment (leaving an obvious white residue) and required a second treatment to dissolve all the remaining cellulose.
- Distilled water bagged in a polyurethane sleeve and passed through the cellulose filter. The sample was then processed alongside the ice core samples.
- 56.3 mg of glacial sediment adjacent to the Baldwin Glacier in the McMurdo Dry Valleys. After acetolysis and washing, 54.2 mg of sediment remained (96% recovery).

Sample	Error	Source of error
Control 1: unused filter paper	0.003g gained	Cover slide had a faint white residue - dissolved cellulose from the filter paper. Quartz grains also noted.
Control 2: distilled water	0.000g	No error
Control 3: Four unused filter papers	0.001g gained	Minimal error, cover slide had a faint white residue, inferred to be dissolved cellulose from the filter paper
Control 4: Baldwin Glacier	0.003g lost	4% loss during lab processing

Table 8: Ice core control sample results.

2.18.3 Determining the rate of sedimentation

The volume of sediment per cubic metre of ice was determined by dividing the weight of dry sediment (per metre) by the volume of one metre of the ice core. The volume of the ice core was determined by multiplying the cross-sectional area of the core (πr^2 , where $r=0.0508$ m) by its length. Therefore, the volume of a one metre length of ice core is 0.0081 m^3 .

The equivalent thickness of settled sediment is determined by dividing weight of sediment per cubic metre (g/m^3) by the average density of the sediment. As the majority

of sediment is likely to have been derived from the local basaltic geology (McMurdo Volcanic Group), the average density of basalt ($2.9 \times 10^6 \text{ g/m}^3$) is used. The sedimentation rate is determined by multiplying the equivalent thickness by a value of 3 (assuming an ice accumulation rate of 0.33 m yr^{-1}).

2.18.4 Results

The sediment flux of material passing through the ice shelf ranges between 0.00005 and $0.00055 \text{ mm yr}^{-1}$ (Table 9). This accounts for between 0.1 and 1% of the sedimentation rate for the sediment core HWD03-2 (0.05 mm yr^{-1}). Sand grain provenance is restricted to minerals derived from the MVG. However, no provenance analysis was conducted due to potential contamination of quartz grains during processing, as some isolated quartz grains were noted in the control samples. The source of this contamination could not be determined, but visual examination of thin slides indicates that the error associated with the weight measurements is likely to have been insignificant (see control 1).

Depth (m)	Weight(g)	Sediment volume(g/m ³)	Settled sediment (mm)	Sed rate (mm yr ⁻¹)
0-1	0.0215	2.65	0.00092	0.00031
1-2	0.0038	0.47	0.00016	0.00005
2-3*	0.0043	0.53	0.00018	0.00006
3-4	0.0092	1.14	0.00039	0.00013
4-5*	0.0134	1.65	0.00057	0.00019
5-6*	0.0097	1.20	0.00041	0.00014
6-7	0.0196	2.42	0.00083	0.00028
7-8*	0.0386	4.77	0.00164	0.00055
8-9*	0.0042	0.52	0.00017	0.00006
9-10	0.0094	1.16	0.00040	0.00013
10-11	0.0243	3.00	0.00103	0.00034
11-12	0.0126	1.56	0.00054	0.00018
13-14	0.0142	1.75	0.00060	0.00020
15-16	0.0161	1.99	0.00069	0.00023
17-18	0.0026	2.20	0.00076	0.00025

Table 9: Ice core sediment results.*- possible leak of polyurethane bag, although integrity of samples appeared intact. Samples 12-13, 14-15, and 16-17 were lost during processing, due to polyurethane bag leakage.

References

Erdtman, G. 1960. The acetolysis method. A revised description. *Svensk Botanisk Tidskrift*.v.54, 561-564.

CHAPTER 3

**The stratigraphic signature of Late Cenozoic
oscillations of the Antarctic Ice Sheet
in the Ross Embayment, Antarctica**

Abstract

The Late Cenozoic history of the Antarctic Ice Sheets (AIS) is not well understood, in particular, the response of the AIS to Late Neogene warm periods is poorly constrained. This is addressed in a 1284.87-m-long sediment core (AND-1B) from beneath the McMurdo sector of the Ross Ice Shelf that provides the most complete record to date of sedimentary processes associated with fluctuations of the marine-based sector of the AIS in the Ross Embayment over the last 13 Myr. The core contains a succession of sub-glacial, glacimarine and marine sediments that comprise ~60 orbital-scale depositional sequences. Each sequence represents an advance and retreat cycle of past ice sheets in the Ross Embayment. On the basis of the characteristic facies within these sequences, three types of facies associations or sequence “motifs” are identified. These are linked to major changes in areal extent of the AIS, glacial thermal regime, and climate.

Motif 1 is dominated by diamictite of sub-glacial (i.e., grounded ice) origin, overlain by thin mudstones interpreted as ice shelf deposits. Motif 1 lacks evidence of subglacial melt-water, and represents glaciation under cold, polar conditions during the past ~1 Myr and the Mid to early Late Miocene.

Motif 2 is characterised by subglacial diamictite, overlain by a relatively thin proglacial-marine facies succession deposited during glacial retreat. Glacial minima are represented by diatom-bearing mudstones, and diatomite. Motif 2 represents glacial retreat and advance under a “sub-polar” to “polar” glacial regime during the Pliocene that was warmer than present, but with limited amounts of subglacial meltwater.

Motif 3 consists of subglacial diamictite that grades upwards into a 5 to 10 m-thick proglacial retreat succession that includes a combination of stratified diamictite, graded conglomerate and sandstone, graded sandstone, and rhythmically stratified mudstone. Mudstone, rather than diatomite dominated deposition during glacial minima, suggesting increased input of meltwater from nearby terrestrial sources during glacial minima. Motif 3 represents Late Miocene “sub-polar” glaciation with significant volumes of subglacially derived melt-water.

3.1 Introduction

The history of the Antarctic ice sheets through the Cenozoic remains poorly known due to Antarctica's remoteness and ice cover for the last 34 million years. Direct physical records of Antarctic Cenozoic glacial history have become available only recently, and then largely from off-shore shelf basins through seismic surveys (e.g., De Santis *et al.*, 1999; Bart *et al.*, 2000) and geological drilling programs (e.g., Ocean Drilling Program (ODP), Cape Roberts Project (CRP), SHALDRIL, and ANDRILL (Hambrey *et al.*, 2002; Naish *et al.*, 2007)). The number of sites drilled is small and mainly confined to three areas: McMurdo Sound (e.g., Barrett *et al.*, 1989; Barrett, 2007), Prydz Bay (e.g., Barron *et al.*, 1989; Hambrey *et al.*, 1991; O'Brien *et al.*, 2001) and the Antarctic Peninsula (e.g., Barker *et al.*, 1999). Even in McMurdo Sound, where Oligocene and Lower Miocene strata are well-documented, research has focused on the evolution and relative stability of the larger East Antarctic Ice Sheet (EAIS), whereas the mid-Miocene to Quaternary history of both EAIS and the West Antarctic Ice Sheet (WAIS) remains largely unknown and poorly dated.

The $\delta^{18}\text{O}$ record indicates a profound cooling ~14 million years ago, interpreted as expansion of the EAIS to perhaps its present-day extent (Zachos *et al.*, 2001). A number of lines of evidence, including geomorphic studies from the Transantarctic Mountains (Sudgen *et al.*, 1993), have suggested that EAIS has been more or less stable and cold for the last ~14 million years. This is based largely on $^{40}\text{Ar}/^{39}\text{Ar}$ tephrochronology from the Dry Valleys region, which places a shift from wet-based terrestrial glaciation to less dynamic dry-based terrestrial glaciation at ~13-15 Myr (e.g., Sudgen *et al.*, 1993; Sudgen and Denton, 2004; Lewis *et al.*, 2006, 2007). Despite this evidence for a stepwise shift in climate and glacial regime, deep-ocean oxygen isotope records indicate that moderate oscillations of global ice volume continued until the development of Northern Hemisphere ice sheets ~3 Myr (e.g., Raymo, 1994), capable of producing global sea-level fluctuations of up to 25 m (Kennett and Hodell, 1993). These ice volume changes are thought to have involved an ice cap on Greenland, and the marine-based WAIS and EAIS margin.

The occurrences of marine diatom- and *Nothofagus*-bearing tills of the Sirius Group at a number of locations high in the Transantarctic Mountains (TAM) led Webb *et al.* (1984) to propose that diatomaceous sediments had been deposited in interior seas in East Antarctica, and subsequently glacially eroded and transported to their present sites. This concept requires one or more significant deglaciations of East Antarctica, with wet-based (subpolar to temperate) glaciation suggested until ~3 Myr. CIROS-2, a sediment drill core collected at the mouth of Ferrar Fjord, McMurdo Sound, recovered a discontinuous record of this critical Pliocene-to-Pleistocene interval. The Pleistocene section of CIROS-2 contains interbedded subglacial and glacialacustrine facies, thought to indicate periods of Ferrar Glacier expansion (recorded by the subglacial facies) that alternated with periods of AIS expansion in the Ross Embayment. Expansion of the grounded AIS into the McMurdo Sound region is interpreted to have dammed a deglaciated Ferrar Fjord, as recorded by glacialacustrine facies (Barrett and Hambrey, 1992). The Pliocene section of CIROS-2 is dominated by diamictite facies, interpreted as subglacial deposits of an expanded Ferrar Glacier (an EAIS outlet glacier). Although these diamictites are interstratified with glacialmarine muds, there is no evidence of substantial volumes of subglacial meltwater, suggesting that Pliocene glaciation was not much warmer than the present day (Barrett and Hambrey, 1992).

Although uncertainty remains about the scale of Antarctic ice sheet dynamism (e.g., Webb and Harwood, 1991; Sudgen *et al.*, 1993), the Early and Middle Pliocene (5-3 million years) generally is regarded as a time of global warmth (e.g., Crowley, 1996), and an important window into Earth's future climate if projections of anthropogenic global warming (IPCC, 2007) are correct.

The Quaternary evolution and stability of the WAIS is poorly documented, although its behaviour since the Last Glacial Maximum (~18 000 yrs BP) is relatively well-known. Since the Last Glacial Maximum, the WAIS has lost up to two-thirds of its mass, with ice cover in the Ross and Ronne-Filchner embayments shifting from ice sheets to ice shelves. However, a high resolution chronology and understanding of the dynamics involved in this retreat of the AIS in the Ross Embayment are yet to be fully resolved

(Bindschadler *et al.*, 1998; Conway *et al.*, 1999; Domack *et al.*, 1999; Stone *et al.*, 2003; McKay *et al.*, 2008).

The response of the WAIS to late Quaternary orbital cycles remains unclear. Scherer *et al.* (1998) provided physical evidence that parts of the WAIS which are now grounded collapsed at least once during the past 0.75 Myr, based on marine diatoms recovered from beneath Ice Stream B (Figure 36), which is also partially supported by modelling studies of the WAIS by MacAyeal (1992). Marine sediments from DSDP Site 270 indicate that continental glaciation extended onto the Ross Sea continental shelf episodically since at least the late Oligocene (Hayes *et al.*, 1975; Leckie and Webb, 1983; Bart *et al.*, 2000). To date, no well-constrained and detailed physical record of past oscillations of the marine-based sector of the AIS in the Ross Embayment (which is likely to have been intimately tied to the state of the WAIS; see Chapter 1 for details) has been available to test these hypotheses.

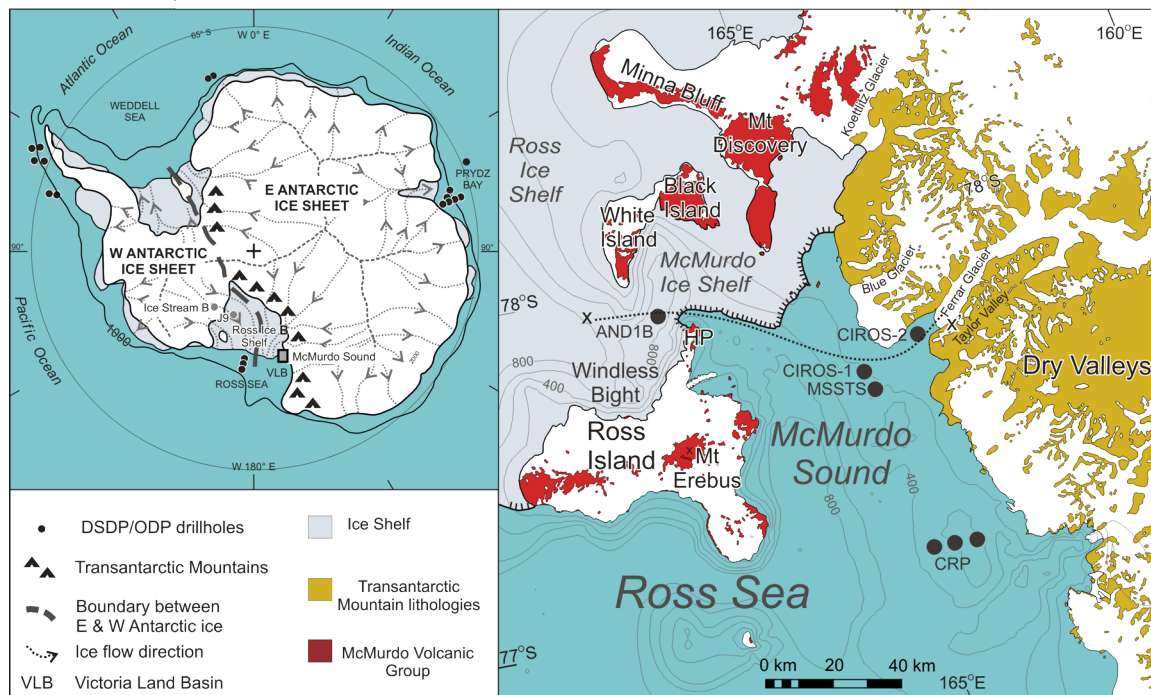


Figure 36: Insert map shows Antarctic continent with present day glacial flowlines (after Barrett, 1999; Drewry, 1983), location of McMurdo Sound (boxed). Larger map shows McMurdo Sound region and the AND-1B drill site near Hut Point (HP), as well as previous drill cores (MSSTS, CIROS, CRP) collected in the region. Transect x-x' shows approximate cross section for sedimentation model cartoons (Figure 42 to Figure 44).

In the austral summer of 2006-07, the latest Antarctic geological drilling program, ANDRILL, successfully cored a 1284.87-m-long record of climate and glacial/marine history spanning the last 13 Myr. The core (AND-1B) was recovered from beneath the northwestern corner of the Ross Ice Shelf (Figure 36; Naish *et al.*, 2007), referred to as the McMurdo Ice Shelf (77.89°S, 167.09°E) project, and contains ~60 sequences recording advance and retreat of a grounded ice margin (Figure 37). Ice shelf thickness at the drill site presently is ~82 m, and water depth is ~835 m. This unique core represents the most complete record to date of past ice sheet oscillations, with a range of lithofacies that can accurately identify periods of glacial advance and retreat within the Ross Embayment.

In this chapter, the lithofacies scheme for AND-1B is presented. This scheme is based on classifications developed from previous drill holes, and is used to track changes in glacial and marine depositional environments as recorded in AND-1B. Three vertical facies successions (Figure 38 to Figure 41), or “motifs”, occur repeatedly in AND-1B. In this chapter, these “motifs” are defined and related to glacial-interglacial oscillations of the grounding line under three different styles of glaciation, or thermal regimes, for the Late Cenozoic ice sheets. Based on data from AND-1B and previous drill cores from McMurdo Sound, a depositional model for each “motif” is presented that accounts for AIS grounding line oscillations within the Ross Embayment, the influence of local EAIS outlet glaciers, and coastal processes in the western Ross Sea.

3.1 Previous high-latitude glacimarine depositional models

Previous work on sedimentary models, as well as process studies from high-latitude continental shelf settings, have identified stratigraphic subdivisions and sedimentary characteristics for different glacial thermal regimes, (i.e., “polar”, “sub-polar” and “temperate”; Table 10) that are highly dependent on climatic setting, local physiography/oceanography, and glacial processes (e.g., Elverhøi *et al.*, 1983; Anderson and Ashley, 1991; Powell and Molnia, 1989; Powell and Domack, 2002; Dowdeswell *et al.*, 1998; Ó Cofaigh *et al.*, 2001; Ó Cofaigh and Dowdeswell, 2001; Desloges *et al.*,

2002). The use of polar, sub-polar, and temperate terminology was chosen over other terminologies for glacial style (i.e., “wet-based” versus “dry based” or polythermal etc), as there are clear glaciological definitions for these terms, and they allow for ready comparison with modern analogues from these modern latitude bands.

Late Quaternary sedimentation associated with the cold “polar” glacial regime of WAIS and EAIS represent the coldest end member for present-day glacimarine deposition (see Table 10), with no significant surface melt and limited subglacial meltwater influence. This produces low ($<0.05 \text{ mm yr}^{-1}$) terrigenous sedimentation rates in the glacimarine/ice shelf environment relative to higher biogenic sedimentation rates ($>0.2 \text{ mm yr}^{-1}$) in nearby open marine environments, including the immediate vicinity of ice shelf calving lines (Domack *et al.*, 1999; McKay *et al.*, 2008). These studies examined sedimentary processes associated with the transition from a grounded ice sheet to open-marine environments in continental shelf basins within the Ross Sea (including under the McMurdo Ice Shelf) since the Last Glacial Maximum. They have identified a facies succession that comprises, in ascending stratigraphic order:

- Massive mud-rich diamict(ite), interpreted as subglacial till deposited beneath grounded ice.
- Stratified diamict(ite) with a sandy mud component, interpreted as a basal debris melt-out zone associated with lift-off and development of a floating ice shelf.
- Sparsely fossiliferous ($<10\%$ biosiliceous, mostly reworked diatom frustules) and non-bioturbated mud(stone) lacking limestones, interpreted as a sub-ice shelf facies.
- Diatom-bearing to diatom-rich (i.e., $10\text{--}50\%$ diatomaceous) mud(stone) and diatom(ite) ooze ($>50\%$ diatomaceous) with limestones, indicative of open marine conditions and iceberg rafting.

“Temperate” glaciers (i.e., those at the pressure melting point throughout) represent the warmest end-member for glacimarine sedimentation, and are characterised by large meltwater plumes with high sediment load. Terrigenous sedimentation rates are several orders of magnitude higher (e.g., $2\text{--}20 \text{ m yr}^{-1}$) than their polar glacimarine counterparts, diluting or suppressing the biogenic component to a few percent (Cowan and Powell, 1991; Powell and Domack, 2002). Graded laminae and rhythmic bedding with iceberg-

rafted debris are characteristic of glacimarine sedimentation under a temperate glacial regime, due to the abundance of meltwater.

“Sub-polar” glacimarine deposition is more difficult to characterise, as it represents an intermediate phase between temperate and polar glaciation. Therefore, glacimarine sedimentation under a sub-polar regime varies widely in response to the extent of surface and subglacial melting or iceberg influences, even in similar climatic settings (see Table 10). In modern glacial environments, an increase in subglacial meltwater is likely to produce a higher terrigenous sedimentation rate during grounding line retreat/advance (Table 10). Deposition of rhythmically-laminated sediments and outwash facies, such as sands and conglomerates, is also more probable in a meltwater-dominated regime, but these facies have also been documented in some colder subpolar environments, such as East Greenland (Dowdeswell *et al.*, 1998; Ó Cofaigh *et al.*, 2001; Ó Cofaigh and Dowdeswell, 2001). An additional complication is that the extent of subglacial meltwater discharge is also likely to be spatially variable along the grounding line (Powell, 1990).

The three ‘motifs’ defined in this chapter for AND-1B are used to further enhance sequence stratigraphic models of high-latitude continental margins, as well as to provide insight into the Late Cenozoic evolution of the Antarctic ice sheets. These “motifs” represent a continuum of glacial regime, from a system dominated by cold polar ice (similar to that of today) during the Mid to early Late Miocene, to a warmer regime with abundant subglacial meltwater discharge during the Pliocene, and back into the present-day style of cold polar glacimarine sedimentation during the Pleistocene. The stratigraphic architecture of the motifs are entirely controlled by variations in the position of the grounding/calving lines as they have accumulated in deep water, below the direct influence of the wave-base and sea level fluctuations.

Table 10 (next page): Modern (post-LGM) analogues from various glacial thermal regimes. Increases in subglacial outwash can be related to sedimentation rates and facies assemblages. Sedimentation rates in temperate regimes (not shown) are orders of magnitude higher than Spitsbergen example (2-20 m yr⁻¹ within 1km from grounding line; Cowan and Powell, 1991). No temperate regime is inferred for AND-1B.

AND-1B interpretation	Glacial regime	Type example	Grounding line proximity	Subglacial/marine conditions	Characteristic glacialine sedimentary processes	Characteristic lithofacies	Climatic setting	References
<div> <div>Motif 1</div> <div>Motif 2a</div> <div>Motif 2b</div> </div>	Polar	Ross Embayment, Antarctica (large and fringing ice shelves)	Proximal	Basal melting rate of Ross Ice Shelf at grounding line <4m/yr to >40m/yr. Subglacial meltwater discharging from Siple Coast grounding line is unknown, but appears to rare and localised during LGM retreat. TAM outlet glacier (MacKay Glacier) basal melting rate is 1.7m/yr, with no conduit flow observed. Suspended Particulate Matter (SPM) beneath Ross Ice Shelf, ~100km from grounding line (site J9) is 0.68 mg/l. SPM up to 14mg/l within 5km of MacKay Glacier grounding line.	Subglacial till deformation and lodgment. Melt-out of debris entrained in basal ice expected close to grounding +/- sediment gravity flows. Subglacial till accumulation rate is 4.1mm/yr at Mackay Glacier. Proximal glacialine accumulation rate is 5.5mm/yr at Mackay Glacier. Tidal pumping of grounding zone. Slope instability after grounding line retreat.	Massive diamicton (subglacial till) beneath present-day, grounded WAIS ice streams. Overthickening of subglacial till packages in grounding zone wedges during still-stands. Massive or stratified diamicton (meltout of basal debris and debris flows near grounding line). Strong to weakly (non-cyclic) laminated muds with occasional sand beds and minor biosiliceous component.	Mean Annual Temp (McMurdo) -17°C Mean Summer Temp (McMurdo) -3°C Sub-Ice-Shelf Water Temp -2°C	Carter et al., 1981 MacPherson, 1987 Powell et al., 1996 Dawber and Powell, 1997 Tulaczyk et al., 1998 Domack et al., 1999 Rignot and Jacobs, 2002 McKay et al., 2008
			Distal	Basal melting rate of ice shelves near calving line is estimated at 0.4m/yr, but is usually lacking sediment. Open marine environment with high biogenic productivity and iceberg calving. SPM at McMurdo Ice Shelf edge <5mg/l (includes biogenic component)	Suspension settling of fine particles advected from open water under the ice shelf +/- sediment gravity flows. If ice shelf is narrow and fringing epibenthic communities may occur. Sediment accumulation rates are ≤0.05mm/yr beneath McMurdo Ice Shelf. Biogenic sedimentation dominates in open water (sed. rate ≤0.2 mm/yr)	Weakly laminated muds with occasional sand beds and minor reworked biosiliceous component (debris-free ice shelf). Biosiliceous ooze with iceberg rafted debris (open marine environment). Local bioturbation and macrofossils if ice shelf is fringing.		
	Polar to Subpolar (iceberg dominated)	Western Antarctic Peninsula (fringing ice shelf or tidewater cliffs)	Proximal	Ice front melting and iceberg calving. Some subglacial meltwater discharge. SPM generally 8-15 mg/l, but rare meltwater generated surface plumes up to 35 mg/l. Meltwater discharge is spatially variable.	Englacial debris released by ice front melting. Melting of basal debris from calved icebergs. Sediment accumulation rate ~ 3 mm/yr (250 m from grounding line)	Massive or stratified diamicton (meltout of basal debris near grounding line). Sandy muds to muddy sands. Sand laminae common.	Mean Annual Temp -3°C Mean Summer Temp 2°C Sea Surface Temp -1 to 1.6°C	Domack and Williams, 1990 Domack and Ishman, 1993 Ashley and Smith, 2000 Powell and Domack, 2002 Domack et al., 2001
			Distal	At distances >5km from grounding line: -SPM higher in surface layer of water column due to phytoplankton blooms. -SPM below 50m water depth is <2mg/l.	Biogenic dominated sedimentation with sed. rate up to 2 mm/yr (due to high productivity and sediment focussing)	Diatomaceous ooze and biosiliceous pebbly muds (contains iceberg rafted debris) common at distances >5km from grounding line.		
	Subpolar (iceberg dominated, some meltwater influence)	East Greenland (fjord - tidewater cliff)	Proximal	Meltwater production varies between fjords. Icebergs dominate some E. Greenland fjords (e.g. Scoresby Sund), others are dominated by meltwater production (e.g. Kejser Franz Joseph Fjord (KFJ)). SPM at head of Kangerlussuaq fjord (iceberg dominated) is ~2 mg/l.	Meltwater process can dominate iceberg sedimentation, even in iceberg dominated fjord. Sed rate in Kangerlussuaq is 24 mm/yr at head of fjord.	Massive or stratified diamicton (meltout of basal debris near grounding line + iceberg scouring). Stratified (including cyclopsels/ cyclopsams) and massive non-bioturbated muds with dispersed clasts dominate inner KJF Fjord and Scoresby Sund. Sediment gravity flows also common.	Mean Annual Temp -7.6°C Mean Summer Temp 2.6° Sea Surface Temp -1 to 3°C	Dowdeswell et al., 1994 Syvitski et al., 1996 Azetzu-Scott and Syvitski, 1999 Evans et al., 2002 Ó Cofaigh et al., 2001
			Distal	Icebergs dominate outer Scoresby Sund. Meltwater production dominates in KFJ. SPM in mouth of Kangerlussuaq fjord <0.5 mg/l.	Iceberg rafting and scouring dominates outer fjords in Scoresby Sund. Meltwater plumes dominate in outer KFJ Fjord and continental shelf with sed. rate ~ 1.1 mm/yr. Sedimentation rate in Kangerlussuaq is 0.6 mm/yr at mouth of fjord	Massive Diamicton deposited in iceberg-dominated Scoresby Sund Ice recession from inner shelf to outer-mid KFJ fjord is marked by change from laminated mud to bioturbated mud.		
Motif 3	Subpolar (meltwater dominated)	Spitsbergen (fjord with tidewater cliffs)	Proximal	Meltwater dominated. Icebergs contribute 1-8 mm/yr to sediment accumulation rate. SPM up to 300-500 mg/l in Konsfjord.	Basal debris deposited close to grounding line. Settling of mud and rare sand from meltwater plumes dominates near ice front. Sediment accumulation rate of 100 mm/yr near ice front in Kongsfjord.	Massive or stratified diamicton (meltout of basal debris near grounding line). Fine-grained muds with layers or lenses of sand/pebbles (iceberg rafted debris) and cyclopsels/cyclopsams. Sand laminae and gravels common within 1km of ice front (sed. gravity flows).	Mean Annual Temp -6.4°C Mean Summer Temp 5.1°C Sea Surface Temp -1 to 3°C	Dowdeswell et al., 1998 Dowdeswell and Dowdeswell, 1989 Elverhøi et al., 1980/1983
			Distal	Meltwater dominated (Icebergs contribute 1-8 mm/yr to sedimentation rate). SPM values of 1-5 mg/l (5-15km from grounding line) in Kongsfjord.	Settling of mud from meltwater plumes still dominates 10 km from ice front. Sedimentation accumulation rate of 1 mm/yr, 10 km from ice front.	Fine grained muds with an increase in bioturbation relative to ice proximal deposits (due to lower sed. rate).		

3.2 Geological setting

AND-1B was drilled in the southern portion of the Victoria Land Basin (Figure 36), one of three major north-south trending sedimentary basins that form the West Antarctic Rift System. The drillhole is located on the western margin of the Victoria Land Basin within the Terror Rift, a 70-km-wide structure extending from Mt. Erebus in the south to Mt. Melbourne, ~350 km to the north (e.g., Cooper *et al.*, 1987). Within McMurdo Sound, the Terror Rift contains ~3.5 km of sediments, accumulated along its central axes since the middle Miocene (Henrys *et al.*, 2007). Sediment in the western Ross Sea today is accumulating primarily in the north-south-trending basin troughs between 600 and 1200 m deep. These troughs are thought to be the sites of former ice streams that drained the WAIS- and EAIS-sourced outlet glaciers during the Last Glacial Maximum (Hughes, 1977; Denton and Hughes, 2000; Mosola and Anderson, 2006). The AND-1B drillsite is situated within a ~900 m deep basin that surrounds most of Ross Island. Termed a “flexural moat”, this basin is believed to have formed through a combination of localised lithospheric loads emplaced by the development of Ross Island’s volcanoes, beginning around 4.6 Myr, superimposed on the regional pattern of rift subsidence (Stern *et al.*, 1991; Horgan *et al.*, 2005).

3.3 Glacial setting

AND-1B was drilled at Windless Bight beneath the McMurdo Ice Shelf (Figure 36), which is considered to be an extension of the Ross Ice Shelf at its northwest margin. The McMurdo ice shelf has a surface snow accumulation of ~0.3 m/year (McCrae, 1984), and the present day calving line is ~5 km from the drillsite. Basal melting of the ice shelf is currently occurring at the AND-1B drill site, but the ice is likely free of sediment (McCrae, 1984; Barrett *et al.*, 2005). The Ross Ice Shelf itself is a major component of the WAIS system with approximately two-thirds of the ice shelf being nourished by ice streams that drain the WAIS, yet its western margin is fed by EAIS outlet glaciers (Fahnestock *et al.*, 2000; Figure 36). Glaciological reconstructions of grounded ice expansion within the Ross Embayment during the LGM (Denton and Hughes, 2000) indicate an ice sheet that extended to near the edge of the continental shelf and was fed by a contribution from both East and West Antarctic (Figure 6),

although uncertainty over the exact contribution from each source during the LGM remains (e.g. Licht et al., 2005).

The glacimarine cycles in AND-1B are interpreted as documenting retreat and advance of a large marine-based ice sheet within the Ross Embayment. This ice sheet was susceptible to large variations in spatial extent through glacial/interglacial cycles. The provenance of clasts within subglacially deposited diamictites in the AND-1B record are consistent with transport by glacial ice sourced from EAIS outlet glaciers to the south of the drill site (Pompilio et al., 2007; Talarico and Sandroni, 2007), indicating that grounded ice events in AND-1B were the result of a large scale advance of the ice sheet across the Ross Embayment, rather than localised glacial advance from Ross Island or outlet glaciers in the McMurdo Sound region.

Ice sheets that occupied the Ross Embayment during past glacial maxima were separated from the land-based sector of the EAIS by the Transantarctic Mountains, but linked by large outlet glaciers (Figure 6). Therefore, the marine-based ice sheets in the Ross Embayment would have had significantly different mass balance controls and responses to past warm periods than the land-based sector of the EAIS. Subglacial sediments in AND-1B were deposited by an ice sheet that was grounded well below sea level and was likely to be highly responsive to oceanographic-related mass balance controls, such as eustasy, iceberg calving and sub-ice melting. Of critical importance with regard to ice sheet retreat within the greater Ross Embayment (including sections of the presently-grounded WAIS) is that marine ice sheet grounding lines are inherently unstable on reverse bedslopes (Weertman, 1974; Thomas and Bentley, 1978; Schoof, 2007). When combined with an overdeepened bed, forcings such as rising sea levels, decreased accumulation rates, increased ice sheet temperature profile and/or basal slipperiness may result in the marine ice sheet being forced into an irreversible retreat. This implies that once retreat was initiated for past configurations of the ice sheet in the Ross Embayment, it was likely to occur across the entire embayment, similar to the pattern of retreat documented for the last deglaciation (e.g. Conway et al., 1999, Denton and Hughes, 2002; Licht et al., 1999, Domack et al., 1999; Shipp et al., 1999). Therefore on a glacial/interglacial timescale, the record in AND-1B of advance and retreat of the ice sheets in the Ross Embayment is likely to be intimately tied to the overall state of the WAIS. The AND-1B record

documents past changes not only in the extent of the marine-based ice sheet in the Ross Embayment over the past 13 Myr, but also provides insight into changes in the ice sheet temperature profile (i.e., thermal regime) and basal slipperiness (i.e., basal meltwater)

3.4 AND-1B lithofacies scheme

AND-1B was described at the Crary Science and Engineering Centre, in McMurdo Station, Antarctica, using standard sedimentological techniques to produce detailed stratigraphic logs (Figure 37; Krissek *et al.*, 2007). From the initial descriptions, eleven lithofacies were defined in the core (Table 11).

3.4.1 Facies 1: Diatomite

Description: Facies 1 consists of massive to weakly-stratified diatomite (e.g., Figure 39A). Stratification is defined by colour changes or laminae/beds of sandstone and gravel. Dispersed pebbles, granules and coarse sand are common throughout and may deform the laminae beneath. The degree of bioturbation is variable and commonly consists of simple horizontal, mm-scale ovoid burrows, although several different types of mm- to cm-scale trace fossils are present. Micro-faulting with mm- to cm-scale offsets is common throughout, although usually more intense in intervals overlain by diamictites (Facies 9 and 10). Pure diatomite (e.g., Figure 39A), lacking a significant terrigenous component but with occasional lonestones, is common, although some intervals comprise up to 50% terrigenous material (e.g., Figure 40B).

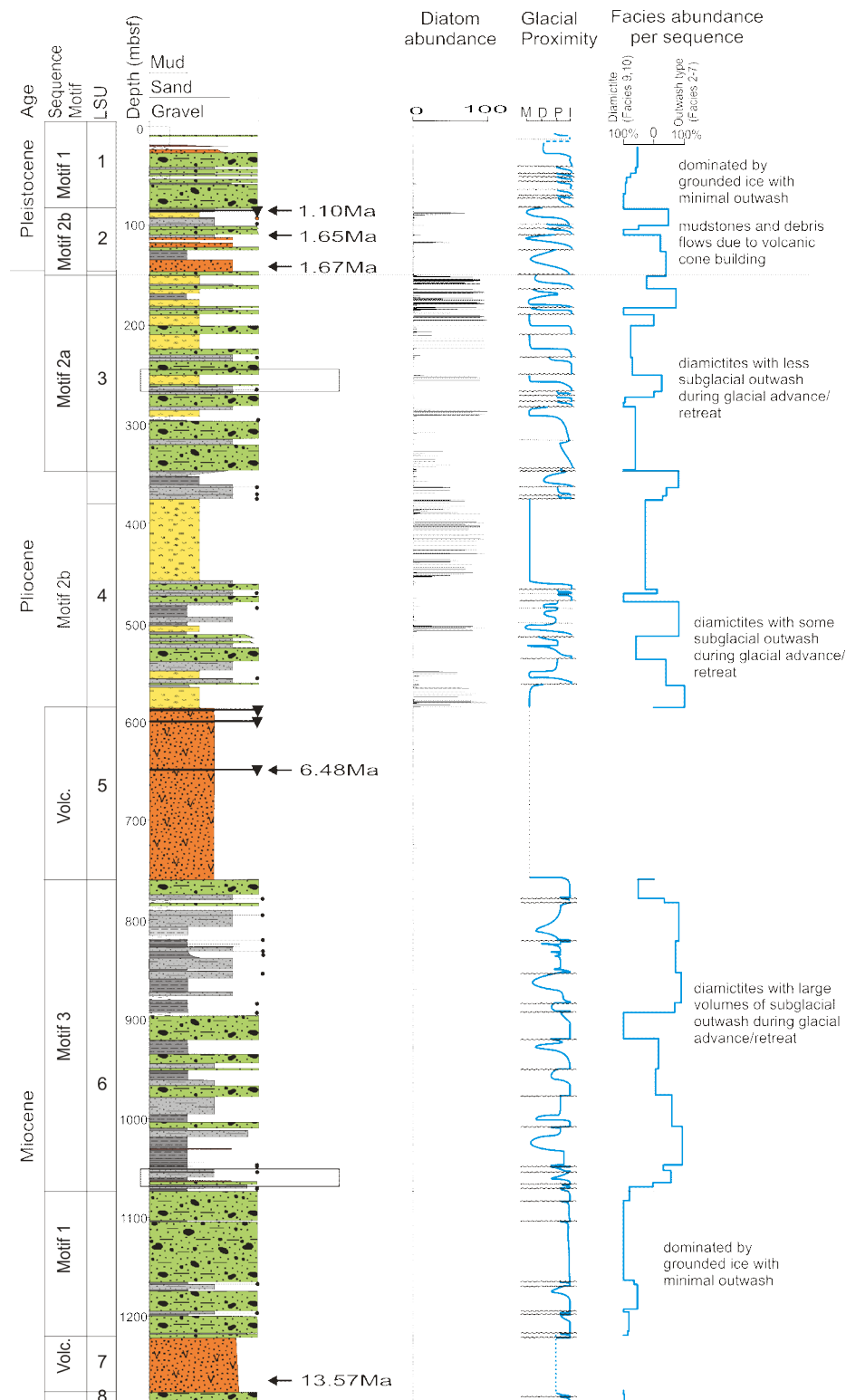
Interpretation: Facies 1 represents biopelagic sedimentation, with a variable contribution from hemipelagic deposition in a high nutrient, marine environment. Periods of iceberg rafting are recorded throughout.

Facies number and name	Predominant Process interpretation	Motif 1 (%)	Motif 2 (%)	Motif 3 (%)
1 - Diatomite	-Pelagic rain +/- hemipelagic suspension settling	0	37	0
2 - Mudstone	-Hemipelagic suspension settling	1	8	22
3 - Interstratified mudstone and sandstone	-Low to mod. density sediment gravity flow -Hemipelagic suspension settling +/-IRD -Redeposition by marine outwash	2	6	10
4 - Mudstone with dispersed/common clasts	-Subglacial deposition -Hemipelagic suspension settling -Rainout from ice rafting	4	11	29
5 - Rhythmically interlaminated mudstone with siltstone or sandstone	-Suspension settling from turbid plumes -Low-density turbidity current deposition -Rainout from ice rafting	0.3	0.2	6
6 - Sandstone	- Sediment gravity flow	0	2	3
7 - Conglomerate	-Redeposition by marine outwash -Redepositional by mass flow	0.7	0	2
8 - Breccia	-Sediment redeposition by mass flow. -Volcanic debris flow.	0	0.5	0.1
9 - Stratified diamictite	-Subglacial deposition -Rainout with currents -Debris flow depositon	24	3	3
10 - Massive diamictite	-Subglacial deposition -Rainout without currents -Debris flow depositon	68	31	26
11 - Volcanic sediments	-Primary volcanics deposits/volcanic debris	0	1	0

Table 11: Summary of lithofacies documented in the core. Percentage of facies that contribute to each motif is also included.

Figure 37: (next page) Stratigraphic log, Lithostratigraphic Units (LSU), and interpretation of AND-1B core. Age intervals are based on the initial age model of Wilson *et al.* (2007). Diatom abundance histogram is based on visual estimates from smear slides. Facies abundance curve measures the relative abundance of diamictite facies (Facies 9, 10) vs. mudstone-rich/"outwash type" facies (Facies 2, 3, 4, 5, 6, 7) within each sequence. It represents a proxy for changes in glacial regime related to subglacial meltwater outwash during glacial retreat, minima and advance. However, this is complicated in some sections by slope processes (e.g., 100-150 mbsf). The glacial proximity curve was determined using the models presented in to Figure 42 to Figure 44. The glacial proximity curve shows the transition from marine(m) to ice distal (d), ice proximal (p) and ice contact/subglacial (i) deposition. GSEs define each sequence boundary.

Chapter 3: Late Cenozoic stratigraphic signature of AIS in the Ross Embayment



LEGEND

- | | | |
|---|--------------------------------------|----------------------------------|
| Diatomite | Sandstone | volcanic ash date |
| Mudstone | Mudst. with dispersed/ common clasts | GSE (glacial surface of erosion) |
| Volcanic sandstone | Diamictite | |
| Rhythmically laminated mudst. with silt/sandst. | Diamictite (<3m thick) | |

3.4.2 Facies 2: Mudstone

Description: This facies is represented by silty claystones to clayey siltstones (e.g., Figure 38A) that are predominantly massive in structure. If present, stratification is identified by a change in either colour or particle size, with sandstone laminae or thin beds (mm to cm scale) present locally. Sandstone laminae and beds are predominantly volcanic in composition, massive or graded, and often display planar or ripple lamination. Bioturbation commonly is absent, although it can be sufficiently intense to obscure primary stratification. Bioturbation usually increases towards contacts with Facies 1. Lonestones are largely absent, but generally are more common where bioturbation is present. Below 759.32 metres below seafloor (mbsf), bioturbation appears to be absent to extremely rare. However, bioturbation may be present but obscured by a significant dark-coloured overprint, attributed to abundant pyrite. A biosiliceous component (e.g., diatom-bearing (10-25%) to diatom-rich (25-50%) mudstone) is also common above 586.59 mbsf but rare to absent below this depth. This distribution of biogenic opal may be due, at least in part, to an opal C-T transformation at ~600 mbsf (Scherer *et al.*, 2007).

Interpretation: Facies 2 records environments that were either distal or proximal to grounded ice and were dominated by hemipelagic suspension settling. Greater bioturbation is thought to imply a more distal environment, with slower sedimentation rates, whereas non-bioturbated mudstone may have been deposited in a more proximal grounding line environment. In the lower part of the core (below 759.33 mbsf), the apparent lack of bioturbation in 5- to 10-m-thick mudstones may indicate an environment where sedimentation rates were too high to support a benthic infauna. Alternatively, the heavy pyritization or dysaerobic condition in this part of the core may have obscured any bioturbation. The lack of diatoms in these units may also be due to rapid input of terrigenous sediment, which would have restricted primary productivity due to turbidity in the water column.

When stratified, the siltstone and sandstone laminae may represent a contribution from distal sediment gravity flows, or the winnowing of fines, perhaps related to submarine outwash or bottom currents. This facies may also include a rare ice-rafted

component in the form of rare lonestones/pebble nests or poorly sorted coarse sand/diamictite beds.

3.4.3 Facies 3: Interstratified mudstone and sandstone

Description: Facies 3 consists of mudstones similar in texture and composition to those of Facies 2, but interbedded with graded and massive sandstones on a cm to dm scale (e.g., Figure 39C). The sandstones are mainly very fine- to medium-grained, but can reach coarse sand grade. The sandstone beds commonly are graded, and are associated with a variety of sedimentary structures, notably planar and ripple lamination. The lower contacts of the sandstones usually are sharp, whereas the upper contacts are gradational (e.g., Figure 39C). Some sandstone intervals are dominated by volcanic grains, whereas others contain a diverse range of minerals. Lonestones of various lithologies are common, and occasionally deform underlying laminae. Bioturbation often is present within finer-grained intervals, and is also more common near contacts with Facies 1.

Interpretation: The fine-grained nature of this facies and the lack of *in situ* macrofossils or benthic diatoms indicate deposition in a deep-water environment. The interstratified nature is probably the result of hemipelagic sedimentation derived from turbid plumes, which alternated with distal to proximal sediment gravity flows or turbidity currents resulting from grounding-line processes or volcanic/tectonic activity. Sandstones with a notable quartzo-feldspathic component and containing planar and ripple-laminae (e.g., Figure 41C) suggest the influence of proglacial grounding-line fan processes. These types of sandstones commonly occur near other facies interpreted as proglacial (e.g., rhythmically interlaminated mudstone with siltstone/sandstone, stratified diamictites, conglomerates, etc). Ice rafting also may have contributed sand grains and clasts with diverse lithologies. Traction currents are another process that probably was active during deposition of this facies, either reworking the tops of gravity flow deposits or as separate (discrete) traction currents.

3.4.4 Facies 4: Mudstone with dispersed/common clasts

Description: Facies 4 comprises mudstones/sandy mudstones with dispersed (trace - <1%) clasts or mudstone with common (1-5%) clasts. Facies 4 differs from Facies 2 (which may also contain rare lonestones) based on the persistence of clasts throughout Facies 4, albeit sometimes in very low abundances. Facies 4 is also very similar to the two diamictite lithofacies (Facies 9, 10), but is distinguished by the relative abundance of sand or gravel, using the classification scheme of Moncreiff (1989). Clasts are predominantly granules to small pebbles with diverse lithologies. Bioturbation can be pervasive locally, but often is absent. Micro-faulting and fracturing are common, particularly when Facies 4 underlies diamictite. Stratification, if present, is defined by changes in colour and grain size. Diatoms are present in some intervals above the volcanic succession at 558.75-759.33 mbsf (Figure 37), but are rare to absent below 759.33 mbsf.

Interpretation: The depositional conditions interpreted for Facies 4 are similar to those interpreted for Facies 2, except that the presence of dispersed/common clasts indicates rainout from floating ice, either beneath an ice shelf or from icebergs. In association with Facies 10, intervals of Facies 4 that lack bioturbation could indicate deposition beneath grounded ice, although intervals with clast nests record deposition beneath iceberg zones (Powell and Cooper, 2002). The presence of bioturbation suggests a marine environment that was relatively distal to the grounding line. The high mud content is interpreted as representing sedimentation from turbid plumes in a pro-grounding-line marine environment, with clasts being contributed from floating ice.

3.4.5 Facies 5: Rhythmically interlaminated mudstone with siltstone or sandstone

Description: Facies 5 consists of rhythmically interlaminated couplets of either siltstone or very fine-grained sandstone that grade upward into claystone with iceberg-rafted debris (e.g., Figure 41B). Claystone and siltstone form fining-upward couplets that are bundled into packages 2 to 5 cm thick. Each package contains 6-10 couplets both above and below a claystone-dominated lamina, which itself is up to 2 cm thick. Individual couplets have a basal lamina of clayey siltstone or very fine sandstone 2 to 5-mm thick, which grades into a claystone lamina 1-2 mm thick.

Thinner couplets appear more discrete and their sandstone/siltstone laminae are well-sorted. Thicker couplets are less well-defined, contain more mudstone, and their sandstone/siltstone is less well sorted. Couplet thicknesses vary systematically within each package, producing a strong rhythmicity. Mudstone laminae can be present within the sandstone in the coarser part of a couplet. Facies 5 also contains lonestones, which have formed impact structures in the underlying laminae, clast nests, and lenses and beds of poorly-sorted, medium- to coarse sandstone and granules (Figure 41A).

Interpretation: Facies similar to Facies 5 have been described from modern temperate to sub-polar glacimarine environments in Alaska and the Greenland margin (Table 10), where they are deposited in quiet-water basins by suspension settling from meltwater plumes (Mackiewicz *et al.*, 1984; Cowan *et al.*, 1999; Ó Cofaigh and Dowdeswell, 2001). A similar origin for this facies in AND-1B is inferred here. These couplets are termed cyclopsams (sandstone/mudstone) for the coarser, more ice-proximal deposits and cyclopels (siltstone/mudstone) for the finer, ice-distal equivalents. The rhythmicity probably resulted from turbid meltwater plumes interacting with tidal currents near the top of the water column. This interaction modulated the settling of suspended sediment to the sea floor (Cowan *et al.*, 1999).

3.4.6 Facies 6: Sandstone

Description: Facies 6 comprises interbedded siltstone, muddy sandstone, and very fine to coarse-grained sandstone. The beds predominantly are volcanic-rich and black in colour, and occasionally contain mud rip-up clasts. Normal grading is common, although some massive beds are present. Planar lamination is the most common stratification type, with rare cases of cross-stratification present. Reverse-graded sandstone beds are also present, but are less common than normal-graded beds. Bed bases usually are sharp and irregular, whereas tops are either gradational or sharp and planar. Soft-sediment deformation structures are common locally. The sandstones are often interbedded with sandy mudstones or siltstones, which are either massive or laminated.

Interpretation: This facies is mostly interpreted as turbidites, usually with incomplete Bouma sequences (Bouma, 1962). Beds grading upward from Ta (massive sandstone) and Tb (planar laminated sandstone) intervals before passing directly into Te (massive

mudstone) intervals are common. Though complete Bouma sequences from Ta to Te divisions do occur, they generally are rare. The incomplete sequences are interpreted as fines-depleted, proximal turbidites. Because these beds generally are volcanic-rich, the turbidity flows that deposited them may have been triggered by co-seismic activity related to volcanism.

3.4.7 Facies 7: Conglomerate

Description: Facies 7 comprises matrix- to clast-supported sandy muddy conglomerate (e.g., Figure 41D), usually with rounded to subrounded clasts of diverse lithologies. The conglomerates often are weakly stratified, and generally are <2 m thick. Rarely, conglomerates are composed of >90% elongate mudstone intraclasts, with horizontally aligned long (a-) axes. Basal contacts of the conglomerate beds are sharp and irregular, and generally have relief of ~1 cm. When associated with Facies 4, 9 or 10, the contacts are often gradational.

Interpretation: Facies 7 is uncommon within the core, and probably records episodes of submarine sediment redeposition, possibly during turbulent discharge from subglacial conduits. Alternatively, they may result from the winnowing of the fine fraction from diamictite deposits.

3.4.8 Facies 8: Breccia

Description: Facies 8 is composed of poorly sorted breccias of sand, granule and gravel clasts in a muddy or sandy matrix. The clasts are dominated by angular to subrounded granules and pebbles of volcanic origin or mud intraclasts. The lower contacts of the breccias generally are sharp and irregular, and vary from horizontal to inclined (<30°).

Interpretation: These breccias are interpreted to have formed by sediment redeposition by submarine mass flow processes, mainly from a volcanic source.

3.4.9 Facies 9: Stratified diamictite

Description: Facies 9 is represented by clast-rich to clast-poor diamictite. Stratification ranges from weak to well-defined, and is identified by changes in

colour, clast concentration or particle size (e.g., Figure 38B). Horizontal alignment of clasts is not used as a criterion for stratification, although preferred long-axes orientation is common. The matrix ranges from muddy to sandy, and the biogenic silica content is variable, ranging from absent to biosiliceous-rich (i.e., comprising up to 50% of the matrix). Clasts are angular to rounded, poorly sorted, and include a wide range of lithologies, such as mudstone intraclasts and volcanics, metasedimentary and sedimentary rocks, granites, dolerites, and marbles. Outsized clasts and pebble nests are present in some intervals (e.g., Figure 41A). Facies 9 is often interbedded with, or grades to, Facies 10. Bioturbation is present in some intervals, but is rare overall.

Interpretation: The origin of the stratified diamictites is diverse. Thinner beds associated with marine facies (e.g., Facies 1) are interpreted to have formed by ice rafting or debris flow deposition. For stratified diamictites that are associated with ice contact or grounding-line proximal facies (e.g., Facies 3, 4, and 10), depositional processes may have included rain-out of basal glacial debris and associated reworking by marine outwash, or debris flows sourced from the grounding line (Powell, 1990). Alternatively, a stratified diamictite may have been deposited beneath grounded ice. Some of the stratified diamictites are dominated by mudstone intraclasts, which may correspond to the granulated facies of Domack *et al.* (1999), interpreted to represent meltout of basal debris during the initial phase of lift-off of grounded ice.

3.4.10 Facies 10: Massive diamictite

Description: In general, the textural and compositional characteristics of Facies 10 are identical to those of the stratified diamictites of Facies 9 (Figure 52 and Figure 53). Although Facies 10 is not stratified, alignment of clast long axes to the horizontal plane is common. Sharp lower contacts are often associated with load features, and fracturing is common. The mud, sand, and clast contents of Facies 10 are variable, and the diamictite may be interbedded with, or grade into and out of, Facies 4 or 9. Clast roundness is also variable, ranging from angular to rounded.

Interpretation: This facies is interpreted as probably recording subglacial deposition from debris-rich basal ice, although rainout from floating ice and icebergs, and

deposition by mass flows originating from the grounding line cannot be excluded. Although the specific depositional process may not be interpretable for a particular diamictite, the occurrences of Facies 10 generally are taken as indicators of ice proximity. When the basal contact of an interval of Facies 10 is sharp and overlies a zone of physical mixing (e.g., Figure 39A), that diamictite is interpreted as a till, deposited beneath grounded ice.

3.4.11 Facies 11: Volcanic rocks and sediments

This facies consists of primary and near-primary volcanic deposits. It includes lapilli tuffs, and one phonolitic lava flow (646.49 to 649.3 mbsf). With the exception of the lava flow, all deposits of Facies 11 have undergone some minor redeposition.

3.5 Sequence stratigraphic framework

Sixty unconformity-bounded glacimarine sequences in the AND-1B core are recognised (Figure 37). Each sequence base is placed at an unconformity interpreted as a *glacial surface of erosion* or GSE (after Fielding *et al.*, 2000). GSEs are identified on the basis of sharp facies dislocations that separate massive diamictite from underlying facies which are usually deformed or intermixed (e.g., Figure 38A/Figure 39 A).

Each GSE is overlain by a vertical succession of lithofacies that are interpreted as recording: 1) the retreat of grounded ice from the site, after a glacial advance and maximum; and after grounding line retreat, 2) the possible development of ice-shelf, and then perhaps open-marine, conditions during a glacial minimum. Subsequent ice readvance led to glacial overriding and development of the overlying GSE. Variations in lithofacies with time primarily reflect changes in depositional energy that are interpreted to reflect changes in glacial proximity. GSEs and glacimarine sequences are not evident in the volcanic successions between 558.75 and 759.33 mbsf, and between 1220 and 1275 mbsf. Although there is considerable lithological variation within these glacial/interglacial sequences, three characteristic facies successions are identified, termed “motifs” (Figure 38 to Figure 41), that are interpreted as recording deposition under distinctly different glacial regimes. The relative abundances of

lithofacies within each motif are detailed in Table 11. Ages discussed in the text (Figure 37) are based on the initial chronostratigraphy of Wilson *et al.* (2007), which incorporates $^{40}\text{Ar}/^{39}\text{Ar}$ ages, microfossil biostratigraphy, and magnetostratigraphy.

3.5.1 Motif 1: Diamictite dominant

The basal portion of Motif 1 is a massive diamictite (Facies 10, 68% of the total facies assemblage), 3 to 30 m thick, that passes upward into stratified diamictite (Facies 9, 24% of the total facies assemblage). The basal diamictites are overlain by thin (0.2 to 6 m-thick) beds of mudstone with dispersed clasts (Facies 4) and silty claystone (Facies 2), with or without interstratified volcanic sandstone. Figure 38 shows an example of Motif 1, with representative photos, in AND-1B. Sequences exhibit a sharp base, underlain by deformed and often stratified diamictite (Facies 9), interstratified sandstone and mudstone (Facies 3), sandstone (Facies 6) or mudstone (Facies 2) of the underlying sequence (e.g., Figure 38A). Sediments directly above and below the GSE often display evidence of soft-sediment deformation and shearing, along with clastic intrusions. In addition, the massive diamictites commonly display a strong fabric of horizontally aligned clasts. This clast fabric together with the extensive deformation at the GSE suggests deposition beneath grounded ice. The diamictite facies are interpreted to record periods of grounded ice or proximal glacimarine sedimentation at the site. Diatom-poor, finer-grained facies that lack an ice-rafted component are inferred to have been deposited in a low-energy environment beneath an ice shelf, while interbedded mudstone and sandstone facies are inferred to represent proximal glacimarine settings, such as near a grounding-line or beneath an ice shelf. Motif 1 dominates the upper 82.7 m of the core (Late Pleistocene) and the interval at 1083-1285 mbsf (Mid to early Late Miocene), except for the volcanogenic interval at 1168-1275 mbsf (see Figure 37).

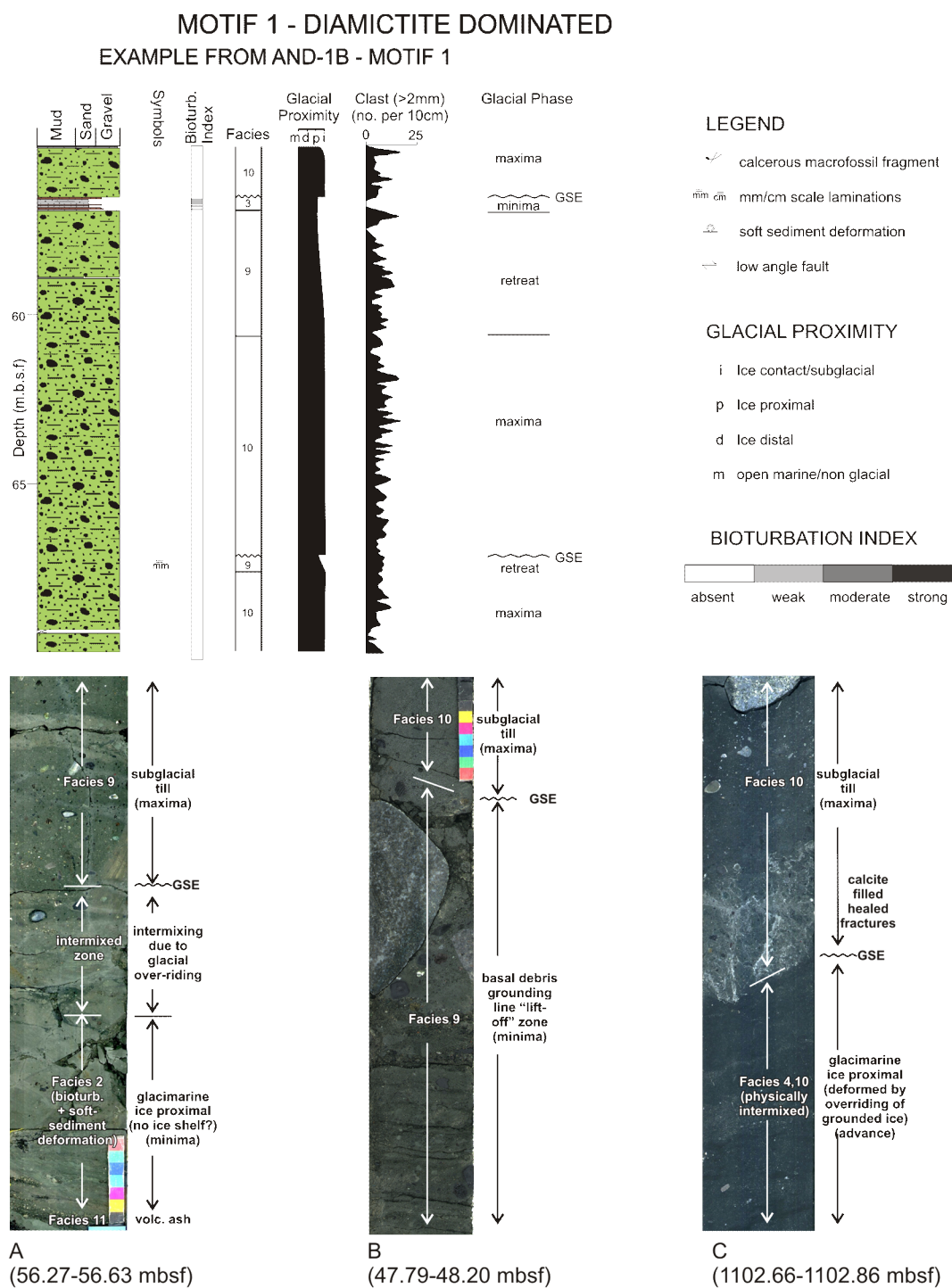


Figure 38: Example stratigraphic log of a Motif 1 sequence from AND-1B (56.0 to 69.5 mbsf) and representative photos of facies assemblages within Motif 1. Interpretations are based on the facies deposition model. The glacial proximity curve shows the transition from marine(m) to ice distal (d), ice proximal (p) and ice contact/subglacial (i) deposition. Sedimentary facies are indicated by the number series 1 to 11 (Table 11). Legend for lithological units is provided in Figure 37.

3.5.2 Motif 2: Interstratified diamictite and diatomite

Sequences of Motif 2 dominate the stratigraphic section at 82.7 to 586.59 mbsf (Figure 37). Each sequence has a basal massive diamictites, 1 to 20 m (Facies 10, 31% of the total facies assemblage), deposited during a glacial maximum. The basal diamictite is overlain by a grounding line retreat succession of stratified diamictite (Facies 9, 3% of the total facies assemblage) or mudstone with dispersed clasts (Facies 4). The grounding-line retreat succession passes upward into increasingly more ice-distal and open marine deposits, including glacial marine biosiliceous mudstone with iceberg-rafted debris (e.g., Facies 3 and 4) and open-marine diatomite (Facies 1, 37% of the total facies assemblage) with minor or rare iceberg-rafted debris. The diatomite records the most open-water and ice-distal depositional conditions developed during glacial minima. The diatomite units range up to 90 m thick (e.g., 376-460 mbsf), and lack significant terrigenous mud. Facies that record glacial readvance may be present above the diatomite in Motif 2, and consist of mudstone- and sandstone-rich facies (Facies 2, 3 and 4). This record of glacial readvance is overlain by stratified diamictites immediately below the next GSE.

Motif 2 is subdivided into two “sub-motifs”, distinguished by the extent of terrigenous sedimentation during the glacial minimum and retreat/advance phases. Motif 2a (150.7 to 376.3 mbsf) contains diatomite with a minor (<10%) terrigenous component throughout, with retreat and advance successions generally 1-2 m thick (e.g., Figure 39). The glacial minimum in Motif 2b (82.7 to 150.7 mbsf; 376.3 to 586 mbsf) is recorded by terrigenous-bearing to terrigenous-rich diatomites (i.e., containing 10-50% terrigenous material), and thicker retreat and advance successions of mudstone-rich facies (e.g. Figure 40).

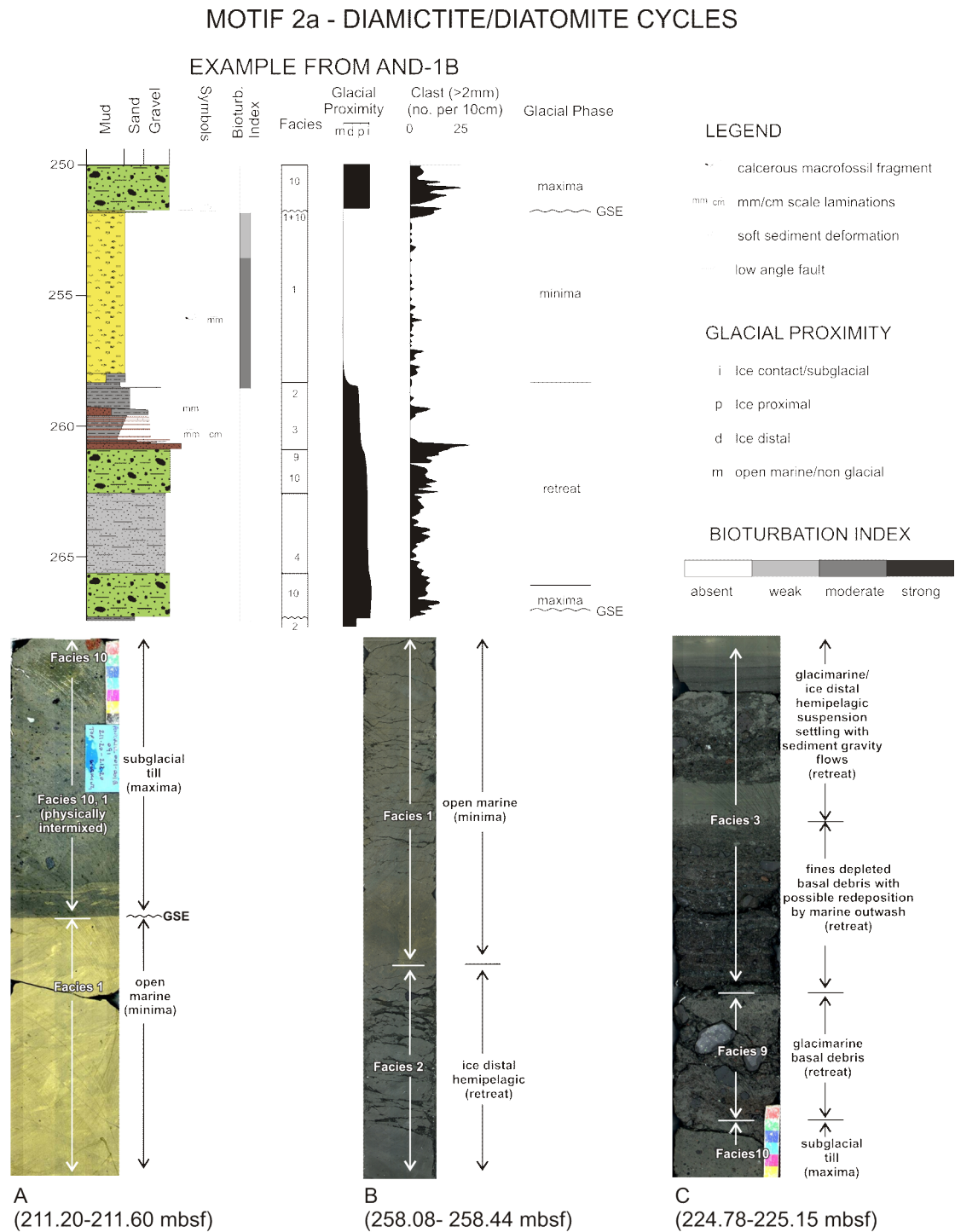


Figure 39: Example stratigraphic log of a Motif 2a sequence from AND-1B (250 to 267.40 mbsf) and representative photos of facies assemblages within Motif 2a. Interpretations are based on the facies deposition model. The glacial proximity curve shows the transition from marine(m) to ice distal (d), ice proximal (p) and ice contact/subglacial (i) deposition. Sedimentary facies are indicated by the number series 1 to 11 (Table 11). Legend for lithological units is provided in Figure 37.

MOTIF 2b - DIAMICTITE/DIATOMITE CYCLES

EXAMPLE FROM AND-1B

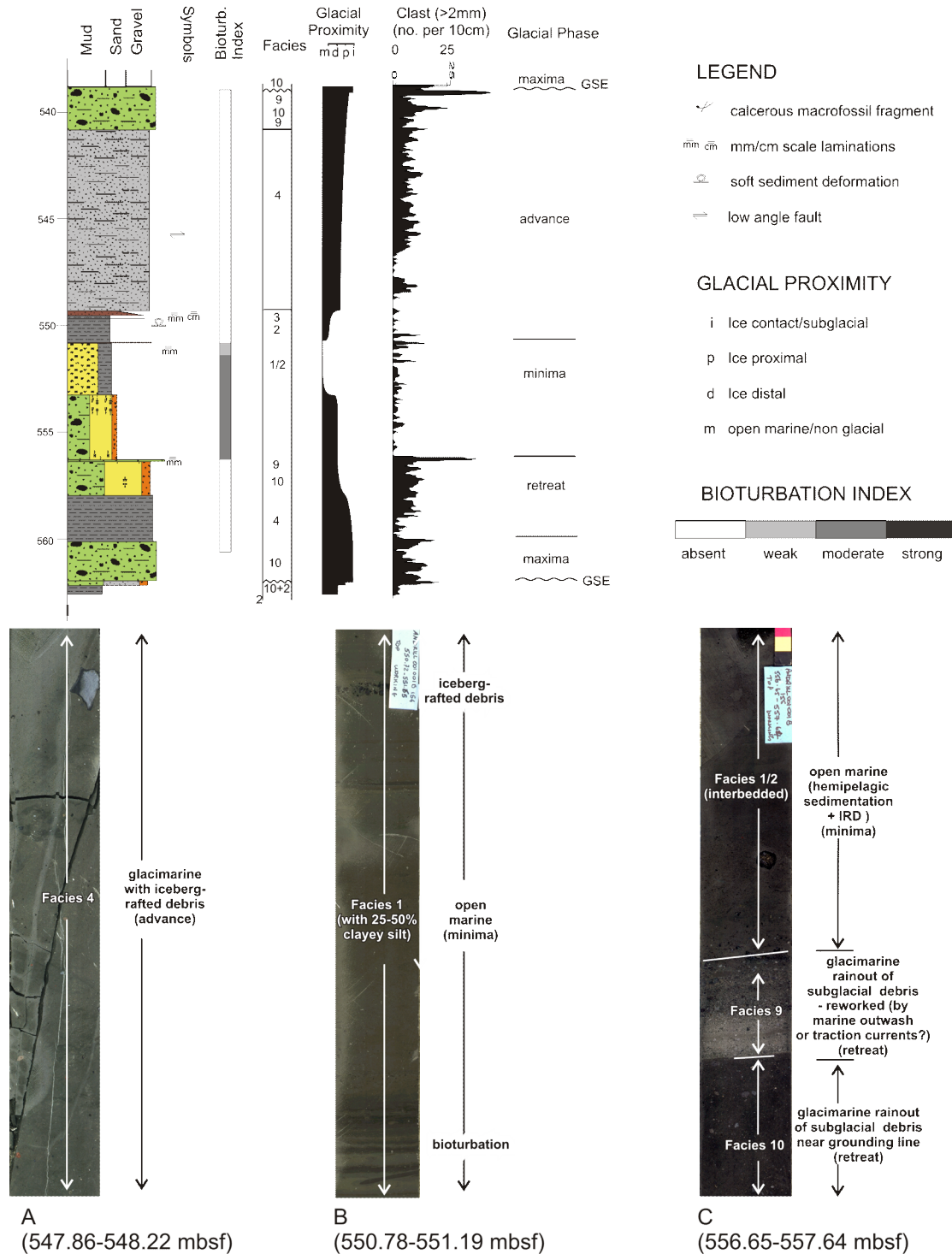


Figure 40: Example stratigraphic log of a Motif 2b sequence from AND-1B (539.00 to 563.80 mbsf) and representative photos of facies assemblages within Motif 2b. Interpretations are based on the facies deposition model. The glacial proximity curve shows the transition from marine(m) to ice distal (d), ice proximal (p) and ice contact/subglacial (i) deposition. Sedimentary facies are indicated by the number series 1 to 11 (Table 11). Legend for lithological units is provided in Figure 37.

Soft-sediment deformation features, clastic dykes, fractures, and brecciation immediately below the GSEs in Motif 2 are attributed to sub-glacial deformation or deformation at the grounding line during ice advance. Many of the transitions from diamictite to diatomite facies appear to have been rapid, with the transition recorded by mudstone-rich facies successions generally less than 1 m thick. Above 295 mbsf, the re-advance successions often are truncated by a GSE, overlain by a thick massive diamictite. The diatomite below the GSE typically is deformed, sheared and intermixed with the subglacial till that lies above that GSE (e.g., Figure 39A).

3.5.3 Motif 3: Interstratified diamictite and mudstone

Motif 3 dominates the interval between 770 and 1083 mbsf in AND-1B. Motif 3 displays some similarities to Motif 2, but lacks diatomite and is composed almost entirely of diamictite (Facies 9, 10; 29% of the total facies assemblage) and terrigenous mudstone-rich facies. Facies 2, 3, 4 and 5 (e.g., Figure 41) together comprise 67% of the facies assemblage within Motif 3. The facies assemblages associated with grounding line retreat and readvance (e.g., Facies 3-5) generally are 10 to 40 m thick in Motif 3 (see Figure 37), which is thicker than their equivalents in Motif 2. This thickness difference may imply a higher sedimentation rate for Motif 3 than for Motif 2. In all cases of Motif 3, a thin massive diamictite (Facies 10) overlies the GSE, and is interpreted as tillite deposited during a glacial maximum. This massive diamictite is overlain by interstratified diamictite (Facies 9 and 10), which passes upward into interbeds of rhythmically interlaminated mudstone and sandstone (Facies 5), interstratified mudstone and sandstone (Facies 3), or mudstone (Facies 2). Conglomerate (Facies 7) and mudstone with dispersed clasts (Facies 4) also are common within this sequence.

MOTIF 3 - DIAMICTITE/MUDSTONE CYCLES

EXAMPLE FROM AND-1B

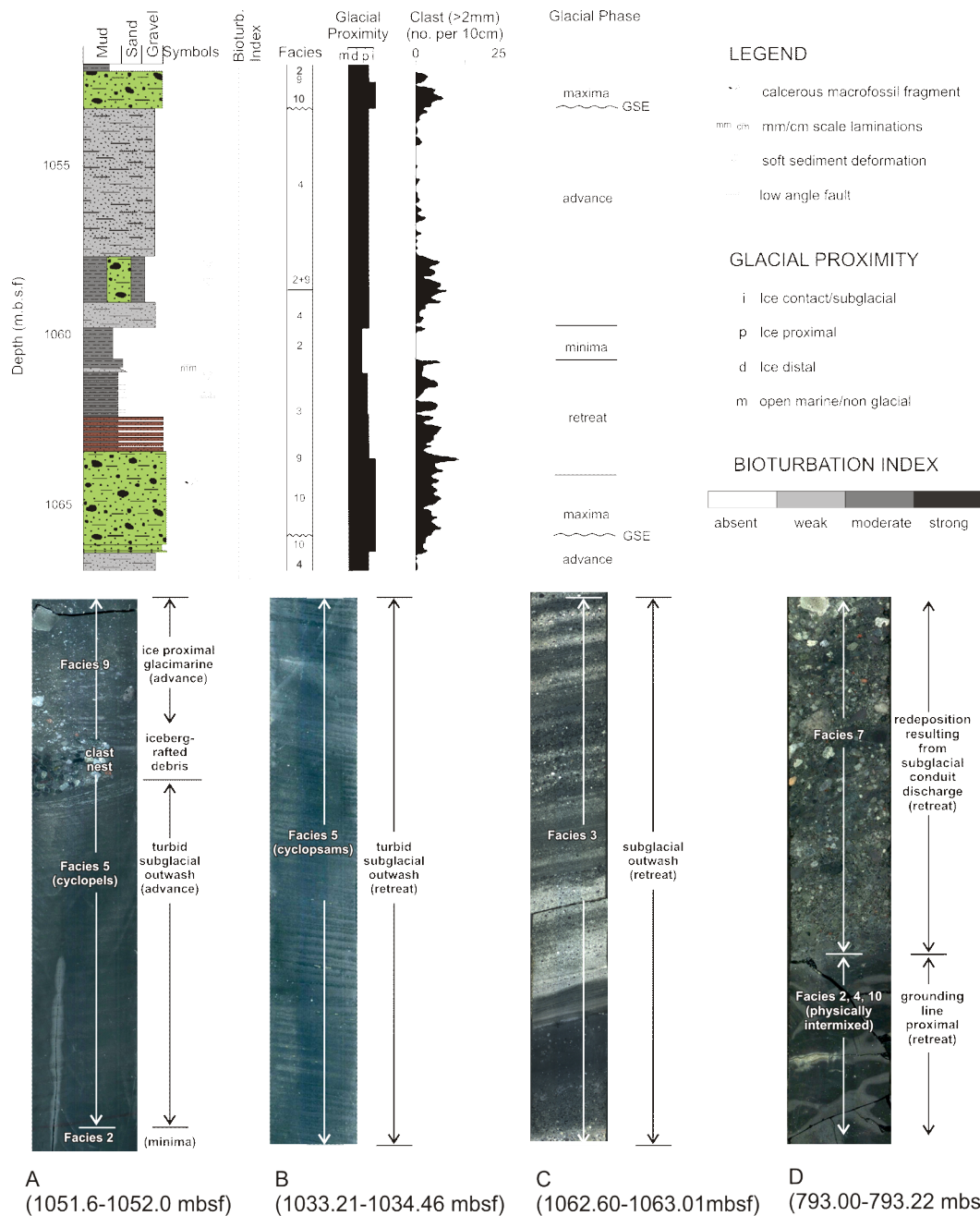


Figure 41: Example stratigraphic log of a Motif 3 sequence from AND-1B (1052.00 to 1067.00 mbsf) and representative photos of facies assemblages within Motif 3. Interpretations are based on the facies deposition model. Sedimentary facies are indicated by the number series 1 to 11 (Table 11). The glacial proximity curve shows the transition from marine(m) to ice distal (d), ice proximal (p) and ice contact/subglacial (i) deposition. Legend for lithological units is provided in Figure 37.

3.6 Discussion: Sedimentation models of glacialmarine deposition at AND-1B

3.6.1 Sedimentation during a cold, polar glacial regime

Motif 1 is consistent with sedimentary models previously derived from the study of modern processes and glacial systems in cold polar regimes, and from successions deposited during the retreat of AIS in the Ross Sea embayment since the Last Glacial Maximum. However, Motif 1 notably lacks open-marine diatomites (e.g., diatom-bearing/rich mudstone and diatomite), similar to those forming in the present-day Ross Sea (e.g., Domack *et al.*, 1999; Dunbar *et al.*, 1989; McKay *et al.*, 2008; Sjunneskog and Scherer, 2005), and there is also a near-complete absence of reworked diatoms within the diamictite facies. The massive diamictites generally are interpreted as either subglacial (basal) till (especially if clast long axes have a strong horizontal alignment and the diamictite overlies a GSE) or proximal glacialmarine deposits of a grounding zone wedge. Diamictites with these attributes are characteristic of LGM deposits collected from the Ross Sea region (e.g., Domack *et al.*, 1999; Licht *et al.*, 1999). The thin interbedded sandstones and mudstones, as well as diamictites with well-defined stratification, are similar to modern sediments collected from the sub-ice shelf zone beneath the McMurdo Ice Shelf (McKay *et al.*, 2008). Although these mudstones and sandstones are thin in Motif 1 sequences, they indicate that glacial retreat and glacial minima conditions produced an ice shelf over the site during the deposition of Motif 1, much like conditions at present. Open water conditions with biogenic-dominated sedimentation are not recorded at the AND-1B drill site during deposition of Motif 1 sequences.

Beneath the present-day McMurdo Ice Shelf, ~60 cm of sediments have accumulated since ice shelf conditions were initiated 10, 000 ^{14}C yrs BP (McKay *et al.*, 2008). This sedimentation rate (0.06 mm yr^{-1}) is much lower than the rate for open-water diatomaceous ooze ($\sim 0.2 \text{ mm yr}^{-1}$) deposited in the Ross Sea (Domack *et al.*, 1999; McKay *et al.*, 2008). Diatom remains are present only in trace amounts in the upper 82.7 m of AND-1B (Figure 37; Scherer *et al.*, 2007), despite the presence of sparsely fossiliferous mudstone and sandstone facies, interpreted as sub-ice shelf deposits. The low diatom abundances within the diamictite facies suggest a minimal amount of erosion within this interval, because erosion of open-marine diatomite should have

recycled more diatomaceous material into the overlying diamictites, as is observed in diamictites of Motif 2 and of the Last Glacial Maximum from the Ross Sea (e.g., Scherer *et al.*, 2004; Sjunneskog and Scherer, 2005). If erosion by over-riding ice was so significant that all traces of underlying diatomite were removed, then it is unlikely that thin sub-ice shelf deposits would have been preserved. Attempts are currently underway to define a higher resolution chronology from these sub-ice shelf deposits to test this hypothesis (see Chapter 4).

The presence of Motif 1 from 1.10 Myr (Figure 37) implies that, for several glacial/interglacial cycles, ancestral configurations of the Ross Ice Shelf and the AIS in the Ross Embayment were similar to the configurations of the Last Glacial Maximum to the Holocene deglaciation. Compared to its extent during the Pliocene, an expanded ice sheet or ice shelf persisted in the Ross Embayment for extended periods, as recorded by the Middle to Upper Pleistocene and Middle Miocene sections of AND-1B, even in a relatively deep water setting. The glacial regime during deposition of Motif 1 was probably similar to the regime of the last glacial cycle - an ice sheet with a cold polar glacial regime, a vertical temperature profile entirely below freezing, and negligible surface melting and subglacial outwash. Ablation was probably controlled by sub-ice shelf melting and calving at the ice shelf margins, so oceanic temperature and circulation, and eustatic sea level change were the major controls on ice volume fluctuations. In the Ross Embayment, this regime persisted through the mid to Late Pleistocene and in Mid to early Late Miocene time.

Motif 1- Diamictite interbedded by mudstone and sandstone

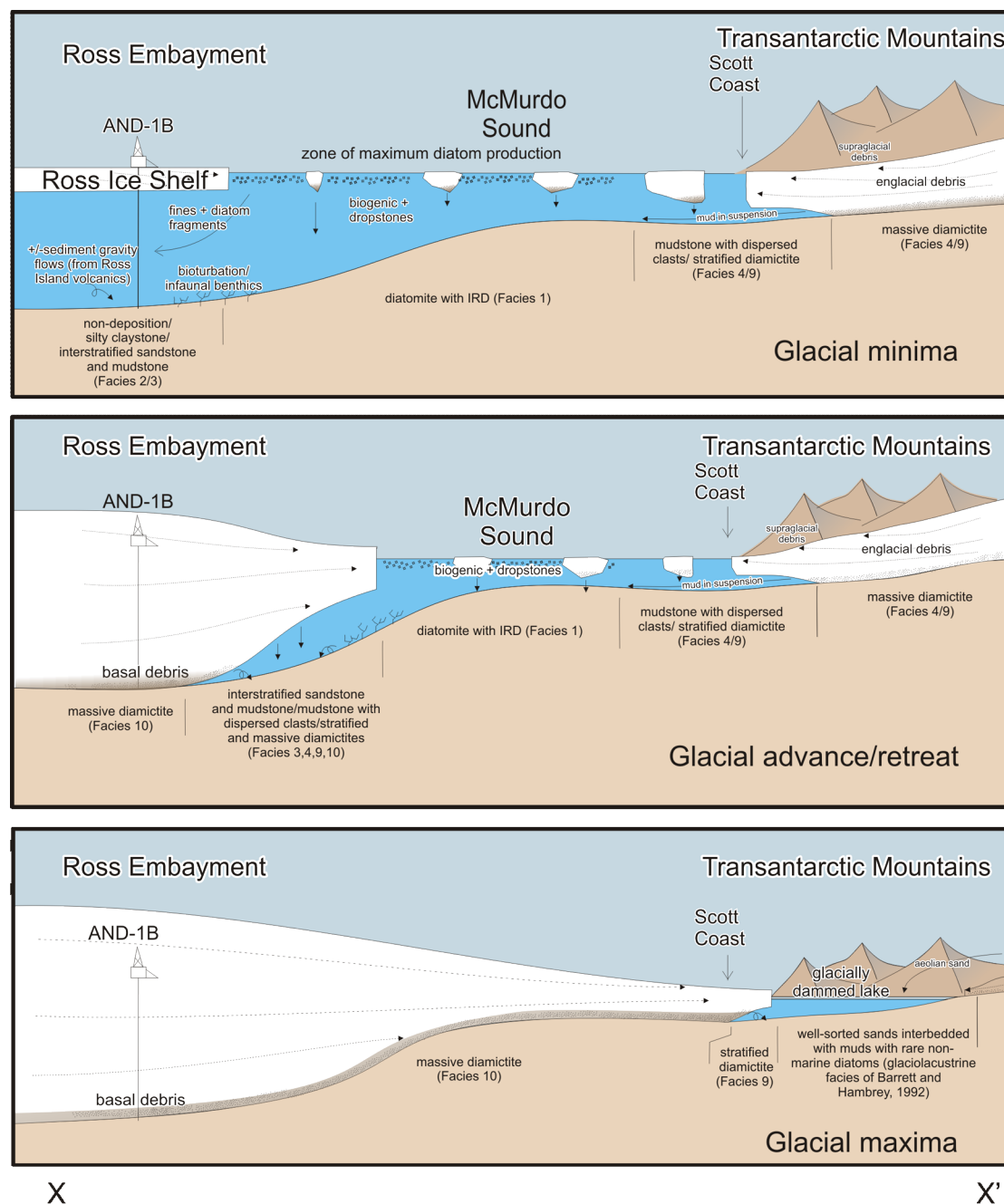


Figure 42: Sedimentary model for Motif 1, along a generalised profile of transect x-x' (see Figure 36). Glacial minima (top) at the drill site are characterised by sub-ice shelf deposition of mudstone interbedded with sediment gravity flows of volcanogenic sandstone. Facies associated with glacial advance/retreat (middle) of ice sheet over the AND-1B drillsite lack significant subglacial meltwater. During glacial maxima (bottom) grounded ice occupies McMurdo Sound, which results in the formation of “ice dammed” lakes during the Pleistocene (e.g., Hall *et al.*, 2000; Barrett and Hambrey, 1992).

The sedimentation model for Motif 1 (Figure 42) also incorporates interpretations made from the drill cores collected closer to the Victoria Land coast (e.g., CIROS-2). This model shows the damming of the mouth of Ferrar Fjord by an expanded ice sheet in the Ross Embayment during glacial maxima, which was interpreted to have caused deposition of glacialacustrine rhythmites in CIROS-2 (Barrett and Hambrey, 1992). According to Motif 1, deposition at the AND-1B site during ice advance was dominated by massive diamictites of subglacial origin (i.e. subglacial till). Based on the assumption that unconformities are minor within the Pleistocene section of Motif 1, interglacial sedimentation at AND-1B occurred almost entirely by sub-ice shelf processes with hemipelagic deposition and sediment gravity flows associated with grounding-line retreat/advance. Where the upper parts of Motif 1 contain locally derived McMurdo Volcanic Group sediments (Figure 36), a depositional environment proximal to the calving line is inferred, probably similar to that of present-day conditions at AND-1B.

3.6.2 Sedimentation during a dynamic polar/sub-polar glacial regime

Motif 2 records more dynamic fluctuations of the ice sheet than Motif 1. Motif 2 sequences dominate the Pliocene section of AND-1B, and are most notable for repetitions of diamictite (34% of the total facies assemblage) overlain by diatomite (37% of the total facies assemblage). The diamictites are interpreted as sub-glacial tills deposited during glacial maxima, whereas the diatomites record open-marine settings during glacial minima. The lack of terrigenous fine-grained sediment (i.e., not iceberg rafted debris) within or associated with the diatomites implies a lack of sub-glacial meltwater entering the Ross Embayment during glacial minima. Episodes with greater meltwater supply may be recorded by the muddy proglacial facies (constituting ~10 to 25% of some sequences; Figure 37) included in a few glacial retreat and advance sequences.

Motif 2 - Diatomite/Diamictite cycles

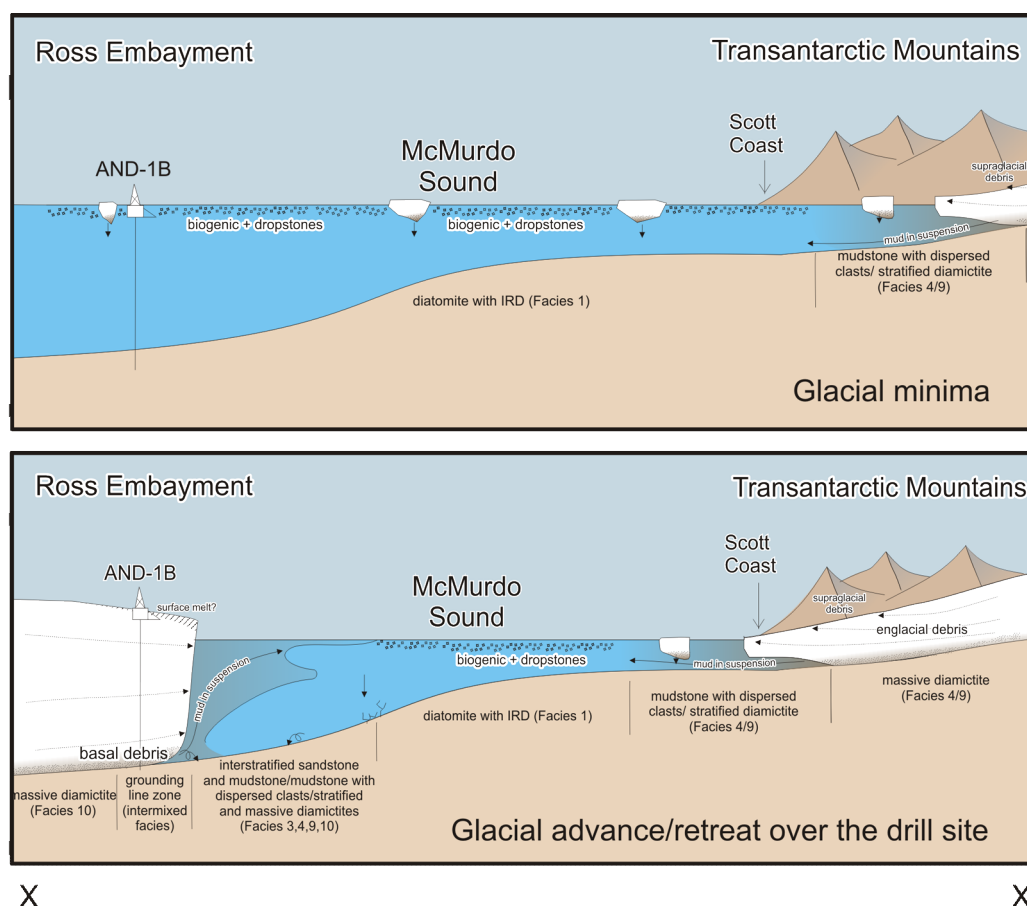


Figure 43: Sedimentary model for Motif 2, along a generalised profile of transect x-x' (see Figure 36). During glacial minima (top) open marine conditions prevail at the drill site with deposition of diatomaceous ooze. During ice sheet glacial advance/retreat (bottom) processes may be similar to those in Motif 1, although sequences within Motif 2b display evidence of an increased meltwater process at the grounding line. During glacial maxima, conditions were similar to that for Motif 1 (Figure 42), although CIROS-2 sediments are dominated by subglacial deposition beneath an expanded Ferrar Glacier, rather than glaciallacustrine sediments (Barrett and Hambrey, 1992).

Motif 2 records a more dynamic AIS in the Ross Embayment than present, with periods of open-water deposition (see Figure 43) during glacial minima. The 90 m-thick diatomite above 459.24 mbsf indicates open-marine conditions in the Ross Embayment for up to 400,000 years, and perhaps spanning several glacial-interglacial cycles in the Early Pliocene (Wilson *et al.*, 2007).

Diatomites deposited during the Holocene have been documented from basinal settings similar to the setting of AND-1B, but located immediately north of Ross Island (McKay *et al.*, 2008) and farther north in the Ross Sea (e.g., Domack *et al.*, 1999). These Holocene deposits indicate that diatomites can accumulate close to an ice shelf calving line, so the Pliocene calving line did not have to retreat significantly from the present-day calving-line position to allow deposition of diatom muds and oozes at AND-1B. However, several indicators of warmer than present conditions do accompany the AND-1B diatomites. While the transitions from glacial to open-marine facies are stratigraphically thinner in Motif 2 than in Motif 3, the transitions in Motif 2 do display clear evidence of elevated rates of sediment delivery (especially in Motif 2b). Evidence is also present that sedimentation was influenced by sub-glacial melt-water during advance and retreat of the grounding-line. This evidence includes turbidites (Facies 6), and ~5- to 10-m-thick intervals of massive mudstone (Facies 2), mudstone with dispersed to common clasts (Facies 4), and graded/stratified outwash sandstone interbedded with mudstone (Facies 3) that contain tractional sedimentary structures, such as ripple-cross-stratification of inferred glaci-fluvial origin (Table 11; Figure 37). These facies commonly lie directly on top of stratified and massive diamictites deposited by grounded ice and during ice lift-off. Preliminary analysis of diatom assemblages also provides strong evidence of warmer-than-present surface waters during the deposition of the Pliocene diatomites (Scherer *et al.*, 2007)

Figure 43 presents a model for the deposition of Motif 2 sequences. During retreat of grounded ice, sedimentation at AND-1B was influenced by variable amounts of meltwater (Motif 2a versus 2b) from the Ross Embayment ice sheet grounding line. Deposition during glacial minima occurred in open-water conditions, with little or no terrigenous input from EAIS outlet glaciers or the Ross Embayment ice sheet via glaci-marine or coastal processes. Although Motif 2 is interpreted to record a more dynamic AIS in the Ross Embayment, it may also reflect moderate warming relative

to present day conditions. Under warmer conditions, a large ice shelf was not sustained in the Ross Embayment, so that glacial minima are represented by open-water sediments, rather than those deposited beneath an ice shelf.

In some cases, the transition from massive diamictite deposited beneath grounded ice (i.e., subglacial till) to marine diatomite with a negligible terrigenous component occurs within 1 m (e.g., 224.20 to 225.20 mbsf), suggesting rapid ice retreat and transition from a grounded ice sheet to an ice-free Ross Embayment. These thin intervals of transitional facies are most common in Motif 2a in the Upper Pliocene section (~150.7 to 295.5 mbsf). The upsection increase in top-truncation of the sequences in the Upper Pliocene may indicate greater erosion during glacial readvance (either due to larger ice volume or a decrease in basin subsidence), or may reflect original deposition of thin readvance successions (i.e., less meltwater supply).

Motif 2 is interpreted to reflect an increased degree of dynamicism of the AIS in the Ross Embayment, under a subpolar to polar glacial regime that was warmer than present, but cooler than conditions during the deposition of Motif 3. If the ice sheet had largely withdrawn from the Ross Embayment during the glacial minima recorded in Motif 2, then the lack of terrigenous sedimentation at AND-1B during those minima indicates limited sediment delivery from local EAIS outlet glaciers. In addition, glacial regimes along the margin of the EAIS and for the TAM outlet glaciers were polar, with little to no meltwater production. However, a warmer ice sheet occupied the Ross Embayment, and episodic meltwater production did deliver moderate volumes of terrigenous sediment to the grounding zone during some times of glacial retreat and advance, as recorded by Motif 2b sequences. Local glaciation in the TAM probably was similar to conditions in modern sub-polar to polar environments dominated by iceberg production (Table 10) during the deposition of Motif 2a sequences in the Late Pliocene. Similar conditions, but with an increased meltwater influence, are interpreted to have existed during the deposition of Motif 2b in the Early Pliocene (Figure 37). The increased abundance of terrigenous mudstone facies at 82.7 - 150.7 mbsf, within glacial minima, retreat, and advance sequences (see Figure 37), is associated with the presence of volcanic sandstone turbidites and debris flow deposits. Alternatively, rather than representing a significant paleoclimatic change, this increased mud input may record increased slope instability during

volcanic cone building on Ross Island, especially on Hut Point Peninsula - which may have also been promoted as a new pinning point for the retreating ice shelf calving line.

3.6.3 Sedimentation during a dynamic sub-polar glacial regime

Motif 3 is interpreted as the record of glacial retreat, minimum and advance phases dominated by deposition of terrigenous siliciclastic sediments. At AND-1B, large volumes of glacial outwash mud, supplied from nearby sources, prevented diatomite from accumulating. This mud supply suggests that significant subglacial meltwater was provided from local EAIS outlet glaciers and from the glacial advance and retreat of the ice sheet that occupied the Ross Embayment. Supporting evidence includes the greater abundance of mud-rich proglacial facies (Facies 2, 3, 4, 5), which form 67% of the total facies assemblage in Motif 3. Within glacial retreat and advance sequences, conglomerate (Facies 7), sandstone (Facies 6) with ripple cross-stratification, and rhythmically interlaminated mudstone with siltstone or sandstone (Facies 5) are all more abundant than in the other two motifs. These facies probably represent deposition influenced by considerable sub-glacial marine outwash and mass flows near the grounding line of an expanded ice sheet in the Ross Embayment. Rhythmically interlaminated mudstone and sandstone constitute 6% of the total facies assemblage in Motif 3 (whereas they are rare to absent in Motifs 1 and 2), and form intervals up to 8 m thick, with cyclopsams (sandstone/mudstone couplets) grading upward into cyclopels (siltstone/mudstone couplets; Figure 41A/B). Lonestones that deform underlying laminae, and poorly sorted sandstone beds, are also associated with occurrences of Facies 5. Although diatoms may have been deposited with these muds, and subsequently destroyed by diagenesis, there is no evidence of the extremely high productivity conditions recorded by Motif 2. The dominance of siliciclastic lithofacies in Motif 3, together with the apparent lack of bioturbation and diatoms, suggest an environment with high sedimentation rates, principally of fine-grained material, in a deep-water setting influenced by iceberg-rafting. The rapid input of terrigenous mudstone during glacial minima is interpreted to have diminished biosiliceous productivity or diluted the input of biosiliceous debris.

The facies successions within Motif 3 are consistent with Holocene sedimentation models for sub-polar environments dominated by large and relatively consistent input of subglacial outwash (c.f. Table 10). These environments are dominated by suspension settling from turbid meltwater plumes, sediment gravity flows, and associated iceberg rafting (e.g., Ó Cofaigh and Dowdeswell, 2001; Dowdeswell *et al.*, 1998). Supporting evidence in the AND-1B core includes the higher abundance of facies deposited in proximal glacial and subglacial environments (i.e., massive/stratified diamictites, conglomerates, rhythmically interlaminated mudstone and sandstones), which are interpreted to record retreat/advance of a grounded ice sheet in the area of the drill site. Intervals of rhythmically interlaminated mudstone with siltstone/ sandstone (Facies 5) are interpreted to have been deposited during grounding-line retreat, in the presence of large volumes of subglacial meltwater. Cyclopsams grade upward into cyclopels, indicating the transition from a proximal to a more distal glacialmarine environment. Taken together, these changes in depositional environment imply significant glacial dynamism and ice volume changes on West Antarctica during the deposition of Motif 3.

Terrigenous sediments dominate the record of deposition during the glacial minimum in Motif 3, from which the largest extent of subglacial melting and outwash recorded in AND-1B is inferred. This evidence of significant subglacial melting and outwash suggests major fluctuations in volume of grounded ice that occupied the Ross Embayment. The significance of mudstones being deposited during glacial minima (when the AIS in the Ross Embayment was no longer influencing sedimentation at AND-1B), raises questions about the thermal state of the EAIS margin in the Ross Embayment during these times. In the absence of a proximal Ross Embayment AIS grounding line, the persistent supply of terrigenous muds during glacial minima required a local meltwater source. Therefore, terrestrial or marine-terminating TAM outlet glaciers (e.g., the Ferrar and Blue Glaciers) probably provided this source, and that meltwater processes were occurring on the EAIS margin/outlet glaciers at this time (Figure 44).

Motif 3 - Mudstone/Sandstone/Diamictite cycles

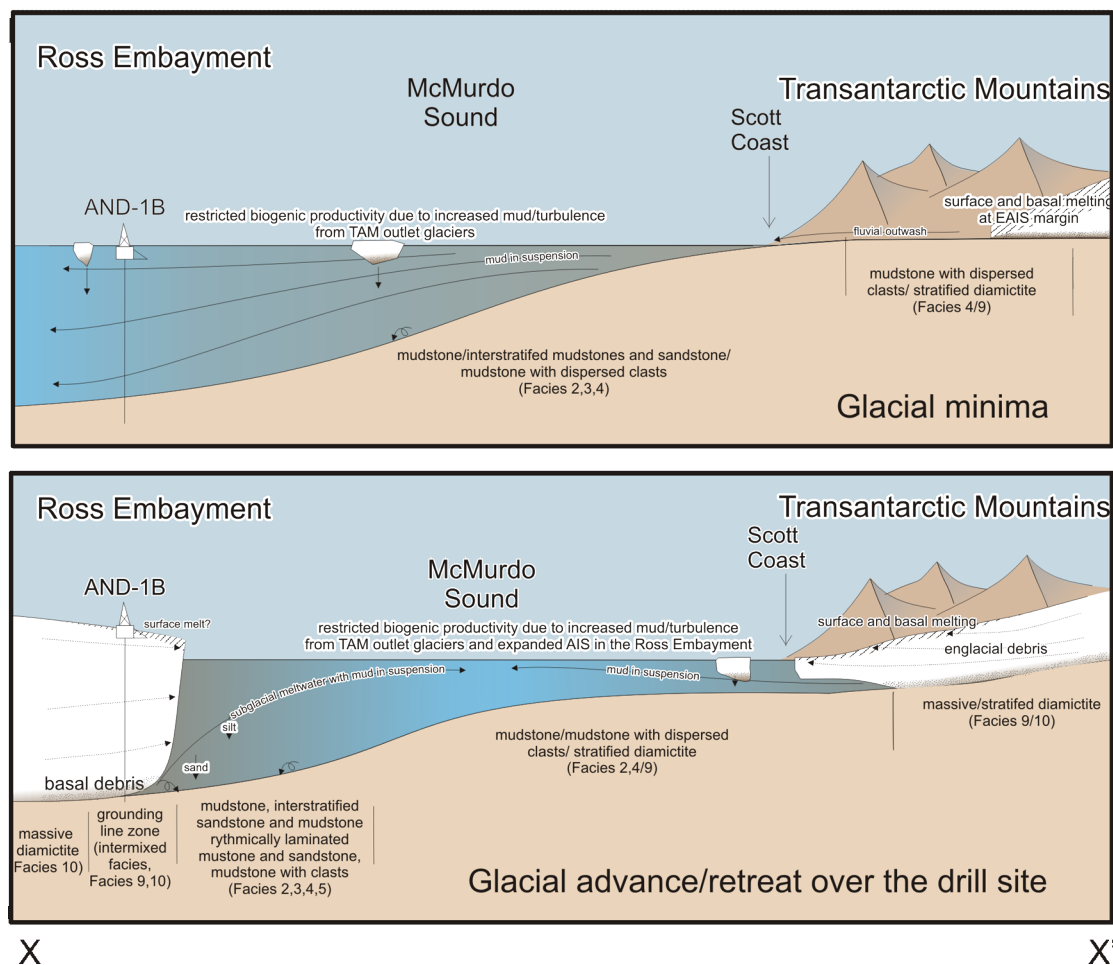


Figure 44: Sedimentary model for Motif 3, along a generalised profile of transect x-x' (see Figure 36). During glacial minima (top), sedimentation during open marine conditions at the drill site are dominated by hemipelagic suspension settling associated with increased meltwater derived from TAM outlet glaciers, relative to Motif 1 and 2. During ice sheet glacial advance/retreat over the drill site, there is a significant increase in facies associated with meltwater process at the grounding line, (Facies 5, 7, 9) and other mudstone rich facies (Facies 2, 3, 4). The ice sheet configuration for the glacial maxima is expected to be similar to that for Motif 1 (Figure 42).

3.7 Conclusions

The AND-1B drill core provides the most continuous, high-resolution record of AIS oscillations and evolution over the past 13 Myr yet recovered. Stratigraphic signatures for repetitive oscillations of AIS extent in the Ross Embayment under three different glacial regimes since the Middle Miocene are identified. Development of a high resolution age model for AND-1B is currently underway, and will allow the observations made in this chapter to be correlated with other proxy climate records (e.g., ice and marine isotope records), thus providing new insight into Antarctica's influence, and response to, Late Cenozoic climate events.

All three motifs display evidence of subglacial erosion and of deposition by a grounded ice sheet. Ice-proximal conditions were followed by a period of proglacial-marine or open-marine sedimentation during retreat of the ice terminus, and succeeded by additional proglacial-marine deposition or erosion during subsequent AIS readvance in the Ross Embayment. The different motifs record changes in the areal extent of the ice sheet, with its mass balance controlled by changes in surface/basal melting and calving processes through the Late Cenozoic.

During the Middle Miocene, sedimentary sequences of Motif 1 were deposited beneath grounded ice and floating ice shelves. Evidence for subglacial melt-water or erosion generally is lacking in these sequences, suggesting a cold, polar glacial regime for both the WAIS and the EAIS during this time. Sequences deposited during the Late Miocene (Motif 3) contain strong evidence for significantly higher volumes of subglacial melt-water and terrigenous sediment supply by both the ice sheet that occupied the Ross Embayment and local EAIS outlet glaciers. This evidence includes the repeated presence of outwash facies deposited during AIS grounding line retreat and advance in the Ross Embayment, as well as the deposition of mudstone facies, rather than diatomite, during glacial minima. In contrast, the Pliocene sequences of Motif 2 document dynamic fluctuations of the marine-based AIS in the Ross Embayment, in the form of subglacial till (diamictites) alternating with open-marine diatomites. The meltwater influence on sequences of Motif 2 appears to have decreased through time, as evidenced by the progressive upsection thinning of

outwash facies deposited during the transitions from subglacial to open marine conditions. This is interpreted as representing a decrease in meltwater influence, recording the transition from a sub-polar glacial regime in the Early Pliocene to a polar glacial regime in the Late Pliocene. Pleistocene sequences of Motif 1 record a return to cold polar glaciations, dominated by subglacial and ice shelf deposition with a general lack of subglacial meltwater influence. This style of glaciation is consistent with modern conditions beneath the Ross Ice Shelf.

3.8 References

- Anderson, J. B., and Ashley, G. M., 1991. Glacial marine sedimentation; paleoclimatic significance; a discussion, in Anderson, J. B., and Ashley, G. M., eds., *Glacial Marine Sedimentation; Paleoclimatic Significance. Geological Society of America Special Paper* v.261, p.223-226.
- Ashley, G.M., and Smith, N.D., 2000. Marine sedimentation at a calving glacier margin: *Geological Society of America, Bulletin* v.112, p.657-667.
- Azetsu-Scott K., Syvitski J.P.M., 1999. Influence of melting icebergs on distribution, characteristics and transport of marine particles in an East Greenland fjord: *Journal of Geophysical Research* v.104 (C3), p.5321-5328.
- Barker, P. F., Camerlenghi, A., Acton, G. D., Brachfeld, S. A., Cowan, E. A., Daniels, J., Domack, E. W., Escutia, C., Evans, A. J., Eyles, N., Guyodo, Y. J. B., Iorio, M., Iwai, M., Kyte, F. T., Lauer, C., Maldonado, A., Moerz, T., Osterman, L. E., Pudsey, C. J., Schuffert, J. D., Sjunneskog, C. M., Vigar, K. L., Weinheimer, A. L., Williams, T., Winter, D. M., and Wolf-Welling, T. C. W., 1999. *Proceedings of the Ocean Drilling Program; initial reports* v.178, 60p.. College Station, TX.
- Barrett, P. J. (ed.), 1989. Antarctic Cenozoic history from CIROS-1 drillhole, McMurdo Sound: *DSIR Bulletin* v.245, 251 p.
- Barrett, P., 1999. Antarctic climate history over the last 100 million years: *Terra Antarctica Reports* v.3, p.53-72.
- Barrett, P.J., 2007. Cenozoic climate and sea level history from glacial-marine strata off the Victoria Land coast, Cape Roberts Project, Antarctica. *International Association of Sedimentologists Special Publication* v.39, p.259-287.
- Barrett, P.J., and Hambrey, M.J. 1992. Plio-Pleistocene sedimentation in Ferrar Fiord, Antarctica.: *Sedimentology* v.39, p.109-123.
- Barrett, P.J., Carter, L., Dunbar, G.B., Dunker, E., Giorgetti, G., Harper, M.A., McKay, R.M., Niessen, F., Nixdorf, U., Pyne, A.R., Riesselmann, C., Robinson, N., Hollis, C., and Strong, P., 2005. Oceanography and sedimentation beneath the McMurdo Ice Shelf in Windless Bight, Antarctica. *Antarctic Data Series* v.25, Antarctic Research Centre, Victoria University of Wellington, 100 p.
- Barron, J., and Larsen, B., et al. 1989. *Proceedings of the Ocean Drilling Project Initial Reports*, v.119, College Station, TX (Ocean Drilling Program). 942 p.

- Bart, P.J., Anderson, J.B., Trincardi, F., Shipp, S.S., 2000. Seismic data from the Northern basin, Ross Sea, record extreme expansions of the East Antarctic Ice Sheet during the late Neogene. *Marine Geology* v.166, p.31-50.
- Bindschadler, R.A., Alley, R.B., Anderson, J., Shipp, S., Borns, H., Fastook, J., Jacobs, S., Raymond, C.F., and Shuman, C.A., 1998. What is happening to the West Antarctic ice sheet? *Eos, Transactions* v.79, p.257, 264-265.
- Bouma, A.H., 1962. Sedimentology of some Flysch Deposits: A Graphic Approach to Facies Interpretation: Amsterdam, Elsevier, 168 p.
- Carter, L., Mitchell, J.S., and Day, N.J., 1981. Suspended sediment beneath permanent and seasonal ice, Ross Ice Shelf, Antarctica. *New Zealand Journal of Geology and Geophysics* v.24, p.249-262.
- Conway, H., Hall, B. L., Denton, G. H., Gades, A. M., and Waddington, E. D., 1999. Past and future grounding-line retreat of the West Antarctic Ice Sheet: *Science* v.286, p.280-283.
- Cooper, A. K., Davey, F. J., and Behrendt, J. C., 1987. Seismic stratigraphy and structure of the Victoria Land Basin, western Ross Sea, Antarctica. In: Cooper, A. K., and Davey, F. J., eds., *The Antarctic Continental Margin: Geology and Geophysics of the Western Ross Sea*: Houston, Texas, Circum-Pacific Council for Energy and Mineral Resources, Earth Science Series, p.93-118.
- Cowan, E.A., and Powell, R.D., 1991. Ice-proximal sediment accumulation rates in a temperate glacial fjord, southeastern Alaska, in Anderson, J.B., and Ashley, G.M., eds., *Glacial marine sedimentation; paleoclimatic significance*. *Geological Society of America, Special Paper* v.261, p.61-73.
- Cowan, E.A., Seramur, K.C., Cai, J., and Powell, R.D., 1999. Cyclic sedimentation produced by fluctuations in meltwater discharge, tides and marine productivity in an Alaskan fjord. *Sedimentology* v.46, p.1109-1126.
- Crowley, T. J., 1996. Pliocene climates; the nature of the problem. Climates and climate variability of the Pliocene. *Marine Micropaleontology* v.27, p.3-12.
- Dawber, M., and Powell, R. D., 1997. Epifaunal distributions at Antarctic marine-terminating glaciers; influences of ice dynamics and sedimentation. In: Ricci, C.A. (ed.) *The Antarctic region; geological evolution and processes; proceedings of the VII international symposium on Antarctic earth sciences, VII international symposium on Antarctic earth sciences*. Siena, Italy, p.875-884.
- De Santis, L., Prato, S., Brancolini, G., Lovo, M. and Torelli, L., 1999. The eastern Ross Sea continental shelf during the Cenozoic and implications for the West Antarctic ice sheet development. *Global and Planetary Change* v.23, p.173-196.
- Denton, G.H., and Hughes, T.J., 2000. Reconstruction of the Ross Ice Drainage System, Antarctica, at the Last Glacial Maximum. *Geografiska Annaler, Series A: Physical Geography* v.82, p.143-166.
- Desloges, J.R., Gilbert, R., Nielsen, N., Christiansen, C., Rasch, M., and Øhlenschläger, R., 2002. Holocene glacimarine sedimentary environments in fiords of Disko Bugt and West Greenland. *Quaternary Science Reviews and Research* v.21, p.947-963.
- Domack, E. W., and Ishman, S. E., 1993. Oceanographic and physiographic controls on modern sedimentation within Antarctic fjords. *Geological Society of America Bulletin* v.105, p.1175-1189.

- Domack, E. W., and Williams, C. R., 1990. Fine structure and suspended sediment transport in three Antarctic fjords. Contributions to Antarctic Research, *Antarctic Research Series* v.50, p.71–89.
- Domack, E. W., Jacobson, E. A., Shipp, S., and Anderson, J. B., 1999. Late Pleistocene-Holocene retreat of the West Antarctic ice-sheet system in the Ross Sea; Part 2, Sedimentologic and stratigraphic signature. *Geological Society of America Bulletin* v.111, p.1517-1536.
- Domack, E.W., Leventer, A., Dunbar, R., Taylor, F., Brachfeld, S., Sjunneskog C., and ODP Leg 178 Scientific Party, 2001. Chronology of the Palmer Deep site, Antarctic Peninsula. a Holocene palaeoenvironmental reference for the circum-Antarctic. *The Holocene* v.11, p.1–9.
- Dowdeswell, J. A., and Dowdeswell, E. K., 1989. Debris in icebergs and rates of glacial marine sedimentation. Observations from Spitsbergen and a simple model. *Journal of Geology* v.97, p.221–231.
- Dowdeswell, J.A., Whittington, R.J., Marienfeld, P., 1994. The origin of massive diamicton facies by iceberg rafting and scouring, Scoresby Sund, East Greenland. *Sedimentology* v.41, p.21-35.
- Dowdeswell, J.A., Elverhøi, A., and Spielhagen, R., 1998. Glacial marine sedimentary processes and facies on the Polar North Atlantic margins. *Quaternary Science Reviews* v.17, p.243-272.
- Drewry, D. J., 1983. Antarctica: Glaciological and geophysical folio. Cambridge, United Kingdom, University of Cambridge, Scott Polar Research Institute, 9 p.
- Dunbar, R. B., Leventer, A. R., Stockton, W. L., 1989. Biogenic sedimentation in McMurdo Sound, Antarctica. *Marine geology* v.85, p.155-179.
- Elverhøi, A., Liestøl, O., Nagy, J., 1980. Glacial erosion, sedimentation and microfauna in the inner part of Kongsfjorden, Spitsbergen. *Norsk Polarinstitutt Skrifter* v.172, p.33-58.
- Elverhøi, A., Lønne, O., Seland, R., 1983. Glaciomarine sedimentation in a modern fjord environment, Spitsbergen. *Polar Research* v.1, p.127-149.
- Evans, J., Dowdeswell, J.A., Grobe, H., Niessen, F., Stein, R., Hubberten, H.W., and Whittington, R.J., 2002. Late Quaternary sedimentation in Kejser Franz Joseph Fjord and the continental margin of East Greenland, in Dowdeswell, J.A., and Ó Cofaigh, C., eds., Glacier-influenced sedimentation on high-latitude continental margins. *Geological Society of London Special Publication* v.203, p.149–179.
- Fahnestock, M.A., Scambos, T.A., Bindshadler, R.A., Kvaran, G., 2000. A millennium of variable ice flow recorded by the Ross Ice Shelf, Antarctica. *Journal of Glaciology* v.46, p.652-664.
- Fielding C.F., Naish T.R., Woolfe K.J., and Levelle M.A., 2000. Facies analysis and sequence stratigraphy of CRP-2/2A, Victoria Land Basin, Antarctica. *Terra Antarctica* v.7, p.323-338.
- Hall, B.L., Denton, G.H., Hendy, C.H., Denton, G.H., and Hall, B.L., 2000. Evidence from Taylor Valley for a grounded ice sheet in the Ross Sea, Antarctica. *Geografiska Annaler: Physical Geography* v.82, p.275-303.
- Hambrey, M.J., Ehrmann, W.U., Larsen, B. 1991. The Cenozoic glacial record from the Prydz Bay continental shelf, East Antarctica . In: J. Barron and B. Larsen (eds.), *Leg 119, Ocean Drilling Program, Scientific Results* p.77–132. Ocean Drilling Program, College Station, TX.

- Hambrey, M. J., Barrett, P. J., Powell, R. D., 2002. Late Oligocene and early Miocene glacial-marine sedimentation in the SW Ross Sea, Antarctica; the record from offshore drilling. In: Dowdeswell, J. A., and Ó Cofaigh, C. (eds.) *Glacier-influenced sedimentation on high-latitude continental margins. Geological Society of London Special Publications* v.203, p.105-128.
- Hayes, D. E., Frakes, L. A., Barrett, P. J., Burns, D. A., Chen, P.-H., Ford, A. B., Kaneps, A. G., Kemp, E. M., McCollum, D. W., Piper, D. J. W., Wall, R. E., and Webb, P. N., 1975. *Initial Reports of the Deep Sea Drilling Project* v.28, p.1017.
- Henrys, S.A., Wilson, T.J., Whittaker, J., Fielding, C.R., Hall, J., and Naish, T.R., 2007. Tectonic History of Mid-Miocene to Present Southern Victoria Land Basin, inferred from Seismic Stratigraphy, in McMurdo Sound, Antarctica. In: Cooper, A.K., and Raymond, C.R., (eds.) *Antarctica: A Keystone in a Changing World—Online Proceedings for the Tenth International Symposium on Antarctic Earth Sciences, USGS Open-File Report 2007-1047*, Short Research Paper 049.
- Horgan, H., Naish, T., Bannister, S., Balfour, N., and Wilson, G. S., 2005. Seismic stratigraphy of the Plio-Pleistocene Ross Island flexural moat-fill; a prognosis for ANDRILL Program drilling beneath McMurdo-Ross Ice Shelf. *Global and Planetary Change* v.45, p.83-97.
- Hughes, T., 1977. West Antarctic ice streams. *Reviews of Geophysics and Space Physics* v.15, p.1-46.
- IPCC, 2007. *Climate Change 2007: The Physical Science Basis. Contribution of Working Group I to the Fourth Assessment Report of the Intergovernmental Panel on Climate Change*. Cambridge University Press, 996 p.
- Kennett, J. P., and Hodell, D. A., 1993. Evidence for relative climatic stability of Antarctica during the early Pliocene; a marine perspective. *Geografiska Annaler. Series A: Physical Geography* v.75, p.205-220.
- Krissek, L.A., Browne, G.H., Carter, L., Cowan, E.A., Dunbar, G.B., McKay, R.M., Naish, T., Powell, R., Reed, J., Wilch, T.I and the Andrill MIS Science Team 2007. Sedimentology and Stratigraphy of the AND-1B Core, ANDRILL McMurdo Ice Shelf Project, Antarctica. *Terra Antarctica* v.14, p.185-222.
- Leckie, R.M., and Webb, P.-N., 1983. Late Oligocene-early Miocene glacial record of the Ross Sea, Antarctica; evidence from DSDP Site 270. *Geology* v.11, p.578-582.
- Lewis, A.R., Marchant, D.R., Kowalewski, D.E., Baldwin, S.L., and Webb, L.E., 2006. The age and origin of the Labyrinth, western Dry Valleys, Antarctica: Evidence for extensive middle Miocene subglacial floods and freshwater discharge to the Southern Ocean. *Geology* v.34, p.513-516
- Lewis, A.R., Marchant, D.R., Ashworth, A.C., Hemming, S.R., and Machlus, M.L., 2007. Major middle Miocene global climate change: Evidence from East Antarctica and the Transantarctic Mountains. *Geological Society of America Bulletin* v.119, p.1449-1461.
- Licht, K. J., Dunbar, N. W., Andrews, J. T., and Jennings, A. E., 1999. Distinguishing subglacial till and glacial marine diamictos in the western Ross Sea, Antarctica; implications for a last glacial maximum grounding line. *Geological Society of America Bulletin* v.111, p.91-103.
- Licht, K.J., Lederer, J.R., Swope, J., 2005. Provenance of LGM glacial till (sand fraction) across the Ross embayment, Antarctica. *Quaternary Science Reviews* v.24, p.1499-1520.

- MacAyeal, D.R., 1992. Irregular Oscillation of the West Antarctic Ice Sheet. *Nature* v.359, p.29-32.
- Mackiewicz, N.E., Powell, R.D., Carlson, P.R., Molnia, B.F., 1984. Interlaminated ice-proximal glacial marine sediments in Muir Inlet, Alaska. *Marine Geology* v.57, p.113-147.
- MacPherson, A., 1987. The MacKay Glacier/Granite Harbour Glacial Marine Sedimentation System. *Unpublished PhD thesis*. Victoria University of Wellington.
- McCrae, I.R., 1984. A summary of glaciological measurements made between 1960 and 1984 on the McMurdo Ice Shelf, Antarctica. Auckland. School of Engineering Report 360, Department of Theoretical and Applied Mechanics, University of Auckland.
- McKay R.M., Dunbar G.B., Naish T.R., Barrett P.J., Carter L., and Harper M., 2008. Retreat history of the West Antarctic Ice (Sheet) Shelf in Western Ross Sea since the Last Glacial Maximum from Deep-Basin Sediment Cores. *Palaeogeography, Palaeoclimatology, Palaeoecology* v.260, p 168-183.
- Moncrieff, A.C.M., 1989. Classification of poorly sorted sedimentary rocks. *Sedimentary Geology* v.65, 191-194.
- Mosola, A.B., and Anderson, J.B., 2006. Expansion and rapid retreat of the West Antarctic Ice Sheet in eastern Ross Sea: possible consequence of over-extended ice streams? *Quaternary Science Reviews* v.25, p.2177–2196.
- Naish, T.R., Powell, R.D., Levy, R.H., and the ANDRILL MIS Science Team 2007. Initial Science results from AND-1B, ANDRILL McMurdo Ice Shelf Project, Antarctica. *Terra Antartica* v.14, p.111-328.
- O'Brien, P.E., A.K. Cooper, C. Richter, *et al.* 2001. *Proceedings of the Ocean Drilling Project Initial Reports* v.188, College Station, TX.
- Ó Cofaigh, C., and Dowdeswell, J.A., 2001. Laminated sediments in glacial marine environments: diagnostic criteria for their interpretation. *Quaternary Science Reviews* v.20, p.1411-1436.
- Ó Cofaigh, C., Dowdeswell, J. A. and Grobe, H., 2001. Holocene glacial marine sedimentation, inner Scoresby Sund, East Greenland: the influence of fast-flowing ice-sheet outlet glaciers. *Marine Geology* v.175, p.103-129.
- Pompilio M., Dunbar N., Gebhardt, A.C., Helling D., Kuhn, G., Kyle P., McKay R., Talarico F., Tulaczyk S., Vogel, S., Wilch T., and the ANDRILL-MIS Science Team. 2007. Petrology and Geochemistry of the AND-1B Core, ANDRILL McMurdo Ice Shelf Project, Antarctica. *Terra Antartica* v.14, p.255-288.
- Powell, R. D., 1990. Grounding-line fans and their growth to ice-contact deltas. *Geological Society of London Special Publication* v.53 p.53-73.
- Powell, R. D., Dawber, M., McInnes, J. N., and Pyne, A. R., 1996. Observations of the grounding-line area at a floating glacier terminus. *Annals of Glaciology* v.22, p.217-223.
- Powell, R. D., and Cooper, J. M., 2002. A glacial sequence stratigraphic model for temperate, glaciated continental shelves. *Geological Society of London Special Publications* v.203, p.215-244.
- Powell, R. D., and Domack, E. W., 2002. Glacial marine environments, in Menzies, J., ed., *Modern and Past Glacial Environments*. Boston, Butterworth-Heinemann, p.361-390.

- Powell, R.D., and Molnia, B., 1989. Glacimarine sedimentary processes, facies and morphology of the south-southeast Alaska shelf and fjords. *Marine Geology* v.85, p.359–390.
- Raymo, M. E., 1994. The initiation of Northern Hemisphere glaciation. *Annual Review of Earth and Planetary Sciences* v.22, p.353–383.
- Rignot, E., and Jacobs, S.S., 2002. Rapid bottom melting widespread near Antarctic ice sheet grounding lines. *Science* v.296, p.2020–3.
- Scherer, R.P., Aldahan, A.A., Tulaczyk, S., Possnert, G., Engelhardt, H., and Kamb, B., 1998. Pleistocene collapse of the West Antarctic ice sheet. *Science* v.281, p.82–85.
- Scherer, R.P., Sjunneskog, C.M., Iverson, N., and Hooyer, T. 2004. Assessing subglacial processes from diatom fragmentation patterns. *Geology* v.32, p.557–560.
- Scherer R., Hannah M., Maffioli P., Persico D., Sjunneskog C., Strong C.P., Taviani M., Winter D. and the ANDRILL-MIS Science Team., 2007. Palaeontologic Characterisation and Analysis of the AND-1B Core, ANDRILL McMurdo Ice Shelf Project, Antarctica. *Terra Antartica*, v.14, p.223–254.
- Schoof, C. 2007. Ice sheet grounding line dynamics: steady states, stability and hysteresis. *Journal of Geophysical Research*, v.112, F03S28, doi:10.1029/2006JF000664.
- Shipp, S., Anderson, J. B., and Domack, E. W., 1999, Late Pleistocene-Holocene retreat of the West Antarctic ice-sheet system in the Ross Sea; Part 1, Geophysical results: Geological Society of America Bulletin, v.111, p.1486–1516.
- Sjunneskog, C., and Scherer, R. P., 2005. Mixed diatom assemblages in glacial sediment from the central Ross Sea, Antarctica. *Palaeogeography, Palaeoclimatology, Palaeoecology* v.218, p.287–300.
- Stern, T. A., Davey, F. J., and Delisle, G., 1991. Lithospheric flexure induced by the load of Ross Archipelago, southern Victoria Land, Antarctica, in Thomson, M. R. A., Crame, J. A., and Thomson, J. W., eds., *Geological Evolution of Antarctica*. Cambridge University Press. International Symposium on Antarctic Earth Sciences, p.323–328.
- Stone, J. O., Balco, G. A., Sugden, D. E., Caffee, M. W., Sass, L. C., III, Cowdery, S. G., and Siddoway, C., 2003. Holocene deglaciation of Marie Byrd Land, West Antarctica. *Science* v. 299, p.99–102.
- Sugden, D., and Denton, G., 2004. Cenozoic landscape evolution of the Convoy Range to Mackay Glacier area, Transantarctic Mountains; onshore to offshore synthesis. *Geological Society of America Bulletin*, v. 116, p.840–857.
- Sudgen, D.E., Marchant, D.R. and Denton, G.H., 1993. The case for a stable East Antarctic Ice Sheet. *Geografiska Annaler* v.75, p.151–353.
- Syvitski, J.P.M., Andrews, J.T., Dowdeswell, J.A., 1996. Sediment deposition in an iceberg-dominated glacimarine environment East Greenland: basin fill implications. *Global and Planetary Change* v.12, p.251–270.
- Talarico, F.M., and Sandroni, S. 2007. Clast provenance and variability in MIS (AND-1B) core and their implications for the paleoclimatic evolution recorded in the Windless Bight - southern McMurdo Sound area (Antarctica), in Cooper A.K et al.,(eds). Program book for the 10th ISAES, *IUGS Open-File Report 2007*, 104, 14p.

- Thomas, R.H., and Bentley C.R., 1978. A model for Holocene retreat of the West Antarctic ice sheet. *Quaternary Research*, v.10, 150–170.
- Tulaczyk, S., Kamb, B., Scherer, R.P. and Engelhardt, H.F., 1998. Sedimentary processes at the base of a West Antarctic ice stream: constraints from textural and compositional properties of subglacial debris. *Journal of Sedimentary Research* v.68, p.487–496.
- Webb, P.N., and Harwood, D.M., 1991. Late Cenozoic Glacial History of the Ross Embayment, Antarctica. *Quaternary Science Reviews* v.10, p.215-223.
- Webb, P.-N., Harwood, D.M., McKelvey, B.C., Mercer, J.H., and Stott, L.D., 1984. Cenozoic marine sedimentation and ice volume variation in the east Antarctic craton. *Geology* v.12, p.287-291.
- Weertman, J. 1974. Stability of the junction of an ice sheet and an ice shelf. *Journal of Glaciology* v.13, p. 3–13.
- Wilson, G., Levy, R., Browne, G., Dunbar, N., Florindo, F., Henrys, S., Graham, I., McIntosh, W. McKay, R., Naish, T., Ohneiser, Powell, R., Ross, J., Sagnotti, L., Scherer, R., Sjunneskog, C., Strong, C., Taviani, Winter, D. and the ANDRILL MIS Science Team. 2007. Preliminary Chronostratigraphy of the AND-1B Core, ANDRILL McMurdo Ice Shelf Project, Antarctica. *Terra Antarctica* v.14, p.297-316.
- Zachos, J.C., Pagani, M., Sloan, L., Thomas, E., and Billups, K., 2001. Trends, rhythms, and aberrations in global climate 65 Myr to present. *Science* v.292, p.686-693.

3.9 Supplementary report: Grain size analysis

3.9.1 Grain size method

Between 10 and 30 g of sample was disaggregated by drying and crushing gently between wooden blocks. After crushing, the samples were tested for carbonate, and if present, were treated in 10% HCL until the reaction was complete. The samples were then stirred in calgon (1g/L) in an ultrasonic bath until disaggregated, which could take several hours. Once fully disaggregated, the sample was wet sieved into sand and mud fractions. The sand fraction (63 μ m to 2 mm; 4 ϕ to -1 ϕ) was dry sieved at 0.5 ϕ intervals, while a 1.5 g sub-sample of the mud fraction was stirred in calgon for 15 minutes in an ultrasonic bath and analysed by SedigraphTM 5100. Data for material >63 μ m, recovered during the dry sieving phase, were then merged with the Sedigraph data. Given the same sample size, the gravel fraction (>2 mm) cannot be reliably estimated, and although recorded, was excluded from the statistical analysis. The relative abundance of gravel was recorded at 10-cm intervals by visual analysis during core characterization (Krissek *et al.*, 2007).

While the removal of aggregates within the diamictite samples was difficult without destroying the original grain-size distribution, it was successful in most cases. The presence of aggregates can be identified by significant jump in the distribution between the sieve and Sedigraph (~4 ϕ), as well as during thin-section analysis of the sand fraction, allowing the magnitude of any aggregate error to be determined qualitatively. However, mudstone and diamictite intraclasts were a relatively common component in some diamictite deposits, and this error could not be determined. Given the consolidated and sometimes cemented nature of these deposits, and that the intraclasts were composed of the same material as the diamictite matrix, it was impossible to record grain-size distribution and maintain the original depositional grain size of many of these samples, and this is an accepted error. The results are presented according to the facies assigned during initial core characterisation, and confirms in most case, the initial descriptions.

3.9.2 Facies 1: Diatomite

Eight samples of diatomite were selected for grain size analysis, with the primary aim to extract the sand fraction for thin section analysis. Due to the small sample sizes and low proportion of terrigenous sediment, no attempt was made to dissolve the biogenic silica. In most samples, there are small peaks in the sand fraction, probably representing an IRD component. Although the grain-size distribution fits into the silty-clay to clay mode, this may be an artefact of the physical crushing of the fragile diatom frustules during processing. The line chart in Figure 45 shows the grain-size distribution for AND-1B diatomite (black lines) plotted alongside diatomites from DF80-189 (red lines; see Chapter 2), which were not crushed during processing. This indicates that errors resulting from physical crushing were minimal. However, both samples were disaggregated in an ultrasonic tank, which may also damage diatom frustules.

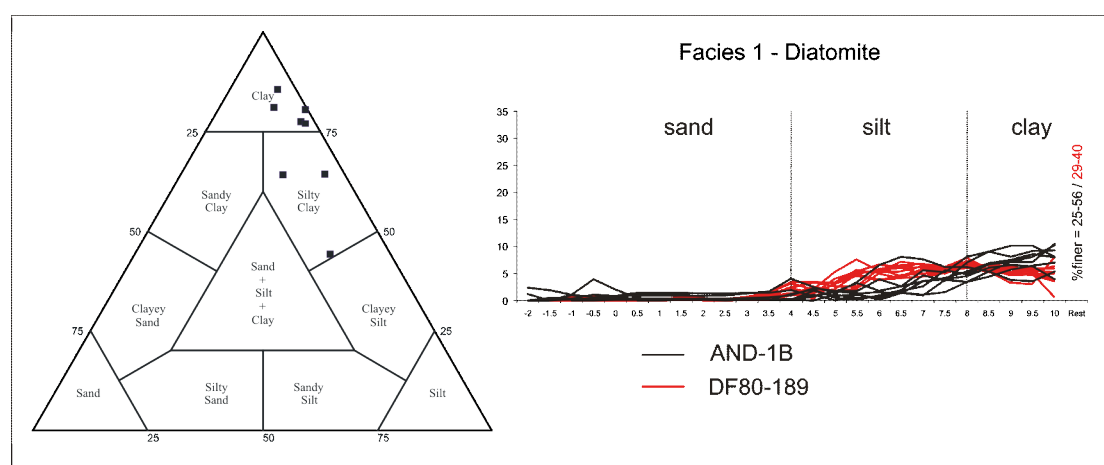


Figure 45: Grain-size results for Facies 1: Shepard diagram (left) showing textural classification and frequency curve for AND-1B (black lines) and DF80-189 core (red lines (presented in Chapter 2 of thesis).

3.9.3 Facies 2: Mudstone

Twenty-two samples of mudstones were processed for grain size analysis. All but one sample fit into the silty-clay to clay mode, and in some samples the clay fraction (>80) reaches 80%. Only one sample has a distinct fine sand mode that shows a jump between the sieve and Sedigraph, and is suspected to have incompletely disaggregated during processing. The sand fraction is absent in most samples (Figure 46), indicating little to no input of ice-rafted debris (from either a floating ice shelf or ice-bbergs).

Figure 46 shows the comparison of AND-1B mudstones versus those from the HWD and DF80-189 cores (red lines; presented in Chapter 2 of this thesis) and those from the Cape Roberts Project (blue lines; Dunbar and Barrett, 2004). The distribution in AND-1B correlates well with those of the HWD and DF cores, in which the mudstone facies are interpreted to have been deposited beneath a floating ice shelf that is free of basal debris. The Cape Robert Project mudstones all have a distinct fine sandstone mode, which is likely to be the result of either the distal component of coastal processes (i.e., suspension settling), or proximal grounding line processes associated with the MacKay Glacier (Fielding *et al.*, 2000).

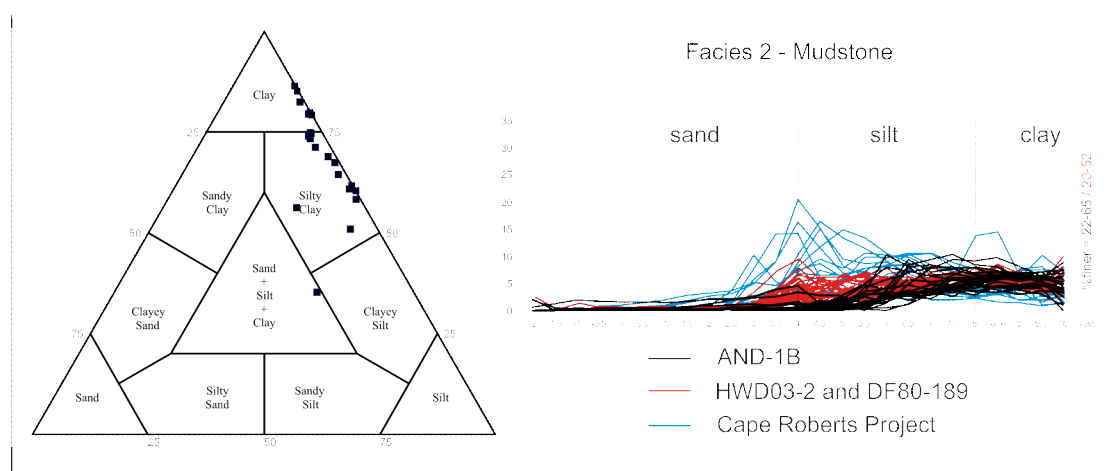


Figure 46: Grain-size results for Facies 2: Shepard diagram (left) showing textural classification; and frequency curve (right) for AND-1B (black lines) and similar facies from the Cape Robert Project (Dunbar and Barrett, 2004), and HWD03-1/DF80-189 core (red lines; presented in Chapter 2 of this thesis).

3.9.4 Facies 3: Interstratified mudstone and sandstone

The grain-size frequency distribution of Facies 3 (34 Samples; Figure 47) is highly variable, making it difficult to define any significant pattern. The distribution of this facies in AND-1B (black lines) correlates well with the interstratified sand and mudstone from HWD03-1 between 0 and 24 cm (red line), indicating that this facies can be deposited in a sub-ice shelf environment, although open marine environments are also a possibility. Sediment gravity flows or grounding line processes, including possible tidal pumping (Domack and Williams, 1990; Domack *et al.*, 1999; Powell and Domack 2002; Anandakrishnan, and Alley, 1997), are the probable depositional processes for these interstratified mudstone and sandstone.

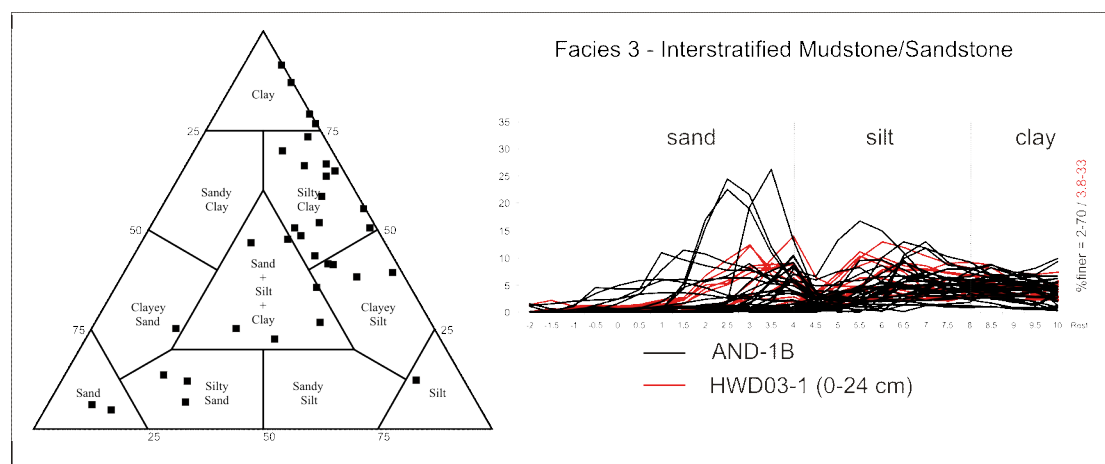


Figure 47: Grain-size results for Facies 3: Shepard diagram (left) showing textural classification; and frequency curve (right) for AND-1B (black lines) and similar facies in HWD03-1 (red lines; presented in Chapter 2).

3.9.5 Facies 4: Mudstone with dispersed/common clasts

Sixteen samples were analysed for grain size, with the frequency distribution of the facies (Figure 48) lying between that of Facies 2 (mudstone; Figure 46) and Facies 10 (massive diamictite; Figure 53). The coarser fraction is indicative of either ice-rafted debris, or deposition in a glacial marine environment that is (relative to Facies 2) more proximal to the grounding line. The clay fraction ($>8\phi$) can be as high as 80%, which is a similar value to that observed for Facies 2. One sample shows a spike at 4ϕ (Figure 48), which is likely due to incomplete disaggregation during processing.

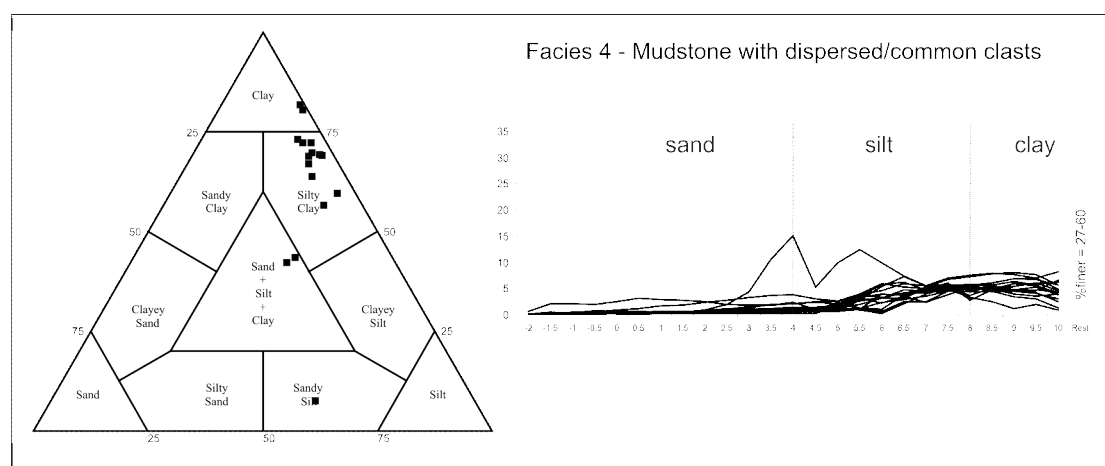


Figure 48: Grain size results for Facies 4: Shepard diagram (left) showing textural classification; and frequency curve (right) for AND-1B (black lines).

3.9.6 Facies 5: Rhythmically interlaminated mudstone with siltstone or sandstone

Five samples were selected for grain size analysis, all of which are lacking any coarse sand. Although the clay fraction dominates all samples and the distribution is similar to Facies 2 (mudstone), there are broad modes in the silt range for three of the samples (Figure 49). The other two samples show similar distributions to those of Facies 2.

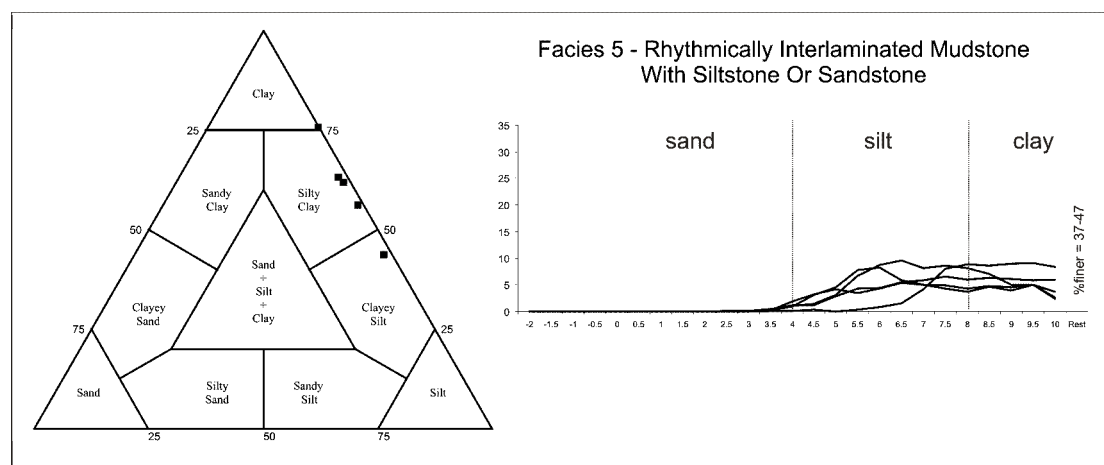


Figure 49: Grain-size results for Facies 5: Shepard diagram (left) showing textural classification; and frequency curve (right) for AND-1B (black lines).

3.9.7 Facies 6: Sandstone

A total of 11 sandstone samples were analysed for grain-size distribution. Seven of these were taken from >1-m thick intervals of graded volcanic sandstones and siltstone (grey lines in Figure 50). The graded volcanic sandstones all have well-defined modes in the very-fine sand or silt range, as well as a notable clay component. The range of different modes, and the high proportion of clay in the volcanic sands reflects the graded nature of these sandstones, suggesting the influence of turbidity currents. The clay is suggestive of suspension settling as the distal component of sediment gravity flows. Two more samples were taken from a sandstone (100.10 and 100.61 mbsf) that directly over Facies 9 (stratified diamictite), and another from a sandstone (1032.47 mbsf) that is interstratified with Facies 5. The sandstones (black lines in Figure 50) associated with Facies 5 or 9 have well-defined modes, contain little clay, and correspond well with the sand unit in HWD03-1 (24-31 cm), which is also directly overlying a diamictite interpreted as melt-out of basal debris. This, along with their association with grounding line proximal facies suggests re-sedimentation and sorting by traction currents associated with grounding line processes (possibly tidal pumping). A fine volcanic sandstone interval (0.48-m thick) with pebble size

clasts within the ~90 m thick diatomite interval was also sampled and has a broad silt mode, consists of 40% clay, and may represent either a IRD or debris flow interval.

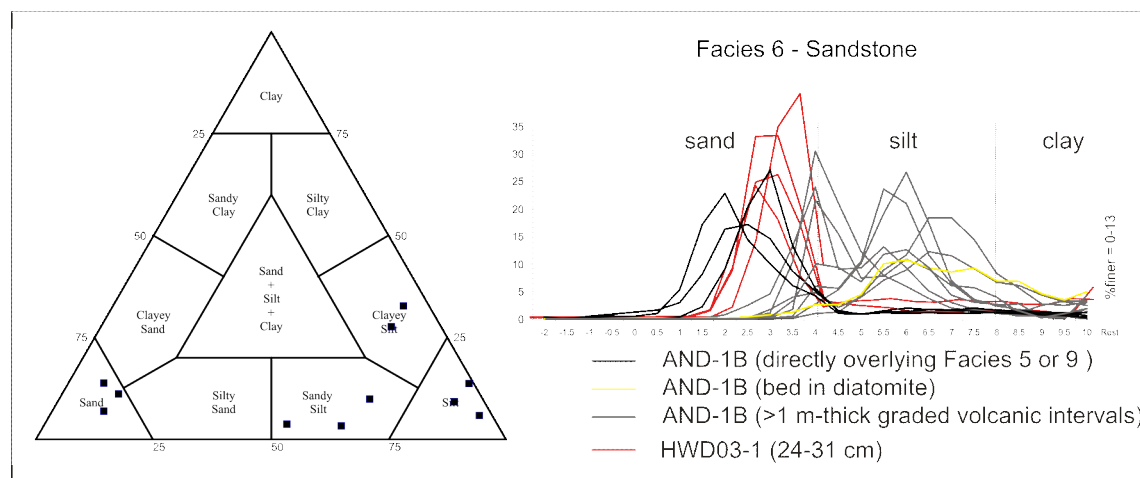


Figure 50: Grain-size results for Facies 6: Shepard diagram (left) showing textural classification; and frequency curve (right) for AND-1B (black lines) and similar facies from the Cape Robert Project (Dunbar and Barrett, 2004), and HWD03-1/DF80-189 core (red lines; presented in Chapter 2).

3.9.8 Facies 7: Conglomerate

Only three samples (Figure 51) were collected for processing, due to the difficulties in obtaining statistically significant result for facies with a high proportion of gravel (and the small sample size). One sample (790.74 mbsf) did not contain enough fine material for Sedigraph analysis, and the coarse nature of the sample is indicative of a conduit discharge deposit (e.g., Figure 41D). The sample at 48.03 mbsf was designated a conglomerate during core description, but displays a uniform distribution that is more akin to Facies 9 and 10 (stratified and massive diamictite; Figure 52 and Figure 53). Reassessment of this description reveals that this conglomerate is only 26-cm thick, matrix-supported, and clast-rich (but dominated a single clast). It is better classified as clast-rich diamictite, with deposition by basal debris meltout from floating ice inferred. The third sample (1221.8 mbsf) is a volcanic conglomerate, that has a well-defined sandstone mode and a broad clay “tail”, and given its association with volcanic sands above and below, is probably a volcanic debris flow.

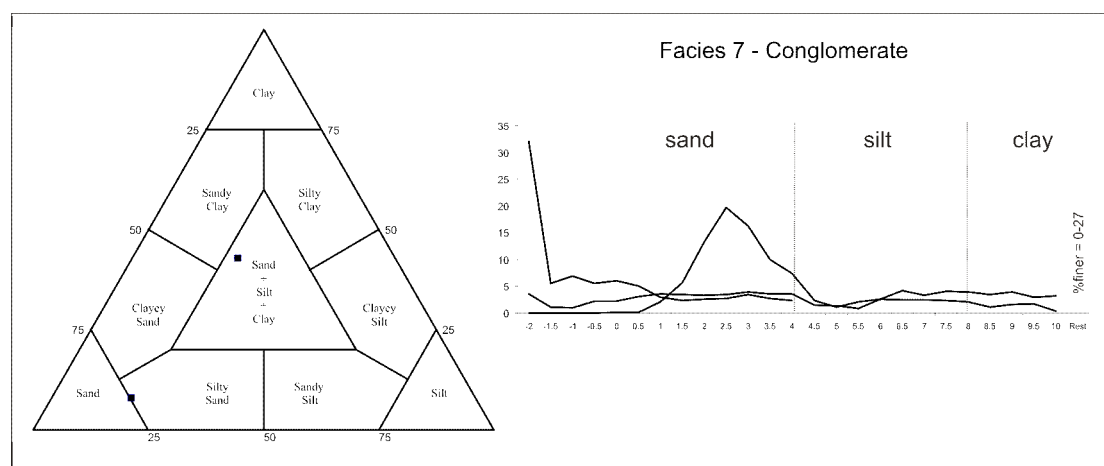


Figure 51: Grain-size results for Facies 7: Shepard diagram (left) showing textural classification; and frequency curve (right) for AND-1B (black lines).

3.9.9 Facies 8: Breccia

No grain size samples analysis due to coarse nature of deposits.

3.9.10 Facies 9: Stratified diamictite

All 22 stratified diamictites analysed for grain size lacked a well-defined mode (Figure 52), although some display a very broad medium-silt mode, which is not as common in Facies 10 (massive diamictites; Figure 53). Most stratified diamictites are a muddy diamictites, but the clay fraction ($>8\phi$) is highly variable in abundance (ranges from 17-74%).

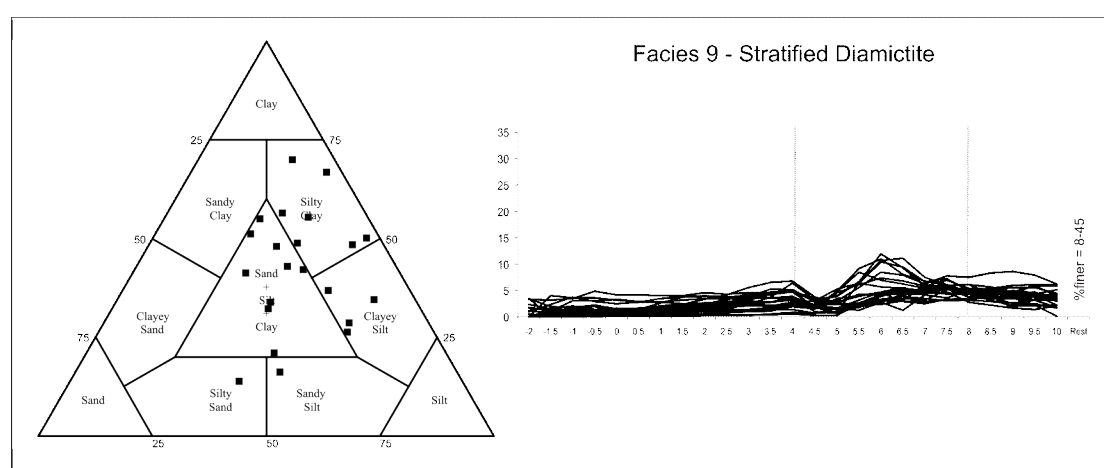


Figure 52: Grain-size results for Facies 9: Shepard diagram (left) showing textural classification; and frequency curve (right) for AND-1B (black lines).

3.9.11 *Facies 10 – Massive diamictite*

Twenty-six massive diamictites were analysed for grain size (Figure 53). They lack any well-defined mode, which is similar to Facies 9 (stratified diamictites). Some display a very broad mode combining the fine sand to fine silt modes, but this is not as common as for Facies 9. Most are classified as muddy diamictite and the proportion of clay fraction (>8 ϕ) is generally higher than Facies 9 (ranges from 22-78%). The massive diamictites in AND-1B have significantly higher clay proportions than other diamictites from the Ross Sea embayment and adjacent TAM till deposits (e.g., Figure 53). Cape Roberts Project diamictites (blue lines in Figure 53) have a well-defined fine sand mode, which is absent in AND-1B diamictites. The most logical explanation for this difference is that diamictites within Cape Roberts Project drill core were deposited by expansion of the TAM outlet glacier corresponding to the present-day MacKay Glacier (Powell *et al.*, 2000; Fielding *et al.*, 2000). Therefore, CRP diamictite are expected to contain a higher proportion of basement rocks as part of their basal bed load.

Diamictites deposited by an expanded AIS in the Ross Embayment at the AND-1B site are expected to be entraining older diamictite units as the grounding line migrates across the seafloor of the Ross Embayment, and therefore incorporating mud-rich facies into the glacial bed load. The uniform distribution in AND-1B correlates better with the average for Ice Stream B till (Tulaczyk *et al.*, 1998; Figure 53), but is slightly finer grained. Although the processes at both sites are likely to be similar (i.e., deposition beneath a marine-based ice sheet), AND-1B is more distal to a source of subglacially exposed bedrock, and therefore more subglacial sediment deposited at AND-1B is likely to be entrained from (mud-rich) diamictites that are believed to blanket the majority of the sea floor of the Ross Embayment continental shelf (Webb *et al.*, 1979; Bart *et al.*, 2003). Differences in glacial process could also explain this variance in grain-size distributions (e.g., grounding zone deposition versus subglacial till; extent of the ice streaming versus slower-moving ice at AND-1B). The textural classification of AND-1B diamictite appears to be consistent with diamictites from the Ross Ice Shelf Project (RISP) and DSDP 272 from the Ross Sea continental shelf (Figure 53). This observation also supports deposition by expansion of the marine-based AIS in the Ross Embayment eroding soft sediments from the Ross embayment continental shelf, rather than direct erosion of Paleozoic to Mesozoic bedrock by expanded TAM outlet glaciers.

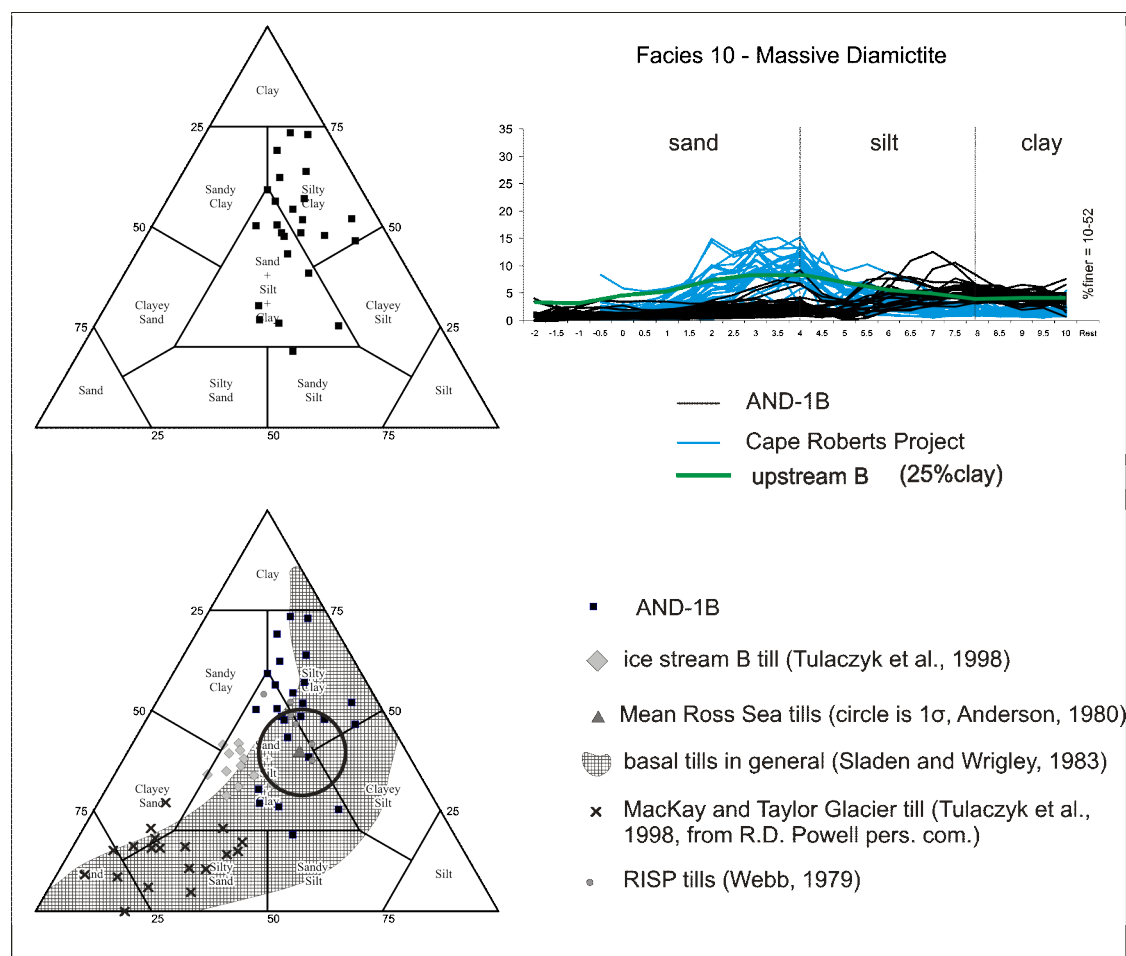


Figure 53: Top: Grain-size results for Facies 10 - Shepard diagram (left) showing textural classification; and frequency curve (right) for AND-1B (black lines) and similar facies from the Cape Robert Project (Dunbar and Barrett, 2004), and the average frequency curve for upstream B tills (green line; Tulaczyk *et al.*, 1998); Bottom: Comparison of textural classification to other Ross Embayment diamictites interpreted as subglacial till (modified from Tulaczyk *et al.*, 1998).

3.10 References

- Anderson, J.B., Kurtz, D.D., Domack, E.W., and Balshaw, K.K., 1980. Glacial and glacial marine sediments of the Antarctic continental shelf. *Journal of Geology* v.88, p.399–414.
- Anandakrishnan, S., Alley, R.B., 1997. Tidal forcing of basal seismicity of Ice Stream C, West Antarctica, observed far inland. *Journal of Geophysical Research* v.102, 15183–15196.
- Bart, P.J., 2003. Were West Antarctic Ice Sheet grounding events in the Ross Sea a consequence of East Antarctic Ice Sheet expansion during the middle Miocene? *Earth and Planetary Science Letters* v.216, p.93–107.
- Domack, E. W., and Williams, C. R., 1990. Fine structure and suspended sediment transport in three Antarctic fjords: Contributions to Antarctic Research, *Antarctic Research Series* v.50, p.71–89.
- Domack, E. W., Jacobson, E. A., Shipp, S., and Anderson, J. B., 1999. Late Pleistocene-Holocene retreat of the West Antarctic ice-sheet system in the Ross Sea; Part 2, Sedimentologic and stratigraphic signature: *Geological Society of America Bulletin* v.111, p.1517–1536.
- Dunbar, G.B and Barrett, P.J., 2004. A compilation of textural data for modern and ancient sediments in the McMurdo Sound area, Antarctica. Victoria University of Wellington, *Antarctic Data Series* v.24. 18 p.
- Fielding C.F., Naish T.R., Woolfe K.J., and Levelle M.A., 2000. Facies analysis and sequence stratigraphy of CRP-2/2A, Victoria Land Basin, Antarctica: *Terra Antartica* v. 7, p.323–338.
- Krissek, L.A., Browne, G.H., Carter, L., Cowan, E.A., Dunbar, G.B., McKay, R.M., Naish, T., Powell, R., Reed, J., Wilch, T.I and the Andrill MIS Science Team 2007. Sedimentology and Stratigraphy of the AND-1B Core, ANDRILL McMurdo Ice Shelf Project, Antarctica: *Terra Antartica* v.14, p.185–222.
- Powell, RD., Krissek, L.A. and van der Meer, J.J.M, 2000. Preliminary depositional environmental analysis of CRP-2/2A, Victoria Land Basin, Antarctica: Palaeoglaciological and palaeoclimatic inferences. *Terra Antartica* v.7, p.313–322.
- Powell, R. D., and Domack, E. W., 2002. Glacimarine environments, in Menzies, J., (ed.) *Modern and Past Glacial Environments*. Boston, Butterworth-Heinemann, p.361–390.
- Sladen, J.A., and Wrigley, W., 1983. Geotechnical properties of lodgement till—a review. In: Eyles, N., (ed.), *Glacial Geology, An Introduction for Engineers and Earth Scientists*. Oxford, U.K., Pergamon Press, p.184–212.
- Tulaczyk, S., Kamb, B., Scherer, R.P. and Engelhardt, H.F., 1998. Sedimentary processes at the base of a West Antarctic ice stream: constraints from textural and compositional properties of subglacial debris. *Journal of Sedimentary Research* v.68, p.487–496.
- Webb, P.N., 1979. Initial report on geological materials collected at RISP Site J9: *RISP Technical Report* v.79-1, Ross Ice Shelf Project Management Office, Lincoln, Nebraska, 126 p.
- Webb, P. N., Ronan, T. E. Jr, Lipps, J. H. and DeLaca, T. E., 1979. Miocene Glaciomarine Sediments from Beneath the Southern Ross Ice Shelf, Antarctica. *Science* v.203, p.435–437.

3.10.1.1 Supplementary data: Grain-size frequency from AND-1B

Class limits (phi)	Facies	-2.0	-1.5	-1.0	-0.5	0.0	0.5	1.0	1.5	2.0	2.5	3.0	3.5	4.0	4.5	5.0	5.5	6.0	6.5	7.0	7.5	8.0	8.5	9.0	9.5	10.0	Rest
Depth (mbsf)																											
9.99	10	0.00	1.20	1.39	1.06	1.06	1.25	1.48	1.71	1.90	1.90	2.17	2.04	2.17	0.81	1.91	1.30	3.24	3.97	4.86	6.16	5.27	4.94	4.78	3.97	3.56	35.89
20.01	4	0.00	0.00	0.06	0.34	0.40	0.40	0.46	0.57	0.69	0.80	0.92	0.86	0.98	0.79	1.69	2.81	3.00	4.12	4.12	4.50	5.53	4.31	3.28	2.91	1.22	55.22
20.27	3	0.14	0.00	0.53	0.96	0.57	0.72	0.91	1.05	1.20	1.20	1.39	1.24	1.44	0.77	0.27	2.05	2.14	2.49	3.47	3.47	4.54	4.27	3.21	2.76	3.29	55.92
20.51	4	0.00	0.45	0.00	0.11	0.23	0.34	0.57	0.57	0.57	0.68	0.80	0.91	1.02	1.08	0.92	1.11	2.22	2.77	3.42	4.34	5.08	4.71	3.78	3.42	3.78	57.13
25.93	3	0.00	0.00	0.14	0.41	1.52	3.38	7.65	11.38	10.69	9.03	8.07	5.86	5.44	2.85	3.84	3.95	4.79	4.86	4.26	2.97	2.20	1.64	0.87	0.59	1.22	2.38
25.96	3	0.00	0.00	0.00	0.00	0.37	0.75	1.87	4.48	5.97	6.34	6.34	5.22	4.85	2.47	3.13	4.67	7.10	9.53	5.69	4.09	4.60	2.43	2.30	1.28	3.58	12.92
26.53	3	0.00	0.00	0.00	0.00	0.09	0.09	0.37	0.82	1.37	1.83	3.30	3.75	3.30	2.68	3.74	3.57	5.70	9.10	7.48	5.95	5.27	4.93	4.08	3.91	1.87	26.78
31.63	10	1.27	0.70	1.27	1.58	1.39	0.95	1.08	1.14	1.33	1.33	1.52	1.27	1.20	2.29	0.58	1.66	1.83	2.08	2.66	2.58	3.32	3.16	2.41	3.32	4.49	53.61
42.1	4	0.00	0.00	0.00	0.00	0.04	0.04	0.18	0.31	0.66	0.92	1.45	1.67	2.02	2.36	2.53	3.22	3.87	3.59	4.60	5.98	2.67	4.70	4.70	4.51	6.44	43.55
42.36	2	0.00	0.00	0.00	0.00	0.00	0.00	0.00	0.06	0.06	0.18	0.53	1.05	1.58	0.77	1.78	2.77	3.37	3.17	3.47	2.57	4.65	3.66	2.97	3.57	3.37	60.41
42.58	4	0.00	0.00	0.00	0.10	0.10	0.20	0.29	0.49	0.59	0.59	0.69	0.69	0.69	0.97	1.45	2.50	2.98	4.62	4.33	4.81	4.23	4.43	4.33	4.62	4.23	52.07
44.84	9	0.00	0.00	1.33	1.33	1.00	1.16	1.28	1.83	2.11	2.16	2.33	2.22	2.27	2.08	4.66	8.52	6.99	6.19	5.38	5.54	5.30	3.45	3.45	3.13	1.69	24.58
48.03	7	3.56	1.07	0.94	2.22	2.22	3.02	3.56	3.43	3.29	3.49	3.96	3.56	3.56	1.46	1.35	0.91	2.56	4.20	3.29	4.02	3.90	3.47	3.90	2.98	3.17	26.92
48.19	9	0.54	0.18	0.18	0.36	0.45	0.58	0.89	1.12	1.39	1.56	2.41	3.80	6.35	3.15	4.04	6.64	10.70	11.17	7.50	6.17	4.76	4.06	1.64	3.28	3.36	13.74
50.14	10	0.00	0.39	1.75	0.78	0.91	1.10	1.49	1.95	2.86	3.57	5.52	6.81	9.15	4.92	3.32	6.63	8.81	7.57	6.09	4.02	3.73	3.19	1.95	2.25	0.65	10.59
50.61	10	4.04	2.24	2.54	3.66	3.44	3.59	3.44	3.14	3.06	2.91	3.29	3.44	3.36	1.19	2.74	4.45	5.08	4.79	3.77	4.17	3.94	3.48	3.54	3.08	2.40	15.24
52.97	3	1.14	1.55	1.96	2.23	2.42	3.28	3.60	3.56	3.19	2.60	2.46	2.19	2.23	1.21	1.32	1.65	2.32	3.18	3.51	4.96	4.83	5.16	5.03	4.77	5.63	24.02
53.1	3	0.00	0.00	0.00	0.00	0.00	0.00	0.00	0.00	0.09	0.18	0.27	0.18	0.54	0.47	0.70	2.20	3.70	9.80	11.80	10.20	9.30	6.90	6.80	5.50	6.20	25.19
53.23	9	0.93	2.42	3.73	2.89	2.46	2.80	3.44	3.73	3.99	3.82	4.03	4.12	4.92	2.91	3.05	5.62	8.46	7.90	6.23	4.73	2.78	2.23	1.61	1.39	2.06	7.74
56.81	3	0.00	0.00	0.00	0.00	0.00	0.00	0.00	0.00	0.05	1.75	19.22	26.18	13.31	3.30	2.14	2.75	4.67	4.63	3.80	3.69	2.60	2.57	1.81	1.56	0.29	5.68
58.97	9	2.34	1.48	2.06	1.40	1.60	1.44	1.81	2.22	2.43	2.47	2.67	2.71	3.50	1.78	0.83	2.05	3.04	4.17	4.88	5.30	4.52	4.52	4.59	4.03	4.31	27.84
67.8	10	1.46	0.53	0.81	0.93	1.06	1.62	1.87	2.18	2.62	2.68	2.87	2.55	2.68	0.81	1.25	1.22	3.12	4.12	9.37	10.59	8.16	5.79	3.89	3.35	1.83	22.64
70.75	10	0.86	1.60	1.66	1.43	1.31	1.48	1.94	2.57	3.37	3.48	3.94	3.31	3.20	1.52	1.62	2.12	2.53	3.43	2.88	3.22	4.25	5.21	4.38	3.77	3.08	31.85
74.71	10	0.85	1.24	1.08	0.91	0.88	1.70	2.05	2.25	2.64	2.77	3.06	2.74	2.87	1.54	0.66	1.56	2.07	2.59	5.11	7.71	6.59	5.48	4.22	3.48	2.37	31.57
77.52	10	0.00	1.75	1.75	0.75	0.75	1.50	1.94	2.44	2.82	2.94	3.13	2.69	2.69	1.48	2.12	0.66	1.75	3.14	4.16	6.21	6.43	6.35	4.75	4.46	3.94	29.36
82.4	9	1.07	1.01	1.66	1.96	1.25	1.19	1.37	1.54	1.72	1.78	2.26	2.08	2.79	2.39	2.38	2.62	4.15	4.69	4.77	5.15	5.00	4.92	4.15	4.08	4.23	29.77
83.5	2	0.00	0.16	0.45	0.20	0.24	0.28	0.24	0.20	0.20	0.20	0.20	0.24	0.49	0.30	0.00	1.64	2.03	2.90	3.96	5.99	5.99	6.28	6.57	5.61	1.16	54.43
83.97	2	1.99	0.00	0.35	0.41	0.18	0.29	0.29	0.23	0.18	0.18	0.29	0.41	0.70	0.18	0.09	0.76	1.52	3.32	4.65	6.46	7.98	7.31	6.46	5.89	6.27	43.60
84.31	2	0.00	0.00	0.00	0.00	0.00	0.00	0.07	0.00	0.14	0.22	0.29	0.36	0.65	0.55	0.95	0.00	1.36	4.85	7.67	9.32	9.12	9.71	8.15	6.41	4.66	35.52
85.2	2	0.00	0.00	0.00	0.00	0.00	0.00	0.00	0.00	0.00	0.06	0.18	0.24	0.42	1.07	0.88	0.20	2.15	8.42	9.30	10.28	8.42	8.03	6.27	5.78	5.19	33.10
86.05	3	0.00	0.00	0.00	0.00	0.00	0.00	0.00	0.00	0.05	0.05	0.05	0.05	0.05	1.18	0.88	0.49	0.29	1.28	4.02	6.38	5.99	6.58	6.77	6.48	4.52	54.87
86.31	3	0.00	0.00	0.00	0.00	0.00	0.00	0.00	0.00	0.15	0.46	1.83	3.51	5.80	2.80	1.46	3.19	4.65	5.60	7.41	6.20	5.08	5.94	5.17	4.39	4.05	32.30

Class limits (phi)	Facies	-2.0	-1.5	-1.0	-0.5	0.0	0.5	1.0	1.5	2.0	2.5	3.0	3.5	4.0	4.5	5.0	5.5	6.0	6.5	7.0	7.5	8.0	8.5	9.0	9.5	10.0	Rest
Depth (mbsf)																											
86.74	2	0.00	0.00	0.00	0.06	0.06	0.06	0.25	0.50	1.24	1.86	2.48	3.84	4.59	1.37	2.00	4.63	3.96	4.63	3.87	4.30	4.13	5.22	4.63	5.22	4.13	36.97
90	2	0.58	0.00	0.24	0.29	0.38	0.48	0.62	0.86	1.30	1.97	2.98	3.46	4.81	1.22	0.95	1.97	2.71	4.10	5.25	4.26	5.00	5.41	4.59	5.58	6.40	34.60
93.15	3	0.00	0.00	0.00	0.00	0.00	0.00	0.04	0.04	0.04	0.04	0.26	1.95	2.18	1.17	0.19	0.00	2.56	5.60	6.55	7.98	7.98	8.83	6.84	6.74	4.37	36.65
95.3	3	0.00	0.00	0.00	0.00	0.00	0.00	0.00	0.00	0.00	0.00	0.06	0.06	0.12	0.26	0.20	2.22	1.91	10.47	12.89	9.27	7.25	6.24	5.84	4.63	1.31	37.26
95.55	3	0.00	0.00	0.00	0.00	0.00	0.00	0.00	0.00	0.05	0.10	1.33	5.89	10.41	3.52	1.22	4.01	2.49	4.74	5.14	5.38	5.14	5.70	5.70	5.46	2.97	30.75
96.58	2	0.00	0.00	0.00	0.00	0.00	0.00	0.00	0.04	0.09	0.13	0.17	0.21	0.34	0.28	1.09	0.20	3.57	7.24	6.34	6.84	5.95	7.04	5.65	5.85	5.25	43.71
97.35	9	0.00	0.67	0.77	0.86	0.81	1.01	0.72	1.05	1.24	1.34	1.44	1.82	2.63	2.16	1.67	3.26	4.68	5.60	4.60	4.43	4.60	4.60	4.43	4.10	2.17	39.31
99.92	2	0.00	0.00	0.12	0.06	0.12	0.06	0.06	0.06	0.06	0.06	0.12	0.18	0.36	1.69	0.59	3.15	10.23	8.16	4.82	4.72	4.62	4.23	4.13	4.13	0.06	48.19
100.1	6	0.43	0.00	0.54	0.86	1.18	1.56	2.90	8.11	16.22	17.08	14.55	8.65	4.99	1.54	0.86	1.23	1.39	1.72	1.63	1.98	1.63	1.50	1.28	1.10	1.17	5.92
100.61	6	0.00	0.12	0.23	0.51	0.51	0.94	5.35	17.14	22.80	14.41	10.00	6.01	4.14	1.03	0.84	1.52	2.00	1.71	1.56	1.30	1.06	0.99	0.75	0.65	0.31	4.14
100.79	9	1.76	1.29	1.50	0.93	1.19	1.14	1.19	1.55	1.92	1.92	2.12	2.12	2.59	3.02	3.89	6.72	11.98	9.27	5.87	6.03	4.71	3.86	3.55	2.24	0.07	17.54
109.19	9	3.50	0.10	0.80	0.90	0.20	0.50	0.40	0.40	0.60	0.80	1.20	1.50	2.10	1.86	4.91	9.11	11.00	8.07	6.87	6.01	6.10	4.47	3.87	3.18	3.18	18.38
109.74	2	0.00	0.00	0.00	0.00	0.00	0.00	0.00	0.00	0.00	0.05	0.05	0.05	0.10	0.35	0.70	2.51	4.22	7.94	8.34	7.64	6.43	6.53	6.03	6.23	4.62	38.19
111.17	3	0.00	0.16	0.07	0.05	0.05	0.11	0.05	0.11	0.11	0.11	0.22	1.79	7.86	6.58	13.12	16.68	14.95	10.86	6.52	5.04	3.39	2.43	1.91	1.13	3.22	3.48
117.63	1a	1.15	0.00	0.97	0.61	0.73	0.91	0.97	0.91	0.85	0.91	1.27	1.70	4.06	2.48	1.29	3.50	6.50	8.08	7.58	6.16	6.25	5.33	3.83	3.58	5.41	24.99
118	4	0.55	2.05	1.96	1.87	2.37	3.01	2.74	2.69	2.37	1.83	1.78	1.78	2.19	0.93	1.80	3.74	4.53	5.82	5.46	5.68	4.53	5.03	4.67	4.10	2.37	24.15
118.62	3	0.00	0.00	0.00	0.00	0.00	0.00	0.00	0.08	0.08	0.08	0.16	0.41	0.97	2.04	0.97	1.94	3.99	6.13	6.42	6.03	5.83	6.51	6.22	5.83	6.13	40.16
119.15	6V	0.00	0.00	0.00	0.00	0.00	0.00	0.00	0.00	0.00	0.12	1.76	3.99	4.82	2.15	4.00	7.06	8.92	12.18	11.48	9.18	6.71	6.00	4.33	3.09	2.47	11.74
122	2	0.62	1.24	1.92	1.73	1.61	1.61	1.42	1.67	1.98	1.98	2.23	2.48	3.40	2.76	2.78	4.74	7.90	7.22	6.32	5.64	4.81	4.29	3.76	3.01	0.90	21.97
124.39	9	0.00	0.23	0.46	0.05	0.23	0.14	0.14	0.14	0.23	0.23	0.32	0.51	0.83	0.71	0.97	6.39	10.36	9.40	6.68	7.27	4.94	5.13	4.65	4.26	5.13	30.61
125.95	2	0.00	0.00	0.00	0.00	0.04	0.00	0.08	0.08	0.08	0.12	0.16	0.16	0.27	0.12	0.69	1.09	1.98	2.67	2.77	3.96	3.36	4.55	4.55	4.85	3.76	64.69
126.39	4+2	0.00	0.00	0.00	0.04	0.00	0.04	0.09	0.09	0.09	0.13	0.17	0.21	0.47	0.61	2.25	0.98	0.39	3.52	2.45	4.31	4.99	4.70	5.38	4.60	3.03	61.46
128.78	2	0.00	0.00	0.00	0.00	0.00	0.00	0.00	0.00	0.00	0.00	0.00	0.05	0.00	0.50	0.50	0.50	2.48	3.67	2.78	4.46	5.25	5.65	6.54	6.25	7.34	54.04
131.72	2	0.00	0.00	0.00	0.00	0.00	0.00	0.00	0.00	0.00	0.00	0.00	0.07	0.43	1.76	1.18	2.56	1.57	2.95	3.35	3.74	2.85	4.33	4.43	4.43	4.92	61.41
133.48	3	0.00	0.00	0.00	0.00	0.00	0.00	0.00	0.05	0.58	1.97	4.08	5.81	8.21	3.69	2.03	2.18	3.90	5.61	5.69	4.36	4.21	4.68	3.98	3.90	3.12	31.96
134.68	4	0.00	0.00	0.20	0.61	0.47	0.54	0.34	0.41	0.81	1.83	4.26	10.41	15.01	5.11	9.77	12.32	9.77	7.28	5.43	4.72	3.13	2.43	1.02	1.85	0.77	1.53
141.29	6V	0.00	0.00	0.00	0.00	0.00	0.00	0.00	0.00	0.00	0.00	0.09	0.09	1.00	1.28	4.16	8.91	11.59	18.32	18.32	14.36	8.22	5.54	2.67	2.48	2.97	0.00
141.4	6V	0.00	0.00	0.00	0.00	0.00	0.00	0.00	0.00	0.00	0.00	0.04	0.13	2.68	5.31	10.14	19.07	26.64	17.38	6.92	3.55	2.34	1.78	0.84	0.19	1.40	1.59
141.58	6V	0.00	0.00	0.00	0.00	0.00	0.00	0.00	0.00	0.00	0.00	0.12	0.47	5.90	5.59	10.48	23.58	20.90	11.61	6.43	3.30	2.50	2.68	0.36	0.00	4.29	1.79
141.72	6V	0.00	0.00	0.00	0.00	0.00	0.00	0.05	0.05	0.05	0.11	1.16	10.29	30.41	21.00	12.16	7.83	5.89	3.70	1.94	1.51	1.26	0.52	0.49	0.43	0.00	1.14
141.84	6V	0.00	0.00	0.06	0.00	0.00	0.00	0.00	0.06	0.70	2.49	4.53	13.15	23.85	9.03	9.23	13.08	9.27	5.08	3.01	1.74	0.94	0.80	0.66	0.42	1.88	0.00
146.58	3	0.00	0.00	0.00	0.00	0.00	0.00	0.00	0.00	0.23	1.70	5.56	7.57	9.12	2.52	4.12	9.52	9.59	7.79	5.92	5.17	4.35	4.95	2.85	3.82	1.87	13.34
146.83	10	0.56	0.00	0.65	1.08	1.51	1.42	1.68	1.90	2.29	2.42	2.89	2.94	3.54	2.02	1.29	3.33	5.82	10.89	12.55	9.98	6.28	4.61	2.72	2.57	3.86	11.19
147.76	10	0.00	5.97	19.89	7.46	5.47	6.46	6.96	7.46	11.93	13.42	11.43	3.48	0.00	0.00	0.00	0.00	0.00	0.00	0.00	0.00	0.00	0.00	0.00	0.00	0.00	0.00
148.32	10	0.00	1.93	1.29	1.65	1.36	1.43	0.93	1.22	1.58	1.58	1.72	1.93	2.44	0.57	1.96	3.03	6.46	5.07	4.09	5.07	4.50	4.82	4.58	4.66	3.52	32.62
150.42	9	3.42	1.95	1.81	2.28	1.54	1.68	2.01	2.15	2.55	3.22	4.43	4.63	5.16	2.81	2.43	2.30	3.93	5.20	5.07	5.32	4.59	4.89	4.05	3.93	3.87	14.80

Class limits (phi)	Facies	-2.0	-1.5	-1.0	-0.5	0.0	0.5	1.0	1.5	2.0	2.5	3.0	3.5	4.0	4.5	5.0	5.5	6.0	6.5	7.0	7.5	8.0	8.5	9.0	9.5	10.0	Rest
Depth (mbsf)																											
150.95	4	0.00	0.00	0.38	0.38	0.38	0.33	0.33	0.33	0.33	0.27	0.27	0.27	0.38	0.74	2.30	1.15	0.96	3.74	4.70	5.75	4.99	5.94	6.71	6.90	8.15	44.29
151.5	4	0.00	0.35	0.17	0.17	0.17	0.09	0.09	0.09	0.09	0.09	0.09	0.09	0.17	0.17	1.84	1.17	0.49	2.43	2.43	4.37	5.44	5.54	6.21	5.54	6.21	56.52
151.71	1b	0.00	0.00	1.12	3.98	1.99	0.43	0.09	0.09	0.09	0.09	0.09	0.09	0.09	0.00	1.10	0.46	0.55	1.38	1.01	3.77	3.49	4.41	5.70	6.43	7.07	56.50
178.98	1a	2.41	1.95	1.09	0.63	0.40	0.40	0.40	0.34	0.34	0.29	0.23	0.23	0.29	1.10	0.00	1.17	0.09	1.44	1.08	1.53	3.51	5.31	7.11	7.11	10.44	51.11
180.38	1a	0.00	0.00	0.20	0.20	0.26	0.33	0.40	0.40	0.40	0.26	0.26	0.20	0.13	0.67	1.72	1.34	1.53	1.34	3.53	4.11	5.35	6.88	7.55	8.60	7.93	46.43
180.68	1b	0.00	0.00	0.00	0.00	0.00	0.00	0.00	0.07	0.07	0.00	0.07	0.07	0.15	1.75	0.79	1.08	0.39	1.77	2.66	5.61	4.92	6.69	7.18	8.07	10.23	48.41
181.22	2	0.00	0.00	0.00	0.00	0.00	0.00	0.00	0.00	0.00	0.09	0.19	0.19	0.28	0.78	2.37	1.48	2.76	2.66	2.17	4.04	3.55	3.35	3.95	4.64	3.26	64.22
181.89	2	1.90	0.47	0.27	0.34	0.14	0.00	0.07	0.00	0.14	0.54	0.61	0.34	0.34	0.14	0.76	1.61	2.27	3.32	4.83	4.07	4.93	6.63	5.40	6.35	4.45	50.11
181.94	9	0.00	4.04	3.63	3.63	3.15	2.74	2.74	2.46	2.60	2.81	3.56	3.56	3.90	2.01	1.50	2.59	3.37	3.85	3.43	3.01	3.25	2.95	2.65	3.13	1.86	27.61
191.24	1+10	0.00	0.38	0.21	0.14	0.17	0.19	0.23	0.24	0.24	0.31	0.31	0.30	0.45	0.14	0.03	0.39	3.48	3.97	3.77	5.90	6.09	5.80	5.71	5.61	5.13	50.79
211.74	1a	0.00	0.00	0.00	0.00	0.10	0.10	0.10	0.10	0.10	0.10	0.10	0.10	1.24	1.96	0.49	0.07	0.98	1.86	4.60	3.72	7.05	9.01	10.09	10.09	8.13	39.87
224.53	3	1.59	0.64	0.00	0.21	0.64	0.74	0.85	0.85	0.85	0.85	0.96	0.85	0.96	0.59	0.63	1.44	2.34	3.24	4.40	6.20	6.56	8.18	6.92	6.65	6.65	36.22
224.67	3	0.00	0.00	0.00	0.00	0.00	0.00	0.00	0.00	0.07	0.44	2.29	5.47	8.57	2.15	3.03	2.13	3.44	6.31	6.72	7.95	7.95	6.89	5.08	4.84	4.18	22.46
224.88	3	0.00	0.00	0.00	0.17	0.17	0.23	0.35	0.23	0.23	0.35	0.64	0.58	0.52	0.12	0.68	1.55	0.10	3.19	4.55	5.32	7.64	8.70	7.35	6.87	9.28	41.20
225	9	3.28	3.23	3.53	4.82	4.13	4.23	4.08	4.08	4.62	4.28	4.62	4.62	4.67	1.96	2.84	4.12	4.62	4.76	5.17	5.63	4.30	3.16	2.11	2.15	2.20	2.79
225.38	10	0.00	0.00	0.32	0.24	0.32	0.24	0.32	0.40	0.40	0.48	0.64	0.64	0.88	1.36	0.28	1.42	2.93	3.12	3.02	4.81	5.38	5.66	6.51	6.04	7.55	47.01
258.55	3	0.00	0.00	0.00	0.00	0.00	0.00	0.00	0.00	0.00	0.00	0.00	0.00	0.11	2.73	0.00	0.39	0.68	0.10	1.16	1.55	1.84	4.45	7.16	8.03	9.87	61.93
260.42	3	0.00	0.00	0.00	0.00	0.00	0.00	0.00	0.00	0.00	0.08	0.08	0.08	0.08	0.00	1.19	0.89	1.09	2.18	2.08	2.38	2.77	3.96	4.56	4.56	3.57	70.44
260.7	3	0.00	0.00	1.32	3.45	4.85	5.80	6.09	5.43	4.48	3.08	2.86	3.08	3.60	2.30	3.39	4.50	5.17	4.27	4.10	3.60	3.77	3.43	3.04	2.87	3.09	12.42
267.88	4	0.00	0.00	0.00	0.00	0.09	0.18	0.27	0.27	0.44	0.62	0.89	1.06	1.33	1.28	1.60	3.10	2.06	3.47	2.25	3.75	5.16	4.79	5.82	5.44	4.13	51.99
283.2	4	0.00	0.00	0.00	0.00	0.00	0.00	0.08	0.08	0.08	0.08	0.08	0.16	0.41	0.83	1.17	0.78	0.10	1.96	3.82	5.09	3.52	4.99	5.29	5.97	6.07	59.42
293.23	2	0.00	0.00	0.00	0.10	0.00	0.10	0.10	0.10	0.10	0.20	0.20	0.31	0.51	0.31	1.47	2.94	3.04	5.59	5.30	5.49	5.20	6.37	5.98	6.47	5.79	44.32
296.72	10	0.00	0.80	0.22	1.02	1.16	1.24	1.75	1.89	2.18	2.33	2.98	3.71	4.00	0.69	0.93	3.78	4.24	5.48	4.78	4.55	5.09	4.24	5.09	5.02	5.09	27.71
307.04	10	0.96	0.00	0.17	0.35	0.17	0.35	0.52	0.70	1.04	1.22	1.48	1.65	1.91	1.06	1.97	2.24	2.69	3.95	3.95	5.83	4.57	5.65	5.65	6.10	1.43	44.39
316.23	4	0.00	0.00	0.46	0.46	0.84	1.07	1.53	1.76	2.30	2.68	3.22	3.52	3.68	2.94	2.56	3.80	5.82	5.20	4.89	5.28	4.74	5.28	4.35	3.96	2.87	26.78
358.94	3	0.00	0.00	0.00	0.00	0.00	0.00	0.00	0.00	0.00	0.17	1.44	5.60	10.19	3.90	3.83	4.24	5.38	5.13	3.18	4.32	4.07	3.91	4.32	4.24	4.56	31.53
359.95	3	0.00	0.33	0.17	0.17	0.08	0.08	0.17	0.08	0.08	0.08	0.17	0.33	1.51	2.46	2.89	2.22	3.37	4.53	4.92	5.40	4.63	4.34	4.92	5.59	5.40	46.08
361.6	3	0.00	0.00	0.00	0.76	0.54	0.76	0.65	0.76	0.65	0.44	0.76	1.74	6.96	5.99	7.47	8.14	5.62	5.12	3.86	3.69	4.78	3.61	4.03	4.20	3.86	25.60
381.92	1b	0.00	0.42	0.32	1.05	0.84	1.37	1.37	1.37	1.27	1.27	1.48	1.48	1.90	0.81	1.66	3.19	1.81	2.59	3.62	3.97	4.57	6.04	6.55	6.30	3.97	40.79
413.16	6	0.00	0.00	0.00	0.00	0.13	0.13	0.00	0.13	0.13	0.38	0.77	1.28	2.56	2.60	4.45	10.03	10.68	9.30	8.56	9.20	6.90	6.81	4.51	3.50	4.88	13.07
460.09	3	0.00	0.00	0.12	0.47	0.35	0.83	0.71	0.71	0.83	0.71	0.71	0.94	1.53	1.30	2.93	4.86	4.21	4.86	5.04	4.86	5.59	5.04	5.50	5.22	4.67	38.02
464.07	10	0.00	0.62	0.44	0.35	0.79	0.53	0.35	0.44	0.53	0.44	0.53	0.62	0.97	0.54	2.59	2.96	7.59	7.87	7.04	6.94	6.39	6.39	4.72	5.37	3.06	31.94
473.22	2+4	0.00	0.00	0.00	0.00	0.00	0.00	0.00	0.00	0.00	0.00	0.00	0.11	0.00	0.00	0.00	0.00	0.60	1.00	1.00	4.10	4.80	5.60	6.90	6.60	6.00	63.29
479.18	10	1.53	0.61	0.31	0.82	0.92	0.71	0.92	1.02	1.22	1.22	1.63	2.04	2.55	2.52	3.25	1.83	4.33	3.91	3.83	4.74	4.33	4.16	5.08	4.49	6.49	35.53
481.15	4	0.00	0.00	0.45	0.09	0.09	0.18	0.09	0.18	0.18	0.27	0.36	0.54	0.90	0.75	0.68	3.78	3.20	3.98	4.75	4.85	5.63	4.27	5.24	5.92	4.46	49.18
488.58	2	0.00	0.00	0.00	0.00	0.00	0.00	0.00	0.00	0.00	0.00	0.00	0.10	0.00	0.00	0.10	0.20	0.00	1.20	3.91	3.21	4.71	5.62	6.12	7.02	7.32	60.47

Class limits (phi)	Facies	-2.0	-1.5	-1.0	-0.5	0.0	0.5	1.0	1.5	2.0	2.5	3.0	3.5	4.0	4.5	5.0	5.5	6.0	6.5	7.0	7.5	8.0	8.5	9.0	9.5	10.0	Rest
Depth (mbsf)																											
494.33	3	0.00	0.00	0.00	0.00	0.00	0.00	0.00	0.00	0.00	0.00	0.00	0.00	0.00	0.00	0.90	2.01	4.32	3.12	4.22	3.72	4.92	3.92	5.13	4.92	4.22	58.59
501.2	2	0.00	0.00	0.00	0.00	0.00	0.00	0.00	0.00	0.00	0.00	0.00	0.07	0.00	0.00	0.00	0.50	0.50	1.10	3.01	3.82	5.72	5.92	5.92	6.03	7.53	59.85
504.55	1b	0.00	0.00	0.31	0.20	0.20	0.31	0.31	0.41	0.41	0.31	0.51	0.61	0.92	2.29	1.78	1.78	3.94	2.63	5.63	5.26	8.07	9.01	8.07	9.20	9.29	28.54
519.11	9	0.00	1.16	3.10	3.02	3.33	2.94	2.71	3.18	3.49	3.33	3.72	5.27	5.19	3.04	5.23	6.40	5.70	5.47	5.00	4.36	4.30	3.95	2.44	2.56	1.63	9.48
523.39	5	0.00	0.00	0.00	0.00	0.00	0.00	0.00	0.00	0.00	0.09	0.17	0.43	1.12	1.39	3.12	6.73	8.77	9.55	8.19	8.68	8.09	7.02	5.07	5.07	3.70	22.81
523.65	3	1.03	0.00	0.16	0.40	0.40	0.55	1.03	1.66	2.37	2.69	3.32	3.95	3.95	2.64	5.54	5.76	6.53	6.69	5.61	5.15	5.46	4.84	3.38	3.69	2.15	21.06
523.93	4+9	3.38	0.82	0.64	0.91	1.19	1.01	1.28	1.19	1.46	1.46	1.55	1.55	1.92	1.21	3.83	6.04	5.38	4.89	4.81	4.98	4.08	3.91	3.75	4.49	4.16	30.09
545.15	4	0.00	0.00	0.00	0.10	0.20	0.31	0.41	0.51	0.72	1.02	1.23	1.84	2.05	2.26	2.02	3.30	5.69	6.05	4.59	5.41	5.69	5.41	4.68	5.14	3.67	37.70
778.7	10	0.00	0.00	0.71	0.83	0.47	0.59	1.07	1.42	1.54	1.90	2.37	2.73	3.08	2.26	1.88	2.04	3.02	2.94	2.78	3.35	3.11	3.60	3.02	2.94	2.37	49.95
790.74	7	32.09	5.54	6.93	5.54	6.00	5.08	3.00	2.31	2.54	2.77	3.46	2.77	2.31	19.63	0.00	0.00	0.00	0.00	0.00	0.00	0.00	0.00	0.00	0.00	0.00	0.00
827.21	3	0.00	0.28	1.12	4.49	4.21	4.21	5.76	6.04	5.62	6.60	8.85	5.90	3.93	1.46	1.05	1.89	2.10	2.43	2.98	2.98	3.15	3.10	2.85	2.73	2.64	13.63
830.64	9	0.00	0.27	0.18	0.53	0.53	1.33	2.66	3.72	3.90	3.81	4.07	3.54	3.63	0.97	0.72	1.98	4.59	2.96	2.89	3.25	3.46	4.09	5.01	4.59	3.81	33.52
850.95	2	0.00	0.00	0.00	0.00	0.00	0.00	0.00	0.00	0.00	0.00	0.00	0.00	0.00	0.14	0.00	4.19	5.59	6.98	7.88	8.08	6.78	7.18	5.98	5.39	2.49	39.30
852.19	3	0.00	0.00	0.00	0.00	0.00	0.00	0.45	5.25	16.94	22.49	19.04	10.94	5.70	2.46	2.02	2.07	2.07	1.97	1.56	1.22	1.17	0.92	0.81	0.78	0.73	1.41
853.25	9	0.00	0.38	0.58	1.35	1.35	1.54	2.02	2.41	2.60	2.69	3.08	2.79	3.86	1.70	1.51	2.42	3.02	2.87	2.57	3.40	3.47	3.55	3.77	3.77	3.70	39.62
854.36	10	3.48	2.26	1.39	2.26	2.70	1.83	2.00	1.91	1.74	1.57	1.74	1.48	1.65	0.90	0.97	1.54	2.13	2.72	3.31	3.38	3.97	4.63	4.56	4.56	4.19	37.12
856.01	4	0.00	0.00	0.00	0.00	0.24	0.24	0.37	0.49	0.61	0.61	0.86	0.98	1.10	1.22	1.21	1.87	2.99	2.99	4.86	4.95	5.51	5.98	6.73	6.64	5.61	43.92
891.17	2	0.00	0.00	0.00	0.00	0.00	0.00	0.00	0.00	0.00	0.00	0.00	0.00	0.00	0.00	0.50	0.90	2.01	2.71	3.41	5.62	5.62	6.32	5.92	6.53	6.83	53.61
902.8	10	0.00	0.00	1.25	0.67	1.00	1.25	1.75	1.84	2.09	2.09	2.67	2.84	3.42	2.04	1.87	3.34	2.64	3.27	3.27	3.27	3.66	3.97	3.89	3.81	3.81	40.29
1032.47	6	0.00	0.00	0.00	0.00	0.00	0.00	0.37	2.25	9.15	20.19	26.99	13.13	5.54	1.40	0.88	1.11	1.02	1.09	0.98	1.02	1.17	1.13	1.13	0.94	0.62	9.87
1032.83	5	0.00	0.00	0.00	0.00	0.00	0.00	0.00	0.00	0.00	0.00	0.09	0.36	1.18	1.21	2.83	4.30	4.39	5.47	5.86	6.54	5.96	6.35	6.15	5.86	5.96	37.49
1033.58	5	0.00	0.00	0.00	0.00	0.00	0.00	0.00	0.00	0.00	0.00	0.00	0.18	1.92	3.20	4.22	3.45	4.32	5.37	4.99	4.89	4.32	4.80	4.61	4.99	2.59	46.15
1043.53	5	0.00	0.00	0.00	0.00	0.00	0.00	0.00	0.00	0.00	0.00	0.06	0.19	0.93	3.07	4.60	7.73	8.22	5.87	4.99	4.31	3.72	4.70	3.92	4.99	2.35	40.34
1053.27	9	1.61	0.00	0.32	0.65	0.32	0.73	0.56	0.81	0.97	1.05	1.13	1.45	1.37	0.76	1.68	1.24	2.74	1.24	4.15	3.62	4.94	5.38	6.00	6.18	6.18	44.93
1060.4	2	0.00	0.00	0.00	0.00	0.00	0.00	0.00	0.15	0.08	0.38	0.68	0.98	1.13	1.23	2.48	1.15	3.15	1.81	2.86	4.96	5.73	7.26	6.87	7.07	4.77	47.26
1062.87	3	0.00	0.00	0.00	1.25	2.41	4.15	10.91	9.65	8.59	7.72	7.72	6.66	5.79	3.37	2.53	2.68	2.75	2.94	2.14	2.78	2.40	2.72	2.49	1.95	0.93	5.46
1063.66	10	0.00	2.68	1.22	1.46	1.09	1.58	1.22	1.58	1.70	1.82	1.70	2.68	2.92	1.78	1.07	4.14	2.68	4.22	5.21	6.44	6.21	5.29	5.52	4.60	4.83	26.36
1066.17	10	0.00	0.95	0.58	0.58	0.36	0.51	0.66	0.80	0.95	1.02	1.09	0.95	1.09	1.53	0.09	0.45	1.80	1.80	2.96	4.76	4.67	4.40	5.66	5.66	4.58	52.10
1095.46	9	0.00	1.42	0.99	1.28	0.78	0.78	1.14	1.42	1.85	2.06	2.41	2.77	3.20	2.06	1.39	1.86	2.87	3.41	3.18	5.12	4.81	5.20	5.59	5.51	4.50	34.38
1164.3	2+10	2.02	2.61	1.49	1.49	1.27	1.49	1.42	1.57	2.02	2.09	2.39	2.76	2.91	1.64	2.21	3.76	3.10	3.76	4.13	5.09	5.16	4.94	5.31	5.24	4.65	25.45
1164.48	4	0.00	0.00	0.00	0.32	0.08	0.16	0.24	0.16	0.24	0.24	0.24	0.32	0.48	0.53	0.58	0.87	3.79	3.59	5.15	6.61	7.19	7.68	7.97	7.58	5.54	40.42
1167.68	10	1.00	2.36	1.43	1.00	1.28	1.43	1.28	1.64	2.28	2.64	3.14	3.71	4.28	3.48	2.97	3.11	4.10	4.03	4.66	4.31	4.59	4.59	4.38	4.45	3.46	24.38
1168.08	4	0.00	0.00	0.00	0.08	0.08	0.16	0.16	0.23	0.31	0.39	0.62	0.85	1.17	0.95	0.56	2.69	5.29	7.12	5.48	6.83	7.41	7.89	7.60	6.92	4.71	32.51
1196.18	10	1.44	0.40	0.40	0.64	0.48	0.80	0.64	1.04	1.28	1.52	1.76	2.33	2.89	2.53	3.34	3.77	4.85	5.36	5.61	6.28	5.86	5.86	4.35	4.94	3.93	27.70
1197.4	5	0.00	0.00	0.00	0.00	0.00	0.00	0.00	0.00	0.00	0.00	0.00	0.08	0.08	0.30	0.00	0.41	0.81	1.52	4.15	8.00	8.91	8.61	9.01	9.11	8.40	40.60
1198.43	9	0.00	0.00	0.37	0.22	0.22	0.29	0.29	0.37	0.59	0.81	0.96	1.18	1.91	1.52	4.59	6.09	7.31	6.84	5.81	6.93	5.43	5.34	4.50	5.90	3.84	28.67

Class limits (phi)	Facies	-2.0	-1.5	-1.0	-0.5	0.0	0.5	1.0	1.5	2.0	2.5	3.0	3.5	4.0	4.5	5.0	5.5	6.0	6.5	7.0	7.5	8.0	8.5	9.0	9.5	10.0	Rest
Depth (mbsf)																											
1198.43	10	0.00	0.00	0.37	0.22	0.22	0.29	0.29	0.37	0.59	0.80	0.95	1.17	2.64	2.79	3.68	7.44	7.72	7.07	5.97	5.51	5.51	4.78	5.33	4.69	4.13	27.47
1199.74	10	0.00	0.95	2.27	2.42	1.90	1.90	1.83	2.49	3.22	3.59	4.10	5.34	6.52	4.40	3.83	6.71	5.67	5.17	4.31	4.56	3.76	3.14	2.83	4.19	2.89	12.01
1220.27	3	0.00	0.00	0.00	0.00	0.00	0.00	0.09	0.09	0.09	0.09	0.19	0.66	0.85	1.66	1.66	3.91	9.97	12.90	11.73	8.70	8.01	6.74	5.18	5.57	3.22	18.67
1221.8	7	0.00	0.00	0.00	0.00	0.06	0.06	2.12	5.72	13.30	19.73	16.26	9.96	7.39	2.32	1.10	2.07	2.54	2.45	2.45	2.38	2.05	1.13	1.58	1.67	0.33	3.32
1248.12	6V	0.00	0.00	0.00	0.10	0.00	0.10	0.10	0.10	0.10	0.10	0.30	1.69	21.53	15.45	7.41	7.71	10.86	8.97	5.98	5.72	3.99	1.05	2.41	3.15	3.15	0.00
1275.18	3V	0.00	0.00	0.19	0.19	0.19	0.37	0.65	0.74	0.46	0.46	0.56	7.13	10.46	5.33	5.87	13.11	13.83	11.38	8.43	7.20	4.75	2.88	1.73	3.02	1.08	0.00
1275.6	9	0.00	0.00	0.00	0.14	0.28	0.28	0.21	0.28	0.42	0.35	0.35	0.42	0.56	0.28	0.29	2.43	2.34	3.02	6.23	7.79	7.50	8.37	8.67	7.89	6.23	35.64
1277.45	9	0.00	0.00	1.56	0.93	0.70	0.93	1.24	1.63	2.41	2.80	3.27	4.74	4.82	1.54	3.49	4.00	4.45	5.27	4.82	5.27	3.78	4.45	4.38	4.00	3.49	26.03
1279.84	3	0.00	0.00	0.00	0.00	0.00	0.00	0.13	0.20	0.39	0.46	0.66	2.63	5.98	4.86	5.04	7.03	8.57	6.43	7.37	6.34	5.74	6.00	6.00	6.52	4.80	14.83
1280.2	9	0.00	0.99	0.99	0.85	1.05	0.92	1.51	2.30	3.29	4.14	5.52	6.50	6.77	3.78	2.55	4.34	4.27	4.34	4.27	5.61	4.46	4.08	4.53	4.78	2.93	15.24
1281.6	9	0.00	0.00	0.57	0.71	0.50	0.85	1.06	1.28	1.84	2.27	3.19	4.25	4.75	3.64	2.74	3.84	4.78	4.85	4.93	5.95	6.11	5.72	4.78	5.95	5.79	19.65
1282.04	10	1.11	1.66	0.74	0.99	1.48	1.54	1.97	2.46	3.64	4.74	6.04	7.33	6.72	3.71	3.39	3.68	4.79	4.50	4.32	4.67	4.67	4.03	4.14	4.14	1.87	11.68
1275.60(d)	9	0.00	0.00	0.00	0.16	0.08	0.16	0.24	0.33	0.41	0.49	0.49	0.49	0.24	0.97	1.32	1.06	1.63	1.92	4.03	4.90	4.90	5.57	6.43	7.40	7.30	49.46
133.48(r)	3	0.00	0.00	0.00	0.00	0.00	0.00	0.00	0.00	0.10	0.31	1.87	2.70	3.74	3.27	2.75	4.24	6.18	6.44	6.44	4.85	6.27	5.21	4.15	4.59	2.74	34.15
141.84(r)	6V	0.00	0.00	0.00	0.00	0.00	0.00	0.00	0.00	0.00	0.00	0.56	4.37	12.81	11.93	8.59	15.00	16.10	11.99	5.55	3.84	3.43	1.92	0.27	1.23	2.40	0.00
48.19(r)	9	0.00	0.00	0.30	0.59	0.44	0.30	0.89	1.18	1.63	1.78	2.07	2.22	2.37	1.79	2.00	4.17	8.94	9.46	8.07	6.77	7.29	5.21	3.73	4.60	4.17	20.05
50.14(r)	10	0.00	1.67	0.93	0.74	0.93	1.30	1.49	1.86	2.42	2.60	2.79	2.60	2.97	3.69	3.65	5.93	11.02	9.95	7.14	6.99	5.70	4.25	2.20	3.50	7.29	6.38
852.19(d)	3	0.00	0.00	0.00	0.00	0.00	0.00	0.57	4.32	15.57	24.43	21.59	11.93	5.80	1.48	1.04	1.39	1.46	1.26	1.29	0.95	0.88	1.02	0.64	0.43	0.36	3.59
86.31(r)	3	0.00	0.00	0.00	0.00	0.00	0.00	0.00	0.00	0.00	0.00	0.31	1.38	2.45	3.00	2.92	4.96	9.35	9.74	9.07	8.21	6.59	6.20	4.39	5.15	5.25	21.00
90.00(r)	2	0.00	0.00	0.00	0.44	0.44	0.44	0.44	0.66	0.88	0.99	1.10	0.88	1.21	0.66	1.59	3.46	4.02	9.35	7.01	7.58	7.86	6.17	5.33	5.99	8.79	24.69

Table 12: Grain-size frequency data for AND-1B. (d) Duplicate sample. (r) Sample reprocessed due to incomplete disaggregation of original sample.

3.10.1.2 *Supplementary data: Grain-size statistical data from AND-1B*

		Percentiles								Moment				Graphic				Inman		Proportions			
		1%	5%	16%	25%	50%	75%	84%	95%	Mean	StDev	Skew	Kurt	Mean	StDev	Skew	Kurt	StDev	Skew	Gravel	Sand	Silt	Clay
9.99	10	-1.52	0.12	3.22	5.76	8.32	11.67	13.37	16.83	8.11	4.16	-0.58	2.34	8.30	5.07	0.01	1.16	5.08	0.00	2.59	16.75	27.51	53.15
20.01	4	0.26	3.21	6.16	7.22	12.12	23.04	28.23	38.76	9.79	3.39	-0.91	2.84	15.50	10.90	0.48	0.92	11.03	0.46	0.06	6.43	26.57	66.94
20.27	3	-0.78	1.55	5.87	7.36	10.88	14.89	16.80	20.66	9.65	3.77	-1.13	3.25	11.18	5.63	0.05	1.04	5.46	0.08	0.67	10.67	19.20	69.45
20.51	4	0.31	3.38	6.75	7.79	10.92	14.39	16.03	19.37	10.05	3.27	-1.17	3.66	11.23	4.74	0.08	0.99	4.64	0.10	0.46	5.80	20.92	72.82
25.93	3	-0.29	0.45	1.15	1.53	2.86	5.58	6.52	8.54	3.65	2.76	1.02	3.82	3.51	2.57	0.38	0.82	2.68	0.36	0.14	63.42	29.73	6.71
25.96	3	0.44	1.27	2.22	2.92	5.75	7.72	9.56	11.65	5.87	3.46	0.53	2.42	5.84	3.41	0.09	0.88	3.67	0.04	0.01	36.19	41.29	22.51
26.53	3	1.32	2.58	4.21	5.51	7.24	10.49	13.36	19.18	7.79	3.39	0.10	1.94	8.27	4.80	0.39	1.36	4.58	0.34	0.00	14.93	43.49	41.58
31.63	10	-2.26	-	3.99	6.61	10.40	13.36	14.77	17.63	9.12	4.40	-1.07	2.93	9.72	5.43	-0.19	1.10	5.39	-0.19	3.23	12.78	17.00	66.99
42.1	4	1.86	3.43	5.58	6.74	9.50	11.58	12.56	14.57	9.28	3.27	-0.50	2.03	9.22	3.43	-0.11	0.94	3.49	-0.12	0.00	7.27	28.83	63.89
42.36	2	3.11	4.73	6.60	7.90	11.49	15.30	17.11	20.78	10.32	2.94	-0.92	2.44	11.73	5.06	0.11	0.89	5.25	0.07	0.00	3.46	22.56	73.98
42.58	4	1.34	4.31	6.41	7.39	10.24	13.40	14.90	17.94	9.86	3.12	-0.82	2.68	10.52	4.19	0.11	0.93	4.25	0.10	0.00	4.42	25.90	69.68
44.84	9	-1.04	0.57	3.34	4.92	6.74	9.88	12.91	19.09	7.15	3.82	-0.05	2.22	7.66	5.20	0.31	1.53	4.79	0.29	1.33	17.69	44.66	36.31
48.03	7	-4.12	-	0.92	2.25	6.75	10.32	12.03	15.52	6.41	4.80	-0.13	1.75	6.57	5.32	0.00	0.85	5.55	-0.05	5.57	32.30	21.68	40.44
48.19	9	-0.84	1.77	3.72	4.76	6.25	8.13	9.66	11.95	6.62	3.16	0.25	3.02	6.54	3.03	0.13	1.24	2.97	0.15	0.89	18.91	54.12	26.08
50.14	10	-1.24	0.53	2.62	3.35	5.41	7.17	8.41	15.69	5.56	3.32	0.48	3.02	5.48	3.75	0.19	1.63	2.89	0.03	2.14	34.13	45.09	18.63
50.61	10	-3.35	-	0.01	1.33	5.44	8.39	9.84	13.19	5.20	4.52	0.10	1.99	5.10	4.72	-0.03	0.87	4.91	-0.11	8.82	33.33	30.12	27.73
52.97	3	-2.07	-	0.98	2.40	7.44	9.91	10.84	12.75	6.68	4.59	-0.26	1.84	6.42	4.54	-0.27	0.75	4.93	-0.31	4.65	27.76	22.99	44.61
53.1	3	3.79	5.56	6.41	6.81	8.04	10.02	10.89	12.66	8.71	2.50	0.37	2.08	8.45	2.19	0.29	0.91	2.24	0.27	0.00	1.26	48.15	50.58
53.23	9	-1.98	-	0.62	1.83	5.07	6.80	7.82	10.85	4.67	3.72	0.25	2.63	4.50	3.63	-0.14	1.00	3.60	-0.24	7.09	36.19	41.70	15.03
56.81	3	2.40	2.67	2.93	3.09	3.60	6.17	7.29	11.26	4.84	2.60	1.56	4.80	4.61	2.39	0.74	1.14	2.18	0.69	0.00	60.51	27.58	11.90
58.97	9	-2.79	-	1.84	3.55	7.48	10.35	11.64	14.26	7.08	4.52	-0.39	2.09	6.99	4.79	-0.14	0.93	4.90	-0.15	5.88	22.25	26.57	45.30
67.8	10	-2.59	0.07	2.54	4.64	7.30	9.42	12.05	17.52	7.11	3.96	-0.33	2.46	7.30	5.02	0.09	1.49	4.75	0.00	2.80	21.05	38.65	37.50
70.75	10	-1.93	-	1.97	3.21	7.80	11.20	13.08	16.92	7.25	4.55	-0.31	1.86	7.62	5.44	-0.01	0.90	5.56	-0.05	4.11	26.03	21.57	48.30
74.71	10	-1.91	0.01	2.44	3.99	7.78	11.48	13.92	18.87	7.57	4.30	-0.42	2.13	8.05	5.73	0.12	1.03	5.74	0.07	3.16	21.88	27.83	47.13
77.52	10	-1.57	-	2.39	3.97	7.91	10.59	12.03	14.95	7.51	4.25	-0.41	2.11	7.44	4.67	-0.10	0.93	4.82	-0.15	3.51	21.68	25.95	48.86
82.4	9	-2.05	-	2.82	4.70	7.72	10.60	11.95	14.70	7.50	4.26	-0.45	2.27	7.50	4.61	-0.08	1.07	4.56	-0.07	3.74	17.94	31.16	47.15
83.5	2	-0.10	5.48	7.18	7.93	11.90	23.40	28.86	39.96	10.13	2.95	-1.12	4.16	15.98	10.64	0.60	0.91	10.84	0.57	0.61	2.52	22.82	74.05
83.97	2		3.65	7.00	7.67	9.49	11.63	12.64	14.70	9.53	3.32	-1.35	5.43	9.71	3.08	0.03	1.14	2.82	0.12	2.34	3.16	24.97	69.53
84.31	2	3.39	6.05	6.94	7.43	8.79	11.24	12.54	15.19	9.40	2.56	-0.07	2.05	9.42	2.79	0.37	0.98	2.80	0.34	0.00	1.73	33.82	64.44
85.2	2	4.06	5.96	6.64	7.11	8.53	10.85	12.00	14.34	9.19	2.57	0.14	1.74	9.06	2.61	0.34	0.92	2.68	0.30	0.00	0.91	40.73	58.36
86.05	3	4.38	6.59	7.61	8.33	10.53	13.46	14.85	17.68	10.45	2.43	-0.66	2.17	11.00	3.49	0.24	0.88	3.62	0.19	0.00	0.26	20.52	79.22
86.31	3	2.67	3.39	5.00	6.11	8.16	10.98	12.43	15.38	8.49	3.23	-0.05	1.75	8.53	3.67	0.18	1.01	3.72	0.15	0.00	11.75	36.39	51.86
86.74	2	1.54	2.72	4.39	5.77	8.60	11.59	13.08	16.10	8.59	3.54	-0.29	1.81	8.69	4.20	0.08	0.94	4.34	0.03	0.00	14.94	28.89	56.17
90	2	-0.67	2.07	3.81	6.02	8.63	10.83	11.78	13.71	8.41	3.73	-0.50	2.32	8.07	3.76	-0.17	0.99	3.98	-0.21	0.82	17.16	25.46	56.57
93.15	3	3.24	4.21	6.66	7.29	8.84	11.46	12.86	15.72	9.31	2.76	-0.20	2.04	9.45	3.29	0.25	1.13	3.10	0.30	0.00	4.54	32.03	63.43

		Percentiles								Moment				Graphic				Inman		Proportions			
		1%	5%	16%	25%	50%	75%	84%	95%	Mean	StDev	Skew	Kurt	Mean	StDev	Skew	Kurt	StDev	Skew	Gravel	Sand	Silt	Clay
95.3	3	5.12	6.01	6.53	6.89	8.42	15.08	19.73	29.18	9.25	2.66	0.19	1.42	11.56	6.81	0.75	1.16	6.60	0.71	0.00	0.24	44.47	55.29
95.55	3	2.90	3.37	3.93	5.31	8.05	11.04	12.97	16.89	8.22	3.37	0.01	1.64	8.32	4.31	0.20	0.97	4.52	0.09	0.00	17.77	31.64	50.58
96.58	2	4.02	5.88	6.72	7.39	9.41	11.95	13.16	15.62	9.74	2.66	-0.26	1.73	9.76	3.08	0.22	0.88	3.22	0.16	0.00	0.99	31.51	67.50
97.35	9	-1.24	1.08	4.38	5.88	8.50	13.59	16.44	22.23	8.46	3.91	-0.56	2.38	9.77	6.22	0.31	1.12	6.03	0.32	1.44	12.92	31.02	54.62
99.92	2	3.64	5.26	5.97	6.49	9.29	222	330.51	550.14	9.54	3.07	-0.35	1.79	115.25	163.69	0.98	1.03	162.27	0.98	0.12	1.15	37.99	60.74
100.1	6	-0.97	0.59	1.52	1.81	2.54	3.79	6.56	10.45	3.57	3.09	1.59	5.00	3.54	2.76	0.60	2.05	2.52	0.59	0.97	76.10	11.97	10.96
100.61	6	-0.34	0.81	1.29	1.51	2.08	3.24	4.99	9.07	3.02	2.71	2.11	7.27	2.79	2.18	0.63	1.95	1.85	0.57	0.35	81.80	11.01	6.84
100.79	9	-2.47	-	2.88	4.60	6.17	8.29	21.42	142.29	6.41	3.79	-0.09	2.79	10.16	26.31	0.77	15.89	9.27	0.65	4.56	16.68	51.50	27.27
109.19	9	-	-	4.62	5.30	6.65	8.97	10.41	13.27	7.00	3.61	-0.37	3.42	7.23	3.56	0.13	1.56	2.89	0.30	4.40	8.60	53.93	33.07
109.74	2	4.81	5.67	6.50	7.05	8.92	11.57	12.91	15.63	9.41	2.65	0.01	1.51	9.44	3.11	0.30	0.90	3.20	0.24	0.00	0.26	38.14	61.60
111.17	3	2.91	3.70	4.41	4.81	5.60	6.65	7.45	9.73	5.97	1.97	1.19	5.94	5.82	1.67	0.30	1.34	1.52	0.22	0.23	10.46	77.14	12.17
117.63	1a		0.84	4.20	5.72	7.45	10.00	10.99	12.99	7.68	3.65	-0.38	2.80	7.55	3.54	-0.02	1.16	3.39	0.04	2.12	12.91	41.83	43.14
118	4	-1.82	-	1.27	3.50	7.05	9.82	11.97	16.36	6.77	4.39	-0.27	2.05	6.77	5.29	0.00	1.12	5.35	-0.08	4.56	22.64	32.48	40.32
118.62	3	3.62	5.06	6.44	7.15	9.18	11.36	12.39	14.47	9.47	2.79	-0.24	1.80	9.34	2.91	0.10	0.92	2.98	0.08	0.00	1.79	33.35	64.86
119.15	6V	2.87	3.42	4.90	5.57	6.72	8.21	9.20	11.95	7.12	2.52	0.73	3.14	6.94	2.37	0.19	1.32	2.15	0.16	0.00	10.70	61.67	27.63
122	2	-1.79	-	2.55	4.21	6.56	9.14	13.67	24.45	6.71	4.04	-0.14	2.33	7.59	6.58	0.35	2.08	5.56	0.28	3.77	20.11	42.18	33.93
124.39	9	0.13	4.92	5.74	6.17	7.98	10.59	11.72	14.02	8.57	3.05	-0.11	2.51	8.48	2.87	0.29	0.84	2.99	0.25	0.69	2.80	46.72	49.79
125.95	2	4.13	6.03	7.77	8.82	11.82	15.09	16.64	19.78	10.81	2.48	-1.15	3.23	12.08	4.30	0.12	0.90	4.43	0.09	0.00	0.97	16.63	82.39
126.39	4+2	3.67	5.42	7.52	8.45	11.81	16.01	18.00	22.05	10.59	2.63	-1.03	3.00	12.44	5.14	0.21	0.90	5.24	0.18	0.00	1.33	19.49	79.18
128.78	2	4.96	6.16	7.61	8.43	10.27	12.07	12.92	14.65	10.45	2.41	-0.62	1.97	10.27	2.61	0.01	0.96	2.65	0.00	0.00	0.06	20.13	79.82
131.72	2	4.21	5.33	7.29	8.52	11.10	13.67	14.88	17.36	10.59	2.63	-0.95	2.49	11.09	3.72	0.02	0.96	3.80	0.00	0.00	0.51	19.97	79.52
133.48	3	2.15	2.84	3.73	4.65	7.72	11.20	13.07	16.87	8.03	3.59	0.01	1.59	8.17	4.46	0.23	0.88	4.67	0.15	0.00	20.70	31.68	47.62
134.68	4	-0.28	2.45	3.34	3.69	5.01	6.21	6.94	8.58	5.10	2.06	0.58	4.81	5.10	1.83	0.12	1.00	1.80	0.07	0.20	34.69	57.51	7.60
141.29	6V	3.95	4.85	5.52	5.92	6.62	7.38	7.84	9.07	6.70	1.22	0.30	3.32	6.66	1.22	0.11	1.19	1.16	0.05	0.00	1.19	85.15	13.67
141.4	6V	3.79	4.25	4.91	5.20	5.74	6.30	6.67	8.21	5.91	1.34	2.19	11.05	5.77	1.04	0.15	1.47	0.88	0.06	0.00	2.86	91.34	5.79
141.58	6V	3.59	3.93	4.71	5.06	5.59	6.33	6.91	9.59	5.90	1.59	1.77	7.47	5.74	1.41	0.31	1.82	1.10	0.20	0.00	6.50	84.39	9.11
141.72	6V	2.89	3.27	3.60	3.76	4.19	4.99	5.57	7.11	4.57	1.41	2.63	13.47	4.45	1.07	0.46	1.28	0.98	0.40	0.00	42.12	55.29	2.59
141.84	6V	2.06	2.73	3.35	3.60	4.29	5.45	5.91	7.41	4.62	1.51	1.05	4.68	4.51	1.35	0.30	1.04	1.28	0.27	0.07	44.78	51.39	3.77
146.58	3	2.33	2.84	3.56	4.16	6.00	8.18	9.39	13.21	6.60	2.96	0.72	2.65	6.32	3.03	0.28	1.06	2.92	0.16	0.00	24.19	48.98	26.83
146.83	10	-1.13	0.43	2.93	4.54	6.65	8.00	9.31	11.18	6.43	3.31	-0.12	2.97	6.30	3.22	-0.16	1.27	3.19	-0.17	1.21	21.68	52.16	24.96
147.76	10	-1.68	-	-	-	0.84	2.11	2.45	2.90	0.68	1.60	0.00	1.87	0.70	1.58	-0.09	0.58	1.82	-0.12	25.86	74.08	0.04	0.02
148.32	10	-1.58	-	3.34	5.53	8.02	11.17	12.85	16.25	7.83	4.17	-0.52	2.37	8.07	4.91	0.00	1.21	4.75	0.02	3.22	15.83	30.74	50.20
150.42	9	-3.19	-	1.31	2.78	6.16	8.70	9.84	11.94	5.80	4.24	-0.09	2.20	5.77	4.18	-0.14	0.94	4.26	-0.14	7.18	29.64	31.64	31.54
150.95	4	-0.18	4.64	6.88	7.70	9.65	11.30	12.08	13.67	9.70	3.00	-0.95	3.77	9.53	2.67	-0.09	1.03	2.60	-0.07	0.39	3.29	24.32	72.00
151.5	4	0.73	5.68	7.64	8.46	10.51	12.61	13.61	15.63	10.43	2.71	-1.28	4.89	10.59	3.00	0.03	0.98	2.98	0.04	0.52	1.13	18.32	80.02
151.71	1b	-1.02	-	7.45	8.56	10.45	12.28	13.16	14.93	9.98	3.74	-1.71	5.29	10.35	3.77	-0.23	1.70	2.85	-0.05	1.13	7.00	11.76	80.11
178.98	1a	-2.66	-	7.59	8.56	10.05	11.32	11.92	13.15	9.71	3.93	-1.75	5.51	9.85	3.26	-0.35	2.13	2.17	-0.14	5.45	3.56	9.92	81.07
180.38	1a	0.52	4.89	7.36	8.18	9.77	11.47	12.27	13.91	9.94	2.85	-1.03	4.04	9.80	2.60	-0.03	1.12	2.46	0.02	0.20	2.83	19.58	77.38

		Percentiles								Moment				Graphic				Inman		Proportions			
		1%	5%	16%	25%	50%	75%	84%	95%	Mean	StDev	Skew	Kurt	Mean	StDev	Skew	Kurt	StDev	Skew	Gravel	Sand	Silt	Clay
180.68	1b	4.24	6.17	7.66	8.42	9.92	11.23	11.85	13.11	10.26	2.43	-0.62	2.42	9.81	2.10	-0.08	1.01	2.09	-0.08	0.00	0.45	18.97	80.59
181.22	2	4.19	5.38	7.38	8.64	12.05	15.85	17.66	21.32	10.68	2.63	-1.06	2.72	12.36	4.98	0.13	0.91	5.14	0.09	0.00	0.76	19.82	79.42
181.89	2	-3.35	3.79	6.80	7.80	10.01	13.03	14.46	17.37	9.76	3.40	-1.44	5.39	10.42	3.97	0.12	1.06	3.83	0.16	2.64	2.51	21.92	72.93
181.94	9	-1.65	-	0.29	2.00	6.22	10.73	13.64	19.57	6.20	4.90	-0.04	1.66	6.72	6.51	0.19	0.98	6.68	0.11	7.67	31.14	23.00	38.19
191.24	1+10	0.26	5.71	7.10	7.85	10.08	12.69	13.93	16.45	10.02	2.91	-1.04	4.04	10.37	3.33	0.16	0.91	3.42	0.13	0.59	2.59	23.78	73.04
211.74	1a	3.60	5.72	7.52	8.13	9.40	11.01	11.79	13.36	9.80	2.53	-0.53	2.86	9.57	2.22	0.08	1.09	2.13	0.12	0.00	2.07	20.74	77.19
224.53	3	-2.65	1.20	6.16	7.20	8.97	10.93	11.86	13.74	8.88	3.60	-1.03	3.92	9.00	3.32	-0.11	1.38	2.85	0.02	2.23	7.76	25.39	64.62
224.67	3	2.68	3.25	3.96	5.62	7.59	9.69	10.89	13.34	7.84	3.11	0.17	1.98	7.48	3.26	0.05	1.02	3.47	-0.05	0.00	16.85	39.70	43.45
224.88	3	1.17	5.25	7.23	7.90	9.53	10.96	11.65	13.03	9.73	2.74	-0.74	3.42	9.47	2.28	-0.07	1.04	2.21	-0.04	0.00	3.47	23.13	73.40
225	9	-2.74	-	-	0.72	3.55	6.74	7.58	9.50	3.79	3.67	0.20	2.25	3.59	3.68	0.04	0.76	3.97	0.02	10.04	44.16	33.40	12.40
225.38	10	0.25	4.04	6.84	7.80	9.80	11.58	12.42	14.14	9.78	3.06	-0.96	3.53	9.69	2.93	-0.10	1.10	2.79	-0.06	0.32	4.58	22.32	72.78
258.55	3	4.31	6.93	8.73	9.31	10.56	11.79	12.38	13.57	10.96	2.18	-1.23	3.82	10.55	1.92	-0.05	1.10	1.82	0.00	0.00	0.12	8.44	91.44
260.42	3	4.85	6.36	8.40	9.40	12.52	15.69	17.19	20.25	11.14	2.25	-1.36	3.61	12.70	4.30	0.09	0.90	4.40	0.06	0.00	0.33	12.58	87.08
260.7	3	-1.04	-	0.55	1.33	5.03	7.98	9.41	11.76	5.09	4.11	0.35	2.06	5.00	4.07	0.05	0.75	4.43	-0.01	1.32	42.73	31.10	24.85
267.88	4	1.75	3.95	6.41	7.73	10.24	13.48	15.02	18.14	9.90	3.09	-0.84	2.66	10.56	4.30	0.11	1.01	4.30	0.11	0.00	5.14	22.68	72.17
283.2	4	4.01	6.31	7.69	8.67	10.74	12.85	13.85	15.88	10.63	2.48	-0.98	2.95	10.76	2.99	0.04	0.94	3.08	0.01	0.00	0.98	17.28	81.74
293.23	2	3.14	5.28	6.59	7.43	9.51	11.83	12.93	15.16	9.71	2.79	-0.45	2.19	9.68	3.08	0.11	0.92	3.17	0.08	0.00	1.73	29.33	68.94
296.72	10	-1.04	0.68	3.06	5.01	7.72	10.28	11.38	13.60	7.58	3.96	-0.30	2.11	7.39	4.04	-0.11	1.01	4.16	-0.12	1.02	22.27	29.56	47.15
307.04	10	-1.37	2.31	5.54	6.83	9.16	17.36	21.77	30.75	9.11	3.62	-0.81	2.99	12.16	8.37	0.54	1.11	8.12	0.55	1.13	9.39	26.26	63.22
316.23	4	-0.44	1.19	3.25	4.61	7.31	10.32	12.20	16.03	7.46	3.81	-0.10	1.99	7.59	4.49	0.13	1.06	4.48	0.09	0.46	21.07	35.23	43.24
358.94	3	2.88	3.36	3.95	4.98	7.82	10.77	12.06	14.66	8.13	3.46	0.07	1.53	7.94	3.74	0.13	0.80	4.05	0.04	0.00	17.41	34.04	48.55
359.95	3	0.99	4.37	6.21	7.13	9.64	12.13	13.31	15.71	9.58	3.11	-0.67	2.72	9.72	3.49	0.05	0.93	3.55	0.03	0.50	2.76	30.42	66.32
361.6	3	-0.25	2.79	4.18	4.84	6.97	10.08	11.46	14.27	7.56	3.51	0.10	2.03	7.54	3.56	0.25	0.90	3.64	0.23	0.00	14.03	44.68	41.29
381.92	1b	-0.84	0.87	4.82	6.62	9.08	12.18	13.76	16.98	8.79	3.86	-0.79	2.69	9.22	4.68	0.01	1.19	4.47	0.05	0.74	13.40	22.21	63.65
413.16	6	2.58	3.92	5.19	5.62	6.93	8.60	9.69	11.27	7.38	2.55	0.63	2.98	7.27	2.24	0.20	1.01	2.25	0.23	0.00	5.51	61.72	32.76
460.09	3	0.04	2.71	5.41	6.40	8.81	11.53	12.86	15.55	8.86	3.42	-0.52	2.47	9.02	3.81	0.07	1.03	3.72	0.09	0.12	7.78	33.64	58.46
464.07	10	-1.05	2.98	5.74	6.31	8.12	11.22	13.13	17.00	8.51	3.33	-0.44	2.97	8.99	3.97	0.31	1.17	3.70	0.36	1.06	5.55	41.92	51.47
473.22	2+4	6.18	7.32	8.40	9.07	11.03	13.08	14.05	16.03	11.01	2.06	-0.87	2.31	11.16	2.73	0.11	0.89	2.83	0.07	0.00	0.12	11.50	88.38
479.18	10	-2.60	0.56	4.10	5.72	8.66	10.89	11.84	13.75	8.28	4.01	-0.66	2.66	8.20	3.93	-0.20	1.05	3.87	-0.18	2.45	13.06	28.73	55.76
481.15	4	1.29	5.04	6.53	7.47	9.91	12.92	14.35	17.25	9.81	3.01	-0.78	2.93	10.26	3.80	0.17	0.92	3.91	0.14	0.45	2.87	27.62	69.07
488.58	2	6.31	6.95	8.24	8.99	10.68	12.39	13.21	14.87	10.88	2.12	-0.78	2.16	10.71	2.44	0.04	0.95	2.48	0.02	0.00	0.11	13.34	86.55
494.33	3	5.04	5.78	7.20	8.23	10.99	14.06	15.51	18.48	10.49	2.56	-0.73	1.96	11.23	4.00	0.13	0.89	4.16	0.09	0.00	0.01	23.21	76.78
501.2	2	5.93	6.98	8.12	8.87	10.62	12.30	13.09	14.71	10.83	2.16	-0.75	2.08	10.61	2.42	0.03	0.93	2.49	-0.01	0.00	0.08	14.66	85.26
504.55	1b	0.47	4.13	6.33	7.24	8.82	10.21	10.83	12.10	8.91	2.87	-0.51	3.23	8.66	2.33	-0.14	1.10	2.25	-0.10	0.31	4.18	31.40	64.12
519.11	9	-1.52	-	0.95	2.32	5.10	7.42	8.52	11.83	5.07	3.75	0.26	2.49	4.86	3.81	-0.02	1.02	3.78	-0.10	4.26	36.17	39.50	20.06
523.39	5	3.68	4.82	5.69	6.18	7.61	9.70	11.06	13.83	8.24	2.67	0.49	2.07	8.12	2.71	0.33	1.05	2.69	0.28	0.00	1.81	54.52	43.67
523.65	3	-	1.44	3.31	4.58	6.62	9.25	11.31	15.80	6.99	3.64	0.04	2.37	7.08	4.17	0.23	1.26	4.00	0.17	1.19	20.32	43.37	35.12
523.93	4+9	-4.50	-	3.36	5.14	7.56	10.66	12.04	14.84	7.53	4.27	-0.52	2.52	7.65	4.56	-0.02	1.17	4.34	0.03	4.84	13.53	35.22	46.41

		Percentiles								Moment				Graphic				Inman		Proportions			
		1%	5%	16%	25%	50%	75%	84%	95%	Mean	StDev	Skew	Kurt	Mean	StDev	Skew	Kurt	StDev	Skew	Gravel	Sand	Silt	Clay
545.15	4	0.97	3.15	5.50	6.28	8.63	11.89	13.57	16.99	8.83	3.34	-0.34	2.08	9.23	4.11	0.22	1.01	4.04	0.23	0.00	8.40	35.00	56.59
778.7	10	-0.79	1.47	3.89	5.85	9.99	15.66	18.35	23.82	8.98	4.06	-0.71	2.19	10.74	7.00	0.20	0.93	7.23	0.16	0.71	16.01	21.39	61.89
790.74	7	-8.20	-	-	-	-0.51	2.96	4.03	4.15	0.24	2.64	0.44	1.63	-0.08	3.48	0.04	0.73	3.90	0.16	44.56	35.79	19.64	0.01
827.21	3	-1.11	-	0.66	1.41	3.24	7.99	9.55	12.41	4.76	4.22	0.59	2.12	4.48	4.19	0.42	0.81	4.45	0.42	1.41	55.62	18.02	24.95
830.64	9	-0.47	0.93	2.39	3.57	8.12	11.21	12.77	15.95	7.66	4.25	-0.26	1.71	7.76	4.87	-0.03	0.81	5.19	-0.10	0.44	27.72	20.82	51.01
850.95	2	5.25	5.58	6.44	7.01	8.76	13.13	15.62	20.67	9.40	2.69	0.04	1.42	10.28	4.58	0.54	1.01	4.59	0.49	0.00	0.01	39.64	60.34
852.19	3	1.14	1.47	1.85	2.06	2.63	3.49	4.68	7.84	3.27	2.06	2.21	8.46	3.05	1.67	0.54	1.82	1.41	0.45	0.00	80.81	14.54	4.65
853.25	9	-0.98	0.44	2.68	4.11	8.61	12.17	13.85	17.28	8.04	4.37	-0.45	1.86	8.38	5.34	-0.02	0.86	5.58	-0.06	0.96	23.68	20.94	54.42
854.36	10	-3.08	-	1.02	3.69	8.55	11.58	13.05	16.03	7.58	4.93	-0.62	2.08	7.54	5.69	-0.20	0.92	6.02	-0.25	7.14	18.89	18.92	55.05
856.01	4	1.16	3.78	6.52	7.44	9.46	11.85	12.98	15.29	9.54	3.07	-0.70	2.72	9.66	3.36	0.05	1.07	3.23	0.09	0.00	5.51	25.61	68.88
891.17	2	5.32	6.32	7.58	8.34	10.26	12.20	13.12	14.99	10.44	2.38	-0.55	1.81	10.32	2.70	0.06	0.92	2.77	0.03	0.00	0.01	20.78	79.21
902.8	10	-1.03	0.75	3.25	5.03	8.73	12.20	13.84	17.18	8.27	4.20	-0.50	1.99	8.61	5.14	0.00	0.94	5.29	-0.03	1.25	19.62	23.36	55.77
1032.47	6	1.24	1.70	2.13	2.36	2.84	3.76	6.94	15.12	4.11	3.21	1.81	4.93	3.97	3.24	0.77	3.93	2.40	0.71	0.00	77.63	8.68	13.69
1032.83	5	3.80	4.90	6.16	6.94	8.94	11.16	12.20	14.31	9.27	2.82	-0.11	1.66	9.10	2.93	0.11	0.92	3.02	0.08	0.00	1.64	36.56	61.80
1033.58	5	3.83	4.46	5.86	6.74	9.37	14.44	16.90	21.89	9.49	3.06	-0.32	1.57	10.71	5.40	0.40	0.93	5.52	0.36	0.00	2.11	34.76	63.13
1043.53	5	3.94	4.60	5.47	6.02	8.70	13.57	16.22	21.61	9.04	3.11	-0.05	1.40	10.13	5.27	0.46	0.92	5.38	0.40	0.00	1.18	42.52	56.29
1053.27	9		1.50	5.75	7.31	9.59	11.76	12.79	14.89	9.23	3.75	-1.10	3.68	9.38	3.79	-0.15	1.23	3.52	-0.09	1.94	9.04	20.35	68.67
1060.4	2	2.83	4.59	6.99	7.85	9.71	12.53	13.87	16.58	9.85	2.84	-0.63	2.33	10.19	3.54	0.18	1.05	3.44	0.21	0.00	3.38	23.39	73.23
1062.87	3	-0.53	0.19	0.90	1.34	2.84	5.78	7.49	10.28	3.84	3.30	1.07	3.42	3.74	3.17	0.44	0.93	3.29	0.41	0.00	64.86	21.59	13.55
1063.66	10	-1.61	-	2.98	5.06	7.73	10.15	11.28	13.57	7.44	4.12	-0.46	2.38	7.33	4.22	-0.16	1.14	4.15	-0.14	3.89	17.76	31.75	46.60
1066.17	10	-1.45	1.80	6.64	7.73	10.23	13.15	14.53	17.34	9.68	3.60	-1.24	3.89	10.47	4.33	0.00	1.18	3.94	0.09	1.53	8.01	18.06	72.40
1095.46	9	-1.54	0.34	3.34	5.39	8.50	11.14	12.47	15.19	8.09	4.10	-0.56	2.32	8.11	4.53	-0.11	1.06	4.57	-0.13	2.42	17.68	24.72	55.18
1164.3	2+10	-2.37	-	2.15	3.91	7.57	10.05	11.20	13.55	7.08	4.40	-0.43	2.25	6.98	4.52	-0.20	1.00	4.53	-0.20	6.12	19.42	28.86	45.59
1164.48	4	1.57	5.58	6.91	7.60	9.23	11.53	12.67	14.97	9.59	2.76	-0.55	2.95	9.60	2.86	0.21	0.98	2.88	0.19	0.00	2.50	28.32	69.18
1167.68	10	-2.00	-	2.44	3.72	7.02	9.91	11.41	14.46	6.89	4.25	-0.23	2.13	6.96	4.57	-0.03	1.02	4.49	-0.02	4.78	22.70	31.25	41.27
1168.08	4	1.98	4.51	6.19	6.90	8.61	10.87	12.12	14.67	8.98	2.85	-0.19	2.33	8.97	3.02	0.19	1.05	2.97	0.18	0.00	4.04	36.33	59.63
1196.18	10	-2.72	1.10	4.07	5.46	7.72	10.36	11.77	14.63	7.79	3.78	-0.42	2.66	7.86	3.97	0.04	1.13	3.85	0.05	2.25	13.39	37.59	46.78
1197.4	5	5.60	6.76	7.54	8.05	9.45	11.03	11.78	13.30	9.97	2.26	-0.08	1.64	9.59	2.05	0.14	0.90	2.12	0.10	0.00	0.16	24.10	75.74
1198.43	9	0.35	3.39	5.12	5.72	7.67	10.32	11.65	14.36	8.12	3.24	-0.03	2.23	8.15	3.29	0.22	0.98	3.26	0.22	0.37	7.54	45.69	46.40
1198.43	10	0.34	3.38	5.23	5.89	7.84	10.51	11.97	14.94	8.27	3.22	-0.10	2.29	8.35	3.43	0.23	1.03	3.37	0.23	0.37	6.85	44.53	48.25
1199.74	10	-1.48	-	1.85	3.03	5.39	8.01	9.36	11.76	5.61	3.76	0.22	2.42	5.54	3.75	0.04	1.02	3.75	0.06	3.22	33.31	38.40	25.07
1220.27	3	3.36	4.89	5.86	6.24	7.35	9.21	10.46	13.30	8.01	2.52	0.62	2.54	7.89	2.42	0.38	1.16	2.30	0.35	0.00	2.08	58.53	39.38
1221.8	7	0.84	1.30	1.84	2.11	2.78	4.08	6.27	9.08	3.70	2.58	1.74	5.71	3.63	2.29	0.60	1.62	2.22	0.58	0.00	74.61	17.36	8.03
1248.12	6V	3.05	3.62	3.88	4.03	5.19	6.54	7.29	9.17	5.50	1.75	0.68	2.99	5.46	1.69	0.33	0.91	1.70	0.23	0.00	24.13	66.11	9.76
1275.18	3V	0.57	3.12	3.77	4.35	5.65	6.73	7.31	8.72	5.60	1.80	-0.25	3.58	5.58	1.73	0.01	0.96	1.77	-0.07	0.19	21.20	69.90	8.71
1275.6	9	1.15	5.25	6.86	7.46	8.99	10.94	11.92	13.92	9.35	2.77	-0.49	3.06	9.26	2.58	0.15	1.02	2.53	0.16	0.00	3.32	29.88	66.80
1277.45	9	-1.05	0.86	3.06	4.00	7.13	10.15	11.69	14.82	7.27	3.94	-0.11	2.01	7.29	4.27	0.08	0.93	4.32	0.06	1.56	23.48	32.61	42.35
1279.84	3	2.32	3.56	4.57	5.34	7.02	9.08	9.87	11.59	7.41	2.79	0.43	2.41	7.15	2.54	0.11	0.88	2.65	0.08	0.00	10.45	51.40	38.15

		Percentiles								Moment				Graphic				Inman		Proportions			
		1%	5%	16%	25%	50%	75%	84%	95%	Mean	StDev	Skew	Kurt	Mean	StDev	Skew	Kurt	StDev	Skew	Gravel	Sand	Silt	Clay
1280.2	9	-1.49	0.57	2.50	3.27	6.03	8.77	9.86	12.63	6.20	3.75	0.18	2.22	6.13	3.67	0.07	0.90	3.68	0.04	1.97	32.85	33.62	31.56
1281.6	9	-0.66	1.51	3.44	4.52	7.33	9.54	10.36	12.04	7.26	3.54	-0.09	2.24	7.05	3.33	-0.11	0.86	3.46	-0.12	0.57	20.70	36.84	41.89
1282.04	10	-2.05	-	2.05	2.89	5.34	8.10	9.19	12.51	5.58	3.75	0.22	2.45	5.53	3.73	0.10	1.01	3.57	0.08	3.51	36.91	33.72	25.86
1275.60(d)	9	1.53	4.86	7.21	8.11	9.96	11.80	12.67	14.44	10.04	2.82	-0.93	3.37	9.95	2.82	-0.04	1.06	2.73	-0.01	0.00	3.10	20.73	76.16
133.48(r)	3	2.74	3.50	5.16	5.99	8.08	11.81	13.99	18.41	8.56	3.23	-0.02	1.67	9.07	4.47	0.36	1.05	4.42	0.34	0.00	8.74	40.43	50.83
141.84(r)	6V	3.11	3.50	3.95	4.32	5.39	6.22	6.72	8.20	5.46	1.46	0.76	3.62	5.36	1.40	0.08	1.01	1.39	-0.04	0.00	17.75	76.42	5.82
48.19(r)	9	-0.36	1.91	4.62	5.69	7.13	9.41	10.55	12.87	7.49	3.26	-0.03	2.58	7.43	3.14	0.10	1.21	2.97	0.15	0.30	13.46	48.49	37.75
50.14(r)	10	-1.56	0.29	2.87	4.37	6.17	7.87	9.16	10.14	6.07	3.15	-0.19	3.12	6.07	3.06	-0.12	1.15	3.14	-0.05	2.60	19.70	54.06	23.63
852.19(d)	3	1.12	1.51	1.90	2.11	2.62	3.35	3.98	8.51	3.32	2.34	2.58	9.65	2.83	1.58	0.50	2.32	1.04	0.31	0.00	84.20	9.76	6.04
86.31(r)	3	3.33	4.16	5.56	6.03	7.41	9.61	10.55	12.45	8.05	2.73	0.45	2.14	7.84	2.50	0.24	0.95	2.50	0.26	0.00	4.15	53.84	42.00
90.00(r)	2	0.15	2.83	5.86	6.42	8.08	9.98	10.60	11.86	8.36	3.05	-0.29	2.83	8.18	2.56	-0.05	1.04	2.37	0.06	0.00	7.50	41.53	50.97

Table 13: Grain-size statistics for AND-1B samples. (d) Duplicate sample. (r) Sample reprocessed due to incomplete disaggregation of original sample.

CHAPTER 4

**The Pleistocene glacial history of the
Antarctic Ice Sheet in the Ross Embayment
based on sediment drill core from
beneath the McMurdo Ice Shelf**

Abstract

Past fluctuations of the Antarctic Ice Sheet (AIS) in the Ross Embayment are reconstructed for the Pleistocene by developing a model for the glacimarine depositional sequences documented in detail from the upper 150 m of the AND-1B drill core. This model reveals glacial to interglacial fluctuations of the AIS in the Western Ross Embayment responding at orbital frequencies. Chronology is constrained by an age model based on $^{40}\text{Ar}/^{39}\text{Ar}$ dating of volcanic ashes and magnetostratigraphy. The glacimarine sequences in AND-1B appear to correlate one-to-one with cycles in the benthic $\delta^{18}\text{O}$ record for the past ~ 0.8 Myr (Marine Isotope Stages 20-2). Five sequences between ~ 1.7 and 1.0 Myr can also be matched with specific intervals in the $\delta^{18}\text{O}$ record, and indicate oscillations of the AIS grounding line operating at a 40-kyr frequency. The AND-1B drill core also provides new insight into the response of the AIS in the Ross Embayment across the Mid-Pleistocene Transition. Prior to 1.0 Myr, glacimarine sequences have a 40-kyr duration, whereas subsequently 100-kyr glacimarine cycles can be clearly recognised in the core. During this “100-kyr world”, subglacial (i.e., grounded ice) to grounding-zone sedimentation dominates at the AND-1B site, with only thin intervals of ice-shelf sedimentation during interglacials. An unconformity in AND-1B that spans most (~ 200 kyr) of the Mid-Pleistocene Transition is inferred to represent large scale expansion of AIS in the Ross Embayment at ~ 0.8 Myr. Prior to the Mid-Pleistocene Transition interglacial periods are characterised by open-water conditions with high abundances of volcanoclastic deposits and occasional diatomaceous sediments.

4.1 Introduction

The West Antarctic Ice Sheet (WAIS; Figure 54) is commonly cited as being potentially unstable on account its marine-based nature (Mercer, 1978; Oppenheimer, 1998), yet little is still known about its past dynamics and response, even during Pleistocene warm intervals (Vaughan and Arthern, 2007). The record obtained from AND-1B provides the first opportunity to correlate a record of the marine-based AIS

extent in the Ross Embayment directly with Antarctic ice core records and other proxies of sea level and temperature change from far-field deep-sea and coastal sites.

This Chapter provides insight into the following questions:

- To what extent did the Antarctic Ice Sheet volume vary during past interglacial periods during the Pleistocene?
- What is the response of the AIS in the Ross Embayment to orbital variations; and how did the ice sheets evolve through the onset of the 100-kyr cycles at the Mid-Pleistocene transition?
- What constraints can be placed on AIS contribution to global sea level during the Late Pleistocene “super interglacials” – e.g., Marine Isotope Stages (MIS) 5 and 9, 11?
- What processes were occurring at the grounding line of past ice sheets in the Ross Embayment during glacial retreat?

The marine $\delta^{18}\text{O}$ isotope record provides a proxy for past global ice volume and changes in oceanic temperature (Miller *et al.*, 1987; Shackleton, 2000). However, determining the relative timing and extent of Northern Hemisphere versus Southern Hemisphere ice volume changes during this time, as well as the timing and magnitude of deep-water cooling since the start of the Pliocene (e.g., Miller *et al.*, 2005) makes the $\delta^{18}\text{O}$ isotope record difficult to interpret. This highlights the need for continuous records of past fluctuations in ice sheet extent from around the Antarctic continental margin.

4.2 Proxy records of Pleistocene ice volume and sea level fluctuations

Both the Vostok and EPICA Dome C ice core records show that although each of the past five interglacial periods (since 430,000 yrs BP) have an average periodicity of 100 kyr, each has distinctive climatic characteristics. For example, Marine Isotope Stage 11 is relatively long lasting (~30 kyr) with relatively low CO_2 concentrations of between 266-287 ppm (Petit *et al.*, 1999), while Marine Isotope Stage 5 and 9 are shorter lived (Figure 5), and have significantly higher CO_2 concentrations of between

287 and 300 ppm. Deuterium profiles from the EPICA Dome C record indicate that peak local temperatures during these “super-interglacials” (Marine Isotope Stage 5e, 7, 9 and 11) were between 2 to 4.5°C higher than present-day interglacial values (Jouzel *et al.*, 2007). Kawamura *et al.* (2007) uses O₂/N₂ ratios (a proxy for local summer insolation) to orbitally tune the chronology for the Dome Fuji (Antarctica) ice core record. This improved chronology provides evidence that the timing of temperature and $\delta^{18}\text{O}$ changes in the Dome Fuji record lags Northern Hemisphere insolation by only 1-4 kyr, while they are completely out of phase with Southern Hemisphere insolation. Kawamura *et al.* (2007) interpreted this to imply that the last four glacial terminations were driven by changes in Northern Hemisphere insolation.

Interglacials between 800,000 and 430,000 years ago also have an average periodicity of 100 kyr. However, they are characterised by being significantly cooler and longer duration than the Late Pleistocene “super-interglacial” periods. Peak temperatures at Dome C during earlier interglacial periods (Marine Isotope Stages 13, 15 and 17) are between 1-1.5°C cooler than the present-day interglacial period (Jouzel *et al.*, 2007). As yet, the mechanism for this change in amplitude has not been determined. Changes in the amplitude of obliquity cycles are cited as a possible cause, as are changes in ocean circulation, albedo, carbon dioxide or glacio-eustasy (EPICA Community Members, 2004).

The Antarctic ice core record currently extends back only to 0.8 Myr and correlates well with stacked $\delta^{18}\text{O}$ benthic records from the deep sea (Figure 4). Recently, Lisiecki and Raymo (2005) compiled a record of benthic $\delta^{18}\text{O}$ from 57 globally-distributed deep-sea drilling sites, which extends the high resolution record of glacial cycles back to the start of the Pliocene (5.3 Myr). The benthic $\delta^{18}\text{O}$ record indicates that prior to 0.9 Myr, glacial/interglacial cycles had a period of ~41 kyr, and are of lower amplitude than the Late Pleistocene 100-kyr glacial cycles. While the pattern of cyclicity is well-described, the mechanisms that drove this period of change through the Mid-Pleistocene Transition are not well understood (see Chapter 1).

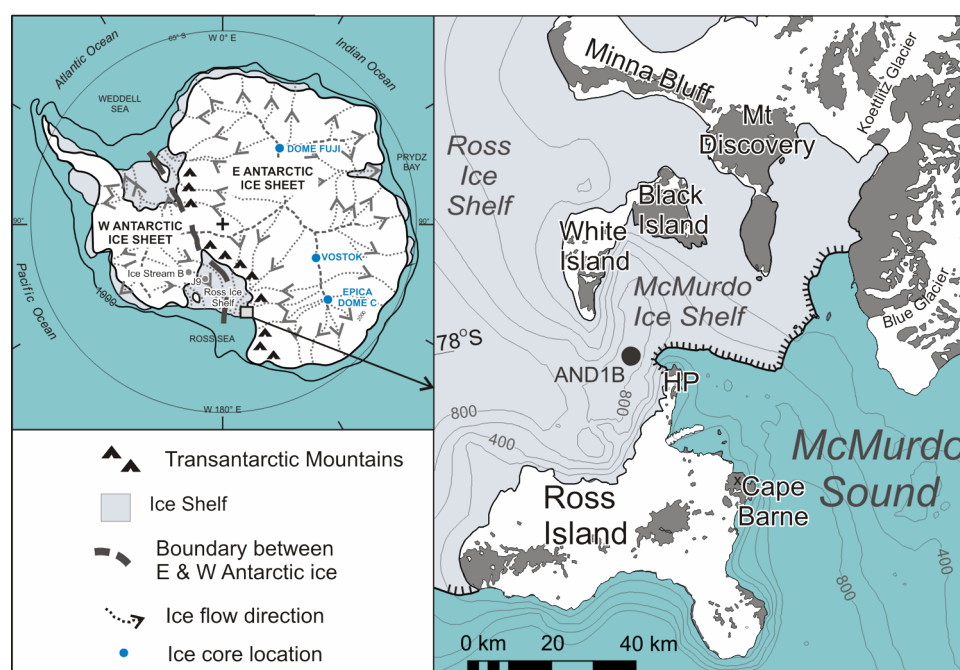


Figure 54: Map of Antarctica and Ross Island (RI) region showing the AND-1B drill core site, and locations mentioned in this chapter.

4.3 Evidence for WAIS “collapse” during the Pleistocene?

Scherer *et al.* (1998) provided diatom and ^{10}Be evidence that parts of the WAIS now grounded were exposed to open marine conditions at least once during the past 0.75 Myr. They constrained the timing of this WAIS “collapse” from the occurrence of *Thalassiosira antarctica* in tills beneath Ice Stream B (Figure 54). However, some argue that the diatom assemblage can not constrain the timing of widespread WAIS retreat more accurately than to the past 1.3 Myr (Kerr, 1998). Despite lacking a high resolution chronology, two intervals in particular (Marine Isotope Stages 5 and 11) were cited by Scherer *et al.* (1998) as most probable candidates for widespread retreat of the WAIS.

Evidence of open marine conditions/extensive ice shelf conditions in McMurdo Sound during Stage 5e is provided by reworked, ice-cored marine sediments at Cape Barne (Figure 54) on Ross Island (Stuiver *et al.*, 1981). This deposit is composed of 20% biogenic material (including sponge spicules, fragmentary carbonate shells, diatoms and foraminifera) and has been $^{230}\text{Th}/^{234}\text{U}$ dated at $120,000 \pm 6,000$ yrs

(Ward and Webb, 1986). Stuiver *et al.* (1981) interpreted this marine deposit as a glacial erratic that was incorporated in the base of an ice shelf (as is happening for the present-day McMurdo Ice Shelf), and transported to Cape Barnes as the ice shelf grounded during the last glacial advance. These marine deposits were therefore seen as providing an age for the last period of extensive ice shelf conditions in McMurdo Sound prior to the Last Glacial Maximum (Stuiver *et al.*, 1981). Coral reef studies in the Bahamas indicate sea levels were ~2 m higher than present day for most of Marine Isotope Stage 5e, although a brief and rapid rise of between 6 to 9 m higher than present is recorded just before the end of Marine Isotope Stage 5e (Neumann and Hearty, 1996; Hearty, *et al.*, 2007). However, there is uncertainty regarding the extent of the Greenland Ice Sheet reductions at this time (North Greenland Ice Core Project members, 2004), and estimates of its contribution to the Stage 5e sea-level highstand are as high as ~4 to 5.5 m (Cuffey and Marshall, 2000).

Scherer *et al.* (1998) cited Marine Isotope Stage 11 as the most probable candidate for “collapse” of the grounded portion of the WAIS. Marine deposits preserved at 20 ± 3 m above sea level on the tectonically stable coastlines of Barbados and Bermuda have been dated at between 390 and 550 kyr (Hearty *et al.*, 1999). Sea levels of 20-m higher-than-present during Marine Isotope Stage 11 would require complete removal of the Greenland and West Antarctic Ice Sheets (~12 m of sea level equivalent), as well as a reduction in volume around the margin of the East Antarctic Ice Sheet. However, accurately determining past sea level highstands from reef and elevated beaches are complicated by uncertainties associated with tectonics, isostatic adjustment following redistribution of water from ice sheets to oceanic basins (Howard, 1997; Chappell, 1998), and somewhat ambiguous chronologies.

Marine Isotope Stage 31 (1.07 Myr) is another potential period for Scherer *et al.*'s (1998) WAIS retreat. Perhaps the assessment of <0.75 Myr for *Thalassiosira antarctica* is indeed too young, as its first stratigraphic occurrence is not yet well defined, and is potentially as old as 1.3 Myr (Barron, 1996; Scherer *et al.*, 1998; Kerr, 1998). Furthermore, Marine Isotope Stage 31 stands out as significantly warmer than the other low-amplitude 41-kyr glacial cycles of the early-Pleistocene (Lisiecki and

Raymo, 2005). In addition, Scherer *et al.* (2008) reported on a warm-water marine carbonate unit deposited during Marine Isotope Stage 31 recovered by the Cape Roberts Project (77°S). The age of this unit is well-constrained by $^{87}\text{Sr}/^{86}\text{Sr}$ dating of carbonate shells, $^{40}\text{Ar}/^{39}\text{Ar}$ dating of volcanic ashes, biostratigraphy, as well as coinciding with a paleomagnetic reversal assigned to the base of the Jaramillo subchron (1.07 Myr). The authors demonstrated from stable isotope measurements, calcareous nannofossils and diatom data that the peak warmth for this deposit, and for ODP site 1094 in the Southern Ocean, occurred during a phase of peak Southern Hemisphere insolation, prior to deglaciation in the Northern Hemisphere. This lends support to the hypothesis of Raymo *et al.* (2006) that local insolation (driven largely by precession) was a key control for determining ice volume in each hemisphere – at least during the periods of extremely high intensity Southern Hemisphere insolation.

MacAyeal's (1992) numerical model of the WAIS indicated the potential for “collapses” of the ice sheet that may be irregularly timed with respect to orbital forcing parameters. He suggested that the distribution of soft, deformable till underlying the WAIS may be critical in determining its likelihood of collapse. Because of isolation from the atmosphere, it takes several thousands of years for climatic changes at the ice sheet surface to reach the ice sheet base, and the presence or absence of till is critical in determining the response of the ice sheet. Therefore extremely warm (but shorter) periods may not necessarily result in WAIS collapse. An example of this potential non-linear behaviour was presented in a numerical ice sheet simulation (forced by a simplified saw-toothed 100-kyr pattern of sea level and air temperature change running over the past 1 Myr) that resulted in only three, irregularly timed collapses. However, MacAyeal was careful to state this sporadic pattern of collapse as a qualitative result, which needed to be tested by the direct geological record.

The glacial-marine record contained in the AND-1B drill core provides the first opportunity to obtain a direct record of AIS variability in the Ross Embayment for the Pleistocene, and thus to test the sensitivity of this integrated EAIS/WAIS system (see Chapter 1) to orbital scale climate forcing. This chapter develops a high-resolution

sequence stratigraphic model for the AND-1B drill core, with a chronology constrained by $^{40}\text{Ar}/^{39}\text{Ar}$ and magnetostratigraphy. It aims to identify the response of past ice sheets that occupied the Ross Embayment in the Pleistocene to past warm periods, especially the “super-interglacials” of the past ~0.4 Myr and Marine Isotope Stage 31. To achieve this, a detailed description of each sequence is provided. This is done in order to identify any potential zones of significant erosion within these sequences. Paleoenvironmental interpretations are also given, and are based on observations and interpretations made in Chapters 2 and 3, as well as the published literature.

4.4 Methods

The methods used in this chapter apply facies analysis techniques involving grain-size, IRD, diatom abundances, etc, as in Chapters 2 and 3, to the upper 150 m of the AND-1B drill core. AND-1B was initially described at the Crary Science and Engineering Centre, in McMurdo Station, Antarctica, using standard sedimentological techniques to produce detailed stratigraphic logs (Krissek *et al.*, 2007), and eleven lithofacies were defined in the core (Chapter 3). T. Naish, R. Powell and I re-examined the upper 150 m of the core at the Antarctic Research Facility during June 2007. This was done to cross-check the initial description, and to confirm correct interpretation of the glacial/interglacial sequences. Several potential volcanic ash horizons suitable for $^{40}\text{Ar}/^{39}\text{Ar}$ dating were also identified (by P. Kyle and J. Ross) during this second phase of description.

The grain-size processing techniques are detailed in Chapter 3 (page 154). Diatom abundances are based on my visual estimates as determined from smear slides, and are presented as log-scale histograms in Figure 55, Figure 58 and Figure 60. Clast frequency data were provided by F. Talarico (University of Sienna) and represent the numbers grains exceeding 2 mm that were exposed at the cut core face, while density data were taken from Niessen *et al.* (2007).

4.5 Pleistocene glacial/interglacial sequence stratigraphy of the AND-1B drill core

The Pleistocene record in AND-1B is represented in the upper 146.79 mbsf (Wilson *et al.*, 2007). Above 82.74 m, the AND-1B drill core can be generalised as “muddy diamictite with thin intervals mudstone and sandstone”. Between 146.79 and 82.74 mbsf, AND-1B contains only 23% diamictite. These diamictites are interbedded with ~10 to 20-m thick successions of volcanic sands, muds, and in two sequences, diatomite.

Nine unconformity-bound glacimarine sequences are defined in the upper 82.74 m of AND-1B, and five are defined between 146.79 and 82.74 mbsf. Each sequence contains a basal *glacial surface of erosion* (GSE) that marks the passage of grounded ice across the site during glacial advance. A GSE is identified by diamictite (most commonly massive) with a sharp basal contact that usually overlies sheared or physically intermixed facies of the underlying sequence. Not all sequences boundaries (GSEs) are erosional, as some glacial readvance/grounding line facies successions are preserved. In this case, the sequence boundary may occur over a zone (generally <1 m) where stratified diamictite passes into massive diamictite with strong horizontal alignment of clast long axes. Recovery was poor for the upper 24.17 m of the drill core, but stratigraphic integrity below 24.17 mbsf is excellent (98% core recovery) and drilling disturbance was rare.

4.5.1 Sequence 1: Diamictite with interbedded sands and muds (10.08 to 0 mbsf)

Description: Although core recovery was limited, the base of Sequence 1 is defined by a stiff diamictite at 10.08 to 9.69 mbsf, and considered to be over-compacted. There was no recovery above this interval in AND-1B, but seven short (gravity and push) sediment cores were collected at the drillsite prior to the drilling of AND-1B. Sections of mud with dispersed clasts were recovered at 2.16 to 1.335 mbsf from a push core (AND-1A), while the other six cores recovered the uppermost 0.5 mbsf of the seafloor sediments (Dunbar *et al.*, 2007). The cores from the 0.5-0 mbsf interval consist of a variety of interbedded sequences of sand and mud, including a <0.35-m

thick basal bed of mud with dispersed clasts of Transantarctic Mountain and McMurdo Volcanic Group lithologies. The sandstone and mudstones are overlain by a thin (<0.07 m) bed of graded very fine volcanic sand with a sharp, erosional base and well-rounded lithics and glassy fragments of mainly volcanic origin. The top of the cores usually consist of a thin (<0.3 m) mudstone commonly with sand and clasts of Transantarctic Mountain and McMurdo Volcanic Group lithologies, and abundant biosiliceous material.

Paleoenvironmental interpretation: The GSE at base of this sequence was not recovered and is inferred somewhere between 17.16 and 10.08 mbsf. The diamictite (10.08 to 9.69 mbsf) and mudstone with dispersed clasts (2.16 to 1.335 mbsf) appear overcompacted relative to overlying sediments, indicating deposition beneath a grounded ice sheet, and possibly at the Last Glacial Maximum. The surface sediments from the gravity and push cores are similar to the HWD cores collected from beneath the McMurdo Ice Shelf (Chapter 2; McKay *et al.*, 2008). This, combined with the lack of diatomaceous-rich muds or oozes, indicates a lack of open marine conditions at the drill site, and that McMurdo Ice Shelf has persisted at the drillsite since the ice sheet grounding line retreated from the region $\sim 10^4$ C kyr BP (McKay *et al.*, 2008).

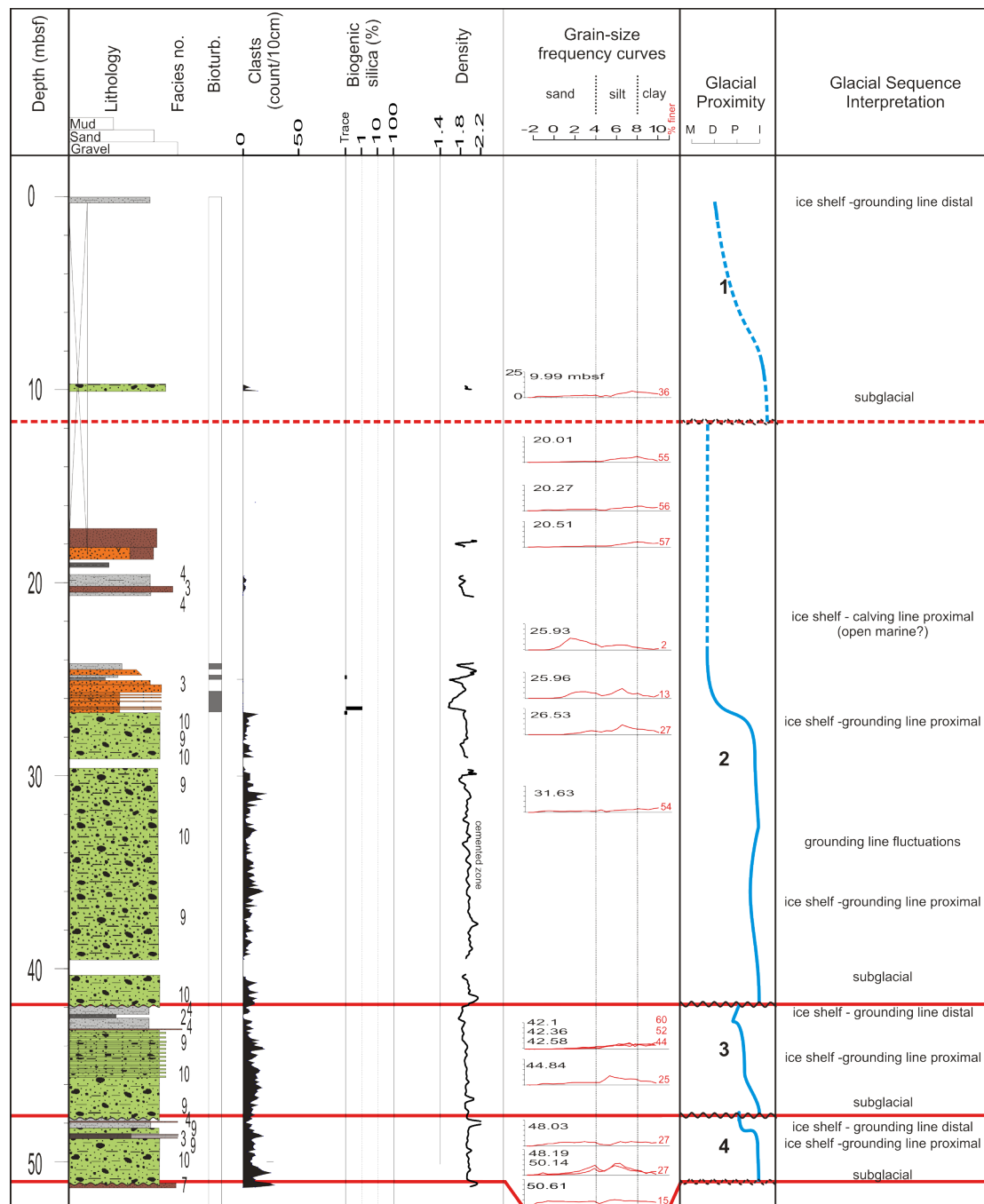


Figure 55: Stratigraphic log (0-52 mbsf), with data plotted showing facies distribution, bioturbation index, clast abundance (Krissek *et al.*, 2007), % biogenic silica, density (Niessen *et al.*, 2007) and grain-size frequency (sample depth(s) shown with each analysis). Glacial proximity curve and sequence interpretation is developed from facies analysis, and shows Sequences 2-4. The glacial proximity curve shows the transition from marine(m) to ice distal (d), ice proximal (p) and ice contact/subglacial (i) deposition. Legend for lithological units is provided in Figure 37.

4.5.2 Sequence 2: Interbedded sandstone and mudstone overlying interbedded stratified and massive diamictite (41.1 to 26.68 mbsf)

Description: The GSE at the base of this sequence (41.90 mbsf) is defined by a sharp contact that overlies a zone of deformed mudstone with clasts in the underlying sequence (Figure 56D). The diamictite (41.90 to 41.10 mbsf) overlying the GSE is massive, and passes upward into a stratified diamictite that contains cm-scale medium to coarse sandy beds. A “pebble nest” from 35.92 to 35.87 mbsf (Figure 56C) passes up into a massive diamictite (35.87 to 31.21 mbsf) that lacks a defined clast orientation and has a high degree of cementation. The diamictite interval has highly variable clast abundance, and alternates between sandy or muddy diamictite.

The diamictite beds are overlain by an interval of cm-scale interbedded volcanic sandstone and mudstone (26.68 to 25.03 mbsf). The basal contact of this interval is a very sharp, planar surface (Figure 56B). The volcanic mudstones are slightly to moderately bioturbated and are interbedded with 0.2- to 0.5-m thick beds of fine to medium-grained graded volcanic sandstone with gradational upper and lower contacts (Figure 56A). Smear slides indicate abundant angular volcanic glass and trace values of diatoms and sponge spicule remains. The volcanic muds are overlain by clayey siltstone/silty claystones (25.03 to 24.17 mbsf) that lack biogenic silica, but have diffuse mm- to cm-scale burrows. This is overlain by a mudstone with dispersed clasts (20.65 to 19.55 mbsf) that lacks bioturbation but contains mm-thick laminae of fine to very fine volcanic sand, and a 29-cm thick bed of interbedded coarse silt/fine sand composed of quartz, feldspar and heavy minerals (see Chapter 5). The top of this sequence was not recovered, due to the unconsolidated nature of volcanic sediments. No core was recovered between 24.17 and 20.65 mbsf and, although unlikely, the possibility of a sequence boundary within this interval cannot be ruled out.

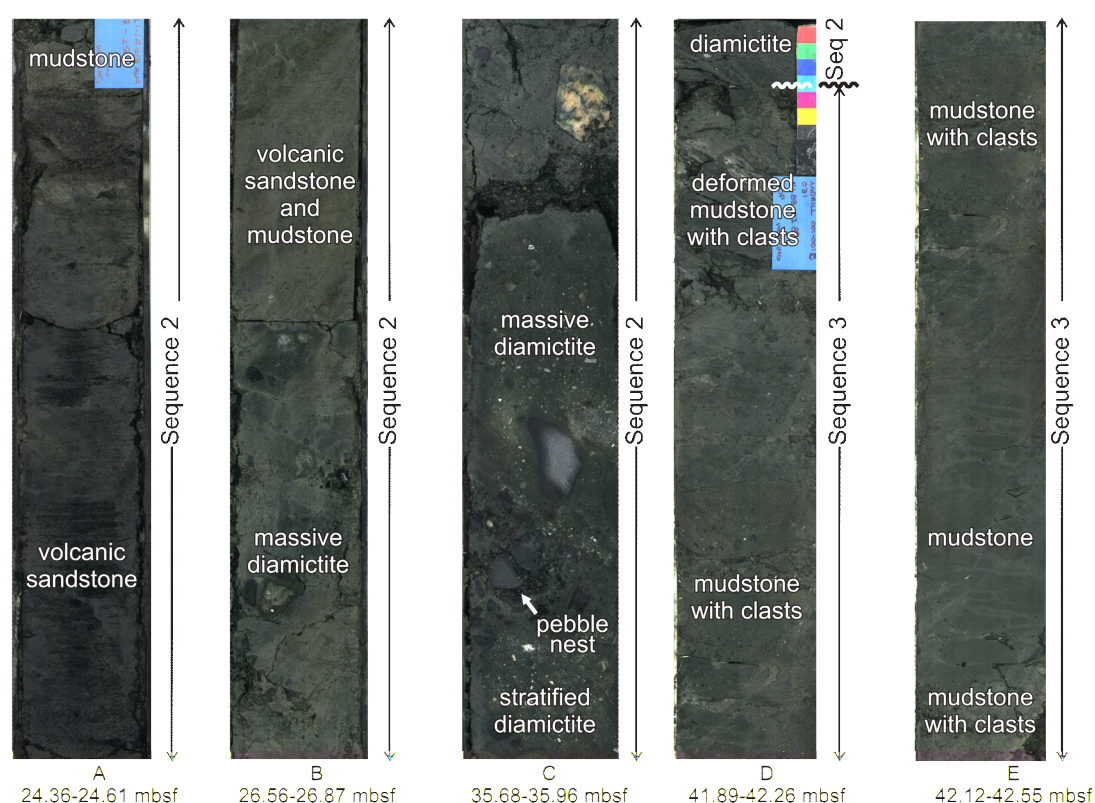


Figure 56: Representative photos of facies and GSEs from Sequences 2 to 3 AND-1B.

Paleoenvironmental interpretation: The massive diamictite overlying the GSE at the base of the sequence is interpreted as subglacial till, due to deformation in the mudstone with dispersed clasts at the top of the underlying sequence (Figure 56D). The intervals lacking clast orientation may represent either subglacial till or grounding zone deposits. Although there is a general lack of confirmed modern examples of grounding zone deposits to support this interpretation, Anderson (1999) noted that grounding zone deposits are expected to have random clast orientation. The presence of the pebble nest (Figure 56C) associates sections of this deposit with periods of floating ice (Powell and Cooper, 2002) and suggests the entire diamictite interval (41.90 to 26.68 mbsf) represents a period of grounding line oscillations as subglacial environments alternated with proximal glacimarine environments. The bioturbated mudstone and volcanic sandstone beds above the diamictite interval indicate a period when grounded ice lifted off the sea floor at the drill site. The moderately bioturbated mudstones/sandstones lack biogenic silica and oversized clasts (i.e., iceberg rafted debris), suggesting deposition beneath a floating ice shelf lacking a basal debris layer, and are consistent with the sub-ice shelf facies inferred in

Chapter 2. The volcanic sand intervals are likely to be reworked, as the sharp planar surface (Figure 56B) separating the volcanic mudstone and sandstone from diamictite and is indicative of an erosive surface, suggesting deposition by a debris flow. This interpretation allows for deposition of the volcanic sandstone and mudstone units beneath a floating ice shelf. The debris flows may be related to submarine volcanism, or slope instability following grounding line retreat. However, an open-marine environment is also a possibility. The mudstones with Transantarctic Mountain clasts at the top of the sequence probably represent readvance of the grounding line, with deposition by grounding-line-related debris flows or ice-proximal basal-debris meltout.

4.5.3 Sequence 3: Diamictite overlain by conglomerate, mud with dispersed clasts and silty claystone (47.70 to 41.90 mbsf)

Description: The GSE at base of this sequence is defined by a sharp surface beneath a 90 cm-thick zone of very weakly-stratified diamictite (defined by mm-scale texture changes) that overlies strongly stratified diamictite in the underlying sequence (Figure 57B). The weakly-stratified diamictite grades into massive diamictite (46.80 to 44.40 mbsf) with a strong fabric defined by horizontal alignment of clast long axes. This is overlain by another stratified diamictite (44.40 to 43.09 mbsf) before passing into a 5.8-cm thick “conglomerate” bed with abundant granule-sized mudstone intraclasts and a sharp irregular lower contact (Figure 57A). The “conglomerate” is overlain by a 51 cm-thick mudstone with dispersed, rounded mudstone intraclasts, and a 19 cm-thick very dark greenish-grey silty-claystone that lacks clasts and has no evidence of bioturbation (Figure 56E). The top of this sequence consists of another mudstone with dispersed mudstone intraclasts (4.3 cm thick). This entire interval is lacking biogenic silica and significant bioturbation.

Paleoenvironmental interpretation: The strong horizontal alignment of clast long axes in the massive diamictite near the base of this sequence, and the presence of deformed sediments immediately beneath the GSE is indicative of deposition beneath grounded ice (i.e., subglacial till). The stratified diamictite above (weakly stratified) and below

(strongly stratified) the GSE suggest the grounding line advance phase of the underlying sequence was preserved, and therefore minimal erosion is inferred. The mudstone with dispersed intraclasts overlying the stratified diamictite (and conglomerate bed) at ~43.03 mbsf shows similarities to the “granulated” facies defined by Domack *et al.* (1999). This granulated zone indicates probable deposition during melt-out from the basal debris zone and is therefore associated with the lift-off of grounded ice, before passing into the silty claystone lacking clasts that was likely deposited beneath a floating ice shelf free of basal debris (c.f. Chapter 2). The lack of any bioturbation and biogenic silica, indicates that the ice-shelf calving line lay seaward of the drillsite before a return to grounding-line proximal glacial marine sediment resumed, as inferred by the mudstone with dispersed clasts at the top of the sequence.

4.5.4 Sequence 4: Diamictite overlain by conglomerate and mudstone with dispersed clasts (51.10 to 47.86 mbsf)

Description: The GSE at the base of this sequence is gradational and inferred on the basis of calcite-cemented massive diamictite with horizontally aligned clasts (51.10 to 48.91 mbsf) overlying a zone of muddy sandy conglomerate (52.96 to 51.10 mbsf) (Figure 57D). At 48.91 mbsf, the massive diamictite grades into a well-stratified diamictite, with abundant mudstone intraclasts and inclined, continuous, planar laminae of mudstone and sandstone (Figure 57C). The upper part of this sequence (48.28 to 47.70 mbsf) consists of mudstone with dispersed clasts (with thin sandstone laminae ~1 grain thick), before passing into a clast-rich diamictite in the upper 0.18 m (Figure 57B).

Paleoenvironmental interpretation: Due to gradational nature of the GSE at the base of this sequence and diagenetic overprint (i.e., mottled texture) in the overlying diamictite, erosion by glacial overriding is difficult to identify. However, it is apparent that a subglacial environment existed at the drillsite. The stratified diamictite with abundant mudstone clasts is indicative of the “granulated facies” of Domack *et al.* (1999) that is associated with sedimentation in the immediate vicinity of the

grounding zone, following “lift-off” of grounding line. Clast-rich zones of stratified diamictite that include mudstone and sandstone laminae (ranging from horizontal to sub-horizontal) are also indicative of this granulated facies. Facies preserved in this sequence are consistent with a proximal grounding-line throughout its deposition.

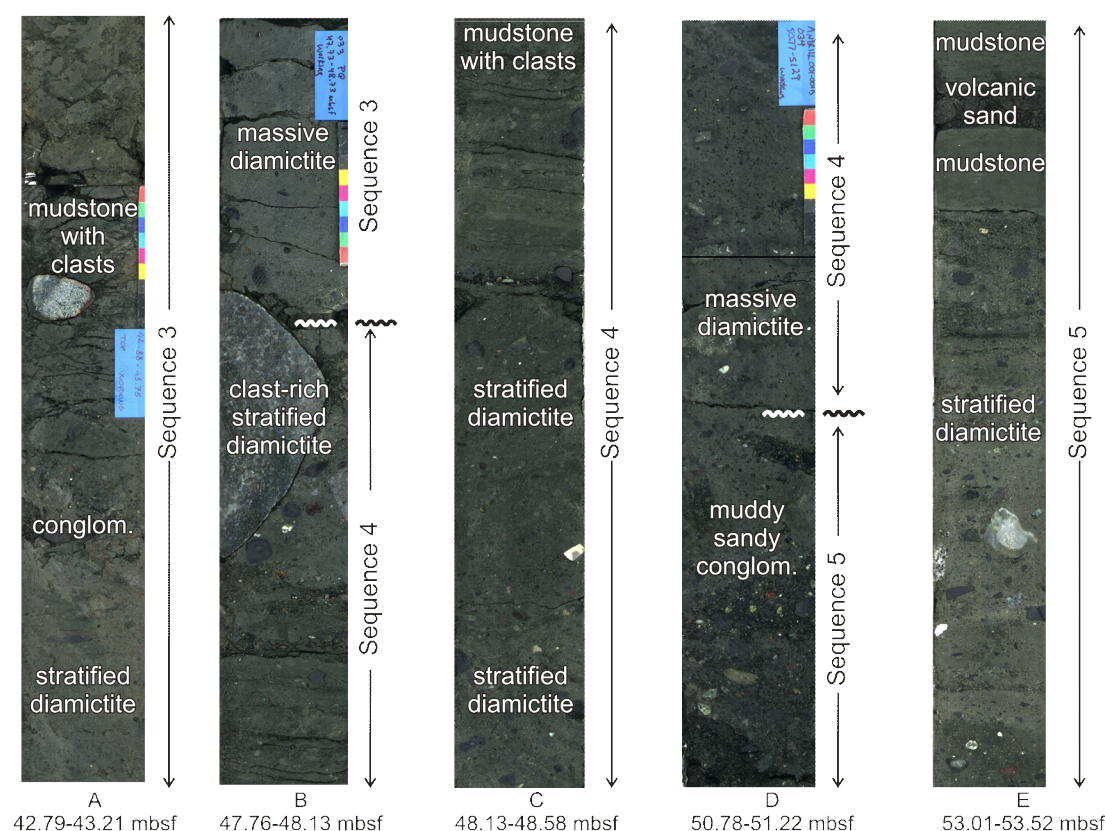


Figure 57: Representative photos of facies and GSEs from Sequences 3 to 5 AND-1B.

4.5.5 Sequence 5: Diamictite overlain by thin interbedded sandstone and mudstone (56.49 to 51.10 mbsf)

Description: The base of this sequence is defined by a GSE with a sharp base (Figure 59A) overlain by a massive diamictite (56.49 to 54.40 mbsf) with clasts horizontally aligned along long axes. This is in turn overlain by a weakly-stratified diamictite (54.40 to 53.47 mbsf), displaying mm-scale clay “stringers” (possible drilling disturbance), before passing into a diamictite with well-defined horizontal stratification characterised by stratigraphic alternations in texture and clast beds (Figure 57E). This facies then passes sharply into a laminated clayey siltstone (53.13

to 52.96 mbsf) with slight to moderate bioturbation and fragments of diatom remains (~1% of matrix; Figure 58). The clayey siltstone is interbedded by a single bed of black volcanic sand before passing back into diamictite. The top of the sequence consists of drilling-disturbed diamictite (e.g. "fall-back debris" of unconsolidated diamictite/conglomerate), and an undisturbed muddy sandy conglomerate in the uppermost 0.22 m of the sequence (Figure 57D).

Paleoenvironmental interpretation: The interpretation for this sequence is similar to Sequence 3, with a strong-clast fabric of the massive diamictite at the base of this sequence suggesting deposition beneath grounded ice, before passing into grounding-zone "lift-off" and then into "debris-free" sub-ice shelf facies. Of note in this interval are the highly-fragment diatom remains, consistent with the sub-ice shelf mud facies documented in Chapter 2. The diatom remains are interpreted as being advected to the drillsite by oceanic circulation beneath an ice shelf free of basal debris during the glacial minima.

4.5.6 Sequence 6: Diamictite overlain by thin interbedded sandstone and mudstone (67.10 to 56.49 mbsf)

Description: The GSE at the base of this sequence directly overlies weakly-stratified diamictite with inclined laminations of concentrated clasts (white arrow in Figure 59C). The diamictite (67.10 to 60.62 mbsf) at the base of this sequence is mostly massive, with random clast orientations, but has intervals of well-defined horizontal alignment of clasts on long axes. The massive diamictite is overlain by a weakly-stratified diamictite (60.60 to 56.90 mbsf), defined by mm- to cm-scale inclined laminations of silty claystone, some containing siliceous microfossils. Mudstone intraclasts are also common within intervals of the stratified diamictite. However, sections of this stratified diamictite are also massive (e.g., 58.15 to 57.45 mbsf). The top of the sequence consists of a slightly bioturbated, laminated clayey siltstone (53.13 to 52.96 mbsf; Figure 59B), that is interbedded by thin (< 0.06 m) sandstone beds, including a volcanic sandstone at 56.50 mbsf (Figure 59A). Diatom remains are relatively common (smear slide estimates between 1-10%; Figure 58) in both the

clayey siltstone (Facies 2) and stratified diamictite (Facies 9) between 58 and 53 msbf. This interval is classified as Diatom Unit 1 by Scherer *et al.* (2007), and consists of Pleistocene, Pliocene and Miocene diatoms. These include the extant species of *Actinocyclus actinochilus* (3.02 Myr to present) and *Thalassiosira antarctica* (~1.1 Myr to present), and the extinct taxa of *Thalassiosira elliptipora* (1.08 to 0.73 Myr) and *Rouxia leventerae* (2.08 to 0.14 Myr). However, the presence of anomalously old (e.g., *Actinocyclus actinochilus*) or long ranging taxa (e.g., *Paralia sulcata*, and *Stephanopyxis*) are characteristic of post-LGM Ross Sea glacimarine sediments that have been reworked, and there are only limited occurrences of *Fragilariopsis* spp, which currently dominate the Ross Sea. (Scherer *et al.*, 2007).

Paleoenvironmental interpretation: The diamictite units within the basal section of this sequence are considerably thicker than most of the overlying sequences, showing in some places evidence of grounded ice (horizontal alignment of clast long axes), and in others grounding-line proximal glacimarine deposition (random clast orientations and laminations). Sequence 6 draws some parallels with Sequence 2, and may represent a prolonged period of grounding zone fluctuations at the drill site during ice volume maxima. The glacial minimum in this sequence is represented by a facies that is consistent with a floating ice shelf (mudstone with sandstone laminae) free of basal debris (i.e., lacking of dropstones), and contains a diatom assemblage characteristic of sediment recycled by subglacial and glacimarine processes (c.f. Sjunneskog and Scherer, 2005), similar to that documented in the Holocene cores reported in Chapter 2 of this thesis.

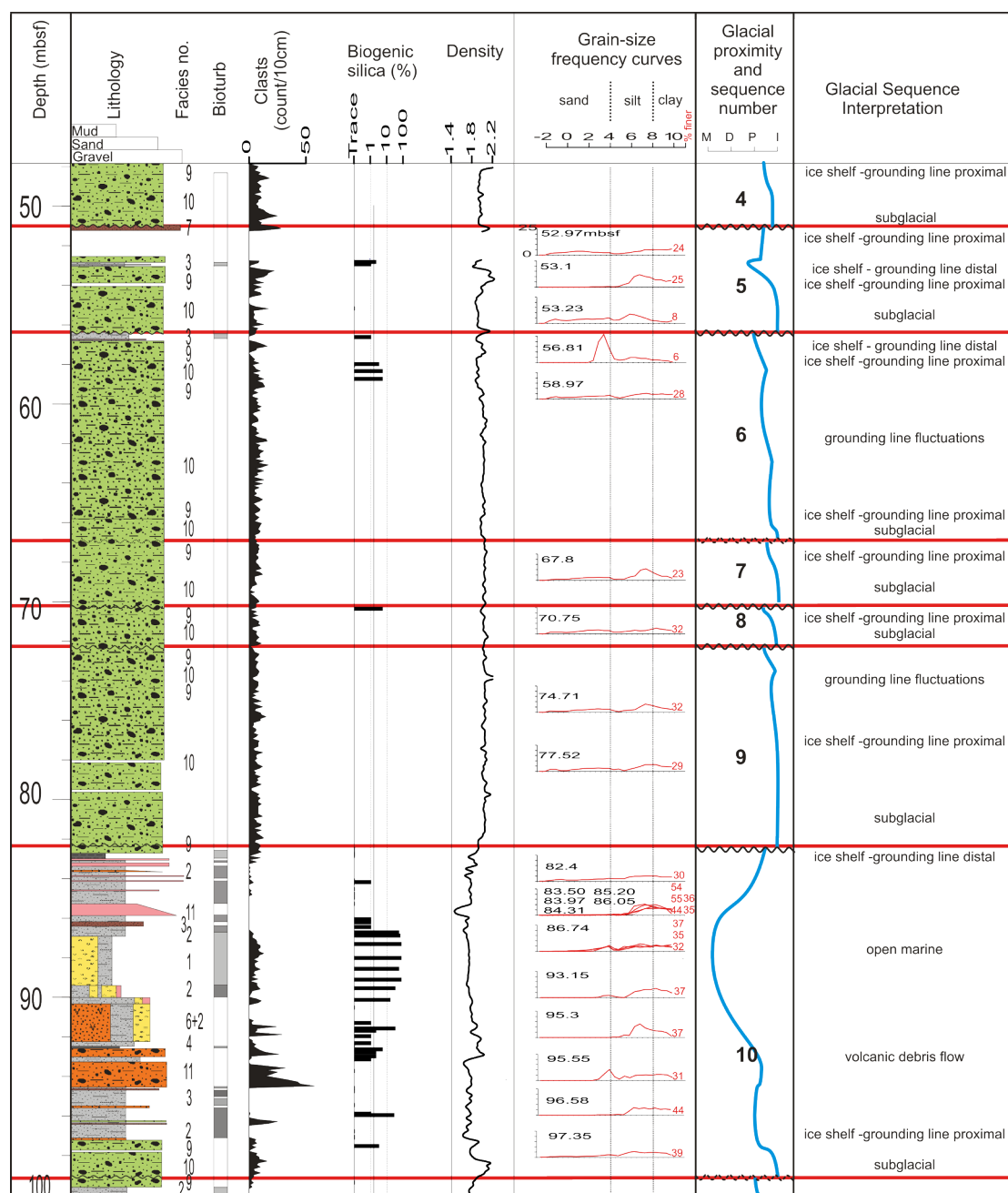


Figure 58: Stratigraphic log (48-100 mbsf), with data plotted showing facies distribution, bioturbation index, clast abundance (Krissek *et al.*, 2007), % biogenic silica, density (Niessen *et al.*, 2007) and grain-size frequency (sample depth(s) shown with each analysis). Glacial proximity curve and sequence interpretation is developed from facies analysis, and shows Sequences 4-10. The glacial proximity curve shows the transition from marine(m) to ice distal (d), ice proximal (p) and ice contact/subglacial (i) deposition. Legend for lithological units is provided in Figure 37.

4.5.7 Sequences 7-9: Interbedded diamictites (82.60 to 67.10 mbsf)

Description: These three sequences consist solely of a series of interbedded massive and stratified diamictites, underlain by GSEs at 82.60, 72.48 and 70.37 mbsf. The basal GSE of Sequence 9 is well defined by a sharp contact, and extensive deformation of the facies at the top of the underlying sequence. The GSE at the base of Sequence 8 (72.48 mbsf) is subtle contact that consists of massive diamictite overlying inclined, weakly-stratified diamictite. The stratified diamictite intervals are between 0.58 and 0.18 m thick, and are characterised by mm-scale laminae with high clast concentrations and horizontal alignment of long-axes. A series of claystone laminae that appear to be highly sheared occur at the top of Sequence 8 (Figure 59D). A smear slide from one of these claystone “stringers” from at 70.49 mbsf contains ~5% fragmented diatoms.

Paleoenvironmental interpretation: These sequences represent fluctuations between a subglacial and ice-proximal glacimarine depositional environment. The contact between Sequences 7 and 8 appears to be erosive due to the sheared claystone laminae with diatom fragments at the top of Sequence 8. These laminae suggest that claving-line deposits at the top of Sequence 8 were subsequently eroded by the glacial advance represented by the base of Sequence 7. The claystone laminae (with 3-5% diatom remains; Figure 59D) also indicate reworking and erosion of sub-ice shelf mudstones during the same glacial advance. While it is possible that open marine sediments were also deposited and eroded, no diatomite or diatom-rich mudstone laminae were found in the diamictite, and it is concluded there were in fact no open marine conditions during the deposition of this sequence, or any of the younger ones.

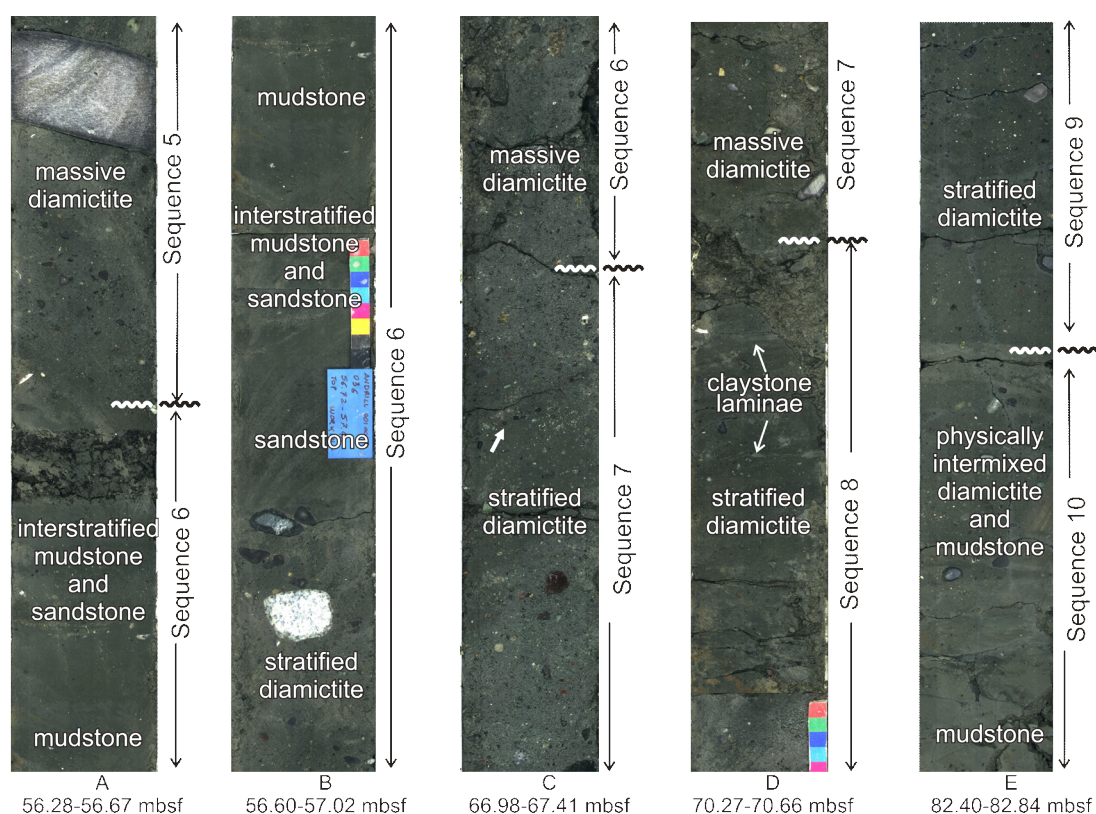


Figure 59: Representative photos of facies and GSEs from Sequences 5 to 10 in AND-1B.

4.5.8 Sequence 10: Interbedded diamictites overlain by mudstone (interbedded with volcanogenic facies), diatomite, and mudstones with lapilli tuff and volcanic ash beds. (99.25 to 82.60 mbsf)

Description: The GSE at the base of this sequence is represented by a transitional zone (rather than an erosional surface) from silty claystone into stratified diamictite (Sequence 11) and then into a massive diamictite (Sequence 10) with horizontally-aligned clasts at 99.25 mbsf (Figure 61C). This passes into a stratified diamictite (98.38 to 97.08 mbsf) with a sharp upper contact overlying silty claystone (97.08 to 94.52 mbsf) that is moderately to highly bioturbated, and has rare thin sandstone interbeds (Figure 61B). The interval between 94.52 and 90.31 mbsf is characterised by clast-rich volcanic diamictites, bioturbated clayey siltstones, and a 2-m-thick interval of physically intermixed clayey volcanic sand (containing calcareous shell debris), diatom rich silty claystone, and silty claystone/clayey siltstone. This passes into a diatom-bearing mudstone with common clasts (90.31 to 90.00 mbsf) of mostly volcanic lithologies, grading upwards into diatom-rich silty claystone with moderate

bioturbation (90.00 to 89.39 mbsf). Then follows a silty-claystone-rich diatomite with dispersed clasts (89.39 and 86.92 mbsf; diatoms constitute up to 70% of the matrix) that passes up into a diatom-rich mudstone. This is overlain by a bioturbated mudstone (86.63 to 82.74) interbedded with laminated sandstone (but lacking clasts), and several volcanic ash and tuff beds ($^{40}\text{Ar}/^{39}\text{Ar}$ dated at 1.014 ± 0.04 Myr; Wilson *et al.*, 2007). This mudstone contains only trace values of very poorly preserved diatom remains. The contact between the mudstone and the underlying diatom-rich mudstone is sharp, inclined and irregular (Figure 61A). The upper portion of this mudstone is highly deformed and physically intermixed with lapilli tuff units. This intermixed zone immediately underlies the GSE in the overlying sequence.

Paleoenvironmental interpretation: The massive diamictite at the base of the sequence is interpreted as subglacial till or grounding-line proximal deposition during the glacial maxima. This passes upward into facies consistent with deposition beneath an ice shelf lacking basal debris (i.e., glacimarine but distal from the grounding line). Though these sediments lack clasts they contain sandstone laminae that probably represent distal sediment gravity flows. The sequence is interrupted between 94.52 and 90.31 mbsf, by a series of debris flows (volcanic diamictites with interbedded sandstones and mudstones) most likely associated with nearby volcanic activity. More than one debris flow is inferred on the basis that the volcanic diamictites and sandstones are interbedded with thin (<0.2 m) intervals of bioturbated silty claystone deposited in a low energy environment. A period of biogenic deposition, with a decreasing contribution from hemipelagic suspension settling followed the deposition of the volcanic debris flows, and is associated with a glacial minimum. Ice-rafted debris was constant throughout the deposition of the silty-claystone-rich diatomite, but is absent in the overlying mudstone (Figure 58). The contact between the mudstone and the underlying diatomite at 86.63 mbsf is sharp and irregular, indicating that it is zone of erosion. After deposition of the mudstone, an advancing grounding line resulted in the deposition of silty claystone with sandstone laminae. The presence of only traces of poorly-preserved diatoms and the lack of clasts also suggest an ice shelf covered the site at this time. However, the presence of several well-preserved volcanic ash and lapilli tuff deposits are difficult to explain if a debris-free ice shelf

was present over the drillsite, and the interval is thicker (~4 m) than expected for ice shelf deposits (> 1 m). Therefore, it may be associated with a renewed phase of volcanism, and was relatively rapidly deposited by distal component of sediment gravity flows, interbedded by volcanic ash and tuff settling through the water column.

4.5.9 Sequence 11: Diamictite, volcanic sandstone and silty claystone (103.72 to 99.58 mbsf)

Description: A well-defined, sharp GSE overlies deformed sediments at 103.72 mbsf (Figure 62A). The base of the sequence consists of a 0.42-m-thick massive diamictite overlain by weakly stratified diamictite. The lithological change is defined by slight changes in clast abundances and claystone laminae with common diatom fragments. The stratified diamictite is clast-rich, containing mostly volcanic lithics or mudstone intraclasts. This is overlain by an interval of sandstone (100.69 to 100.08 mbsf) with deformed ripple cross-stratification, and contains mudstone clasts with common diatom fragments. This sandstone was classified as volcanic during the initial core description, but thin-section analysis indicates that it is non-volcanic, being composed almost entirely of weathered mudstone (including diatom fragments) and diamictite intraclasts. The sandstone interval has a sharp basal contact (Figure 61E). At its top, it passes sharply into a silty claystone (with rare clasts) with slight to moderate bioturbation, but lacking diatoms (Figure 61D) and then into a stratified diamictite (Figure 61C).

Paleoenvironmental interpretation: This sequence marks the transition from grounded ice (massive diamictite interpreted as basal till) to an ice-proximal glacimarine deposition, inferred from the stratified diamictite and deformed rippled sandstone probably deposited by a tidal pumping mechanism (e.g., Figure 64). This passes into a sub-ice shelf silty claystone that is lacking clasts and has slight to moderate bioturbation. Readvance of the grounding line is preserved in the form of the stratified diamictite.

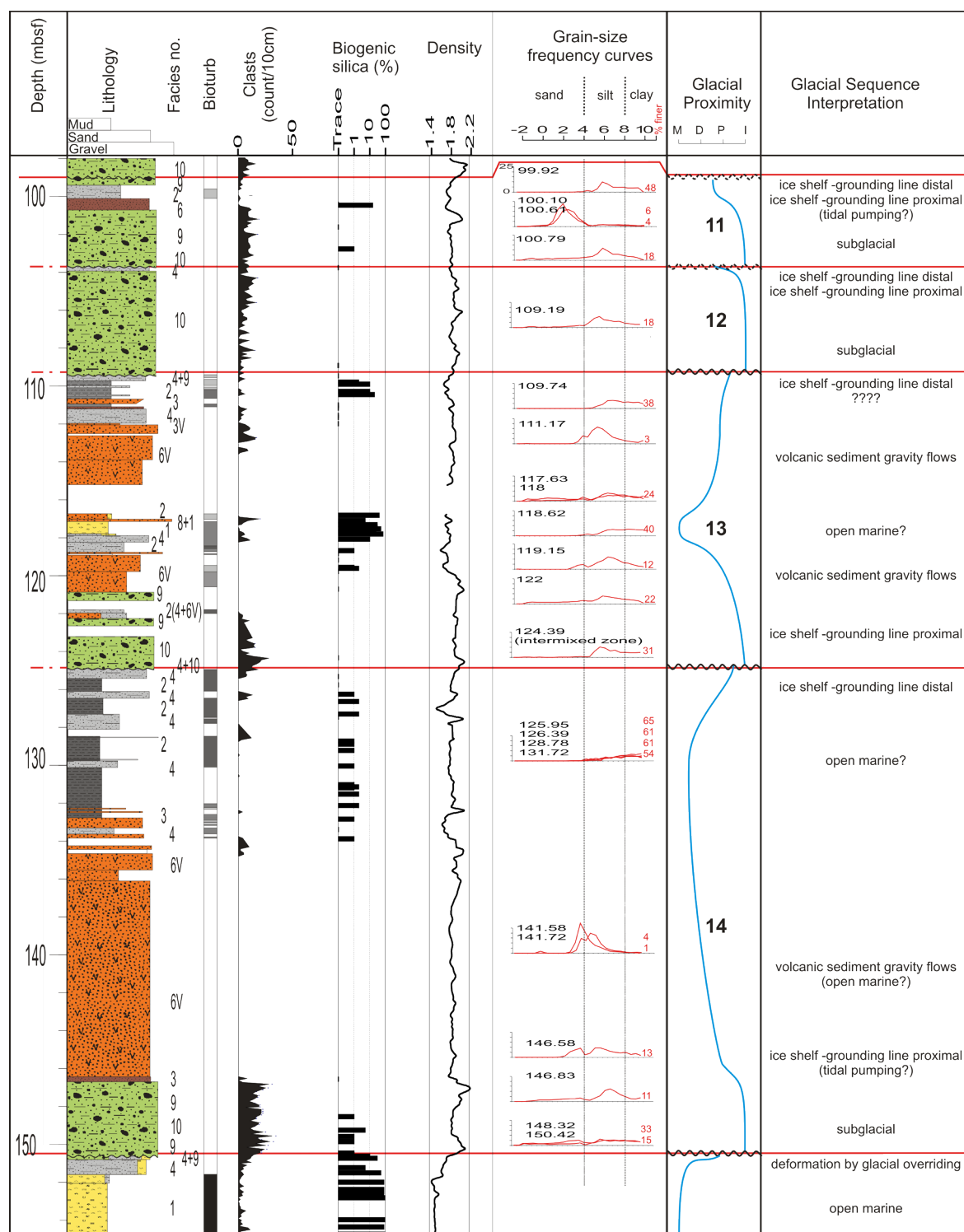


Figure 60: Stratigraphic log (98-154 mbsf), with data plotted showing facies distribution, bioturbation index, clast abundance (Krissek *et al.*, 2007), % biogenic silica, density (Niessen *et al.*, 2007) and grain-size frequency (sample depth(s) shown with each analysis). Glacial proximity curve and sequence interpretation is developed from facies analysis, and shows Sequences 11-15. The glacial proximity curve shows the transition from marine(m) to ice distal (d), ice proximal (p) and ice contact/subglacial (i) deposition. Legend for lithological units is provided in Figure 37.

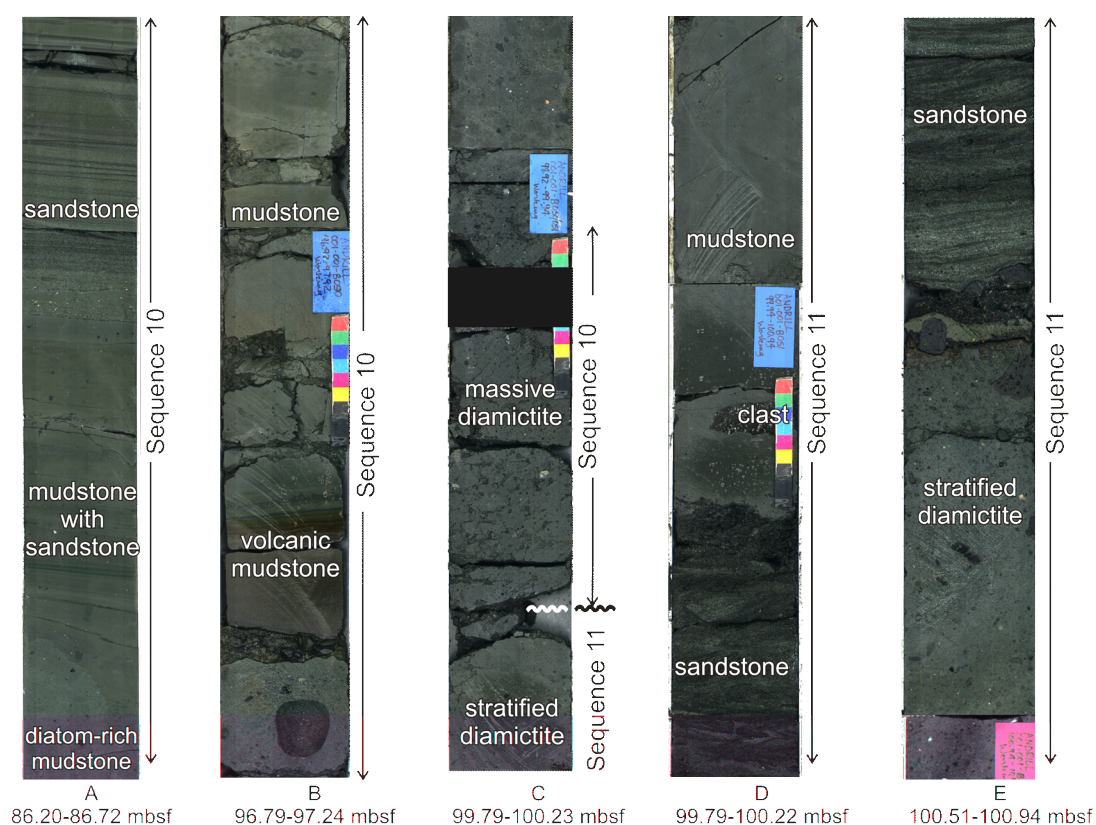


Figure 61: Representative photos of facies and GSEs from Sequences 10 to 11 in AND-1B.

4.5.10 Sequence 12: Diamictite overlain by mudstone with dispersed clasts (109.42 to 103.72 mbsf)

Description: The GSE at the base of sequence overlies deformed facies in the underlying sequence and is overlain by a mostly massive diamictite (109.42 to 103.92 mbsf; Figure 62C). However, the basal section of the diamictite (109.42 to 108.95 mbsf) contains weak, mm-scale stratification defined by texture and colour changes, and evidence of intermixing with mudstone from the underlying sequence. This passes into massive diamictite (109.42 to 103.94 mbsf) with intervals of clast long-axis alignment, and randomly orientated clasts that are well-cemented and contain common diamictite intraclasts (Figure 62B). The top of the sequence (103.92 to 103.72 mbsf) consists of a mudstone with dispersed clasts and rare diatom fragments. The mudstone also includes a thin (0.03 m), poorly sorted, black volcanic sandstone bed (Figure 62A).

Paleoenvironmental interpretation: The diamictite at the base of the sequence deforms underlying glacimarine deposits (Sequence 13), which indicates glacial overriding by grounded ice, before passing into glacimarine/ice shelf deposition close to the grounding line. The diamictite in the overlying sequence contains common diatom remains (Figure 60), suggesting an open marine environment may have occurred some time between the deposition of Sequence 12 and 11.

4.5.11 Sequence 13: Volcanic sandstones and mudstones, mudstone with dispersed clasts, diatomite, and diamictite (125.00 to 109.42)

Description: The massive diamictite (125.00 to 123.23 mbsf) at the base of this sequence contains sections of physical intermixing with stratified diamictite, and passes upward into interbedded stratified diamictite and silty claystones (122.66 to 120.94 mbsf; Figure 62E) with abundant granules of mudstone intraclasts and soft sediment deformation features. This is overlain by an interval of interbedded volcanic sandstones and siltstones (120.94 to 118.91 mbsf). Bioturbated silty claystone and mudstone with common clasts (118.91 to 117.90 mbsf) overlie the volcanic interval before passing into a diatomaceous-rich mudstone and diatomaceous ooze (117.90 to 117.02 mbsf; Figure 62D). These are capped by sandy volcanic breccias and unstratified dm-scale beds of volcanic sandstones (117.02 to 111.94 mbsf). The top of the sequence consists of mudstone with dispersed intraclasts, passing into a bioturbated silty claystone (lacking clasts) with fragmented remains of diatoms that are interbedded with volcanic sandstone beds. An intermixed zone of mudstone with dispersed clasts and diamictite directly underlies the GSE of the overlying sequence (Figure 62C).

Paleoenvironmental interpretation: This sequence records the transition from a subglacial to an open marine environment that is interrupted by sediment gravity flows associated with volcanic activity. Open marine conditions are recorded during the glacial minima, as evidenced by diatom-bearing mudstone and diatomite with associated ice-rafted debris. Readvance of the grounding line appears to have been associated with an ice shelf, on account of silty claystone that lacks clasts, but has common (5-20% smear slide estimate) fragmented diatom remains. However, thick volcanic sand beds complicate this signal.

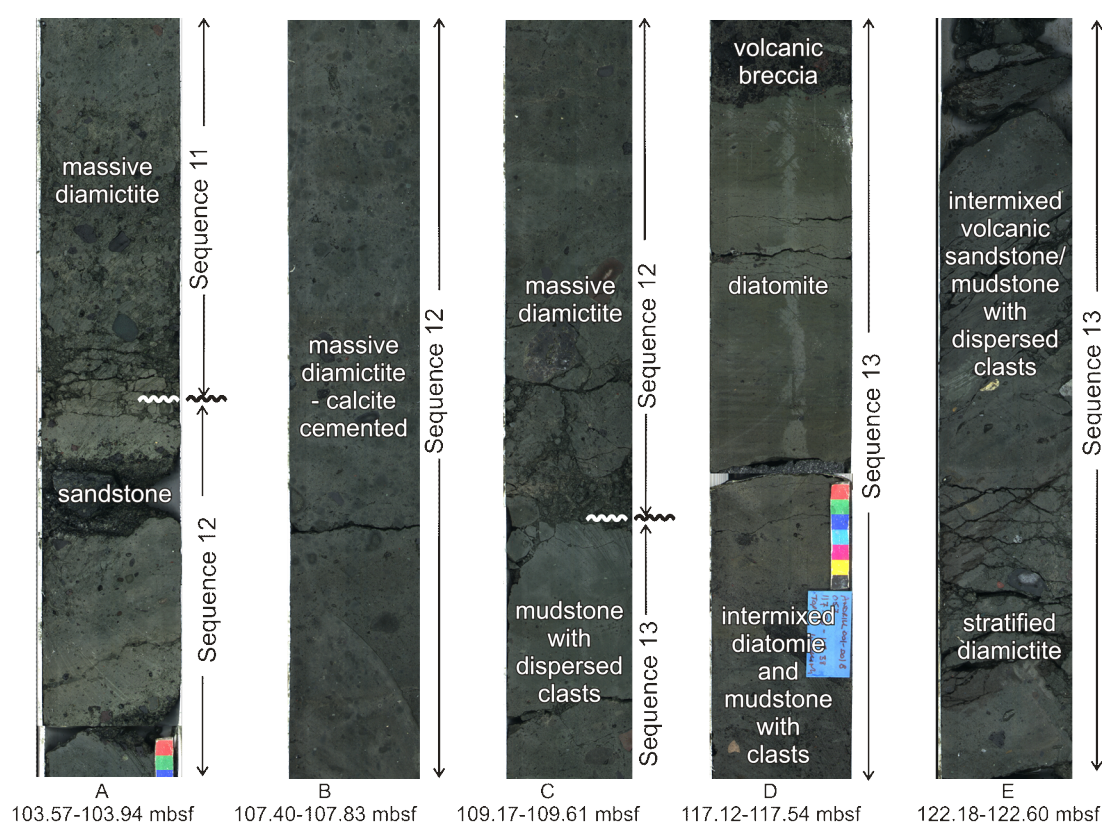


Figure 62: Representative photos of facies and GSEs from Sequences 11 to 13 in AND-1B.

4.5.12 Sequence 14: *Diamictite, volcanic sandstones, mudstone with dispersed clasts and silty claystones (150.73 to 125 mbsf)*

Description: The GSE at the base of this sequence is a gradational contact between 150.73 to 149.30 mbsf characterised by a physically mixed zone of mudstone with dispersed clast and diatomite (underlying sequence) that passes sharply into stratified diamictite (defined by clast concentrations) and then into massive diamictite at 149.30 mbsf (Figure 63D). The massive diamictite contains up to 5% diatom remains (Figure 60). The diamictite becomes stratified again between 147.83 and 146.79 mbsf before passing upward into a sandstone (composed of various lithologies) with mm-scale parallel laminations that is capped by a 3-cm thick stratified (inclined), clast-rich diamictite that is dominated by mudstone intraclasts (Figure 63C). Unconformably overlying the diamictite is a ~12 m thick interval of graded, volcanic sandstone beds, stratified at cm- to dm-scale (Figure 63B). The beds commonly grade upwards, contain occasional flame structures and parallel laminations, and have sharp bases. These volcanic sandstones are overlain by mudstone with dispersed clasts (Figure

63B) interbedded with mm- to cm-scale volcanic sandstone beds (134.72 to 132.84 mbsf) and then into silty claystone and clayey siltstone (132.82 to 125.46 mbsf). Some intervals of the silty claystones and clayey siltstones have rare to moderate bioturbation, and laminae defined by colour changes. Some of the volcanic sandstones contain mudstone lonestones that deform underlying laminae (Figure 63B). The top of the sequence is characterised by a bioturbated mudstone with dispersed clasts. There is some evidence of physical intermixing of mudstone with common clasts and sandy mudstone with dispersed clasts between 126.50 and 126.14 mbsf.

Paleoenvironmental interpretation: This sequence shows evidence for grounded ice at the glacial maximum (massive diamictite interpreted as basal till), followed by grounding line deposition during glacial retreat associated with thin sandstone/diamictite deposits (~0.3 m thick) truncated by volcanic sediment gravity flows (displaying flame structures, parallel laminae, and graded beds). Most of the mudstone and sandstone deposited during the glacial minimum in this sequence are probably related to local volcanism, although some periods of slower sedimentation are recorded by highly bioturbated zones (diatom abundances are between 1-2% in smear slide estimates; Figure 60). Rare mudstone lonestones deform underlying laminae. These lonestones are of an identical lithology to the mudstone beds interstratified with the volcanic sandstone unit (Figure 63B). This suggests that the grounding line was in the immediately vicinity and was actively entraining clasts of mudstone laminae into its basal bedload. The mudstone clasts were then ice-rafted a very short distance before being released by sub-ice shelf melting.

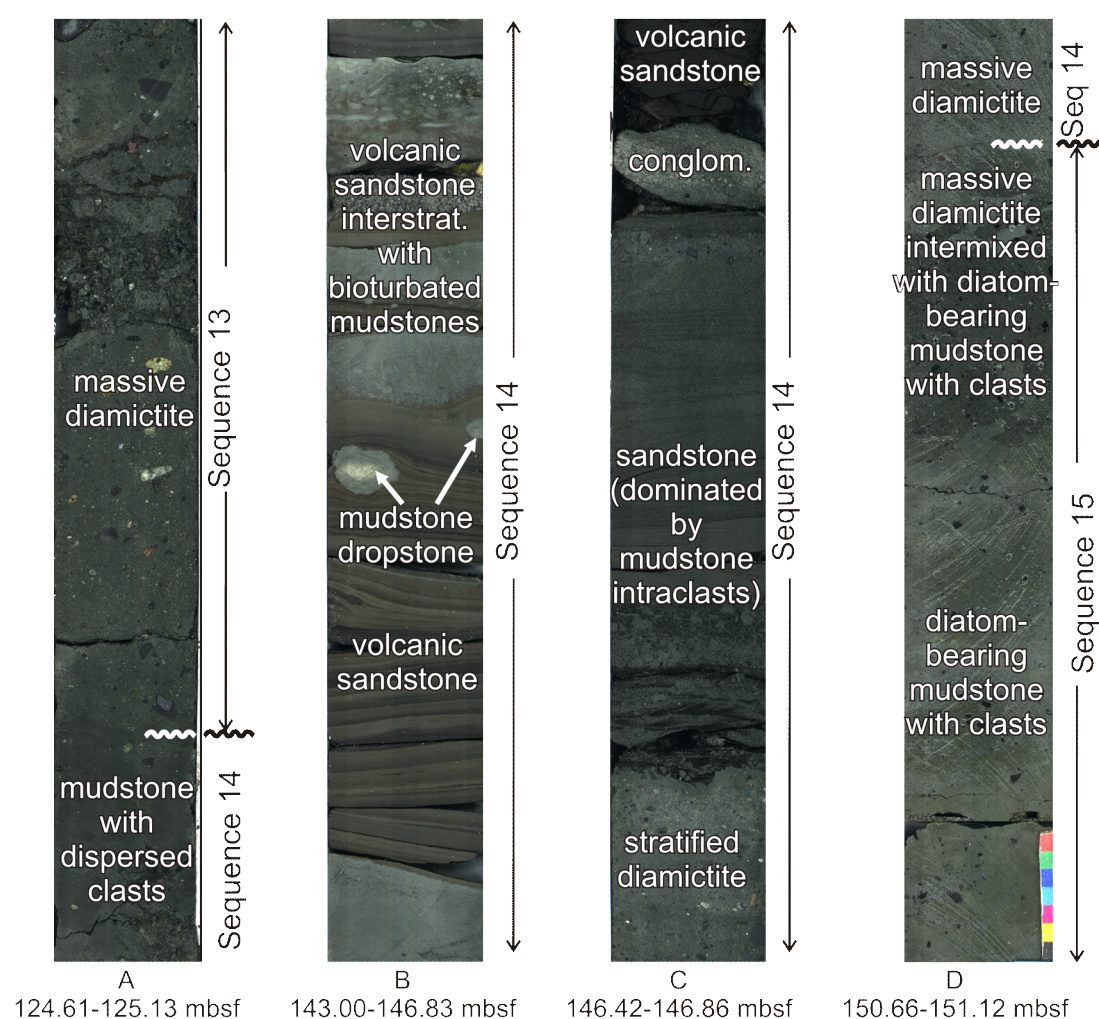


Figure 63: Representative photos of facies and GSEs from Sequences 13 to 15 in AND-1B.

4.6 Subglacial, glacialmarine and marine processes of the Antarctic Ice Sheet system in the Ross Embayment during the Pleistocene

The transitions from subglacial to glacialmarine facies in the AND-1B drill core provide new insight into the subglacial environment and grounding line processes of past ice sheets in the Ross Embayment throughout the Pleistocene. Each sequence described above shows clear transitions from periods of grounded ice overriding the drill site location (or in the immediate vicinity) to a glacialmarine environment, and in several cases open-marine conditions.

The subglacial environment is represented in most sequences by massive diamictite with strong horizontal alignment of clasts a-axes, implying deposition of basal till

beneath grounded ice. This lithology commonly rests on a GSE beneath which deformed and physically intermixed facies can be seen, consistent with overriding and deformation by grounded ice. Intervals of diamictite with a random clast fabric are more difficult to interpret, as they can form in a subglacial (e.g., lodgement/deformation till), glacimarine (e.g., basal debris melt-out), ice shelf or open marine environment (e.g., iceberg-scoured glacimarine debris) (e.g., Anderson *et al.*, 1980; Powell and Molnia, 1989; Dowdeswell *et al.*, 1994; Domack *et al.*, 1999). These along with stratified diamictite facies (commonly with higher proportion of mudstone intraclasts) could also represent a grounding zone wedge system (e.g., Powell and Alley, 1997; Anadakrishnan *et al.*, 2007). The identification of such deposits may ultimately be important, as Alley *et al.* (2007) provide modelling experiments that suggest the presence of a grounding zone wedge system may help to maintain grounding line stability, even during periods of small scale (~10 m) sea level increases. This has the implication that only large-scale sea level rises are likely to result in widespread grounding-line migration.

No facies were found that might represent significant conduit or sediment-laden subglacial meltwater-plume discharge. Several intervals are classified as conglomerates, but all are < 1 m thick. These conglomerate deposits are associated with the final transition from grounding-zone deposition to more distal glacimarine deposition of muds, and are probably equivalent to the granulated deposits of Domack *et al.* (1999), or the clast-rich diamictite deposits associated with grounding line retreat at the base of DF80-189 (Chapter 2). The grain-size frequency distributions of these conglomerates are consistent with those of the diamictite facies (e.g., Figure 51, Chapter 3). As a result, these conglomerates are interpreted as a clast-rich equivalent of the stratified diamictite deposits.

Some sequences (e.g., 11 and 14) contain sandstone beds within subglacial and glacimarine transition facies that represent the initial phase of ice retreat (Figure 60). Some of these sandstones display cross-bedding, which suggests the influence of traction currents. The very well-sorted, cross-bedded sandstone (consisting almost entirely of mudstone/diamictite intraclasts) in the glacial retreat succession within

Sequence 11 (100.69 to 100.08 mbsf) is the most notable unit of this type. The sandstone has a mean grain size range of 700 to 880 μm (see grain-size frequency curves at 100.61 and 100.10 mbsf in Figure 60). Currents of the order of 30-50 cm s^{-1} are required to move sand in this size range (Hjulstrom, 1939). Sand deposits of this grain-size frequency and lithology (i.e., mudstone and diamictite intraclasts) are a consistent facies associated with the initial retreat phase in LGM to Holocene sediment cores collected from the Ross Sea (e.g., Domack *et al.*, 1999), and from sub-ice shelf deposits beneath the McMurdo (e.g., sand unit in HWD03-1 (31 to 24 cm); Chapter 2) and Amery Ice Shelves (Hemer *et al.*, 2007), as well as in the Antarctic Peninsula (Evans and Pudsey, 2002).

In the absence of any evidence for subglacial meltwater discharge, the most likely process for formation of these currents is “tidal pumping” resulting from grounding line migration through a tidal cycle (e.g., Alley *et al.*, 1987; Domack and Williams, 1990). Where the sea floor profile is relatively flat on either side of the ice sheet-ice shelf transition, the “grounding line” may advance and retreat daily as the tide falls and rises. Tidal height variations at the present-day Siple Coast grounding line are of the order of ~ 1 m (Anadakrishnan and Alley, 1997), and may result in the development of a thin water film between the ice sheet and the bed (Alley *et al.*, 1987; Figure 64). In addition, MacAyeal *et al.* (2006) has linked long-period waves derived from Alaskan storms to iceberg calving at the Ross Ice Shelf front, and Domack *et al.* (2007) has suggested that long-period waves may also contribute to grounding-zone “pumping” deposition, as it will result in higher amplitude oscillations than tidal influences.

As the grounding line continues to retreat upstream of the AND-1B drill site, deposition of muds continues, free of basal glacial debris beneath a floating ice shelf. Bioturbation is absent, or of moderate intensity, and diatom remains are absent, or rare and poorly preserved, suggesting limited sub-ice shelf oceanic circulation. These observations are consistent with observations beneath other ice shelves (Domack *et al.*, 1999; Hemer and Harris, 2003; McKay *et al.*, 2008; Chapter 2).

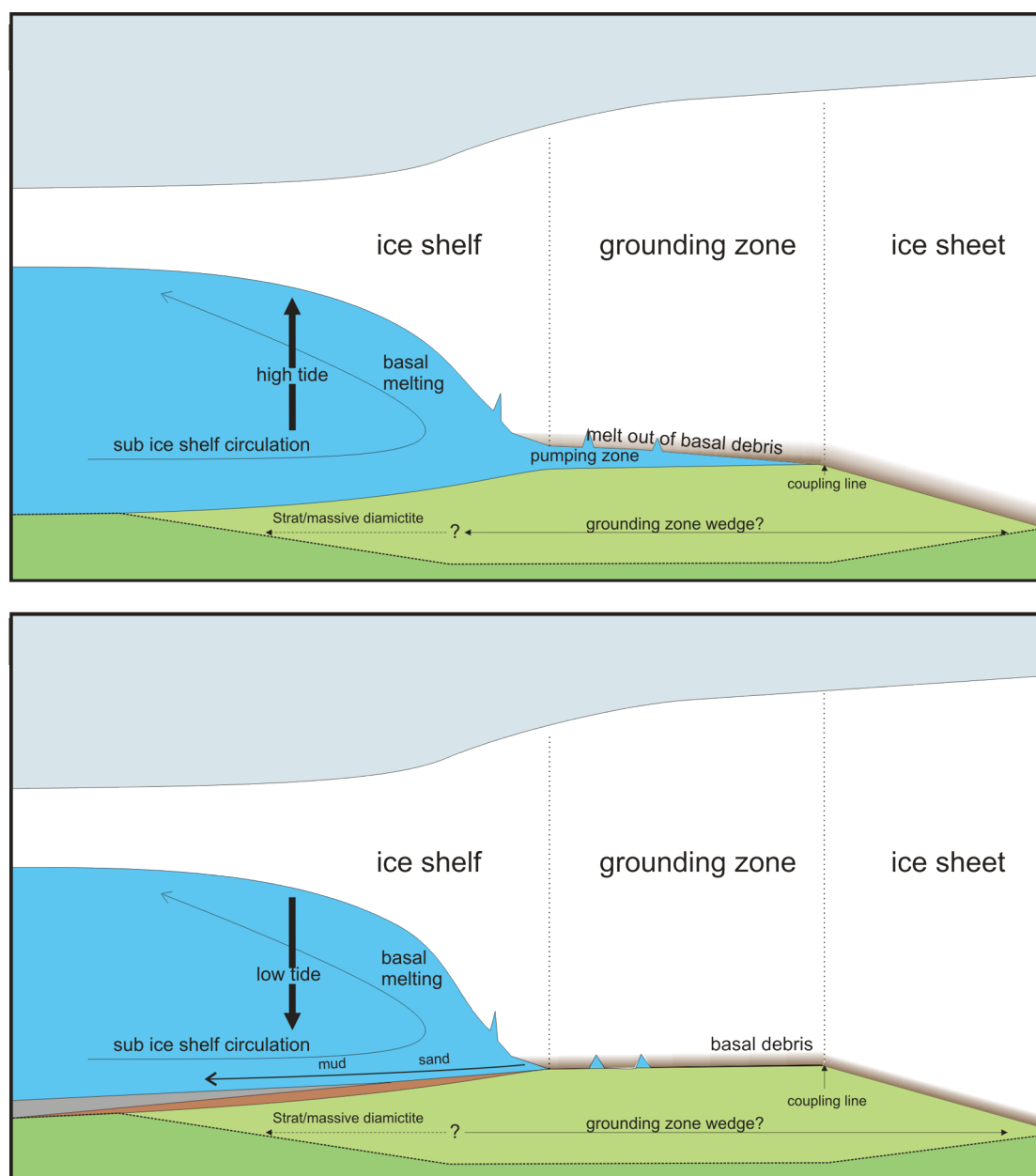


Figure 64: Cartoon to illustrate simply the tidal pumping process (based on cartoons from Domack and Williams, 1990 and Anadakrishnan *et al.*, 2007). The height of the tidal cavity (pumping zone) is of the order of several mm (Alley *et al.*, 1987). Not to scale.

During open marine conditions, volcanic sandstone and mudstone units dominate. Two sequences (Sequences 10 and 13) contain diatomite intervals with ice-rafted debris, indicative of an open marine environment (e.g., Chapter 2). However, both of these intervals contain thick, continuous successions (~5 to 12 m) of volcanoclastic diamictite, sandstones, and mudstone. Some of these volcanic intervals are physically-intermixed and are interpreted to be deposited by volcanic debris flows, turbidity

currents, as well as near-primary volcanic ash fall. The association of these volcanoclastic intervals with open marine diatomite facies suggests a linkage between volcanic-rich sediments and an open marine environment. For sequences where the glacial minima are most likely represented by a floating ice shelf above the drill site (i.e., Sequences 3-9 and 11-12), the maximum thickness of any volcanic-rich bed is 4 cm.

At face value, this observation suggests that Sequences 2 and 14 were also deposited in open water environments. The glacial retreat and minima facies in Sequence 14 consists of volcanic sandstones (including a 12-m thick turbidite sequence) that are interbedded with highly bioturbated mudstones (containing ~1% diatoms). The mudstone at the top of this sequence is 7-m thick, almost an order of magnitude thicker than the mudstones facies deposited in Sequences 9-3 and 12-11, or for mudstones deposited beneath Antarctic ice shelves in the Holocene (McKay *et al.*, 2008; Hemer and Harris, 2003). These observations, combined with the 12-m thick volcanic sandstone succession, point towards an open marine setting for the glacial minima in Sequence 14.

The upper half of Sequence 2 has poor recovery, but subglacial to glacimarine diamictites in this sequence are overlain by at least 1.5 m of volcanic sandstone and mudstone. The basal contact of this volcanic interval is very sharp and planar, suggesting that it is erosional and that the volcanic mudstone is the result of a sediment gravity flow. It is difficult to determine from these criteria alone if open marine waters surrounded the drillsite during the glacial minimum in this sequence, but given the association with volcanoclastic sediments it is a possibility.

4.7 Sedimentary evidence for erosion and unconformities

The presence of ice shelf deposits in Sequences 1 to 6 suggests there are minimal periods of time missing between sequences, despite potential erosion by GSEs. Holocene ice shelf deposits around the Antarctic margin are characteristically thin (<1 m); and have lower sedimentation rates than their open marine counterparts (McKay *et al.*, 2008; Hemer and Harris, 2003; Evans and Pudsey, 2002; Domack *et al.*, 2005).

Therefore, if erosion of open marine sediments had occurred, then it is likely that the thin ice shelf deposits would have also been eroded. In the unlikely situation that the marine deposits have been eroded while the thin ice shelf deposits are preserved, there should be some evidence of recycling of the marine sediments within the basal section of the diamictite in the overlying sequence.

There is no evidence of recycled diatoms in diamictite from Sequences 1 through 7. Trace amounts of diatoms are noted in the basal diamictite from Sequences 11 to 14 (Figure 58 and Figure 60), and these sequences overlie marine sediments. The upper ~20 cm of Sequence 8 contain “wispy” laminae of claystone that are sheared and contain ~5% diatom remains. These laminae (Figure 59D) have a similar style of deformation to those associated with GSEs separating diatomite from diamictite in the Pliocene section of AND-1B (c.f. Figure 39A; Chapter 3).

Sequence 9 is different from the overlying Sequences 10 to 14 in that it lacks trace numbers of diatoms but overlies a sequence that is rich in diatoms. However, the open water diatomite facies is overlain by a silty claystone (sub-ice shelf) and stratified diamictite. This record of grounding line advance in the upper part of Sequence 10 and continuing into Sequence 9, indicates that the advance was largely non-erosive and therefore sediment recycling was minimal. This largely non-erosive nature during the late Pleistocene (0.8 Myr to present) is probably the result of the cold-polar regime of ice sheet that occupied the Ross Embayment during this time period.

4.8 Chronostratigraphy and correlation to the marine oxygen isotope timescale

The age model presented in Figure 65 has been developed from the initial chronostratigraphy of Wilson *et al.* (2007). It integrates $^{40}\text{Ar}/^{39}\text{Ar}$ dates from volcanic ashes and the magnetostratigraphy, with the sequence stratigraphy developed in this chapter. The magnetic reversals at 84.97 and 80.03 mbsf are identified as Brunhes/Matuyama (0.781 Myr) and Matuyama/Jaramillo (0.988 Myr) boundaries, respectively (Wilson *et al.*, 2007). These events provide good age control, as they are constrained by the $^{40}\text{Ar}/^{39}\text{Ar}$ date of 1.014 ± 0.04 Myr from a felsic tephra at 85.53

mbsf (Wilson *et al.*, 2007). The reversed magnetic transition at 91.13 mbsf (Figure 65) almost certainly represents the base of Jaramillo subchron (1.072 Myr). Using these constraints, Sequences 14, 13, 10 and 9 can be accurately tied to excursions in the isotope curve (Figure 65).

Sequences 14 and 13 are dated by $^{40}\text{Ar}/^{39}\text{Ar}$ age of basaltic tephra at 1.67 ± 0.03 Myr and 1.65 ± 0.03 Myr, respectively (Wilson *et al.*, 2007; Figure 65). As there are no magnetic reversals in these sequences, they are not as well constrained, but most they were probably deposited between Marine Isotope Stage 60 to 54 (Figure 65). Sequences 11 and 12 are poorly constrained, most likely being deposited during two ~40,000 year intervals somewhere between Marine Isotope Stages 53 and 34. However, they were most likely to have been deposited within the Matuyama Chron below the Cobb Mountain subchron, due to inferred erosion of the Cobb Mountain subchron by the base of Sequence 10. This implies unconformities totalling ~0.5 Myr between the top of Sequence 13 and the bottom of Sequence 10.

The base of Sequence 9 can be confidently correlated with the glacial advance represented by Marine Isotope Stage 20 on account of the Bruhnes/Matuyama geomagnetic boundary occurring within the diamictite interval at the sequence base. Sequences 1-9 have been tentatively correlated with the nine Marine Isotope Stage interglacial events in the Lisiecki and Raymo (2005) $\delta^{18}\text{O}$ benthic stack (Figure 65). In this age model, every named isotope stage can be linked to particular glacial/interglacial cycle in the AND-1B core for the past ~0.8 Myr. Further $^{40}\text{Ar}/^{39}\text{Ar}$ dates on volcanic ash are currently being obtained to improve the confidence of the correlation of individual glacial minima to Marine Isotope Stage interglacials in the $\delta^{18}\text{O}$ benthic record

Critical to this age model is the age of Sequences 1 and 2. The diamictite at the base of Sequence 2 (at ~10 mbsf) is most likely to have been deposited during the Last Glacial Maximum. Although there is significant core loss between 10 and 24 mbsf this is probably due to difficulty in coring unconsolidated lithologies during this interval (e.g., volcanic sands etc). A volcanic ash sample at ~25 m is currently being

dated to test these assumptions, and provide an age constraint for the top of Sequence 2.

There appear to be at least two periods of erosion in early Pleistocene (>0.8 Myr) part of the AND-1B core. The older occurs between ~ 1.6 and 1.13 Myr and the younger somewhere between ~ 0.99 and 0.8 Myr. The earliest part of the Pleistocene, corresponding to the Olduvai subchron ($1.8 - 1.7$ Myr) is also missing from the record.

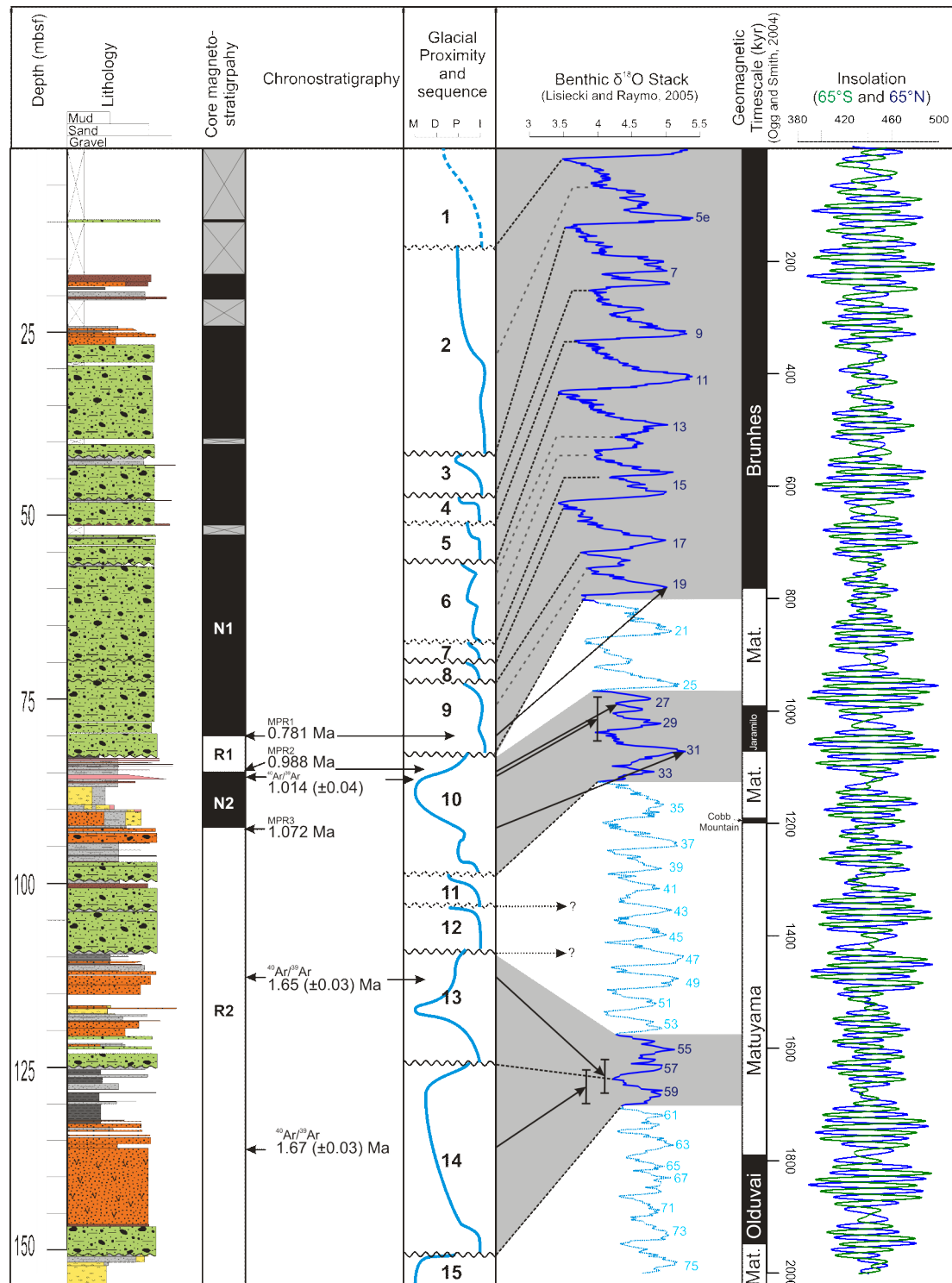


Figure 65: Age model based on integration of magnetostratigraphy, tephrchronostratigraphy and the sequence stratigraphic model. Solid arrows indicate absolute ages (and associated errors), while dashed arrows indicate interpretation based on sequence stratigraphic model, showing the transition from marine(m) to ice distal (d), ice proximal (p) and ice contact/subglacial (i) deposition. Legend for lithological units is provided in Figure 37.

4.9 Identifying periods of past retreat and expansion of the Antarctic Ice Sheet in the Ross Embayment during the Pleistocene

4.9.1 The Late Pleistocene (0.8 Myr to present)

In AND-1B, the Late Pleistocene sequences (Sequences 1-9) characterise a period of relative stability of the AIS in the Ross Embayment, and open-marine conditions are not recorded in the AND-1B drillsite. This stability is interpreted primarily as a consequence of a persistent cold glacial thermal regime (and cold climate) that maintained an extensive ice shelf across the Ross Embayment during interglacial periods. Despite this stability, there is clear evidence of ice shelf grounding and ice sheet deposition during each of the nine glacial cycles over the past 0.8 Myr, implying significant sensitivity of past ice sheets in the Ross Embayment to either climate, sea level, or both.

Over the past 0.8 Myr, only Sequence 2 and Sequence 8 provide evidence of possible calving-line proximal, ice shelf sedimentation. A confident interpretation for Sequence 2 is difficult because several metres of the upper part were not recovered. However, diatom remains abundances are low (~1% of matrix from smear slide estimates) throughout the interglacial mudstone facies in Sequence 2, suggesting sub-ice shelf conditions more extensive or similar to that of today. In the previous section, these facies were tentatively correlated with MIS 5. Geological evidence for calving line proximal, ice shelf conditions in McMurdo Sound supports this interpretation as reworked marine shells, dated as Marine Isotope Stage 5e, have been reported from Cape Barne, ~45 km to the north of the drillsite (Stuiver *et al.*, 1981). The age model developed from this sequence stratigraphic approach is tentative and dating the top of this sequence is critical to its robustness. $^{40}\text{Ar}/^{39}\text{Ar}$ dating of volcanic ashes in glacial minima facies at 25 and 54 mbsf (Jake Ross, New Mexico Tech., pers. comm.) will be available in the near future. There is also potential for obtaining maximum depositional ages of the diamictite deposits by dating enclosed volcanic clasts.

The diamictite in Sequence 2 contains evidence for fluctuations between grounded and marginally floating ice associated with the grounding zone. These fluctuations

could correspond to Marine Isotope Stage 7, a lower amplitude interglacial period just prior to 0.2 Myr.

Sequences 3 to 6 all contain evidence for debris-free ice shelf conditions during glacial minima, but no evidence for open marine conditions. It is difficult to gauge the duration of these periods of sub-ice shelf deposition at MIS, but they are of similar thickness (<1 m) to Holocene ice shelf sediments elsewhere (e.g., Hemer and Harris, 2003; Evans and Pudsey, 2002), implying a similar duration (i.e., several thousand years during the peak of each Marine Isotope Stage interglacial). These periods of deposition beneath a debris-free ice shelves coincide with the higher-amplitude “super-interglacials” of the past ~400 kyr (e.g., Marine Isotope Stage 5e, 9, 11), and correspond to ~120-130 m of sea level fluctuations between glacial and interglacial peaks (Miller *et al.*, 2005) .

Rapid or large (>20 m?) sea level rises are likely to destabilise the grounding line (Alley *et al.*, 2007; Schoof, 2007) and expose the base of the thick ice shelf to warm oceanic masses upwelling onto the Ross Sea continental shelf, in turn leading to rapid basal melting of ice shelf (Payne *et al.*, 2004; Dupont and Alley, 2005). Recent modelling experiments and observations at the Siple Coast grounding line suggest that slower/lower amplitude sea level rises are less likely to have resulted in extensive ice shelf development, as development of sedimentary wedges at the grounding line results in thickening the overlying ice sheet, which in turn helps stabilises the grounding line (Alley *et al.*, 2007; Anadakrishnan and Alley, 1997). If this model is correct, then it may help to explain the lack of extensive ice shelf conditions during the lower-amplitude fluctuations in the benthic $\delta^{18}\text{O}$ record, and suggests that only the high-amplitude 100-kyr interglacial/glacial signal will result in “lift-off” and retreat of the grounding line.

The lack of open marine deposits, and the presence of ice shelf deposits during interglacial periods, implies a cooling of the glacial regime at 0.8 Myr to the extent that an extensive ice shelf persisted across the Ross Embayment during interglacial periods. Large ice shelves require cold ice in order to be sustained (Mercer, 1978;

Alley *et al.*, 1989) – currently ice at the surface of Upstream B site and at J9 (Ross Ice Shelf) averages -25°C (Clough and Hansen, 1979; Engelhardt *et al.*, 1990). The implication of more extensive ice shelves during interglacials in a cooler glacial regime is that they will increase the buttressing effect on the grounded ice sheet that feeds it (Mercer, 1978; Rignot *et al.*, 2004). A cooling in the glacial regime to the extent that large ice shelves could be maintained during interglacials in the Late Pleistocene helps to explain the relative stability of AIS in the Ross Embayment since 0.8 Myr, relative to more dynamic Pliocene, when the Ross Embayment sector of AIS was probably warmer and therefore ice shelves were less likely to form during interglacials.

4.9.2 Mid-Pleistocene Transition

The unconformity at 82.6 mbsf coincides with the onset of the Mid-Pleistocene Transition and is inferred to represent large-scale expansion of AIS in the Ross Embayment at ~ 0.8 Myr. This corresponds to the transition from the earlier 40 kyr glacial/interglacial cycles to the later 100 kyr cycles since that time (Lisiecki and Raymo, 2005). The 100-kyr glacial-interglacial cycles of the Late Pleistocene are documented to be in phase between hemispheres, which has led some to postulate a Northern Hemisphere control on deglaciation of the Antarctic Ice Sheet, though either eustatic forcing or changes in ocean temperature (Thomas and Bentley, 1978; Stuiver *et al.*, 1981; Denton *et al.*, 1986; Denton and Hughes, 2000; Kawamura *et al.*, 2007).

In the current age model (Figure 65), the base of Sequence 7 is correlated with the glacial advance associated with Marine Isotope Stage 16, which is characterised in the benthic $\delta^{18}\text{O}$ record by the first large negative excursion ($\sim 3.5\text{‰}$), suggesting that this was a particular cold glacial period (Figure 65). This advance is inferred to have eroded facies deposited during a period of calving-line proximal ice shelf sedimentation at the drillsite, which is correlated with Marine Isotope Stage 17 (i.e., the top of Sequence 8).

4.9.3 The Early Pleistocene

Prior to the Mid-Pleistocene Transition, the ice sheets in the Ross Embayment were more dynamic, with several periods of open water conditions in McMurdo region. Sequence 10 is the last period of prolonged open marine conditions recorded at the drillsite and its timing coincides with Marine Isotope Stage 27 to 31. However, the magnetic reversal that is correlated to the base of Jaramillo subchron (1.072 Myr) occurs at 91.13 mbsf, within an interval of physically-intermixed volcanic sand and diatomite. This interval is interpreted as a volcanic debris flow. Therefore, the climatic signal associated with the peak warmth during Marine Isotope Stage 31 may not be as well-preserved in AND-1B as it was in CRP-1 drillsite, ~150 km to the north of AND-1B (Scherer *et al.*, 2008). However, the presence of the intermixed diatomite at this time is clear evidence of open-water conditions at the drillsite during Marine Isotope Stage 31. Dating the overlying mudstone via the magnetic reversal at the top of Jaramillo subchron (0.988 Myr), indicates that the sea floor was not eroded at the drillsite during the following glacial maximum of Marine Isotope Stage 30 (Figure 65).

Micropaleontology and isotopic analysis of Marine Isotope Stage 31 deposits at CRP-1 and Southern Ocean drill sites (ODP Site 1094) indicate that ice-free conditions (and minimal sea ice) and high sea surface temperatures occurred in phase with high values of southern latitude insolation and precedes Northern Hemisphere deglaciation (Scherer *et al.*, 2008). Scherer *et al.* (2008) suggest that this in-phase relationship supports the hypothesis of Raymo *et al.* (2006) that prior to 1 Myr local insolation driven primarily by precession, had a direct control on volume changes in the Antarctic Ice Sheets. Scherer *et al.*, (2008) imply that at least for the warmest Southern Hemisphere orbital configuration, that ice sheet growth and decay is antiphased between the northern and Southern Hemisphere, and that glacial cycles in each hemisphere could operate at 20-kyr cyclicity (c.f. Raymo *et al.*, 2006).

According to the age model (Figure 65) Sequences 14 and 13 could represent either a 20 or 40-kyr cycles, but not 100-kyr cycles. This is a consequence of the interglacial facies in Sequences 14 and 13 having $^{40}\text{Ar}/^{39}\text{Ar}$ ages of 1.67 (± 0.03) Myr and 1.65

(± 0.03) Myr respectively. The maximum range of the errors is separated by 80 kyr, but the overlap could also allow for 20 kyr cyclicity. However, direct correlation to the isotope curve suggests that Sequences 14 and 13 are 40 kyr cycles.

4.10 Conclusions

- The nine late Pleistocene glacimarine sequences (0.8 Myr to present) in the AND-1B drill core match the glacial-interglacial cycles of the Antarctic deep ice core and marine deep-sea benthic $\delta^{18}\text{O}$ records. The preservation of thin interglacial ice shelf deposits between all of the sequences indicates that erosion by grounded ice during glacial periods has been minimal.
- There is no evidence of open marine conditions at the AND-1B drill site for the past 0.8 Myr. Claving-line proximal/open marine conditions may have occurred during Marine Isotope Stage 5e, but conclusive proof is lacking, and the ice sheet configuration probably mirrored that of the present day Ross Ice Shelf.
- There is no evidence in AND-1B for the widespread collapse of AIS in the Ross Embayment during Marine Isotope Stage 11, as postulated by earlier workers.
- The early Late Pleistocene (0.8 to 0.5 Myr) is characterised by sequences mostly containing subglacial to glacimarine/grounding-line proximal deposits (e.g., Sequences 9, 7 and 6). These sequences are indicative of minor fluctuations of the grounding line in the vicinity of the drillsite. Not enough is yet known about modern grounding line depositional processes to determine if the facies observed (i.e., alternations of stratified and massive diamictite) are a response to climatic or eustatic forcing, or a result of shorter-term depositional patterns as part of grounding zone wedge sedimentation. However, one subtle contact between massive and stratified diamictite (separating Sequence 7 from 8) at the sequence boundary contains highly sheared, diatom-bearing mudstone intraclasts that suggests some erosion of a thin ice shelf deposit. This may indicate that this sequence boundary was a larger-scale event.
- For the period before 0.8 Myr, the AND-1B sequences record more dynamic ice sheet behaviour in the Ross Embayment, with several sequences documenting subglacial deposition followed by periods of open marine sedimentation at the

drill site and in the Ross Embayment. Sequence 10 spans at least two Glacial-Interglacial cycles (Marine Isotope Stages 31 to 27) as there is no evidence of a subglacial deposition associated with Marine Isotope Stage 30 at AND-1B. This supports the hypothesis that AIS in the Ross Embayment was much smaller during Marine Isotope Stage 31, and was not able to re-establish itself for the following glacial cycle.

- The early Pleistocene sequences (~1.7 to 0.8 Myr) in AND-1B appear to represent 40-kyr cycles (obliquity), although 20-kyr precessional-based pacing can not be ruled out. Either way, the early Pleistocene sequences document a fundamental change in the past response of the ice sheet system in the Ross Embayment to orbital forcing.

4.11 References

- Alley, R. B., Blankenship, D. D., Bentley, C. R., and Rooney, S. T., 1987. Till beneath ice stream B; 3, Till deformation; evidence and implications. Special section. *Journal of Geophysical Research* v. 92, p.8921-8929.
- Alley, R. B., Blankenship, D. D., and Rooney, S. T., 1989. Sedimentation beneath ice shelves; the view from ice stream B. Modern glacimarine environments; glacial and marine controls of modern lithofacies and biofacies. *Marine Geology* v. 85, p.101-120.
- Alley, R. B., Anandakrishnan, S., Dupont, T. K., Parizek, B. R., and Pollard, D., 2007. Effect of sedimentation on ice-sheet grounding-line stability. *Science* v. 315, p.1838-1841.
- Anandakrishnan, S., and Alley, R. B., 1997. Tidal forcing of basal seismicity of ice stream C, West Antarctica, observed far inland. *Journal of Geophysical Research* v. 102, p.15,183-15,196.
- Anandakrishnan, S., Catania, G. A., Alley, R. B., and Horgan, H. J., 2007. Discovery of till deposition at the grounding line of Whillans ice stream. *Science* v. 315, p.1835-1838.
- Anderson, J.B., 1999. Antarctic Marine Geology. Cambridge University Press, UK, 289p.
- Anderson, J. B., Kurtz, D., Domack, E.W., and Balshaw, K., 1980. Glacial and glacial marine sediments of the Antarctic continental shelf. *Journal of Geology* v. 88, p.399-414.
- Barron, J.A., 1996. Diatom constraints on sea surface temperatures and sea ice distribution during the middle part of the Pliocene. *U.S. Geological Survey Open-File Report* 96-713, 1-45,
- Chappell, J., 1998. Jive talking. *Nature* v. 394, p.130-131.
- Clough, J.W., and Hansen, B.L., 1979. The Ross Ice Shelf Project. *Science* v.203, p.433-434.

- Cuffey K.M., and Marshall, S.J., 2000. Substantial contribution to sea level rise during the last interglacial from the Greenland ice sheet. *Nature* v.404, p.591–594.
- Denton, G. H., and Hughes, T. J., 2000. Reconstruction of the Ross ice drainage system, Antarctica, at the last glacial maximum. *Geografiska Annaler. Series A: Physical Geography* v.82, p.143-166.
- Denton, G. H., Hughes, T. J., and Karlen, W., 1986. Global ice-sheet system interlocked by sea level. *Quaternary Research* v. 26, p.3-26.
- Domack, E., 2007. Recognition of long period waves in Antarctic glacial marine (ice shelf) sediments. *Geophysical Research Abstracts* v.9, 04586, SRef-ID: 1607-7962/gra/EGU2007-A-04586.
- Domack, E. W., and Williams, C. R., 1990. Fine structure and suspended sediment transport in three Antarctic fjords. *Antarctic Research Series* v.50, p.71-89.
- Domack, E. W., Jacobson, E. A., Shipp, S., and Anderson, J. B., 1999. Late Pleistocene-Holocene retreat of the West Antarctic ice-sheet system in the Ross Sea; Part 2, Sedimentologic and stratigraphic signature. *Geological Society of America Bulletin* v. 111, p.1517-1536.
- Domack, E., Duran, D., Leventer, A., Ishman, S., Doane, S., McCallum, S., Amblas, D., Ring, J., Gilbert, R., and Prentice, M., 2005. Stability of the Larsen B ice shelf on the Antarctic Peninsula during the Holocene epoch. *Nature* v.436, p.681-685.
- Dowdeswell, J.A., Whittington, R.J., Marienfeld, P., 1994. The origin of massive diamicton facies by iceberg rafting and scouring, Scoresby Sund, East Greenland. *Sedimentology* v. 41, p.21-35.
- Dunbar, G., Niessen, F., Vogel, S., Tulaczyk, S., Mandernack, K., Krissek, L., Carter, L., Cowan, E., Wilch, T., Peng, C., Strong, C.P., Scherer, R., Sjunneskog, C., Winter, D., McKay, R., Talarico, F., Pompilio, M., and the ANDRIL-MIS Science Team. 2007. Late Pleistocene to Holocene Strata from Soft-Sediment Coring at the AND-1B site, ANDRILL McMurdo Ice Shelf Project, Antarctica. *Terra Antarctica* v.14, p141-154.
- Dupont, T. K., and Alley, R. B., 2005. Assessment of the importance of ice-shelf buttressing to ice-sheet flow. *Geophysical Research Letters* v.32, p.4.
- Engelhardt, H., Humphrey, N., Kamb, B., and Fahnestock, M., 1990. Physical Conditions at the Base of a Fast Moving Antarctic Ice Stream. *Science*, v.248, p.57-59.
- EPICA Community Members, 2004. Eight glacial cycles from an Antarctic ice core. *Nature* v.429, p.623-628.
- Evans, J., and Pudsey, C. J., 2002. Sedimentation associated with Antarctic Peninsula ice shelves: implications for palaeoenvironmental reconstructions of glacial marine sediments. *Journal of the Geological Society* v. 159, p.233-237.
- Hearty, P. J., Kindler, P., Cheng, H., and Edwards, R. L., 1999. A +20 m middle Pleistocene sea-level highstand (Bermuda and the Bahamas) due to partial collapse of Antarctic ice. *Geology* v. 27, p.375-378.
- Hearty, P. J., Hollin, J. T., Neumann, A. C., O'Leary, M. J., and McCulloch, M., 2007. Global sea-level fluctuations during the Last Interglaciation (MIS 5e). *Quaternary Science Reviews* v. 26, p.2090-2112.

- Hemer, M. A., and Harris, P. T., 2003. Sediment core from beneath the Amery Ice Shelf, East Antarctica, suggests mid-Holocene ice-shelf retreat. *Geology* v. 31, p.127-130.
- Hemer, M.A., O'Brien P.E., Post A.L., Craven M., Truswell E.M., Roberts D., Harris P.T., 2007. Sedimentological signatures of the sub-Amery Ice Shelf circulation. *Antarctic Science* v.19, p.497-506.
- Hjulstrom, F. 1939. Transportation of detritus by moving water. In *Recent Marine Sediments* (Trask, P. D., ed.). Dover Publications Inc., New York, p.5–31.
- Howard, W.R., 1997. A warm future in the past. *Nature* v.388, p.418–419.
- Jouzel, J., Masson-Delmotte, V., Cattani, O., Dreyfus, G., Falourd, S., Hoffmann, G., Minster, B., Nouet, J., Barnola, J. M., Chappel-laz, J., Fischer, H., Gallet, J. C., Johnsen, S., Leuenberger, M., Lulergue, L., Luethi, D., Oerter, H., Parrenin, F., Raisbeck, G., Raynaud, D., Schilt, A., Schwander, J., Selmo, E., Souchez, R., Spahni, R., Stauffer, B., Steffensen, J. P., Stenni, B., Stocker, T.F., Tison, J. L., Werner, M., and Wolff, E. W., 2007. Orbital and millennial Antarctic climate variability over the last 800 000 years. *Science* v.317, p.793–796.
- Kawamura, K., Parrenin, F., Lisiecki, L., Uemura, R., Vimeux, F., Severinghaus, J. P., Hutterli, M. A., Nakazawa, T., Aoki, S., Jouzel, J., Raymo, M. E., Matsumoto, K., Nakata, H., Motoyama, H., Fujita, S., Goto-Azuma, K., Fujii, Y., and Watanabe, O., 2007. Northern Hemisphere forcing of climatic cycles in Antarctica over the past 360,000 years. *Nature* v. 448, p.912-916.
- Kerr, R. A., 1998. Global change: Signs of past collapse beneath Antarctic ice. *Science* v. 281, p.17.
- Krissek, L.A., Browne, G.H., Carter, L., Cowan, E.A., Dunbar, G.B., McKay, R.M., Naish, T., Powell, R., Reed, J., Wilch, T.I and the Andrill MIS Science Team 2007. Sedimentology and Stratigraphy of the AND-1B Core, ANDRILL McMurdo Ice Shelf Project, Antarctica. *Terra Antarctica* v.14, p.185-222.
- Lisiecki, L. E., and M. E. Raymo, M.E., 2005. A Pliocene-Pleistocene stack of 57 globally distributed benthic $\delta^{18}\text{O}$ records. *Paleoceanography* v.20, PA1003, doi:10.1029/2004PA001071.
- MacAyeal, D. R., Okal, E. A., Aster, R. C., Bassis, J. N., Brunt, K. M., Cathles, L. M., Drucker, R., Fricker, H. A., Kim, Y.-J., Martin, S., Okal, M. H., Sergienko, O. V., Sponsler, M. P., and Thom, J. E., 2006. Transoceanic wave propagation links iceberg calving margins of Antarctica with storms in tropics and Northern Hemisphere. *Geophysical Research Letters* v. 33, L17502, doi:10.1029/2006GL027235.
- MacAyeal, D.R., 1992. Irregular Oscillation of the West Antarctic Ice Sheet. *Nature* v. 359, p.29-32.
- McKay, R.M., Dunbar, G.B., Naish, T., Barrett, P.J., Carter, L., and Harper, M., 2008. Retreat history of the Ross Ice Sheet (Shelf) since the Last Glacial Maximum from deep-basin sediment cores around Ross Island. *Palaeogeography, Palaeoclimatology, Palaeoecology* v.260, p 168-183.
- Mercer, J. H., 1978. West Antarctic ice sheet and CO₂ greenhouse effect; a threat of disaster. *Nature* v.271, p.321-325.

- Miller, K. G., Fairbanks, R.G., and Mountain, G.S., 1987. Tertiary Oxygen Isotope Synthesis, Sea Level History, and Continental Margin Erosion. *Paleoceanography* v.2, p.1–19.
- Miller, K.G., Kominz, M.A., Browning, J.V., Wright, J.D., Mountain, G.S., Katz, M.E., Sugarman, P.J., Cramer, B.S., Christie-Blick, N., Pekar, S.F., 2005. The Phanerozoic record of global sea-level change. *Science* v.312, p.1293–1297.
- Naish, T.R., Powell, R.D., Levy, R.L., and the ANDRILL science team, 2007. AND-1B Initial Science Results, ANDRILL McMurdo Ice Shelf Project. *Terra Antarctica* v.14, p.113–328.
- Neumann, A. C., and Hearty, P. J., 1996. Rapid sea-level changes at the close of the last interglacial (Substage 5e) recorded in Bahamian island geology. *Geology* v. 24, p.775–778.
- Niessen F., Magens D., Gebhardt A.C. and the ANDRILL-MIS Science Team, 2007. Physical Properties of the AND-1B Core, ANDRILL McMurdo Ice Shelf Project, Antarctica. *Terra Antarctica* v.14, p.155–166.
- North Greenland Ice Core Project members, 2004. High-resolution record of Northern Hemisphere climate extending into the last interglacial period *Nature* v. 431, p.147–151.
- Oppenheimer, M., 1998. Global warming and the stability of the West Antarctic Ice Sheet. *Nature* v.393, p.325–332.
- Payne, A.J., Vieli, A. Shepherd, A.P. Wingham, D.J., and Rignot, E., 2004. Recent dramatic thinning of the largest West Antarctic ice stream triggered by oceans. *Geophysical Research Letters* v.31, doi:10.1029/2004GL021,284.
- Petit, J. R., Jouzel, J., Raynaud, D., Barkov, N. I., Barnola, J. M., Basile, I., Bender, M., Chappellaz, J., Davis, M., Delaygue, G., Delmotte, M., Kotlyakov, V. M., Legrand, M., Lipenkov, V. Y., Lorius, C., Pepin, L., Ritz, C., Saltzman, E., and Stievenard, M., 1999. Climate and atmospheric history of the past 420,000 years from the Vostok ice core, Antarctica. *Nature* v. 399, p.429–436.
- Powell, R. D., and Alley, R. B., 1997. Grounding-line systems; processes, glaciological inferences and the stratigraphic record. In: Barker, P. F., and Cooper, A. K., (eds.) *Geology and seismic stratigraphy of the Antarctic margin 2. Antarctic Research Series* v. 71, p.169–187.
- Powell, R. D., and Cooper, J. M., 2002. A glacial sequence stratigraphic model for temperate, glaciated continental shelves. *Geological Society of London Special Publications* v.203, p.215–244.
- Powell, R.D., and Molnia, B., 1989. Glacimarine sedimentary processes, facies and morphology of the south-southeast Alaska shelf and fjords. *Marine Geology* v. 85, p.359–390.
- Raymo, M. E., Lisiecki, L. E., and Nisancioglu, K. H., 2006. Plio-Pleistocene ice volume, Antarctic climate, and the global $\delta^{18}\text{O}$ record. *Science* v. 313, p.492–495.
- Rignot, E., Casassa, G., Gogineni, P., Krabill, W., Rivera, A., and Thomas, R., 2004. Accelerated ice discharge from the Antarctic Peninsula following the collapse of Larsen B ice shelf. *Geophysical Research Letters* v.31, L18401, doi:10.1029/2004GL020697.

- Scherer, R. P., Aldahan, A. A., Tulaczyk, S., Possnert, G., Engelhardt, H., and Kamb, B., 1998. Pleistocene collapse of the West Antarctic ice sheet. *Science* v. 281, p.82-85.
- Scherer R., Hannah M., Maffioli P., Persico D., Sjunneskog C., Strong C.P., Taviani M., Winter D. and the ANDRILL-MIS Science Team., 2007. Palaeontologic Characterisation and Analysis of the AND-1B Core, ANDRILL McMurdo Ice Shelf Project, Antarctica. *Terra Antartica* v.14, p.223-254.
- Scherer, R. P., Bohaty, S.M., Dunbar, R.B., Esper, O., Flores, J-A., Gersonde, R., Harwood, D.M., Roberts, A.P., and Taviani, R., 2008. Antarctic records of precession-paced insolation-driven warming during early Pleistocene Marine Isotope Stage 31. *Geophysical Research Letters*, v.35, L03505, doi:10.1029/2007GL032254.
- Schoof, C. 2007. Ice sheet grounding line dynamics: steady states, stability and hysteresis. *Journal of Geophysical Research* v.112, F03S28, doi:10.1029/2006JF000664.
- Shackleton, N. J., 2000. The 100,000-year ice-age cycle identified and found to lag temperature, carbon dioxide, and orbital eccentricity. *Science* v. 289, p.1897-1902.
- Sjunneskog, C., and Scherer, R. P., 2005. Mixed diatom assemblages in glacial sediment from the central Ross Sea, Antarctica. *Palaeogeography, Palaeoclimatology, Palaeoecology* v. 218, p.287-300.
- Stuiver, M., Denton, G. H., Hughes, T. J., Fastook, J. L., 1981. History of the marine ice sheet in West Antarctica during the last glaciation; a working hypothesis. In: Denton, G. H., and Hughes, T. J. (eds.) *The last great ice sheets*, p.319-436.
- Thomas, R. H. and Bentley, C. R., 1978. A Model for Holocene Retreat of the West Antarctic Ice Sheet. *Quaternary Research* v.10, p.150–170.
- Vaughan, D. G., and Arthern, R., 2007. Why is it hard to predict the future of ice sheets? *Science* v. 315, p.1503-1504.
- Ward, B. L., and Webb, P.-N., 1986. Late Quaternary foraminifera from raised deposits of the Cape Royds-Cape Barne area, Ross Island, Antarctica. *Journal of Foraminiferal Research* v. 16, p.176-200.
- Wilson, G., Levy, R., Browne, G., Dunbar, N., Florindo, F., Henry, S., Graham, I., McIntosh, W., McKay, R., Naish, T., Ohneiser, C., Powell, R., Ross, J., Sagnotti, L., Scherer, R., Sjunneskog, C., Strong, C.P., Taviani, M., Winter, D., and the ANDRILL MIS Science Team, 2007. Preliminary integrated chronostratigraphy of the AND-1B core, ANDRILL McMurdo Ice Shelf Project, Antarctica. *Terra Antartica* v.14, p.297-316.

CHAPTER 5

Sand provenance of the AND-1B drill core

Abstract

The detrital sand grain mineralogy of the Late Cenozoic glacimarine sequences in the AND-1B drill core documents changes in provenance during discrete glacial and interglacial phases of Milankovitch duration cycles. However, there is also a provenance shift from a composition that contains higher abundances of rounded quartz indicative of the Beacon Supergroup (above 80 mbsf), to one that has a more subdued Beacon Supergroup signal. This up-core change at ~0.8 Myr reflects a change in the source or volume of ice derived from Transantarctic Mountain outlet glaciers to the south of the drill site. This change in ice source or volume may be influenced by changes in paleogeography resulting from Plio-Pleistocene volcanic cone building or alternatively, changes in the volume of outlet glaciers passing through the Transantarctic Mountains into the Ross Embayment during glacial maxima – or it may represent a combination of both.

5.1 Introduction

The AND-1B drill core site is currently situated beneath the McMurdo Ice Shelf in a ~900 m deep basin and is surrounded by several large volcanic islands (Figure 66). Sedimentary processes at the drillsite have been influenced by numerous changes in the configurations of glacial extent and thermal regime of the ice sheet, and tectonic activity, as well as the evolution of late Neogene and Quaternary volcanism, that have occurred at drillsite over the past ~13 Myr.

The sand grain (63-500 μm) petrology in the AND-1B region for the LGM to Holocene gravity cores (presented in Chapter 2) highlight the changes in provenance that can occur over a single glacial termination. Typically, Transantarctic Mountain detritus is transported within the basal debris layer of grounded ice during glacial maxima and the initial phase of glacial retreat. During glacial minima, deposition beneath the McMurdo Ice Shelf results in starvation of Transantarctic Mountain detritus at the drillsite, while fine-grained McMurdo Volcanic Group detritus dominates. In open water conditions, such as occurs the Lewis Basin in the present-day Ross Sea, some Transantarctic Mountains lithologies are carried into the region as

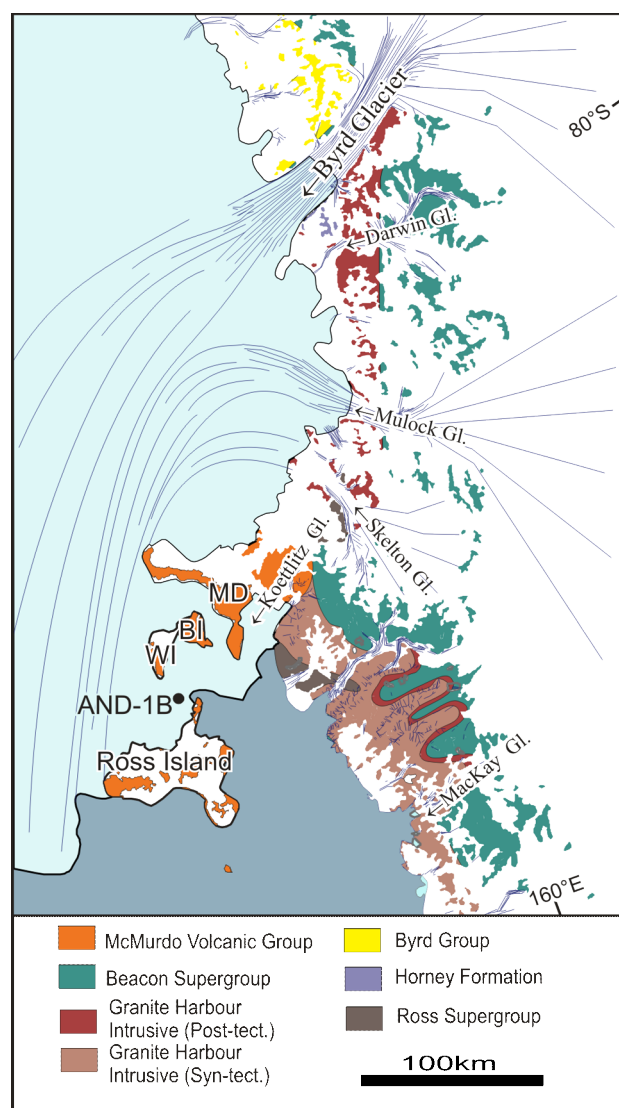


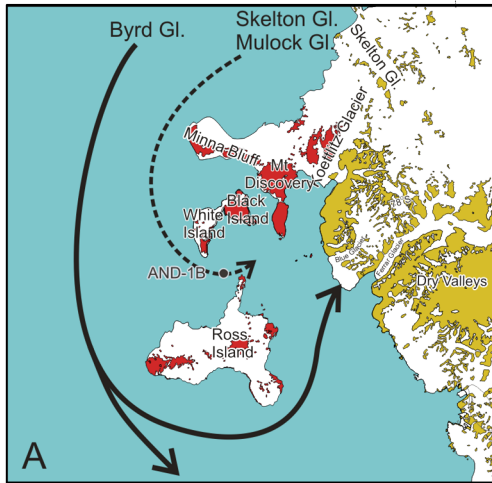
Figure 66: Geological map (after Craddock 1970 and Borg *et al.*, 1989). Also shown are present day glacial flow lines of major outlet glaciers into the Ross Ice Shelf (after Fahnestock *et al.*, 2000; and Drewry, 1983) including inferred catchments (based on elevation data of Drewry, 1983). Table 1 provides details on characteristic minerals derived from the bedrock geology.

a component of Iceberg Rafted Debris from outlet glaciers calving into the Ross Sea, together with volcanic detritus derived from glaciers draining off the local volcanic islands (Chapter 2).

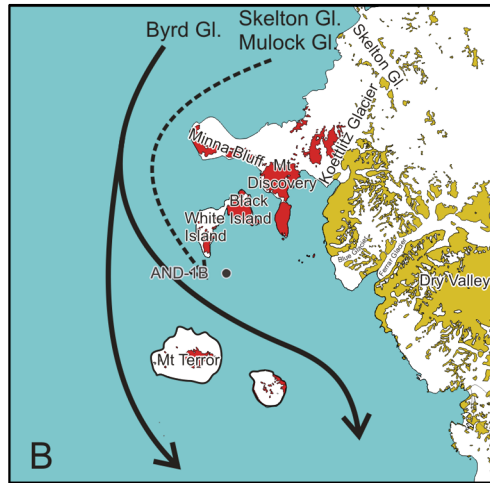
In this chapter, a number of complexities are evaluated that complicate this relatively simplistic provenance signal. The emergence of major volcanic centres during deposition of the drill core is likely to have altered past glacial flow-line pathways. (Figure 67). The most notable of these volcanic emergences are Mt Bird at ~4.6 Myr (Wright and Kyle, 1990a), Mt Terror at ~1.75 Myr (Wright and Kyle, 1990b), and Hut Point Peninsula and Mt Erebus at ~1.3 Myr (Esser *et al.*, 2004). White Island dates back to 7.65 Myr, but its northern margin is as young as 0.17 Myr (Cooper *et al.*, 2007). Minna Bluff formed between 11 and 7.26 Myr, but contains a large unconformity at ~10 Myr that is the presumed result of glacial overriding at this time

VOLCANIC EVOLUTION/PALAEOGEOGRAPHY MECHANISM

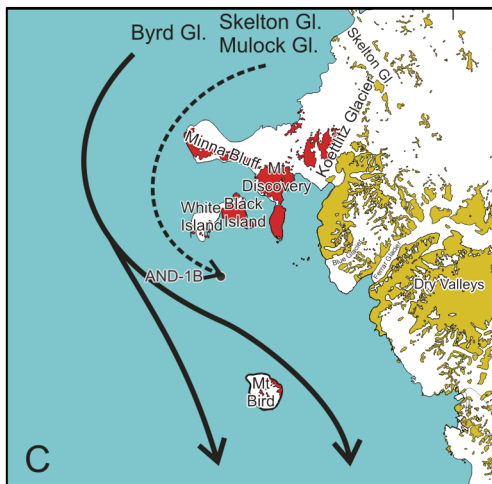
Present day



~1.5 Myr



~2 Myr



~10 Myr

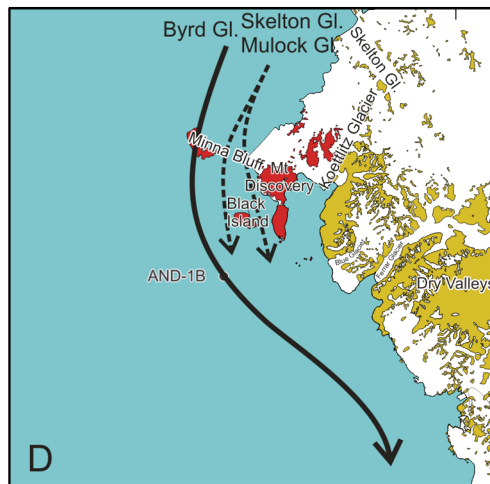


Figure 67: Paleogeography reconstructions based on the known chronology of volcanism in the McMurdo region (Wright and Kyle, 1990a,b,c; Esser *et al.*, 2004; Cooper *et al.*, 2007). Black arrows represent hypothesised glacial flowlines for grounded ice advance from Transantarctic Mountain outlet glaciers as discussed in text. The reconstruction at 10 Myr accounts for glacial overriding of a smaller Minna Bluff, which is documented by an erosional unconformity (Wright and Kyle 1990c).

(Wright and Kyle, 1990c). This chapter questions how changes in paleogeography can influence sediment provenance and glacial flowlines during glacial maxima. It also identifies the competing influences of changing geography and ice volume on sediment composition during past glacial maxima.

Changes in glacial volume over either West or East Antarctica may alter the flow-line paths of Transantarctic Mountain outlet glaciers that feed into the Windless Bight Basin. Conceptually, a thicker WAIS may result in diverting more ice derived from

the Byrd Glacier region, rather than the Mulock or Skelton Glaciers, into the vicinity of AND-1B (Figure 68).

Licht *et al.* (2005) presented a provenance study of tills in the Ross Sea and comparing them to till samples from West Antarctica and the Transantarctic Mountains outlet glaciers. This study concluded that tills deposited in the Central Ross Sea were deposited at the convergence of East and West Antarctic Ice Sheet derived ice (i.e., a similar scenario to Figure 68B), indicating that southern Transantarctic Mountain outlet glaciers are the probable source for sediments in AND-1B.

5.2 Methods

A total of 79 thin sections, from the entire AND-1B drill core were analysed from the sand fraction (63-500 μm) following grain size analysis. Methodology for preparing the thin sections was identical to that in Chapter 2. Following preparation of the grain mount thin sections, modal petrographic analysis (300 grain point count) for the 63-500 μm fraction was undertaken. However, groupings for modal analysis were slightly different than Chapter 2, due to the different objective of this study. Due to the rigorous disaggregating during grain size processing in most samples, sandstones composed of intraclasts were not disaggregated – as they were generally

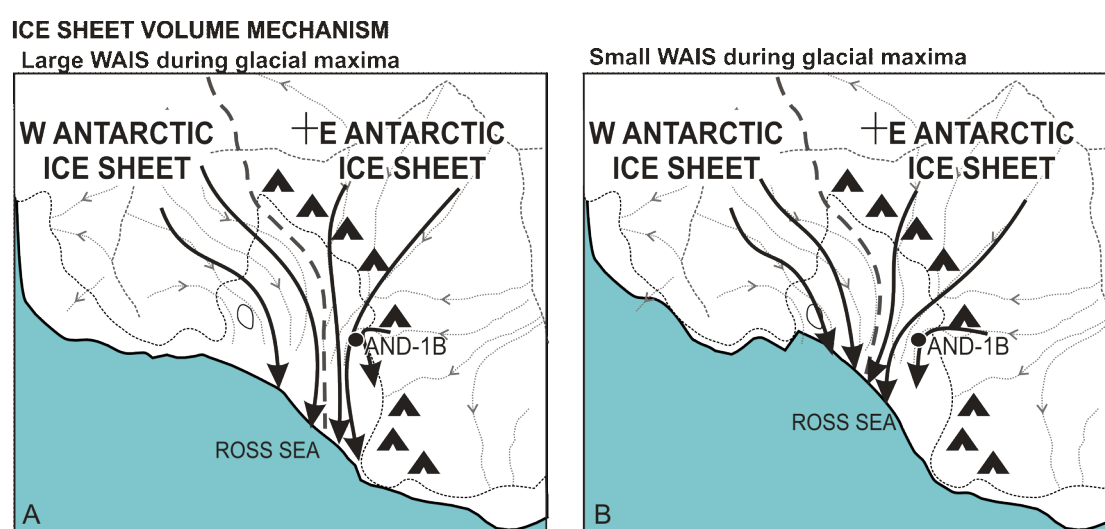


Figure 68: Hypothesised effect on glacial flowlines for two different glacial maxima scenarios, where the relative contribution of East versus West Antarctic Ice Sheets to glacial advance in the Ross Embayment is changed. Under the scenario of a smaller and thinner WAIS, East Antarctic Ice Sheet flow-lines may extend further into the central Ross Sea.

unconsolidated and represent the original depositional grain size. Diamictite or mudstone intraclasts were not counted as they mostly removed during grain-size processing, and to maintain consistency, if they were present they were not counted. The abundances of rock fragments and minerals characterised in these counts are summarised in Table 14.

The most notable change from Chapter 2 was the division of quartz into four sub-categories (angular, rounded, rounded with overgrowths, and metamorphic quartz). Quartz was the most distinctive indicator of the Transantarctic Mountains provenance in Chapter 2, as it is absent in the McMurdo Volcanic Group (Kyle, 1990). Rounded quartz with overgrowths can be directly attributed to Devonian Taylor Group (Beacon Supergroup) sandstones (Korsch, 1974), while metamorphically shocked quartz is attributed to metasediments of the Ross Supergroup or syn-tectonic plutons of the Granite Harbour Intrusive Complex (Gunn and Warren, 1962). Rounded Quartz is likely to also be derived from the Beacon Supergroup. Angular quartz can be attributed to any of these groups.

5.3 Results

The results and the provenance of any given sample is highly facies dependent (Table 14) as was noted in Chapter 2. Diamictite facies tend to contain abundant Transantarctic Mountain detritus, whereas open marine diatomites are rich in volcanic detritus (Table 14). Figure 69 shows the down core variability of volcanic grains relative to facies. The sand fractions in the diatomite samples (yellow data points) contain ~50% or more volcanic glass and lithics, whereas diamictite samples (green data points), with rare exceptions, contain less than 25% volcanic lithics or glass (Figure 69).

Mudstone (dark grey) and mudstone with dispersed clasts (light grey) change composition down core, with samples above 150 mbsf generally containing >25 % volcanic grains, well above the base level for the diamictite samples. Below 150 mbsf, abundances are generally <25% and more closely mirror abundances in the diamictite facies (Figure 69).

Due to the dominance of feldspar and volcanic grains in many of the samples, the majority of mineral assemblages have abundances of <5%, making it difficult to identify statistically significant trends from most mineral or lithic groups. However, quartz usually constitutes between ~10%-30% (Table 14) in the diamictite facies. Figure 69 shows a depth plot for the ratio of Qr (rounded quartz with overgrowths and rounded quartz) to Qa (angular quartz), which allows for identification of provenance signal that is not affected by the abundance of volcanic grains. Above 80 mbsf, the ratio in all but one diamictite sample exceeds 0.2, while below 80 mbsf it never exceeds 0.2 in the diamictite samples.

5.4 Discussion

5.4.1 Long-term provenance signal shifts in diamictite facies

Above ~80 mbsf, the significantly higher proportion of rounded quartz grains (many of which display overgrowths; Table 14) indicates an increase contribution from Devonian Beacon Supergroup sediments. This result agrees strongly with the initial petrology results of the clasts presented in Pompilio (2008) where there is a consistent increase in the abundance of dolerite above 82.74 mbsf. Ferrar Dolerite crops out as sills that intrude Beacon Supergroup sediments in the Transantarctic Mountains (Tingey, 1991). Therefore, an increase in Beacon Supergroup is expected to be associated with an increase in Ferrar Dolerite clasts. Dolerite lithics and pigeonite, a pyroxene characteristic of the Ferrar Dolerite, were noted in the sand fraction, but were rare (<2.3%) in all samples, and no statistically significant trend is observed.

The abundance of quartz in the diamictite facies of the upper 80 m averages ~30%. This value is consistent with quartz abundances from LGM (and retreat-phase) diamictites from the McMurdo region, which range between 30-37% for cores immediately north of Ross Island (Licht *et al.*, 2005; Chapter 2) and from beneath the McMurdo Ice Shelf (Chapter 2). This suggests flow-line paths for periods of grounded ice during the Late Pleistocene (past 0.8 Myr) where similar to those of the LGM throughout the deposition of the diamictites in upper 80 m of the AND-1B drill core.

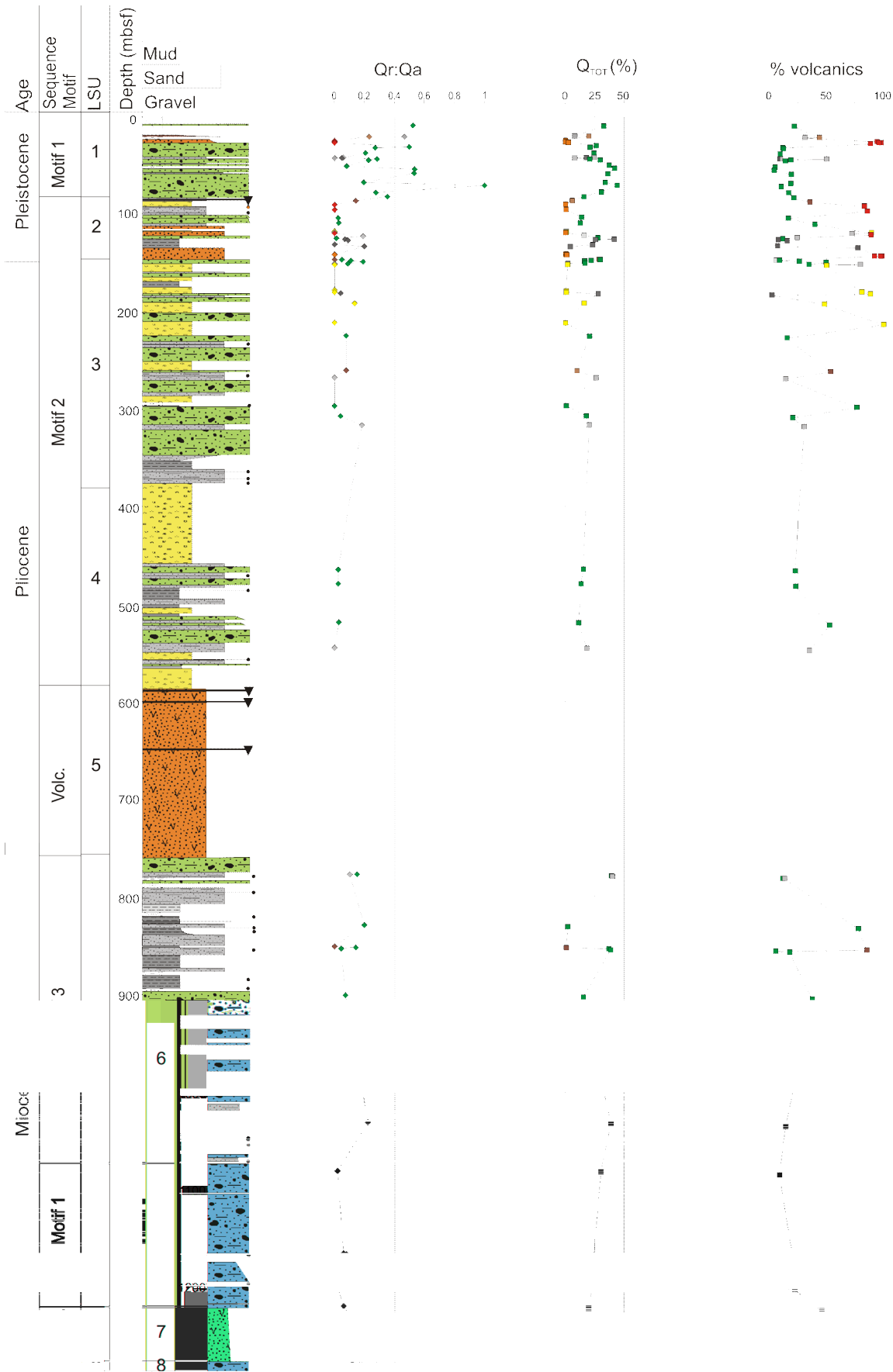


Figure 69: Sequence motifs, Lithostratigraphic Units (LSU) and the lithologic log of AND-1B plotted alongside (left to right): Ratio of Qr (rounded quartz and quartz with overgrowths) to Qa (angular quartz), percentage Q_{TOT} (total quartz grains); and percentage volcanic grains (volcanic lithics and glass). Legend for lithological units is provided in Figure 37.

The increased Beacon Supergroup quartz signal for the upper 80 m suggests that grounded ice during glacial maxima was sourced from the Mulock/Skelton Glacier catchments. The Mulock and Skelton Glacier catchments are contained within a region where the rock strata are known to be dominated by Beacon Supergroup (Craddock, 1970; Figure 66), before overriding over ~30-40 km of Granite Harbour Intrusive Complex and Ross Supergroup (metasediments) outcrops, and passing into the Ross Ice Shelf. In contrast, the catchment of the Byrd Glacier (further south) is significantly larger (Figure 68) and while the bedrock beneath this catchment is largely unknown, the outlet glacier itself predominantly cuts through Granite Harbour Intrusive Complex and Byrd Group (limestone, marble and sedimentary strata) (Craddock, 1970; Figure 66). Till samples studied by Licht *et al.* (2005) from the southern margin of lower Byrd Glacier contain only 5.6% quartz, and 70% calcite, which appear to be representative of the adjacent Byrd Group strata. The Darwin and Hatherton Glaciers, two smaller outlet glaciers immediately to the north of the Byrd Glacier also have catchments that override Beacon Supergroup, and could potentially contribute to the provenance signal observed in the upper 80 m, but relative to the Mulock and Byrd glaciers, the present volume of ice derived from these glaciers is minor.

A provenance from the Mulock/Skelton Glaciers region throughout most AND-1B is also inferred by Talarico *et al.* (2007), who noted that low-grade metasediments, and granite clasts dominate the clast assemblage of this interval of the AND-1B drill core, as well as higher abundances of dolerite clasts. They attributed these metasediments as being sourced from phyllites and low-grade meta-sandstones from the Skelton Group (Ross Supergroup; Figure 66), where the only known outcrops occur between the Skelton and Mulock Glacier.

Below 80 mbsf, the provenance signal is more difficult to determine from the sand fraction. It is clear there is a decrease in Beacon Supergroup quartz, but not an overall decrease in the total abundance of quartz (Figure 69), which is suggestive of an increasing contribution from the Granite Harbour Intrusive Complex. However, the clast data still indicate a Skelton/Mulock Glacier source for most of the Pliocene (Talarico, written communication 2008). The decrease in rounded quartz abundance in the sand fraction below 80 mbsf could represent a change in the relative

contribution of ice sourced from the Mulock or Skelton Glaciers, but geological mapping of the Beacon Supergroup is not of high enough resolution to confirm this possibility. Alternatively, it may be indicative of a thinner EAIS, as this would result in ice entraining stratigraphically lower bedrock, in this case the Granite Harbour Intrusive Complex, underlying the Beacon Supergroup in the Skelton/Mulock Glacier region (Craddock, 1970). In all cases, diamictite deposits interpreted as subglacial till are probably sourced from southern Transantarctic Mountain glaciers, as glaciological models require large-scale expansion of the WAIS in order to deflect southern Transantarctic Mountain outlet glacier ice around Minna Bluff into the AND-1B region (Denton and Hughes, 2002; MacAyeal *et al.*, 1996).

Based on this change in provenance at ~80 msbf, some broad inferences can be made regarding the cause for the change in glacial flowlines during glacial maxima. The depositional processes (Motif 1) responsible for the upper 80 m of AND-1B subglacial strata are likely to be similar to those in Motif 1 from the Mid to early Late Miocene interval of the core (i.e., 1083-1285 mbsf; Chapter 3). Motif 1 is inferred to represent glacial advance of similar magnitudes during deposition of both these intervals. However, unlike the Pleistocene, diamictites in sequences in the Mid to Late Miocene section of core display no increase in Beacon Supergroup-derived quartz, but do contain metasedimentary clasts indicative of the Byrd region (Talarico *et al.*, 2007). The emergence of volcanic islands during the Late Miocene, Pliocene and Quaternary probably had a significant influence on the glacial flowlines orientation over the drill site. In the absence of Ross Island during the Late Miocene, and a smaller Minna Bluff that is overridden by ice during glacial maxima, ice derived from the Byrd Glacier is more likely to flow through the AND-1B drill site (e.g., Figure 67D).

In addition to this, Motif 1 sequences in the early Late Miocene part of the core occur around the time of (or just after) the formation of Minna Bluff (~11 Myr), and there is also a significant glacial unconformity at Minna Bluff at ~10Myr, suggesting that ice flowed over Minna Bluff at this time (Wright and Kyle, 1990c). White Island had probably yet to emerge at this time (Cooper, 2007), and Black Island was probably smaller in size (Wright and Kyle, 1990c). Both of these factors may have resulted in an increased flux of ice derived from the Byrd Glacier region. Deposition of the sequences

above 80 mbsf, coincides with the final phase of the emergence of Ross Island, and the first phase of subaqueous volcanism beginning on Mt Erebus and Hut Point Peninsula just prior to ~1.3 Myr (Kyle 1981; Esser *et al.*, 2004). The development of a larger Ross Island conceivably results in diverting most of the Byrd Glacier to the east of Ross Island (Figure 67A). This agrees well with flow-line reconstructions of Denton and Hughes (2000).

Inferences of changes in the past volume of the WAIS based on sand fraction provenance alone is difficult as changes in local paleogeography may have a significant influence on provenance during glacial maxima. Improved chronology of the volcanic evolution in the McMurdo region should help to resolve some of the uncertainties presented here. In the meantime, numerical models need to be developed to test these hypotheses for past glacial flowlines, and should take into account changes in paleogeography as well as the relative ice fluxes from East and West Antarctica.

5.4.2 *Glacial to interglacial variability*

Figure 70 shows a log of the sand fraction petrology results for upper 150 m of AND-1B, with respect to glacial-marine sequences outlined in Chapter 3. It highlights provenance variability through individual glacial/interglacial cycles. However, not all glacial minima contain the same provenance signal. For example, the glacial minima facies (at ~25 mbsf) in Sequence 2 are characterised almost entirely by volcanic glass before passing upwards in proglacial mudstone and sandstone that have a similar proportion of quartz as the overlying diamictite in Sequence 1. The glacial minima facies in Sequence 3 contains quartz throughout, and although there is an increase in volcanic lithics and glass, it is not the dominant provenance signal, suggesting a relatively closer proximity to the ice sheet grounding line throughout the glacial minima.

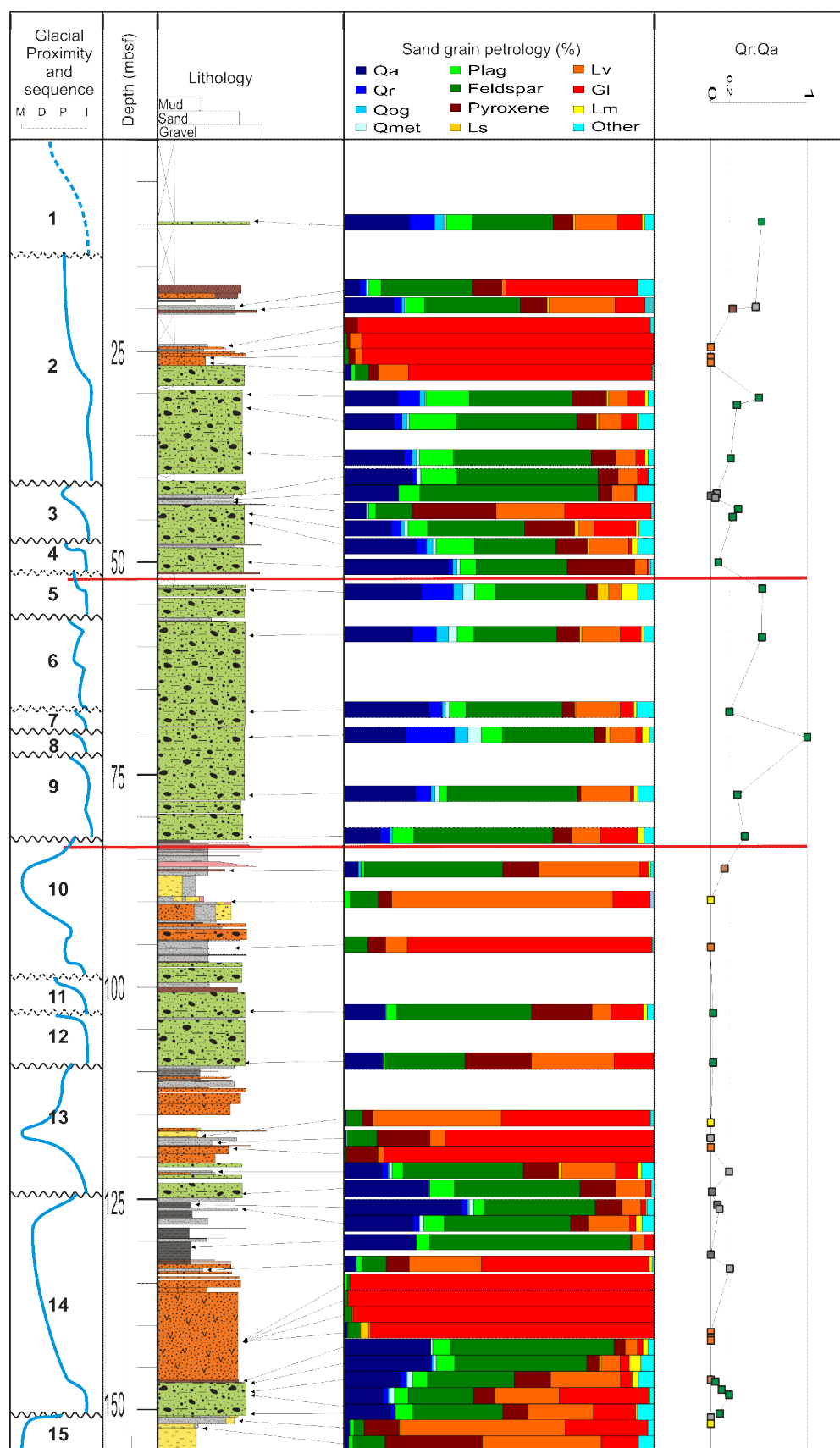


Figure 70: Petrographic results for the upper 150 m of the AND-1B drill core. Also shown is the sequence stratigraphy model present in Chapter 3 showing the transition from marine(m) to ice distal (d), ice proximal (p) and ice contact/subglacial (i) deposition. Legend for lithological units is provided in Figure 37.

During deposition of the open-water diatomites in Sequences 10, 13 and 15, the sand fraction is dominated by well-preserved volcanic lithics and glass, which is similar to Pliocene diatomite, again indicating that iceberg rafting at the drillsite was mostly influenced by calving either from (proto-)Ross Island glaciers, or from the Koettlitz Glacier near the base of Mt. Discovery and Mt. Morning. These glaciers are expected to expand during open water conditions as they have low-altitude catchments, and therefore open water conditions in the McMurdo region would provide increased precipitation.

The diamictite at the base of Sequence 14 has a consistent provenance signal throughout, and this provenance signal continues through to the sandstone unit that caps it. This sandstone contains abundant mudstone and diamictite intraclasts. Unlike the diamictite samples, clasts in this sandstone were not disaggregated, as their grain size was clearly a product of the depositional processes (e.g., cross-rippled, well sorted sandstone; Chapter 3). However, to maintain consistency, these intraclasts were not included in the modal analysis, but visual estimate places their abundance at ~30-40%. Despite this, the provenance of this sandstone is almost identical with that of the underlying stratified diamictite indicating that it associated with grounding line processes, and supports the tidal pumping mechanism for this deposit (discussed in Chapter 4). This sandstone is overlain by a series of volcanic sands consisting almost entirely of angular and vesicular volcanic glass. The mudstone overlying the volcanic sandstone shows a similarity in provenance to that of the diamictite at the base of Sequence 14, as well as the diamictite in the overlying Sequence 13. This similarity in provenance to the overlying diamictite suggests that the mudstones in the upper part of Sequence 14 were probably the product of grounding-line processes associated with glacial re-advance, rather than the fine grained, distal component of volcanic sediment flows associated with the underlying volcanic sandstone.

5.5 Conclusions

- The diamictite and proglacial mudstone-rich facies in the upper 150 m of the AND-1B display a consistent provenance signal that has a notable quartz component and limited volcanic grains. However, the sequences with thicker glacial minima successions contain volcanic sandstone that are dominated by angular volcanic glass.
- The sand fraction in the diatomites units indicate that deposition of clastic detritus during open water conditions at the drillsite is dominated by volcanic lithics, with a minor granite component. This is likely to have been the result of icebergs calving from outlet glaciers off an early Ross Island and the terminus of the ancestral Koettlitz glacier.
- Above 80 mbsf, there is a distinct increase in the Beacon Supergroup provenance signal. From the available data it is difficult to ascertain an exact source area, but it is consistent with rock outcrops exposed in the catchments of the Mulock/Skelton Glacier. The final phase of volcanic cone building in the McMurdo Region during the Quaternary coincides with a significant shift in the provenance signal of AND-1B at ~80 mbsf. Changes in paleogeography throughout the Neogene and Quaternary may complicate any climate signal that may be observed in the provenance signal.
- The provenance signal in the sand fraction of glacial maxima diamictites is consistent with the clast abundance data (Talarico *et al.*, 2007) that indicates a Mulock/Skelton Glacier source.

sample (mbsf)	Facies no.	Qa	Qr	Qog	Qmet	Plag	Ls	Lm	Dolerite + Pigeonite	granite+ microcline	Feldspar	Pyroxen e	Lv	Glass	other
9.99	10	21.0	8.0	3.0	0.7	8.7	0.7	1.0	0.3	1.7	25.7	6.3	13.7	7.7	1.7
20.01	4	5.0	2.0	0.3	0.7	4.0	0.0	0.0	0.3	0.3	29.3	9.3	1.3	42.3	5.0
20.27	3	16.0	2.7	1.0	0.3	6.0	0.7	0.7	0.3	0.3	31.0	8.7	21.3	9.7	1.3
24.73	4	0.0	0.0	0.0	0.0	0.0	0.0	0.0	0.0	0.0	0.0	4.3	0.0	94.3	1.3
25.93	3	0.0	0.0	0.0	0.0	0.3	0.0	0.0	0.0	0.0	0.7	1.0	3.7	94.0	0.3
25.96	3	0.0	0.0	0.0	0.0	0.3	0.0	0.0	0.0	0.0	1.3	2.0	2.3	93.7	0.3
26.53	3	2.3	0.0	0.0	0.0	1.3	0.0	0.0	0.0	0.0	4.3	3.0	9.7	78.7	0.7
30.07	10	17.3	7.0	1.7	0.3	14.0	0.7	1.0	0.3	1.0	33.0	11.0	6.3	5.3	1.0
31.63	10	16.0	2.7	1.7	0.7	15.3	0.7	0.7	0.3	0.7	38.7	6.3	7.3	5.0	4.0
37.87	10	19.3	2.7	1.3	1.0	11.0	0.0	1.0	0.7	0.7	44.3	8.0	6.3	3.0	0.7
42.10	4	22.0	1.3	0.0	1.3	11.7	0.0	0.0	0.3	0.7	45.3	6.3	6.3	3.3	1.3
42.36	2	17.7	0.0	0.0	0.0	6.7	0.0	0.0	0.7	0.0	57.3	4.3	7.3	0.7	5.3
42.58	4	7.0	0.3	0.0	0.7	2.3	0.3	0.0	0.0	0.3	11.7	27.0	22.3	27.7	0.3
43.86	9	15.1	3.3	1.0	1.3	6.3	1.3	1.0	0.3	2.0	31.3	16.1	4.9	13.5	2.6
44.84	9	23.3	3.3	2.0	1.0	12.3	0.7	2.0	0.7	3.0	26.3	10.0	12.7	1.0	1.7
50.14	10	33.7	1.3	1.3	1.0	5.3	0.0	0.3	0.0	0.0	29.3	21.7	4.0	0.7	1.3
53.23	9	25.0	10.3	3.0	3.7	6.7	3.7	5.3	2.0	1.7	29.3	3.7	4.0	0.0	1.7
58.97	9	22.0	7.7	4.0	2.7	5.3	0.7	1.0	1.0	1.0	26.7	7.3	12.3	6.7	1.7
67.80	10	27.3	4.3	1.0	1.3	5.3	0.3	1.0	1.0	3.7	31.0	4.0	14.3	4.3	1.0
70.75	10	20.0	15.7	4.3	4.3	6.7	1.3	2.3	0.3	0.3	29.7	3.7	8.3	2.0	1.0
77.52	10	23.0	5.0	1.3	1.3	2.7	0.0	1.3	0.0	5.3	42.0	1.0	16.0	1.0	0.0
82.40	9	11.7	3.0	1.0	0.0	7.0	0.0	2.0	0.3	2.0	44.3	6.0	9.3	11.7	1.7
86.31	3	4.7	0.0	0.7	0.3	1.0	0.0	0.7	0.0	0.3	44.5	11.6	32.6	2.7	1.0
90.00	2	0.0	0.0	0.0	0.0	2.0	0.0	0.0	0.0	0.0	9.0	4.3	71.3	12.0	1.3
95.55	3	0.3	0.0	0.0	0.0	0.0	0.0	0.0	0.0	0.0	7.3	5.7	7.0	78.7	1.0
103.30	10	13.0	0.3	0.0	0.3	3.3	0.0	1.3	0.3	0.7	43.3	19.3	6.0	10.3	1.7
109.19	9	12.3	0.3	0.0	0.0	0.7	0.0	0.0	0.0	0.0	25.7	21.3	26.7	13.0	0.0
117.63	1a	0.7	0.0	0.0	0.0	0.0	0.0	0.0	0.0	0.0	5.3	3.3	41.3	48.0	1.3
118.62	3	0.7	0.0	0.0	0.0	0.7	0.0	0.0	0.0	0.0	9.3	17.0	5.0	67.3	0.0
119.15	6V	0.0	0.0	0.0	0.0	0.0	0.0	0.0	0.0	0.0	0.7	10.3	2.0	87.0	0.0
122.00	2	12.3	2.0	0.3	1.0	3.7	1.0	1.3	1.0	1.7	38.7	11.3	17.3	7.0	1.3
124.39	9	27.3	0.3	0.0	0.0	8.0	0.0	0.0	0.3	0.3	40.3	11.7	9.7	1.7	0.3
125.95	2	37.7	2.0	0.7	1.3	3.3	0.0	0.3	0.3	1.0	35.7	8.7	6.0	1.7	1.3
126.39	4+2	22.3	2.0	0.0	1.3	6.7	0.0	2.0	0.7	1.3	40.7	5.7	13.3	2.0	2.0
131.72	2	23.3	0.0	0.0	0.0	4.3	0.0	0.0	0.0	0.0	64.7	0.3	4.0	3.0	0.3
133.48	3	3.3	0.7	0.0	0.0	1.7	0.0	1.0	0.0	0.0	8.0	7.3	23.3	54.0	0.7
141.00	6V	0.3	0.0	0.0	0.0	0.7	0.0	0.0	0.0	0.0	1.0	0.0	0.0	98.0	0.0
141.58	6V	0.0	0.0	0.0	0.0	0.0	0.0	0.0	0.0	0.0	1.3	0.0	0.0	98.7	0.0
141.72	6V	0.0	0.0	0.0	0.0	0.0	0.0	0.0	0.0	0.0	2.7	0.0	0.3	97.0	0.0
141.84	6V	1.0	0.0	0.0	0.0	0.3	2.7	0.0	0.0	0.0	4.0	0.0	0.7	91.3	0.0
146.58	3	28.0	0.0	0.0	0.7	5.7	0.0	1.7	0.3	1.0	52.7	3.7	4.0	1.7	0.7
146.83	10	27.7	0.7	0.7	0.7	6.0	0.7	3.7	1.0	1.7	42.3	4.0	6.0	3.0	2.0
147.76	10	18.3	1.7	0.3	1.7	4.7	0.0	2.0	1.7	1.3	28.0	11.3	22.3	4.0	2.7

sample (mbsf)	Facies no.	Qa	Qr	Qog	Qmet	Plag	Ls	Lm	Dolerite + Pigeonite	granite+ microcline	Feldspar	Pyroxen e	Lv	Glass	other
148.32	10	12.7	1.7	0.7	1.3	4.3	0.0	0.3	0.7	0.7	21.0	7.0	20.7	28.7	0.3
150.42	9	15.0	1.3	0.0	0.3	5.7	0.0	0.7	0.3	1.3	29.0	8.0	21.0	13.7	3.7
150.95	4	2.0	0.0	0.0	0.0	1.3	0.3	0.0	0.0	0.0	3.3	11.3	53.0	26.7	2.0
151.71	1b	1.7	0.0	0.0	0.0	1.3	0.3	0.0	0.0	0.0	10.3	31.3	38.0	12.0	5.0
178.98	1a	0.7	0.0	0.0	0.0	1.3	0.0	0.0	0.0	0.0	9.7	7.0	64.3	16.7	0.3
180.38	1a	0.7	0.0	0.0	0.0	0.3	0.0	0.0	0.0	0.0	4.0	5.7	69.3	19.3	0.7
181.94	9	25.3	1.0	0.0	1.7	4.3	0.0	26.3	0.3	2.3	33.3	2.0	2.3	0.0	1.0
191.24	1b+10	12.3	1.7	0.0	2.0	2.3	0.0	1.0	0.3	1.3	18.3	11.7	37.0	11.3	0.7
211.74	1a	0.0	0.0	0.0	0.0	0.0	0.0	0.0	0.0	0.0	0.0	0.0	100.0	0.0	0.0
225.38	10	17.0	1.3	0.0	2.3	5.3	0.7	1.3	0.3	2.0	42.0	12.0	13.3	2.0	0.3
260.70	3	8.7	0.3	0.3	0.3	3.3	1.3	0.3	0.0	0.0	24.0	6.3	31.3	22.3	1.3
267.88	4	25.7	0.0	0.0	0.3	5.3	0.0	0.7	0.3	2.0	42.3	8.3	8.0	6.0	1.0
296.72	10	0.7	0.0	0.0	0.0	1.0	0.0	0.3	0.0	0.0	14.0	6.3	54.7	22.0	1.0
307.04	10	17.0	0.3	0.3	0.0	6.0	0.7	0.3	1.7	0.0	45.7	6.7	12.7	7.7	1.0
316.23	4	16.7	2.7	0.3	0.7	3.4	0.7	0.3	1.0	1.4	33.3	8.5	23.1	7.5	0.3
464.07	10	14.7	0.3	0.0	0.3	5.3	0.0	0.0	0.0	1.7	39.7	13.7	15.3	7.3	1.7
479.18	10	13.0	0.3	0.0	0.0	4.3	0.7	0.0	0.0	1.3	39.3	16.7	17.3	5.7	1.3
519.11	9	11.0	0.3	0.0	0.0	2.0	0.0	0.0	0.7	0.3	22.6	10.0	18.6	33.9	0.7
545.15	4	18.3	0.0	0.0	0.0	2.3	0.0	0.0	0.3	1.0	26.3	15.3	31.7	3.3	1.3
778.70	10	34.3	4.5	0.6	0.0	1.9	0.3	3.6	2.3	1.0	32.0	7.4	11.0	0.6	0.3
778.90	4	36.0	2.7	1.0	0.3	1.7	0.3	0.3	0.3	0.7	37.0	6.0	11.7	1.7	0.3
830.64	9	1.7	0.3	0.0	0.0	2.1	0.0	0.0	0.0	0.3	8.0	8.7	75.9	2.1	0.7
852.19	3	0.7	0.0	0.0	0.0	1.7	0.0	0.0	0.0	0.0	6.0	5.3	81.3	4.0	1.0
853.25	9	30.7	3.0	1.3	2.0	1.7	1.3	0.0	1.3	1.7	48.7	2.7	5.3	0.0	0.3
854.36	10	36.0	1.3	0.3	1.0	1.7	0.3	1.3	0.0	2.3	34.0	4.0	12.3	5.3	0.0
902.80	10	14.0	0.7	0.3	0.3	4.7	0.3	0.7	0.3	2.0	31.0	7.7	31.0	6.7	0.3
1032.47	6	31.7	6.3	0.7	0.3	7.0	0.3	0.0	0.0	1.7	37.0	0.3	10.3	4.0	0.3
1033.58	5	31.0	0.7	0.0	0.0	3.0	0.0	0.0	0.3	0.7	54.3	1.0	8.7	0.3	0.0
1167.68	10	21.7	0.3	1.0	1.3	8.3	0.7	0.0	0.0	3.3	38.7	3.3	19.3	1.7	0.3
1168.08	4	21.0	1.3	0.3	0.3	3.3	0.0	0.3	1.0	0.3	26.7	2.3	18.7	24.0	0.3
1196.18	10	15.9	0.0	0.0	0.0	6.3	1.6	0.0	0.0	0.0	54.0	4.8	12.7	3.2	1.6
1199.74	10	21.0	0.3	0.0	1.7	5.7	0.0	0.0	0.3	0.3	43.0	5.0	15.0	7.3	0.3
1221.80	7	16.7	1.0	0.0	2.0	1.0	0.0	0.3	0.3	2.0	26.3	4.3	17.3	28.7	0.0
1275.60	9	22.7	5.3	1.0	1.0	2.3	0.0	0.0	0.0	0.0	23.3	3.3	36.7	3.7	0.7
1280.20	9	22.6	2.7	0.0	0.7	5.0	1.7	0.3	0.0	1.7	54.5	2.7	6.3	1.3	0.7
1282.04	10	20.7	1.7	0.7	0.7	7.3	3.3	0.3	1.0	1.0	52.0	4.7	5.3	0.3	1.0

Table 14: Percentage data from modal analysis of sand fraction from AND-1B. Angular quartz (Qa), rounded quartz (Qr), rounded quartz with overgrowths (Qog), metamorphic quartz (Qmet), plagioclase (Plag), sedimentary lithics (Ls), metamorphic lithics (Lm), volcanic lithics (Lv). Other category includes Olivine, Kaesurite, Amphiboles, Marble, Opaque, Isotropic minerals, Biotite, Chlorite, Calcite and unidentified heavy minerals.

5.6 References

- Borg S.G., DePaolo D.J., Wendlandt E.D., Drake T.G., 1989. Studies of granites and metamorphic rocks, Byrd Glacier area. *Antarctic Journal of the United States* v.24, p.19–21.
- Cooper, A. F., Adam, L.J., Coulter, R.F., Eby, G.N., and McIntosh, W.C., 2007. Geology, geochronology and geochemistry of a basanitic volcano, White Island, Ross Sea, Antarctica. *Journal of Volcanology and Geothermal Research* v.165, p.189-216.
- Craddock, C., 1970. *Antarctic Map Folio Series* v.12.
- Denton, G. H., and Hughes, T. J., 2002. Reconstructing of the Ross Ice Drainage System, at the last glacial maximum. *Geografiska Annaler, Series A: Physical Geography* v.82, p.143-167.
- Drewry, D. J., 1983. Antarctica: Glaciological and geophysical folio: Cambridge, United Kingdom, University of Cambridge, Scott Polar Research Institute, 9 p.
- Esser R.P., Kyle P.R., and McIntosh W.C., 2004. $^{40}\text{Ar}/^{39}\text{Ar}$ dating of the eruptive history of Mount Erebus, Antarctica: Volcano evolution. *Bulletin of Volcanology* v.66, p.671–686.
- Fahnestock, M.A., Scambos, T.A., Bindshadler, R.A., and Kvaran, G., 2000. A millennium of variable ice flow recorded by the Ross Ice Shelf, Antarctica. *Journal of Glaciology* v.46, p.652-664.
- Gunn, B.M., and Warren, G., 1962. The Geology of Victoria Land from Mawson Glacier to Mulock Inlet. *NZ Geological Survey Bulletin* v.71, p1-157.
- Licht, K.J., and Fastook, J., 1998. Constraining a numerical ice sheet model with geologic data over one ice sheet advance/retreat cycle in the Ross Sea. *Chapman Conference on the West Antarctic Ice Sheet*, University of Maine. p.25–26.
- Licht, K.J., Lederer, J.R., and Swope, J., 2005. Provenance of LGM glacial till (sand fraction) across the Ross embayment, Antarctica. *Quaternary Science Reviews* v.24, p.1499-1520.
- Korsch, R. J., 1974. Petrographic comparison of the Taylor and Victoria groups (Devonian to Triassic) in South Victoria Land, Antarctica. *New Zealand Journal of Geology and Geophysics* v.17, 523-541.
- Kyle P.R., 1981. Mineralogy and geochemistry of a basanite to phonolite sequence at Hut Point Peninsula, Antarctica, based on core from Dry Valley Drilling Project Drillholes 1, 2 and 3. *Journal of Petrology* v.22, p.451–500.
- Kyle, P. R., 1990. McMurdo Volcanic Group, western Ross Embayment; introduction. In: Le Masurier and Thomson (eds.) *Volcanoes of the Antarctic Plate and southern oceans*. *Antarctic Research Series* v.48, p.19-25.
- MacAyeal, D. R., Rommelaere, V., Huybrechts, P., Hulbe, C. L., Determann, J., Ritz, C., 1996. An ice-shelf model test based on the Ross Ice Shelf. *Annals of Glaciology* v.23, p.46-51.
- Pompilio, M., Dunbar, N., Gebhardt, A., Helling, D., Kuhn, G., Kyle, P., McKay, R., Talarico, F., Tulaczyk, S., Vogel, S., Wilch, T., and the ANDRILL MIS Science Team. 2007. Petrology and Geochemistry of the AND-1B Core, ANDRILL McMurdo Ice Shelf Project, Antarctica. *Terra Antarctica* v.14, p.255-288.

- Talarico, F., Sandroni, S., and the ANDRILL-MIS Science Team, 2007. Clast Provenance and variability in MIS (AND-1B) core and their implications for the paleoclimatic evolution recorded in the Windless Bight - southern McMurdo Sound area (Antarctica). In: Cooper, A., and Raymond, C. (eds), *Antarctica; A Keystone in a Changing World--Online Proceedings for the 10th International Symposium on Antarctic Earth Sciences*. *U.S. Geological Survey Open-File Report* 2007-1047.
- Tingey, R.J., 1991. Mesozoic tholeiitic igneous rocks in Antarctica: the Ferrar (Super) Group and related rocks. In: Tingey, R. J. (ed.), *The geology of Antarctica: Oxford Monographs on Geology and Geophysics* v. 17, p.153-174.
- Wright and Kyle, 1990a. Mount Bird. In: Le Masurier and Thomson (eds) *Volcanoes of the Antarctic Plate and southern oceans*. *Antarctic Research Series* v.48. p97-98. American Geophysical Union.
- Wright and Kyle, 1990b. Mount Terror. In: Le Masurier and Thomson (eds) *Volcanoes of the Antarctic Plate and southern oceans*. *Antarctic Research Series* v.48. p99-102.
- Wright and Kyle, 1990c. Minna Bluff. In: Le Masurier and Thomson (eds) *Volcanoes of the Antarctic Plate and southern oceans*. *Antarctic Research Series* v.48. p117-119.

CHAPTER 6

Synthesis

Introduction

The primary aim of this thesis is to identify the sedimentary processes associated with oscillations of the marine-based sector of Antarctic Ice Sheet (AIS) in the Ross Embayment through facies analysis of the AND-1B drill core from the western Ross Embayment. A specific goal is to identify changes in the extent and thermal characteristics of the past ice sheets that occupied the Ross Embayment during glacial/interglacial cycles during Late Cenozoic time (13-0 Myr). The research addresses this issue on a number of timescales, beginning with the development of a sedimentary model that could be applied to the deglaciation in the Ross Sea Embayment since the Last Glacial Maximum (LGM) (Chapter 2). This sedimentary model is then applied to evaluate cyclic sedimentary and glacial processes associated with the behaviour of the AIS in the Ross Embayment over the past 13 Myr, the period covered by the ANDRILL core (Chapter 3). A facies approach for grounding-line fluctuations of polar to sub-polar ice sheets is developed within a sequence stratigraphic framework. This analysis identifies three distinct types of glacimarine cycles, termed “sequence motifs”, each characterised by a specific vertical succession of facies. The differences in these motifs reflects the long-term evolution of the Ross Embayment sector of the AIS from a cold-polar glacial regime through to a relatively warmer, sub-polar style of glaciation, and then back to the cold polar style of glaciation that characterises the Late Pleistocene section of the AND-1B drill core. Each motif is interpreted on the basis of modern analogues of glacimarine sedimentation from a range of climatic/glacial settings, and represents fluctuations of the grounding line of a marine based ice sheet as it advances and retreats from the Ross Embayment. These three motifs are used to infer changes in the controls on AIS mass balance and stability in the Ross Embayment during the Late Cenozoic. Comparisons are also made between the record in AND-1B and other geological records of Neogene and Quaternary age, as well as global proxies of past variability in oceanic temperature and ice volume.

6.1 Development of a sedimentary model for the seafloor beneath the McMurdo Ice Shelf since the Last Glacial Maximum

A sedimentary model was presented in Chapter 2 for the LGM-Holocene deglaciation of the Ross Sea, based on short sediment gravity and piston cores from the beneath the McMurdo Ice Shelf, and from the seasonally open waters of McMurdo Sound and north of Ross Island. This sedimentary model is characterised by a clast-rich diamictite deposited in a grounding-line proximal environment immediately following the retreat of grounded ice at the LGM. The diamictites pass into mudstone-dominated sediments that lack clasts (>2 mm), a facies that is indicative of deposition beneath a floating ice shelf that is free of basal debris. In the present-day seasonally-open water north of Ross Island, pre-Holocene ice shelf muds are overlain by Holocene accumulations of diatom-bearing muds or diatom ooze with IRD. This sediment model represents the modern “type” example for cold-polar, glacial-interglacial cycles within the AND-1B drill core.

6.2 Sedimentary model associated with a cold-polar marine-based ice sheet in the Ross Embayment: Motif 1

The sedimentary model associated with Pleistocene and Mid to early Late Miocene section of the AND-1B sediment drill core (Chapters 3 and 4) is consistent with the model developed for the LGM-Holocene record in Chapter 2, and is characterised by Motif 1 sequences (Chapter 3). Glacial maxima in Motif 1 are represented by massive diamictites deposited beneath grounded ice, as interpreted from the sharp basal contacts of the diamictites and the deformation of underlying sediments due to glacial overriding. The glacial-retreat facies in Motif 1 contain no evidence for conduit discharge from beneath grounded ice, such as well-sorted conglomerates (e.g., Powell, 1990). The facies include some sandy conglomerates and sandy diamictites, but these are regarded as gently winnowed on the basis of their poor sorting and most likely the result of sub-ice shelf currents close to the grounding line, perhaps including a tidal pumping mechanism (e.g., Domack and Williams, 1990). Well-sorted, cross-bedded sandstone deposits cap some of the glacial retreat diamictite (and conglomerate) facies, and most likely result from tidal pumping processes. The facies succession then passes into quiet ice shelf deposition characterised by fine-grained mudstone facies.

Due to a lack of direct modern observations, much remains unknown regarding grounding zone and subglacial processes for marine-based sectors of the AIS. However, the observations of diamictite interpreted as subglacial till from AND-1B can provide some insight. Powell and Alley (1997) predicted that a marine ice sheet in a cold-polar regime would probably result in wedge of diamictite occurring at the end of a diamictite sheet up to tens of metres thick and several kilometres long – a “glacimarine sheet wedge deposit”. Many of the subglacial tills in AND-1B are of comparable thickness and consistent with this view. Even during the cold-polar regime of the Late Pleistocene, where the ice sheet is colder than freezing throughout most of its thickness, the marine-based sectors of the AIS were most probably thawed at parts of its bed, depositing water-saturated and deforming subglacial tills (Alley *et al.*, 1986; Powell and Alley, 1997; Tulaczyk *et al.*, 1998). This is supported in AND-1B by evidence of deformation due to sliding basal ice (e.g., aligned clasts, and minor physical intermixing of underlying deposits) in the diamictites units interpreted as subglacial till deposits, including those deposited under the cold polar regime of the past 0.8 Myr.

6.3 Sedimentary model associated with a dynamic sub-polar marine-based ice sheet in the Ross Embayment: Motif 2

During the Pliocene, the AIS was highly dynamic in the Ross Embayment, and oscillated between states of fully grounded ice and open marine conditions at the drill site. This period is characterised by cyclic sequences of diamictite, mudstones and diatomites (Motif 2; Chapter 3). Two sub-motifs are defined, based on the degree of terrigenous sedimentation during glacial retreat and minima phase. Subglacial to grounding-line proximal diamictite facies in Motif 2a are overlain by thin (<1-5 m) glacial retreat successions of mudstone-rich facies before passing into open water deposition of diatomites. Motif 2a is indicative of some subglacial meltwater at the grounding line during glacial retreat of the AIS in the Ross Embayment. Motif 2b characterises sequences during the lower Pliocene section of the AND-1B drill core, and consist of a basal unit of diamictite overlain by a relatively thick (~10 m) proglacial retreat facies succession consisting of mudstone and sandstones, before passing into diatomite that has variable degrees of (0-50%) terrigenous input. Motif 2b is characteristic of glacial regime where there is a greater abundance of subglacial

meltwater associated with glacial retreat and advance, relative to Motif 2a. Throughout the Pliocene Epoch, the terrigenous proglacial retreat/advance facies become progressively thinner up-section and are particularly thin (<1 m) in the upper Pliocene section of AND-1B (~230 to 152 mbsf). This is indicative of gradual cooling of the glacial regime of the marine-based AIS in the Ross Embayment and the transition from a sub-polar towards a cold-polar regime.

6.4 Sedimentary model associated with a dynamic sub-polar WAIS: Motif 3

During the Late Miocene, there was a warmer glacial regime, as characterised by Motif 3 sequences (Chapter 3). Glacial maxima in Motif 3 consist of massive diamictite deposited beneath grounded ice, before passing into a glacial retreat facies succession that commonly include conglomerate and stratified sandstone. These facies are consistent with significant subglacial meltwater, with conduit discharges and grounding line fan processes (Powell, 1990; Chapter 3). Cyclopels, cyclopsams and thick (>10 m) intervals of mudstone are deposited immediately following grounding line retreat and during the glacial minima phase. Such facies are all indicative of significant discharge of sub-glacially derived meltwater (Mackiewicz *et al.*, 1984; Cowan *et al.*, 1999), and comparison to modern glacial analogues implies a thermal regime for AIS in the Ross Embayment during the Late Miocene that was similar to present-day sub-polar environments (cf. Spitsbergen and Greenland; Table 10), where meltwater processes have a primary influence on ice sheet mass balance controls.

6.5 Response of WAIS to Late Cenozoic climate cycles

The key aim of the ANDRILL McMurdo Ice Shelf project is to determine past ice sheet responses to climate forcings at a variety of timescales (Naish *et al.*, 2005). Chapter 2 provides insight into the response of the AIS in the Ross Embayment to warming since the Last Glacial Maximum. The sedimentary model developed in Chapter 2 is also relevant to the Late Pleistocene record in AND-1B (Chapter 4), for which a cold-polar glacial regime has been inferred for the Ross Embayment sector of AIS (Chapter 3).

Here, I have evaluated the ice sheet record as expressed in high-resolution facies analysis and by comparison to deep-sea sediment core records (past ocean temperature and ice volume). Critical to the accurate assessment of the AND-1B record, with respect to other global climate proxy records, was a robust chronology. Refinement of the age model for the Neogene (and Quaternary) sections will continue to add insight into the response of the AIS to past climatic variability, and this potential is discussed in the following sections.

6.6 Timing of the retreat of AIS in the Ross Embayment since the Last Glacial Maximum and the sub-orbital Holocene record

Deglaciation of the Antarctic Ice Sheets is believed to have contributed ~14-18 m to post-LGM eustatic sea level rise, with approximately two-thirds of this thought to have been sourced from the WAIS (Huybrechts, 2002; Denton and Hughes, 2002). However, there is still considerable debate surrounding the timing (and extent) of the retreat of the AIS since the LGM. Resolving this uncertainty has significant implications for our understanding of Antarctica's recent role in the global climate system, in particular its response to orbital forcing and contribution to thermohaline circulation.

Clark *et al.* (2002) pointed to Antarctica as a source for Meltwater Pulse-1A, a rapid 20-m-sea level rise centred on 12,000 ¹⁴C yr BP (Fairbanks 1989). This led Weaver *et al.* (2003) to suggest on the basis of numerical modelling that meltwater discharge of this magnitude sourced from Antarctica would result in strengthening of North Atlantic Deepwater production, resulting in the Bølling-Allerød warm event (i.e., last glacial termination) in the Northern Hemisphere. This establishment of strong North Atlantic Deepwater formation was then susceptible to the freshwater “forcing” by decay of the Northern Hemisphere Ice Sheets that is inferred to have lead to the Younger Dryas cold event in the Northern Hemisphere (Broecker *et al.*, 1989; Clark *et al.*, 2002; Weaver *et al.*, 2003).

The post-LGM retreat history of marine-based AIS in the Ross Sea Embayment, based on marine sediment cores (Domack *et al.*, 1999; Chapter 2 of this thesis), implies that

the majority of AIS retreat in the Ross Embayment occurred after 11,000 ^{14}C yr BP, and therefore could not have contributed to Meltwater Pulse 1A. The data presented in Chapter 2 indicates that by $\sim 9,000$ ^{14}C yr BP the ice shelf calving line had reached its present-day position. This phase of rapid retreat coincides with Meltwater Pulse 1B between ~ 9.2 and 9.8 ^{14}C yr BP (~ 10 m sea level rise; Fairbanks, 1989). The chronology in Chapter 2 indicates that the retreat of grounding line from the outer Drygalski Trough to Ross Island preceded Meltwater Pulse 1B, while open marine conditions near Ross Island occurred immediately following it. Although this chronology is not sufficiently accurate to constrain the timing of grounding line retreat to one of these meltwater events, it is good enough to show that Antarctica was not a significant contributor to Meltwater Pulse 1A.

A simple interpretation of the chronology presented in Chapter 2 suggests that initial grounding line retreat was probably initiated by eustatic sea level rise associated with disintegration of the Northern Hemisphere ice sheets. Once ice shelf conditions had begun to develop across the outer Ross Sea embayment (following Meltwater Pulse 1A), rapid thinning of ice shelf probably occurred, as exposure of the base of the ice shelf to oceanic processes results in rapid basal melting from beneath (Shepherd *et al.*, 2004; Payne *et al.*, 2004; Alley *et al.*, 2007). This melting event may have contributed to Meltwater Pulse 1B.

Open water conditions were in place immediately north of Ross Island by ~ 9 ^{14}C Kyr, yet the sub-ice shelf record at the HWD sites indicates persistent ice shelf conditions throughout the Holocene (Chapter 2), implying a stable calving line for the Ross Ice Shelf throughout the warmest period of the Holocene. Ice cores from around the Ross Sea sector indicate warmer-than-present temperatures ($\sim 2^\circ$ warmer) between ~ 7.2 and 5.2 ^{14}C Kyr BP (Masson *et al.*, 2000; Steig *et al.*, 2000). This temperature optimum coincides with the first open water conditions in McMurdo Sound proper at 6500 ^{14}C yr BP (Licht *et al.*, 1996; Conway *et al.*, 1999). Chapter 2 reconciles discrepancies between the terrestrial and marine geological for glacial retreat chronology by suggesting that an ice shelf remained in place within McMurdo Sound up to ~ 6.5 ^{14}C yr BP, and its break-up around this time could be related to this temperature optimum. There is also a

notable IRD peak in DF80-189 around this time (Figure 15), which may have resulted from the break-up of the McMurdo Sound ice shelf.

6.7 Determining the response of WAIS to orbitally influenced climate cycles during the Pleistocene

During the late Pleistocene (0.8 Myr to present), the glacimarine sequences in AND-1B were found to have a ~100 kyr cyclicity (Chapter 4). These sequences record a marine-based AIS in the Ross Embayment that had a cold polar regime (Chapter 3) and was relatively stable, with only grounded ice sheet or floating ice shelves recorded. There is no physical evidence of any prolonged marine conditions at the drill site. As the AND-1B record is interpreted as recording advance and retreat of ice sheets across the entire Ross Embayment (see Chapter 1), this implies that there was no large-scale WAIS “collapse” in past 0.8 Myr, a period that included “super-interglacials” centred on 420 and 120 Kyr. Prior to Mid-Pleistocene Transition, the Ross Embayment sector of the AIS was more dynamic and fluctuated between a grounded state and open marine conditions at the AND-1B drill site. These fluctuations occurred at a higher frequency than for the Late Pleistocene sequences, in some if not all episodes, with a period of 40 kyr.

6.8 Comparison with Neogene geologic records from East Antarctica

6.8.1 Prydz Bay region

Comparisons can be made between the AND-1B record and the Neogene strata from the Prydz Bay region of East Antarctica, which is a direct record of variations in extent of ice in the Lambert drainage basin, itself ~7% of the East Antarctic Ice Sheet (Hambrey and Dowdeswell, 1994). However differences between the deep-water facies in the AND-1B drill core and the shallow water facies of the Pagodroma Group need to be kept in mind. The middle to late Miocene Fisher Bench Formation from the Pagodroma Group contains evidence for increased subglacial meltwater in glacial retreat facies with the presence of 2 or 3-m-thick intervals of rhythmically laminated clay and siltstone, as well as a high proportion of boulder/cobble gravels indicative of subglacial conduit

discharge (Hambrey and McKelvey, 2000). The claystone and siltstone laminae form couplets ~1-3 mm thick, and are consistent with the rhythmically-laminated mudstone with siltstone/sandstone documented in Motif 3 from AND-1B (Chapter 3). The pebble to cobble gravels, interpreted as sub-aquatically discharged glacifluvial (e.g., conduit discharges) sediments, might be considered equivalent to conglomerate and stratified sandstone facies in Motif 3 from AND-1B. Diatom biostratigraphy suggests that the Fisher Bench Formation was deposited sometime between 12.7 and 8.5 Myr. This age lies in the range of the Late Miocene Motif 3 strata in AND-1B (Wilson *et al.*, 2007; Chapter 3), and supports the interpretation in Chapter 3 that subglacially-derived meltwater process were common on the margin of EAIS during the Late Miocene.

While the Miocene strata in the Pagodroma Group deposits have sedimentary features indicating a significantly warmer-than-present glacial regime, the Pliocene Bardin Bluff deposits in the Pagodroma do not contain evidence for subglacial meltwater facies such as tidal rhythmites or conduit discharge facies (Hambrey and McKelvey, 2000). Inferences of a “wet-based” glacial regime for the Bardin Bluffs Formation are based on the presence of mud-rich diamictites with striated and faceted clasts. These diamictites are indicative of sliding at the base of the expanded Lambert Glacier. However, basal melting and sliding occur beneath the present-day East Antarctic Lambert Glacier (Allison, 1979). Inferring a warmer-than-present environment strictly on the basis of “wet-based” deposition (e.g., Whitehead and McKelvey, 2001; McKelvey *et al.*, 2001) is equivocal, as lodgement and deformation till appear to be common facies deposited beneath the cold-polar, marine-based portions of WAIS and EAIS in the cold-polar regime of the Pleistocene, as documented in AND-1B and other studies (Domack *et al.*, 1999; Hemmer and Harris, 2003; this study). However, inferences of a warmer-than-present climate can be made from the glacial minima successions in the Bardin Bluff deposits, as there is an absence of ice shelf facies (Hambrey and McKelvey, 2000). Glacial minima facies are represented by ice-berg rafted debris and rockfall deposits, indicating that the glaciers in the Lambert fjord terminated as tidewater cliffs, rather than an ice shelf. The presence of Early Pliocene marine deposits at Marine Plain in the Vestfold Hills also indicates that there was recession of the marine-based margin of EAIS during glacial minima in Pliocene times (Quilty *et al.*, 2000).

These observations are consistent with the Pliocene record in AND-1B drill core, where there are many periods of open-water conditions in the Ross Embayment and little evidence of prolonged ice shelf conditions like those of today (e.g., Motif 2). Comparison of the Pliocene Pagodroma with AND-1B suggests that the marine-based sectors of the WAIS and EAIS both had warmer temperature profiles (sub-polar to polar) relative to the present-day cold polar environment, at least to the extent that they could not support ice shelves in large embayments during glacial minima.

6.8.2 *Transantarctic Mountains*

Terrestrial glacial deposits and related sediments scattered at high elevations throughout the Transantarctic Mountains have been collectively termed the Sirius Group (Mercer, 1972, McKelvey *et al.* 1991). They have long been recognised to be of wet-based glacial origin and deposited from ice flowing from the East Antarctic interior (Mayewski, 1975, Denton *et al.*, 1984), and some deposits contain a coeval *Nothofagus* flora (Francis and Hill, 1996). Pliocene marine diatoms found in the deposits at several locations led some to suggest that the deposits were younger than this, implying open seas in the interior during the geologically recent past. However, a range of circumstantial evidence has shown this to be unlikely (Sugden *et al.*, 1993) and further studies suggest atmospheric contamination as a more probable source for the diatoms (McKay *et al.*, 2008).

The McMurdo Sound region does contain deposits on land of well-established Pliocene age. These include the Pecten Conglomerate, a fjordal deposit now at an elevation of ~200 m in the floor of Wright Dry Valley (Webb, 1974); Late Miocene to Pleistocene glacial-interglacial sequences at least 328 m in thickness in the floor of lower Taylor Dry Valley (McKelvey, 1981); and a comparable sequence ~165 m thick cored in the floor of Ferrar Fiord (Barrett and Hambrey, 1992). These deposits comprise glacial and coastal facies that are little different from those being deposited today.

A feature of the McMurdo Sound region has been the extensive geomorphological research over the last two decades (Summerfield *et al.*, 1999, Sugden and Denton 2004). This has been accompanied by soil studies, surface age dating and tephrochronology (Marchant *et al.*, 1996), and has led most recently to discoveries of moraines and fossiliferous deposits marking the transition from temperate to cold-based ice 14 Myr ago at the edge of the East Antarctic Ice Sheet in this region (Lewis *et al.*, 2007). This body of work implies a persistent cold landscape adjacent to the Ross Embayment throughout the last 14 Myr. However, this is not inconsistent with most of the AND-1B record, as the Pliocene diatomite beds in AND-1B imply very little terrigenous sediment entering the basin despite being adjacent to (100 km west of) a mountain range with peaks exceeding 3000 m. Although there is evidence for significant meltwater in the AND-1B record during the Late Miocene (Motif 3 sequences; Chapter 3), there as yet is no evidence of coeval vegetation growing on land during the deposition of AND-1B sequences, based on initial palynological studies (Scherer *et al.*, 2007). This suggests that Sirius Group deposits were likely deposited prior to the deposition of the AND-1B sequences. Although ice that feeds the AND-1B drill site is sourced from the EAIS, the sedimentary sequences in AND-1B are primarily responses to the expansion and contraction of the marine-based AIS across the entire Ross Embayment (see Chapter 1 and 3). As a grounded ice sheet at the AND-1B drill site will be marine-based at the AND-1B drill site, the mass balance controls (e.g., eustasy, iceberg calving and sub-ice melting) will therefore be the same as for most of the WAIS. Therefore, this disconnection between a cold-polar regime for the EAIS and a subpolar regime for the AIS in the Ross Embayment and low altitude EAIS fjordal outlet glaciers may be explained by the different mass balance controls for terrestrial versus marine-based ice sheets.

6.9 Correlation to global proxies and implication for orbital control of the Late Cenozoic Antarctic Ice Sheets

Chapter 4 developed a high-resolution glacial sequence stratigraphic model for the Pleistocene section of the AND-1B, and this was compared to the composite benthic $\delta^{18}\text{O}$ marine record of Lisiecki and Raymo (2005), a proxy for ice volume and deep-sea temperature. Using the stratigraphic tools developed in this thesis, and with continuing

development of the AND-1B age model, this approach is being applied to older sections of the core (e.g., Naish *et al.*, in review) to determine the past contributions of the Antarctic Ice Sheets to global sea level changes at an orbital (i.e., 40-100 kyr) timescale. Here a comparison is made to a composite benthic $\delta^{18}\text{O}$ marine record (Zachos *et al.*, 2001) on a much broader time scale. This provides insight into the major changes through time in mass balance controls for AIS in the Ross Embayment that are implied by the three distinctive sequence motifs (Figure 71; Chapter 3).

The oldest part of the AND-1B core (Mid to early Late Miocene; 1285 to 1083 mbsf) is characterised by Motif 1 (cold polar glacial regime). This motif represents large-scale expansion of AIS onto the Ross Sea continental shelf, by a cold-polar style of ice sheet similar to that of the late Quaternary. They may correspond to the large positive $\delta^{18}\text{O}$ excursions (Figure 71) during the Mid to early Late Miocene (e.g., Mi-4 and Mi-5; Miller *et al.*, 1991).

The overlying strata in Late Miocene (1083 to 770 mbsf) in AND-1B are characterised by Motif 3 sequences (sub-polar glacial regime with abundant subglacial meltwater). The chronology of this section of the AND-1B is not yet well constrained. There are probably numerous unconformities in this section of the core, but at this stage these are unable to be determined from the initial age model. Motif 3 likely correlates to low amplitude interval in the benthic $\delta^{18}\text{O}$ record between 11 and 6.5 Myr (Figure 71). The Motif 3 sequences between 1083 and 900 mbsf generally have thicker diamictite units than for Motif 3 sequences above 900 mbsf. These thicker diamictites could correspond to some of the late Miocene $\delta^{18}\text{O}$ excursions (e.g., Mi-6 and Mi-7; Figure 71; Miller *et al.*, 1991). Most of the latest Miocene is probably missing from the record and coincides with a ~180 m volcanic succession dated at ~6.5 Myr.

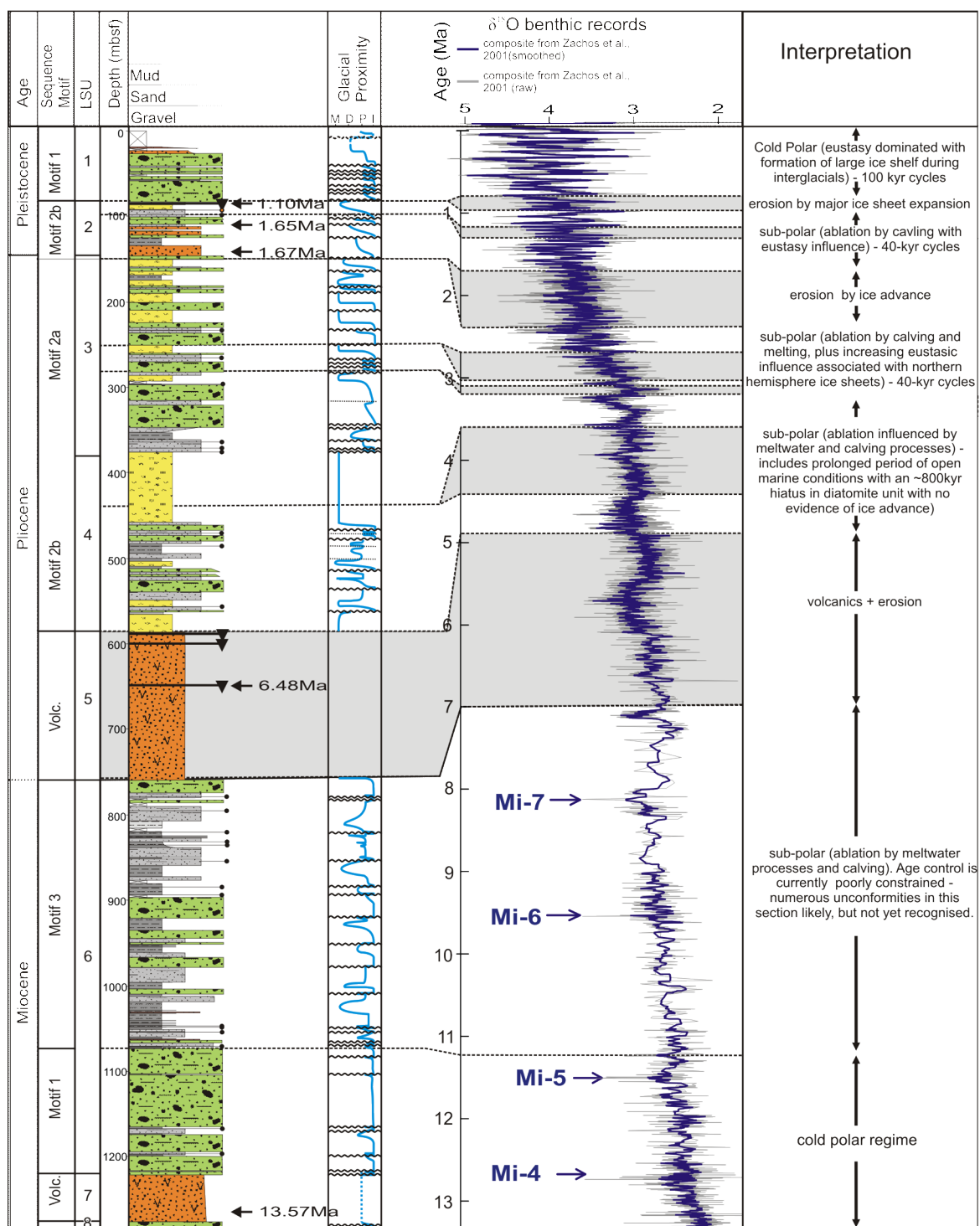


Figure 71: Correlation of AND-1B to $\delta^{18}\text{O}$ marine records, based on data from Zachos *et al.* (2001). Smoothed curve is curve is based on a 5 point running mean. Ages for Mi-events are from Miller *et al.*, 1991. Legend for lithological units is provided in Figure 37.

The Early Pliocene section of AND-1B is characterised by Motif 2b sequences (sub-polar glacial regime with some meltwater influence). Of note here is a 90-m-thick interval of diatomite deposited between 4.4 and 3.5 Myr. Initial diatom biostratigraphy suggests that a ~800 kyr unconformity exists at 440 mbsf (Naish *et al.*, in review), and this is marked stratigraphically by a volcanic debris flow unit at this depth. The entire interval is considered to represent a prolonged period when the AND-1B drill site was ice-free, and due to the long duration of marine deposition it probably represents widespread and prolonged retreat/absence of the marine-based portion of the AIS in the Ross Embayment at this time. This would have resulted in sea levels ~5 m higher than present and there is some support for this in an average $\delta^{18}\text{O}$ value of 3‰, though reaching as low as 2.73‰ in the $\delta^{18}\text{O}$ benthic record (Lisiecki and Raymo, 2005). These low values correspond to sea levels of ~25 m higher than present (Dowsett and Cronin, 1990; Crowley, 1996), and would require almost complete deglaciation of WAIS, as well as the Greenland Ice Sheet and about 10 m sea level equivalent of the margin of EAIS. Thick (>10 m) proglacial retreat facies in Motif 2b indicate that subglacial-derived meltwater played a role in controlling ice sheet mass balance, but this diminishes with time as the AND-1B record passes into the Late Pliocene.

The Late Pliocene section of the AND-1B consists of Motif 2a sequences, which differ from Motif 2b in the rapid transitions from diamictite to diatomite facies. Proglacial retreat facies are generally <1 m thick. This implies a significant reduction in subglacial melting and a general cooling in glacial thermal regime. This interval coincides with the gradual increase in $\delta^{18}\text{O}$ values from marine benthic records between ~3 Myr and 1 Myr (Figure 71). This trend is generally attributed to global cooling from ~3.1 Myr and the development of the Fennoscandian and Laurentide ice sheets from ~2.5 Myr (Shackleton and Opdyke, 1977). The lack of subglacial meltwater associated with glacial retreat implies that mass balance became largely controlled by calving of ice from the marine margin, as well as from basal melting of floating ice shelves that may have fringed the margin of Antarctica. An increasing influence of eustatic sea level control associated with ephemeral Northern Hemisphere ice sheets at this time is also implied.

During the Pleistocene section of AND-1B, the development of the present-day style of cold-polar glaciation is documented by a large scale expansion of AIS in the Ross Embayment at 0.8 Myr, as indicated by a change from Motif 2 sequences to Motif 1 sequences, and an associated unconformity (Chapter 4). Since 0.8 Myr, the AIS has oscillated at a frequency of 100 kyr, whereas before this it responded at a 40-kyr cyclicity (Chapter 4). This change in thermal regime coincides with the Mid-Pleistocene Transition that is well documented in the $\delta^{18}\text{O}$ benthic record (Figure 71). Interglacial periods during the Late Pleistocene are characterised by extensive ice shelf conditions, rather than open marine conditions. This indicates that although it oscillates at a 100-kyr periodicity, the AIS has been a relatively stable feature in the Ross Embayment over the past 0.8 Myr, compared to Pliocene and Late Miocene times.

6.10 References

- Allison, I. E., 1979. The mass budget of the Lambert Glacier drainage basin, Antarctica. *Journal of Glaciology* v.22, p.223-235.
- Alley, R. B., Blankenship, D. D., Bentley, C. R., and Rooney, S. T., 1986. Deformation of till beneath ice stream B, West Antarctica. *Nature* v. 322, p.57-59.
- Alley, R. B., Anandakrishnan, S., Dupont, T. K., Parizek, B. R., and Pollard, D., 2007. Effect of sedimentation on ice-sheet grounding-line stability. *Science* v. 315, p.1838-1841.
- Barrett, P. J., and Hambrey, M. J., 1992. Plio-Pleistocene sedimentation in Ferrar Fiord, Antarctica. *Sedimentology* v. 39, p.109-123.
- Broecker, W. S., Kennett, J. P., Flower, B. P., Teller, J. T., Trumbore, S., Bonani, G., and Woelfli, W., 1989. Routing of meltwater from the Laurentide ice sheet during the Younger Dryas cold episode. *Nature* v. 341, p.318-321.
- Clark, P. U., Mitrovica, J. X., Milne, G. A., and Tamisiea, M. E., 2002. Sea-level fingerprinting as a direct test for the source of global meltwater pulse IA. *Science* v. 295, p.2438-2441.
- Conway, H., Hall, B. L., Denton, G. H., Gades, A. M., and Waddington, E. D., 1999. Past and future grounding-line retreat of the West Antarctic Ice Sheet. *Science* v.286, p.280-283.
- Cowan, E. A., Seramur, K. C., Cai, J., and Powell, R. D., 1999. Cyclic sedimentation produced by fluctuations in meltwater discharge, tides and marine productivity in an Alaskan fjord. *Sedimentology* v. 46, p.1109-1126.
- Crowley, T. J., 1996. Pliocene climates: the nature of the problem. *Marine Micropaleontology* v.27, p.3-12.

- Denton, G. H., Prentice, M. L., Kellogg, D. E., and Kellogg, T. B., 1984. Late Tertiary history of the Antarctic ice sheet; evidence from the dry valleys. *Geology*, v. 12, p.263-267.
- Denton, G. H., and Hughes, T. J., 2002. Reconstructing the Antarctic Ice Sheet at the Last Glacial Maximum. *Quaternary Science Reviews* v. 21, p.193-202.
- Domack, E. W., and Williams, C. R., 1990. Fine structure and suspended sediment transport in three Antarctic fjords. *Antarctic Research Series* v. 50, p.71-89.
- Domack, E. W., Jacobson, E. A., Shipp, S., and Anderson, J. B., 1999. Late Pleistocene-Holocene retreat of the West Antarctic ice-sheet system in the Ross Sea; Part 2, Sedimentologic and stratigraphic signature. *Geological Society of America Bulletin* v.111, p.1517-1536.
- Dowsett, J., and Cronin, T. M., 1990. High eustatic sea level during the middle Pliocene: Evidence from the southeastern U.S. Atlantic Coastal Plain. *Geology* v.18, p.435- 438.
- Fairbanks, R. G., 1989. A 17,000-year glacio-eustatic sea level record; influence of glacial melting rates on the Younger Dryas event and deep-ocean circulation. *Nature* v.342, p.637-642.
- Francis, J. E., and Hill, R. S., 1996. Fossil plants from the Pliocene Sirius Group, Transantarctic Mountains: evidence from climate from growth rings and fossil leaves. *Palaaios* v. 11, p.389-396.
- Hambrey, M. J., and Dowdeswell, J.A., 1994. Flow regime of the Lambert Glacier-Amery Ice Shelf system, Antarctica: structural evidence from Landsat imagery. *Annals of Glaciology* v.20, p.401-406.
- Hambrey, M. J., and McKelvey, B., 2000. Neogene fjordal sedimentation on the western margin of the Lambert Graben, East Antarctica. *Sedimentology* v. 47, p.577-607.
- Hemer, M. A., and Harris, P. T., 2003. Sediment core from beneath the Amery Ice Shelf, East Antarctica, suggests mid-Holocene ice-shelf retreat. *Geology* v. 31, p.127-130.
- Huybrechts, P., 2002. Sea-level changes at the LGM from ice-dynamic reconstructions of the Greenland and Antarctic ice sheets during the glacial cycles. *Quaternary Science Reviews* v. 21, p.203-231.
- Lewis, A.R., Marchant, D.R., Ashworth, A.C., Hemming, S.R., and Machlus, M.L., 2007. Major middle Miocene global climate change: Evidence from East Antarctica and the Transantarctic Mountains. *Geological Society of America Bulletin* v.119, p.1449-1461.
- Licht, K. J., Jennings, A. E., Andrews, J. T., and Williams, K. M., 1996. Chronology of late Wisconsin ice retreat from the western Ross Sea, Antarctica. *Geology* v. 24, p.223-226.
- Lisiecki, L. E., and Raymo, M.E., 2005. A Pliocene-Pleistocene stack of 57 globally distributed benthic $\delta^{18}O$ records. *Paleoceanography*, v.20, PA1003, doi:10.1029/2004PA001071.
- Mackiewicz, N. E., Powell, R. D., Carlson, P. R., and Molnia, B. F., 1984. Interlaminated ice-proximal glacial-marine sediments in Muir Inlet, Alaska. *Marine Geology* v.57, p.113-147.

- Marchant, D. R., Denton, G. H., Swisher, C. C., III, and Potter, N., Jr., 1996. Late Cenozoic Antarctic paleoclimate reconstructed from volcanic ashes in the dry valleys region of southern Victoria Land. *Geological Society of America Bulletin* v.108, p.181-194.
- Masson, V., Vimeux, F., Jouzel, J., Morgan, V., Delmotte, M., Ciais, P., Hammer, C., Johnsen, S., Lipenkov, V. Y., Mosley-Thompson, E., Petit, J.-R., Steig, E. J., Stievenard, M., and Vaikmae, R., 2000. Holocene climate variability in Antarctic based on 11 ice-core isotopic records. *Quaternary Research* v.54, p.348-358.
- Mayewski, P.A., 1975. Glacial geology and Late Cenozoic history of the Transantarctic Mountains, Antarctica. *Institute of Polar Studies report* v.56, The Ohio State University.
- McKay, R., Barrett, P., Harper, M., and Hannah, M., 2008. Atmospheric transport and concentration of diatoms in the Allan Hills, Transantarctic Mountains. *Palaeogeography, Palaeoclimatology, Palaeoecology* v.260, p.245-261.
- McKelvey, B.C., 1981. The lithological logs of DVDP cores 10 and 11, eastern Taylor Valley. In: McGinnis, L.D. (ed.), Dry Valley Drilling Project, *Antarctic Research Series* v.33, p.63-64.
- McKelvey, B.C., Webb, P.N., Harwood, D.M. and Mabin, M.C.G., 1991. The Dominion Range Sirius Group: a record of the Late Pliocene-Early Pleistocene Beardmore Glacier. In: Thompson, M.R.A., Crame, J.A. and Thompson, J.W. (eds.), *Geological Evolution of Antarctica*. Cambridge, Cambridge University Press, p.675-682.
- McKelvey, B. C., Hambrey, M. J., Harwood, D. M., Mabin, M. C. G., Webb, P. N., and Whitehead, J. M., 2001. The Pagodroma Group; a Cenozoic record of the East Antarctic ice sheet in the northern Prince Charles Mountains. *Antarctic Science* v.13, p.455-468.
- Mercer, J.H., 1972. Some observations on the glacial geology of the Beardmore Glacier Area. In: Adie, R.J. (ed.) *Antarctic Geology and Geophysics*. Universitetsforlaget, Oslo, p.427-433.
- Miller, K. G., Wright, J. D., and Fairbanks, R. G., 1991. Unlocking the ice house: Oligocene-Miocene oxygen isotopes, eustasy, and margin erosion. *Journal of Geophysical Research* v. 96(B), p.6829-6848.
- Naish, T., Powell, R., Barrett, P., Horgan, H., Dunbar, G., Wilson, G., Levy, R., Robinson, N., Carter, L., Pyne, A., Niessen, F., Balfour, N., Damaske, D., Henrys, S., Kyle, P., and Wilson, T., 2005. ANDRILL McMurdo Ice Shelf Scientific Prospectus. *ANDRILL Contribution* v.4. University of Nebraska-Lincoln, 18p.
- Naish, T., Powell, R., Levy, R., Krissek, L., Niessen, F., Pompilio, M., Scherer, R., Talarico, F., Wilson, G., Wilson, T., McKay, R., Ross, J., Winter, D., Browne, G., Carter, L., Cody, R., Cowan C., Crampton, J., Dunbar, G., Dunbar, N., Florindo, F., Gebhardt, C., Graham, I., Hannah, M., Harwood, D., Hansaraj, D., Henrys, S., Helling, D., Kuhn, G., Kyle, P., Läufer, A., Maffioli, P., Magens, D., Mandernack, K., McIntosh, W., Millan, C., Morin, R., Ohneiser, C., Paulsen, T., Persico, D., Reed, J., Raine, I., Schmitt, D., Sagnotti, L., Sjunneskog, C., Strong, P., Taviani, M., Vogel, S., Wilch, T., Williams, T., In review. Late Cenozoic variability of the West Antarctic Ice Sheet. In review with *Nature*.

- Payne, A. J., Vieli, A., Shepherd, A. P., Wingham, D. J., and Rignot, E., 2004. Recent dramatic thinning of largest West Antarctic ice stream triggered by oceans: *Geophysical Research Letters* v.31, L23401. doi: 10.1029/2004GL021284.
- Powell, R. D., 1990. Grounding-line fans and their growth to ice-contact deltas. In: Dowdeswell, J. A., and Scourse, J. D., eds., *Glacimarine Environments: Processes and Sediments. Geological Society of London Special Publication*, v.53, p.53-73.
- Powell, R. D., and Alley, R. B., 1997. Grounding-line systems; processes, glaciological inferences and the stratigraphic record. In: Barker, P. F., and Cooper, A. K.(eds.), *Geology and seismic stratigraphy of the Antarctic margin 2. Antarctic Research Series* v. 71, p.169-187.
- Quilty, P.G., Lirio, J.M., and Jillett, D., 2000. Stratigraphy of the Pliocene Sørsdal Formation, Marine Plain, Vestfold Hills, East Antarctica. *Antarctic Science* v. 12, p.205-216.
- Scherer R., Hannah M., Maffioli P., Persico D., Sjunneskog C., Strong C.P., Taviani M., Winter D. and the ANDRILL-MIS Science Team., 2007. Palaeontologic Characterisation and Analysis of the AND-1B Core, ANDRILL McMurdo Ice Shelf Project, Antarctica. *Terra Antartica* v.14, p.223-254.
- Shackleton, N. J., and Opdyke, N. D., 1977. Oxygen isotope and palaeomagnetic evidence for early Northern Hemisphere glaciation. *Nature* v.270, p.216-219.
- Shepherd, A., Wingham, D. J., and Rignot, E., 2004. Warm ocean is eroding West Antarctic ice sheet. *Geophysical Research Letters* v. 31, L23402. doi:10.1029/2004GL021106.
- Steig, E. J., Morse, D. L., Waddington, E. D., Stuiver, M., Grootes, P. M., Mayewski, P. A., Twickler, M. S., Whitlow, S. I., Denton, G. H., and Hall, B. L., 2000. Wisconsinan and Holocene climate history from an ice core at Taylor Dome, western Ross Embayment, Antarctica. *Geografiska Annaler. Series A: Physical Geography* v. 82, p.213-235.
- Sugden, D.E., and Denton, G.H., 2004. Cenozoic landscape evolution of the Convoy Range to Mackay Glacier area, Transantarctic Mountains; onshore to offshore synthesis: *Geological Society of America Bulletin* v.116, p.840-857.
- Sudgen, D.E., Marchant, D.R. and Denton, G.H., 1993. The case for a stable East Antarctic Ice Sheet, *Geografiska Annaler* v.75(A), p.151-353.
- Summerfield, M.E., Sugden, D.E., Denton, G.H., Marchant, D.R., Cockburn, H.A.P. & Stuart, M.F., 1999. Cosmogenic isotope data support previous evidence of extremely low rates of denudation in the Dry Valleys region, southern Victoria Land, Antarctica. *Geological Society (London) Special Publications* v.16, p.255-267.
- Tulaczyk, S., Kamb, B., Scherer, R. P., and Engelhardt, H. F., 1998. Sedimentary processes at the base of a West Antarctic ice stream; constraints from textural and compositional properties of subglacial debris. *Journal of Sedimentary Research* v. 68, p.487-496.
- Weaver, A. J., Saenko, O. A., Clark, P. U., and Mitrovica, J. X., 2003. Meltwater pulse 1A from Antarctica as a trigger of the Bolling-Allerod warm interval. *Science* v.299, p.1709-1713.

- Webb, P. N., 1974. Micropaleontology, paleoecology and correlation of the Pecten Gravels, Wright Valley, Antarctica, and description of *Trochoelphidiella onyxi*. *Journal of Foraminiferal Research* v. 4, p.185-199.
- Whitehead, J.M., and McKelvey, B.C., 2001. The stratigraphy of the Pliocene–lower Pleistocene Bardin Bluffs Formation, Amery Oasis, northern Prince Charles Mountains, Antarctica. *Antarctic Science* v.13, p.79–86.
- Wilson, G., Levy, R., Browne, G., Dunbar, N., Florindo, F., Henry, S., Graham, I., McIntosh, W., McKay, R., Naish, T., Ohneiser, C., Powell, R., Ross, J., Sagnotti, L., Scherer, R., Sjunneskog, C., Strong, C.P., Taviani, M., Winter, D., and the ANDRILL MIS Science Team, 2007. Preliminary integrated chronostratigraphy of the AND-1B Core, ANDRILL McMurdo Ice Shelf Project, Antarctica. *Terra Antarctica* v.14, p.297-316.
- Zachos, J., Pagani, M., Sloan, L., Thomas, E., and Billups, K., 2001. Trends, rhythms, and aberrations in global climate 65 Ma to present. *Science* v.292, p.686-693.